ABSTRACT

Title of Dissertation:	EPIDEMIOLOGY AND FUNGICIDE SENSITIVITY OF GRAPE LATE SEASON BUNCH ROTS IN THE MID-ATLANTIC
	Scott David Cosseboom, Doctor of Philosophy, 2022
Dissertation directed by:	Assistant Professor, Mengjun Hu, Plant Science and Landscape Architecture

This project aims to improve the management of late season bunch rots of grape (LSBR) which can be caused by a wide range of fungal pathogens. LSBR collectively have been an increasing issue in Mid-Atlantic vineyards, severely affecting grape yield and quality. Despite intensive fungicide spray programs and cultural practices, severe LSBR epidemics threaten the budding Mid-Atlantic wine industry. The basic plant pathological variables of host, pathogen, and environment were investigated to improve knowledge of the diseases involved, and therefore improve management strategies. The most common causal agents of LSBR in the Mid-Atlantic were found to be *Botrytis cinerea* and *Colletotrichum* spp. and the species identity of less common fungi was also investigated. The next most prevalent fungi associated with LSBR, *Alternaria alternata, Aspergillus uvarum,* and *Neopestalotiopsis rosae* were evaluated for pathogenicity in field experiments through the artificial inoculation of grape clusters. Second, the sensitivity of *A. uvarum, B. cinerea,* and *N. rosae* to commonly used chemical classes of

fungicides was tested. Lastly, the optimal infection conditions and timing for *Colletotrichum* spp. were evaluated in laboratory, field, and greenhouse experiments, resulting in a quantitative inoculum tracking technique and a disease prediction model. These experiments were focused on solving practical and important disease management issues experienced by local grape growers, while conducting novel research that was applicable to the broader science community. Beyond the increased knowledge of the etiology and epidemiology of LSBR, the conclusions of this research could lead to reformed LSBR management strategies with the elimination of unnecessary and ineffective fungicide applications, increased accuracy and timing of management efforts, and increased marketable grape yield.

EPIDEMIOLOGY AND FUNGICIDE SENSITIVITY OF GRAPE LATE SEASON BUNCH ROTS IN THE MID-ATLANTIC

by

Scott David Cosseboom

Dissertation submitted to the Faculty of the Graduate School of the
University of Maryland, College Park, in partial fulfillment
of the requirements for the degree of
Doctor of Philosophy
2022

Advisory Committee:
Dr. Mengjun Hu, Chair
Dr. Joseph Fiola
Dr. Joseph Roberts
Dr. Kathryne Everts
Dr. Natalia Peres
Dr. Nidhi Rawat

Acknowledgements

I would like to first thank my God, who has provided for me in every way. Huge thank you to my advisor Mengjun Hu for inviting me on this journey. He is a great mentor and collaborator, who offered wise advice and council, yet was also patient and adaptable when things did not go according to plan. I was also under the prudent guidance of an incredible advisory committee and other mentors including Kevin Atticks and Tom Croghan. Further mentoring and professional growth came through my Foundation for Food and Agriculture (FFAR) fellowship, from which I gained so much.

Thank you to the researchers who went before me and gathered knowledge that I built upon in my investigations. I am indebted to the lab mates who were eager to assist me in the many experiments I was juggling, including Anita Schoeneberg, Stephen Boushell, Qiuchen Luo, Chiti Agarwal, Chloe Hinson, Madeline Farrell, Elizabeth Tran, Emily Fang, and Alfred Wirman. There were many others who supported and cooperated in my experiments, including Ron Wates and Boordy Vineyards, Michael Newell, Chris Cochran, and the Wye REC crew, Joseph Fiola, and Shaun, Meghan, and Sydney from the UMD greenhouse complex.

I thank the Maryland Wineries Association and FFAR for financial support and Wonderful Nurseries for donating the many vines which I befouled with ripe rot.

Lastly, I thank those who have been there for me spiritually and emotionally during this season. I cannot overstate how much support I received from my loving wife, Gift, whom I met and married while completing my PhD degree. Finally, shout out to my family, friends, FFAR Fellows, and colleagues who have encouraged me and prayed for me along the way.

Table of Contents

List of Tables

List of Figures

Chapter 1: Review of the Literature: Late Season Bunch Rots

1.1) Wine grape production in the Mid-Atlantic

Commercially grown wine grapes are a relatively new but increasingly important crop in the Mid-Atlantic, with rapidly increasing acreage (USDA-NASS 2017). The production in this region is primarily for the local market, with most vineyards tied to a winery and tasting room. The majority of wine produced by these operations is sold on-site for a premium price, especially if labeled as a Maryland or Virginia wine. In Maryland, a wine bottle labeled as a Maryland wine must be produced by at least 75% grapes grown in Maryland. Similar legislation in other states has created high demand for locally produced grapes.

The grapevine cultivars grown in Mid-Atlantic vineyards are chosen to produce a variety of desirable wines. Wine grapes are generally produced from two types of grapevines. The first, known as French cultivars. are *Vitis vinifera* L., and cultivars from this species are used to create the more widely known and desirable wines such as Merlot, Cabernet Sauvignon, and Chardonnay. The second type are French-American hybrids, such as Chambourcin or Vidal Blanc, which are generally better suited for American climates and more resistant to some diseases (Wilcox et al. 2015). Mid-Atlantic vineyards are primarily non-irrigated, and trained with vertical shoot positioning, and are either cane or spur pruned. Due to somewhat small acreages per vineyard (less than 50) in this region, most cultural management of the vines is conducted manually, such as pruning, shoot positioning, leaf pulling, cluster thinning, and harvesting.

1.2) Fungal pathogens associated with late season bunch rots

The prevention and control of diseases on wine grapes is essential for consistent production of quality fruit. The disease susceptible grapevines cultivated in the Mid-Atlantic region experience a climate that is favorable for fruit rotting pathogens (Kepner and Swett 2018; Oliver 2016; Steel et al. 2007). Many fungi have been reported as primary and secondary pathogens that are responsible for these fruit rots. Late season bunch rots (LSBR) are a particularly devastating group of diseases that cause the fruit to rot just before harvest. *Botrytis cinerea*, *Colletotrichum* spp., and *Greeneria uvicola* are a few examples of fungal pathogens responsible for LSBR (Steel et al. 2007). The diseases caused by the many LSBR pathogens can be difficult to differentiate by the symptoms observed on the fruit, making disease management difficult (Samuelian et al. 2011). The following paragraphs will introduce important background information and research on well-studied and under-studied LSBR pathogens relevant to the Mid-Atlantic.

According to the grape disease compendium, over 70 fungi have been associated with fruit rots of grapevines (Wilcox et al. 2015). Black rot, Botrytis bunch rot, ripe rot, and sour rot are four fruit rotting diseases most frequently encountered by Mid-Atlantic grapevine growers, but only Botrytis bunch rot and ripe rot are pathogen-related LSBR because black rot occurs earlier in the season (Hoffman et al. 2002) and sour rot is primarily resultant from fruit fly damage (Hall et al. 2018). Botrytis bunch rot and ripe rot are caused by the fungal pathogens *Botrytis* spp. and *Colletotrichum* spp., and recently *Alternaria alternata, Aspergillus japonicus,* and *Pestalotiopsis telopeae* have been reported as causing LSBR in the Mid-Atlantic (Kepner and Swett 2018). Multiple species in *Colletotrichum* have been described as fruit rotting pathogens of grapevine in the Mid-Atlantic (Oliver 2016). The most prevalent species belong to two species complexes, the *C. acutatum* complex (Damm et al. 2012) and the *C. gloeosporioides*

complex (Weir et al. 2012). Also, multiple species of *Alternaria, Aspergillus, Botrytis,* and *Pestalotiopsis* have been described in other regions (Dowling et al. 2017; Lorenzini and Zapparoli 2014; Samson et al. 2014; Swart and Holz 1994; Vesth et al. 2018; Xu et al. 1999). Furthermore, certain *Alternaria* and *Aspergillus* species can produce mycotoxins, which have been detected in wine and grape juice (Scott et al. 2006; Serra et al. 2006). *Pestalotiopsis* spp. and *Neopestalotiopsis* spp. have been isolated from other grapevine tissues besides clusters and have been found to cause stem cankers (Jayawardena et al. 2015; Sergeeva et al. 2005).

1.3) Cultivar susceptibility

The cultivars grown in the Mid-Atlantic have been cultivated for their desirability in winemaking rather than for their disease resistance, and a large percentage of acreage is planted with LSBR susceptible, French cultivars such as Chardonnay or Cabernet Sauvignon (Kepner and Swett 2018; Oliver 2016). French cultivars can vary in susceptibility to fungal diseases, but are generally considered more susceptible than the second type of grapevines, French-American hybrids. Hybrid grapevines are generally more resistant to a variety of diseases, such as downy mildew, powdery mildew, and black rot (Wilcox et al. 2015). The resistance of a grapevine cultivar to LSBR depends on many factors such as the cuticle thickness (Herzog et al. 2015), biochemical composition (Deytieux-Belleau et al. 2009), cluster compactness (Vail and Marois 1991), harvest timing preferences (Padgett and Morrison 1990), and the exact pathogen involved (Wilcox et al. 2015). Since many diverse cultivars are grown in the Mid-Atlantic, the susceptibility of these cultivars to LSBR may play a significant role in yield losses. Cultivar susceptibility to *Botrytis* bunch rot has been well characterized (Paňitrur-De La Fuente et al. 2018). A few studies have been conducted to understand cultivar susceptibility to ripe rot and

initial findings show that hybrid grapevine cultivars are not necessarily more resistant than *V. vinifera* cultivars (Shiraishi et al. 2007). Table grapes and muscadine grapes can also be susceptible to ripe rot (Daykin and Milholland 1984; Jang et al. 2011; Shiraishi et al. 2007). The susceptibility of grapevine cultivars to fruit rot caused by *Alternaria, Aspergillus,* or *Pestalotiopsis* has not been characterized.

1.4) Infection conditions and timing

Fruit rotting pathogens of grapevine can infect and cause disease at different times of the season. For example, *Guignardia bidwellii,* the causal agent of black rot, infects clusters and causes disease before veraison (Hoffman et al. 2002), while *B. cinerea* is considered to primarily infect at bloom and remain quiescent until causing disease at fruit maturation (Swart and Holz 1994). The infection timings of *Alternaria* spp., *Aspergillus* spp., *Colletotrichum* spp., and *Pestalotiopsis* spp. on grape bunches are not well characterized. *Colletotrichum* spp. has been isolated from asymptomatic cluster tissues at all phenological stages (Steel et al. 2007), and *C. acutatum* and *C. gloeosporioides* complexes can infect clusters throughout the season, from bloom to harvest, when artificially inoculated (Oliver 2016; Steel et al. 2012). However, the ripe rot disease appears to develop as berries ripen because grapes that were detached and inoculated at pre-veraison more resistant to ripe rot development than grapes that were detached and inoculated post-veraison (Steel et al. 2007). Fungicides applied at susceptible infection windows can be highly effective. For example, fungicide applications targeting *B. cinerea* at bloom have been shown to reduce the severity of Botrytis bunch rot at harvest (Nair 1985). With ripe rot, an effective application at the veraison stage may be more effective than at the bloom stage (Samuelian et al. 2014).

Environmental conditions greatly affect the ability of many fungal pathogens to infect their host, and temperature and wetness duration are the two most important factors for *Colletotrichum* infection on strawberry (Sturgess 1957) and *B. cinerea* infection on grapes (Broome et al. 1995). For example, *C. acutatum* caused the highest incidence of anthracnose fruit rot of strawberry at temperatures between 25 to 30 °C and wetness durations of over 13 hours (Wilson 1990). This information was used to create a mathematical disease model, that can predict infection risk, given the factors of temperature and wetness duration (MacKenzie and Peres 2012). This model is currently implemented in strawberry production and has resulted in better timed fungicide applications for maintaining disease control while reducing the total number of applications per season (Cordova et al. 2017; Pavan et al. 2011; Zhang et al. 2019). A few studies have looked at the pathogenicity of *C. acutatum* on grapes under different temperature and wetness duration treatments, and these two environmental factors appear to be highly correlated with disease (Steel et al. 2007). Disease models have been created for many diseases and cropping systems such as Botrytis bunch rot of grapevine, and the further development and implementation of prediction models for important diseases to the Mid-Atlantic may help reduce the number of excess applications per season (Broome et al. 1995).

1.5) LSBR management and limitations

1.5.1) Cultural methods

Cultural methods that increase aeration in the fruit zone of the canopy or prevent fruit wounding can reduce LSBR pressure (Austin and Wilcox 2011; Wilcox et al. 2015). Fungal diseases are generally favored by longer durations of wetness or high humidity (Bulger et al. 1987; Nair and Allen 1993; Wilson 1990). Leaf removal in the fruit zone is a common practice in the Mid-

Atlantic and has been shown to reduce *Botrytis* bunch rot severity (Gubler et al. 1991; Zoecklein et al. 1992) and allows for greater fungicide coverage (Tardaguila et al. 2010). Furthermore, management of leaf diseases is important for protecting the fruit, because downy and powdery mildew can also appear on the fruit when not sufficiently managed in the canopy. Powdery mildew infection of fruit can be very severe, but even diffuse infections can leave entry wounds for LSBR pathogens (Gadoury et al. 2007). Fruit can be wounded in many other ways, including insects (Mondy et al. 1998), birds (Tracey et al. 2007), heavy winds, hail (Elmer and Michailides 2007), and overly compact clusters (Nair 1985; Vail and Marois 1991). Common methods to reduce wounding include bird netting, insecticide applications, and berry thinning (Nair 1985; Tracey and Saunders 2003). However, these cultural methods do not provide sufficient control alone, especially in growing regions with a disease-conducive climate. One highly effective cultural practice for disease prevention is bagging clusters with wax paper bags, but this practice is highly labor intensive and therefore is not economically viable in the Mid-Atlantic (Karajeh 2018).

1.5.2) Chemical methods

Use of fungicides is considered a major component in integrated grapevine disease management. In almost all Mid-Atlantic vineyards, fungicides are employed for managing LSBR, primarily targeting Botrytis bunch rot and ripe rot. Information on fungicide efficacy against the LSBR caused by *Alternaria*, *Aspergillus*, and *Pestalotiopsis* is very limited, but has been well characterized for *Botrytis* bunch rot. Previous in-field and *in vitro* studies on fungicide efficacy against ripe rot and *Colletotrichum* isolates from grapes have provided helpful information for ripe rot management (Oliver 2016; Samuelian et al. 2014). Currently, Mid-Atlantic grapevine growers take a shotgun approach to control LSBR, applying a variety of fungicides biweekly

during the lengthy growing season. Unfortunately, the excess use of fungicides is costly, has a negative impact on the environment, and may reduce the effective lifespan of fungicides by selecting for resistant subpopulations.

B. cinerea is an example of a pathogen that has become resistant to fungicides. *Botrytis* populations from grapevines and small fruit crops all over the world have been found to contain high frequencies of fungicide resistant members, and some individual isolates can be resistant to multiple chemical classes of fungicides simultaneously (Cosseboom et al. 2019; Fan et al. 2017; Weber 2011). Site-specific fungicides, which target a single site in a critical metabolic pathway (Hahn 2014), are most prone to resistance development. Site-specific fungicides also tend to be highly effective while having low non-target toxicity. Resistance of fungi to site-specific active ingredients has been associated with mutations at the fungicide target sites, overexpression of the target sites, or overexpression of drug efflux pumps (Hahn 2014). Mutations at fungicide target sites generally provide cross-resistance among fungicides within the same chemical class. While multi-fungicide resistance is typically conferred by accumulation of target-site mutations in different genes (Li et al. 2014), the multiple-resistant phenotypes MDR1 and MDR2 have been associated with overexpression of the respective genes *atrB* and *mfsm2* that code for drug efflux pumps (Leroch et al. 2013). Various molecular and mycelial methods can be used to characterize a representative group of isolates for fungicide resistance, further informing LSBR management strategies (Cosseboom et al. 2019).

1.6) Summary

Wine grapes are an increasingly important crop in the Mid-Atlantic United States, with high demand for locally produced wine and grapes. From 1997 to 2017, grapevine acreage in

Maryland has increased from 313 to 1170 acres and in Virginia from 1899 to 4967 acres (USDA-NASS 2017). Unlike the Mediterranean climate of California or France, where the late summer and early fall months (the ripening period) are temperate and dry (Hannah et al. 2013), the climate in the Mid-Atlantic is typically wet, humid, and warm during the ripening season of grapes. These disease-favorable weather conditions, combined with the popularity of growing disease-susceptible *Vitis vinifera* cultivars, sets a perfect stage for losses to LSBR (Nair and Allen 1993; Wilson 1990). To cope with high disease pressure, growers spray an estimated 12 to 18 applications per season with a wide variety of synthetic fungicides. Still, disease management remains a top problem in Mid-Atlantic commercial vineyards. Some of the most problematic and spray-driving diseases are fruit rots that occur just before harvest and are herein called late season bunch rots (LSBR). There have been reports of LSBR caused by many different pathogens including *Botrytis spp., Colletotrichum spp., Alternaria sp., Aspergillus sp.,* and *Phomopsis sp.*, which can be responsible for yield losses of up to 80% in an unfavorable year (Wilcox et al. 2015). However, the common pathogens responsible for LSBR from different cultivars in the Mid-Atlantic have not been characterized in depth (Kepner and Swett 2018). Each pathogen may have a unique life cycle and fungicide sensitivity, complicating LSBR disease management. How the environmental conditions and growth stage of grapevines interact with causal agents of LSBR has yet to be investigated. Further, the actual disease resistance of grapevine cultivars to the lesser-studied LSBR in the Mid-Atlantic is currently unknown. These factors display the urgent need for foundational study of LSBR. Ultimately, the new knowledge gained in this study will enable development of novel LSBR management strategies for improved vineyard sustainability and profitability.

Chapter 2: Diversity and Pathogenicity of Fungal Species Associated with Late Season Bunch Rots of Wine Grape in the Mid-Atlantic United States

2.1) Introduction

In grape production, fruit rotting diseases that occur late in the season cause serious losses every year, especially in the Mid-Atlantic region of the United States. These diseases are known to be caused by *Botrytis* and *Colletotrichum* spp. (Adamo 2016; Oliver 2016), and multiple other fungi have been associated with rotten fruit in the Mid-Atlantic, including *Alternaria, Aspergillus,* and *Pestalotiopsis* (Kepner and Swett 2018). In fact, over 70 fungi associated with fruit rots have been reported on grapes, but their species identity largely remains unknown (Wilcox et al. 2015).The genera of many previously reported fungi have been expanded through taxonomic revisions, and multiple species per genus have been isolated from diseased grapes worldwide (Jayawardena et al. 2015; Lorenzini and Zapparoli 2014; Rousseaux et al. 2014; Walker et al. 2011). Of the many fungal species associated with grape late season bunch rots (LSBR), it is unclear which are most prevalent and contribute significantly to fruit rots in the emerging Mid-Atlantic wine grape industry.

The relatively new wine grape industry in this region lacks a history of foundational pathology research. The first obstacle in controlling LSBR is identification of the causal agent. Symptoms on fruit can appear similar between diseases and multiple fungi can be isolated from the same fruit (Samuelian et al. 2011). In *Botrytis,* two primary species have been identified causing LSBR with *Botrytis cinerea* being the most prevalent followed by *Botrytis*

pseudocinerea (Walker et al. 2011). Similarly, *Alternaria alternata* was more prevalent than *Alternaria tenuissima* (Mikušová et al. 2014). Ripe rot is caused by at least 12 *Colletotrichum* species, the most prevalent belonging to either the *C. acutatum* or *C. gloeosporioides* complexes, and the prevalence of each species appears to vary by region (Echeverrigaray et al. 2019; Lei et al. 2016; Oliver 2018; Pan et al. 2016; Yan et al. 2015; Yokosawa et al. 2020). Within *Aspergillus*, 36 species have been isolated from grapes, with most belonging to *Aspergillus* section *Nigri*, the black aspergilli (Rousseaux et al. 2014). The genus *Pestalotiopsis* was recently split into the genera *Pestalotiopsis, Neopestalotiopsis,* and *Pseudopestalotiopsis* (Maharachchikumbura et al. 2014), and multiple species of *Pestalotiopsis* and *Neopestalotiopsis* have been isolated from rotten grapes (Deng et al. 2013; Jayawardena et al. 2015; Kepner and Swett 2018; Xu et al. 1999). Species identity is important because colonies that look similar in vitro and cause similar disease symptoms may be different species with variable traits such as pathogenicity, fungicide sensitivity, and mycotoxigenicity (Cabañes et al. 2002; Dowling et al. 2020).

Specifically in the Mid-Atlantic, 12 genera have been associated with LSBR: *Alternaria*, *Aspergillus*, *Botrytis*, *Colletotrichum*, *Diaporthe*, *Epicoccum*, *Fusarium*, *Neofusicoccum*, *Neopestalotiopsis*, *Nigrospora*, *Penicillium*, and *Pestalotiopsis* (Encardes 2020; Kepner and Swett 2018). Phylogenic identification through multilocus sequencing has only been conducted for isolates of *Botrytis, Neofusicoccum,* and *Colletotrichum,* identifying isolates as *B. cinerea, N. ribis, C. fioriniae, C. nymphaeae, C. conoides, C. aenigma, C. kahawae,* and *C. gloeosporioides* (Adamo 2016; Encardes 2020; Oliver 2018).

With the diverse set of fungi associated with late season bunch rot of wine grapes, understanding their pathogenic ability is critical to determine how threatening each fungus is to

the grape production industry. The pathogenicity of *Botrytis cinerea* and *Colletotrichum* spp. is well understood (Steel et al. 2011). The pathogenicity of *Alternaria, Aspergillus,* and *Pestalotiopsis/Neopestalotiopsis* has been evaluated on wounded and non-wounded detached fruit (Kepner and Swett 2018). All three fungi were able to initiate fruit rot consistently on wounded fruit, and fungi in these genera have also been isolated from asymptomatic (Barbetti 1980; Da Rocha Rosa et al. 2002; Kakalíková et al. 2009; Serra et al. 2006; Steel et al. 2007) and symptomatic berries in other studies (Barkai-Golan 1980; Jayawardena et al. 2015; Latorre et al. 2002; Lorenzini and Zapparoli 2014; Nair 1985). These fungi may play a significant role in fruit rots of grape, but the ability of these fungi to cause disease in a field setting has not yet been assessed. It is also not known if cultivars differ in susceptibility or if grapes are ontogenically resistant as with black rot (Molitor and Berkelmann-Loehnertz 2011), Botrytis bunch rot (McClellan and Hewitt 1973), and powdery mildew (Gadoury et al. 2003), where the bloom period tends to be more susceptible to infection. Due to the limited sampling and the expanded taxonomy of LSBR associated fungal genera, the objectives of this study were to collect LSBR symptomatic clusters throughout the Mid-Atlantic, identify the fungal species isolated from these clusters through phylogenic analysis, and assess the pathogenicity of the most prevalent, yet understudied fungi.

2.2) Materials and Methods

2.2.1) Isolate collection and initial characterization

In the late summer and early fall seasons from 2014 to 2020, ripe grapes with fruit rot symptoms from 18 Mid-Atlantic (Maryland, Pennsylvania, and Virginia) vineyards were collected, and fungi were isolated from them. If the fungi on the rotten fruit were sporulating, then spores were

aseptically transferred to a 100 mm Petri dish containing potato dextrose agar (PDA). Fruit without sporulation were surface sterilized, cut into small pieces, and plated onto PDA. The fruit were sterilized by submerging in a solution of 1% sodium hypochlorite for one minute followed by rinsing with sterile deionized water. After fungi had grown on the medium, a hyphal tip was transferred to a new plate of PDA containing ten, 25 mm^2 pieces of sterile filter paper and incubated for three to four days at 22 °C. Once the mycelium had grown to the edge of the plate, these filter paper pieces were dried in a desiccator for two weeks, then placed in a 1.5 ml centrifuge tube containing silica gel beads and stored at -20 °C.

The isolates were then categorized into groups according to their morphology, and up to 15 isolates of each morphological group were saved per vineyard. DNA was extracted from mycelia of a random selection of isolates from each morphology group (Chi et al. 2009). The internal transcribed spacer (*ITS*) region of these isolates was amplified through PCR with previously described primers (ITS1 and ITS4) and thermocycling protocol. All primer sequences and references of thermocycling protocols used in this study are listed in Table A1. All PCR reactions in this chapter contained a total volume of 20 µl with 1X Taq Master Mix (Apex Bioresearch Products, San Diego, CA), 1 µl DNA template, 0.5 µM of each primer, and purified water. Purification and sanger sequencing of amplicons was either conducted by the Arizona State University Genomic Facility (Tempe, AZ) or by Genewiz (genewiz.com), and the sequences were identified using BLAST.

A small sampling of fungi from asymptomatic fruit was also conducted. Asymptomatic grape berries (cv. Cabernet Sauvignon) were collected from a commercial Maryland vineyard at regular intervals from bloom until harvest in 2020 to determine which fungi were present throughout the season in Maryland vineyards. Every two to three weeks, four to five Cabernet

Sauvignon berries were collected from the same vineyard rows and were surface sterilized in 1% sodium hypochlorite for one minute followed by rinsing twice with sterile deionized water. For two berries per cluster, four pieces of the berry skin was transferred onto potato dextrose agar (PDA) and incubated at 22 °C for four days. The genera of fungi from asymptomatic fruit were then morphologically characterized and identified. If the identity of the fungi based on morphology was not possible the internal transcribed spacer (*ITS*) region was amplified in PCR with primers ITS1/ITS4 as described above and identified with BLAST (https://blast.ncbi.nlm.nih.gov/Blast.cgi).

Additional sampling was conducted for *Botrytis* to observe differences in species distribution or fungicide sensitivity profiles between small fruit crops in the Mid-Atlantic. Samples were collected from 2014 to 2019 from strawberry, blackberry, black raspberry, and red raspberry. Up to 30 isolates per farm were collected for this additional sampling.

2.2.2) Multilocus sequencing

Randomly selected isolates from each of the commonly occurring genera identified with the *ITS* sequencing were then identified to the species level by sequencing more genetic loci. *Pestalotiopsis* was not included because it has recently been identified from Mid-Atlantic vineyards (Kepner and Swett 2018). The *tef1* gene was additionally sequenced for *Cladosporium, Diaporthe,* and *Fusarium* with the primers EF1T and EF2T. Also, the Actin gene was sequenced for *Cladosporium* with primers ACT512F and ACT783R and the partial β-tubulin gene for *Diaporthe* (aka *Phomopsis*) with primers BT2A and BT2B. For *Alternaria,* the RNA polymerase subunit II (*rpb2*) gene was amplified with primers and Rpb2-5f2 and Rpb2-7cr. The β-tubulin and translation elongation factor 1-α (*tef1*) genes of *Neopestalotiopsis* isolates

were amplified with primers BT2A and BT2B and 728F and EF2, respectively. *Aspergillus* was identified according to sequences of the calmodulin gene with primers cmd5 and cmd6.

Forty-five *Colletotrichum* isolates from symptomatic grapes and three from asymptomatic grapes were plated on PDA for seven days and then were separated into groups based on their colony morphology. DNA was extracted from each isolate as mentioned above, and then the partial β-tubulin, glyceraldehyde-3-phosphate dehydrogenase (*gapdh*), and chitin synthase 1 (*chs-1*) genes of a selection of isolates in each morphological group were amplified in PCR. For *Botrytis,* the *gapdh* gene was amplified for sixty-five *Botrytis* isolates representing the different small fruit crops and farms with the primers g3pdhfor+ and g3pdhrev+. All amplicons were Sanger sequenced as mentioned above.

2.2.3) Phylogenic analysis

The phylogenic analysis was conducted for each genus separately. The sequences were aligned with sequences of previously identified species of each genus and trimmed to the same length (Table A2). If multiple loci were sequenced for a genus, then the aligned sequences were concatenated. All of the following phylogenic analyses were conducted with the software MEGA version X (Kumar et al. 2018). Sequences of previous phylogenic studies were included in the analyses to include each relevant species for each genus including *Alternaria*, *Aspergillus*, *Botrytis*, *Cladosporium*, *Colletotrichum*, *Diaporthe*, *Fusarium*, and *Neopestalotiopsis* (Jayawardena et al. 2015; Maharachchikumbura et al. 2014; Samson et al. 2014; Woudenberg et al. 2013).

For *Botrytis,* an isolate of *Sclerotinia sclerotiorum* was used as the outgroup strain. For *Colletotrichum,* two separate analyses were conducted for the *C. acutatum* and *C. gloeosporioides* species complexes with sequences of these isolates and ex-type strains and both

were rooted with *C. orchidophilum* (Table A2) (Damm et al. 2012; Weir et al. 2012). Two separate analyses were conducted for the *Cladosporium cladosporioides* and *Cladosporium herbarum* species complexes, which were unrooted trees (Bensch et al. 2015). The *Diaporthe* tree was also unrooted (Hilário et al. 2021; Santos et al. 2017) and so was the *Aspergillus* tree (Samson et al. 2014). The *Fusarium* tree was rooted with *F. verticillioides* as the outgroup (Bolton 2016) and the *Neopestalotiopsis* tree was rooted with *Pestalotiopsis rhododendri* as the outgroup (Baggio et al. 2021). The *Alternaria* isolates were identified to the section level according to Woudenberg et al. (2012) with *Stemphylium herbarum* as the outgroup. All trees were constructed with Maximum Parsimony analysis and the robustness of the tree was estimated with 1,000 bootstrap replications with Tree Bisection Reconnection search method and 1000 random sequence additions. The max number of trees was set at 5000 and branches of zero length were collapsed (Jayawardena et al. 2016). All references for GenBank accessions used for each phylogenic analysis are listed in the appendix (Table A2).

2.2.4) In-field pathogenicity of *A. alternata*, *A. uvarum*, *B. cinerea*, and *N. rosae*

Three commonly occurring but understudied fungi, *Alternaria alternata, Aspergillus uvarum,* and *Neopestalotiopsis rosae,* were tested for their ability to cause fruit rot diseases in a vineyard after being collected and identified to the species level as described above. Three isolates of each fungus plus three isolates of the well-established pathogen *Botrytis cinerea* were selected to be prepared as inoculum. To induce sporulation, *A. uvarum* and *B. cinerea* were cultured on PDA at 22 °C in the dark, *A. alternata* was cultured on quarter-strength PDA at 22 °C in the dark, and *N. rosae* was cultured on PDA at 25 °C under constant fluorescent light. Spore suspensions of a mixture of the isolates of each species were created by flooding the plates with sterile water and liberating the conidia by rubbing with a sterile cell-spreader. The spore suspensions were filtered

through sterile, double-layered cheesecloth and diluted to 1 x 10^5 conidia/ml and were kept in a chilled atomizer for no more than four hours before inoculation in the field (Amiri et al. 2018).

The trials took place at an experimental vineyard at the University of Maryland Wye Research and Education Center in 2019 and 2020. At three phenological timings, bloom (BBCH 65), veraison (BBCH 83), and pre-harvest (BBCH 85), healthy-appearing grape clusters of four cultivars, Chardonnay, Chambourcin, Cabernet Franc, and Merlot, were inoculated with spore suspensions or water as a control by misting with an atomizer until runoff (Lorenz et al. 1995). For the first and second year, 30 and 16 clusters per pathogen-timing-cultivar combination were inoculated, respectively. Half of the clusters per pathogen-timing-cultivar combination were wounded by piercing the cuticle of ten berries per cluster with a sterile toothpick. Clusters inoculated at the bloom timing were wounded at pre-harvest. For the other two inoculation timing treatments of veraison and pre-harvest, the clusters were wounded immediately prior to inoculation. Since the cultivars in the trial matured at different rates, the inoculation, wounding, and harvest dates differed by cultivar (Table A3). Any fungicides applied during the two trials were not effective against the inocula and were primarily targeting foliar downy mildew with limited applications for powdery mildew.

Immediately after inoculation, the clusters were covered with white, wax-paper bags to promote infection by prolonging wetness duration and to prevent unwanted infection or injury from other fungi, birds, or insects (Karajeh 2018). The bags were left on the clusters until harvest. For the bloom-inoculated clusters, the bags were temporarily removed at the pre-harvest stage, wounded, and immediately replaced. The wounded-bloom inoculated treatment was not included for the *B. cinerea* and water inoculum in 2019. At harvest, the clusters were cut from the vines, weighed, and evaluated for disease severity. Disease severity was measured by

visually estimating the percentage of berries with disease per cluster. If more than one disease was observed on a cluster, the severity of each disease was noted. Fungi causing the different diseases were isolated from the clusters and were identified according to their morphology.

2.2.5) Statistical analysis

All statistical analyses in this project were conducted using the software JMP Pro 14.1 (SAS Institute, Cary, NC). The severity of four different diseases (Alternaria fruit rot, Aspergillus fruit rot, Botrytis bunch rot, and Neopestalotiopsis fruit rot) was recorded at harvest. The severity of each disease occurring on clusters inoculated with five different inocula (*A. alternata, A. uvarum, B. cinerea, N. rosae,* and water) was compared to the disease severity on clusters inoculated with water. This was conducted separately for each year, disease, inoculation timing, and wound treatment with a Steel multiple comparisons test with the water inoculum as the control. The water control treatment was not included for non-wounded clusters at the bloom timing in 2019, and therefore no statistical analysis was conducted on this disease severity data. The cluster weight data was square root transformed to meet ANOVA assumptions of homogeneity of variance and normal distribution of residuals. The effect of the inoculum, wounding, cultivar, and inoculation timing and interactions of these factors on the square root of the cluster weights was evaluated by ANOVA. Post hoc comparisons of the variables on cluster weight were conducted with a Tukey's honestly significant difference test. The square root transformed cluster weight data was then back-transformed to present results. The fungicide sensitivity data was analyzed by determining the percent inhibition at each concentration, then regressing the log of the concentration against the average percent inhibition at each concentration. This regression was then used to estimate the concentration that inhibits growth by 50% compared to the control for each isolate.

2.3) Results

2.3.1) Isolate collection and distribution

From 2014 to 2020, clusters with various LSBR symptoms were collected. In total, 265 fungal isolates were obtained from 37 cultivars grown in 18 vineyards located in Maryland (238 isolates), Pennsylvania (18 isolates), and Virginia (9 isolates). Sequences of the *ITS* region revealed that the isolates belonged to 15 genera, and the most common genera were *Botrytis, Colletotrichum, Aspergillus, Alternaria, Pestalotiopsis, and Neopestalotiopsis* (Fig. 2.1A; B). Isolates collected from *V. vinifera* cultivars (as opposed to hybrid cultivars) constituted 87, 94, and 100% of total isolates collected from Maryland, Pennsylvania, and Virginia, respectively (Fig. 2.1B). Of the isolates collected from asymptomatic fruit in 2020, many similar genera were isolated, with the genera *Alternaria*, *Cladosporium*, and *Fusarium* being frequently isolated throughout the season (Table A4). With the additional *Botrytis* sampling, a total of 249 isolates were collected from blackberry (n=13), black raspberry (n=33), grape (n=92), red raspberry (n=36), and strawberry (n=75) from 14 farms in Maryland and two farms in Pennsylvania during the 2014 to 2019 seasons.

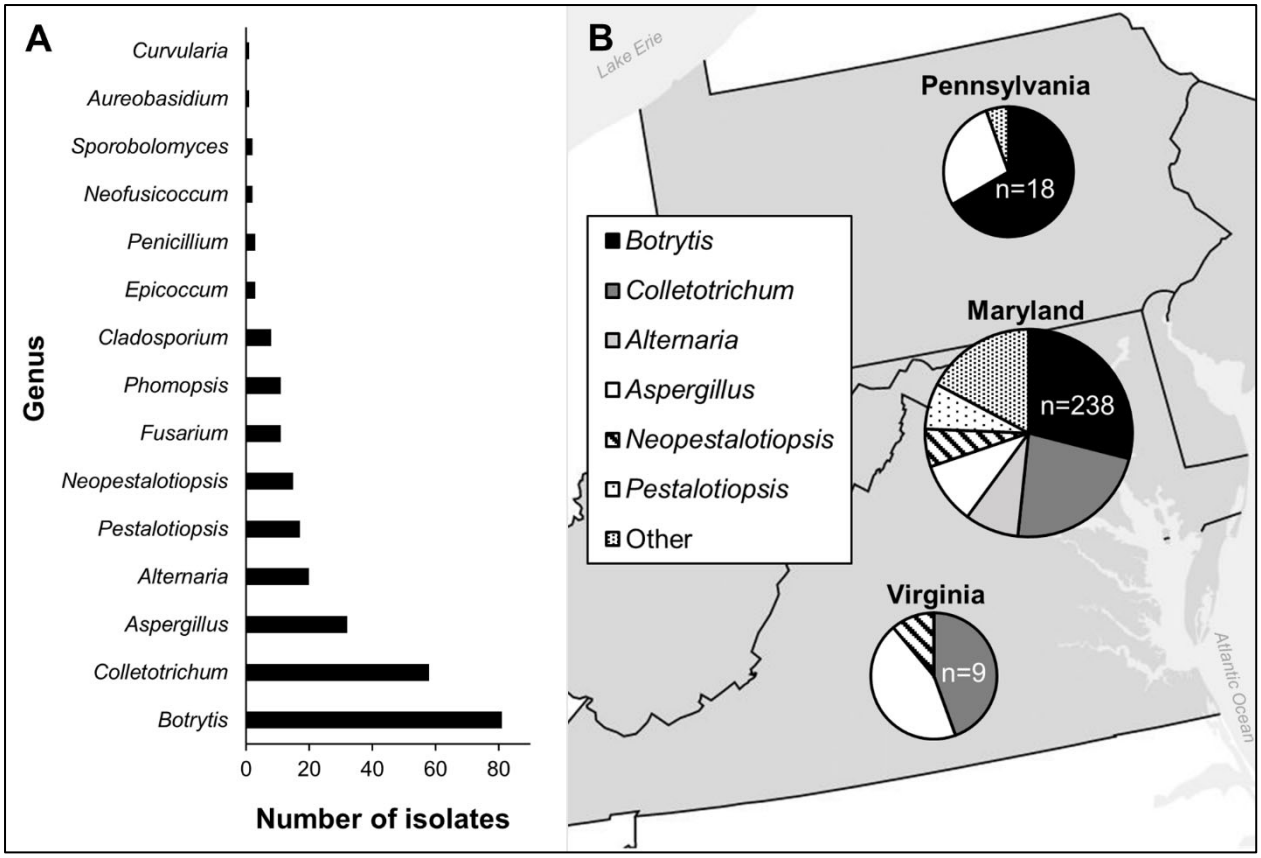

Fig. 2.1. Distribution of (A) 15 Genera of fungal isolates (n = 265) collected from ripe, rotten grape berries from 2014 to 2020 from 18 Mid-Atlantic vineyards that were identified through sequencing of the internal transcribed spacer region in (B) Pennsylvania, Maryland, and Virginia.

A variety of symptoms were observed on the clusters sampled in this study, and it was not always possible to predict which fungus would be isolated from each cluster. However, some symptoms and fungi were consistently associated with each other. *Botrytis* spp. were associated with soft fruit, water-soaked lesions, and profuse whitish gray sporulation (Botrytis bunch rot; Fig. 2.2C; D). *Colletotrichum* spp. were isolated from fruit that were shriveled, had rough skin, or orange sporulation (ripe rot; Fig. 2.2B; E; F). *Aspergillus* was mostly isolated from clusters with shriveled berries and light to dark brown powdery sporulation (Aspergillus fruit rot; Fig. 2.2A; F). *Alternaria* was isolated from berries with dense, dark brown to dark green mycelium

(Alternaria fruit rot; Fig. 2.2C). *Pestalotiopsis* and *Neopestalotiopsis* were consistently isolated from fruit with white mycelial growth (Pestalotiopsis/Neopestalotiopsis fruit rot; Fig. 2.2E; F). *Aspergillus, Alternaria, Pestalotiopsis,* and *Neopestalotiopsis* were also frequently isolated from clusters displaying ambiguous symptoms of shriveling, bruising, or rough skin, and fungi of more than one genus could often be isolated from the same cluster (Fig. 2.2C; E; F).

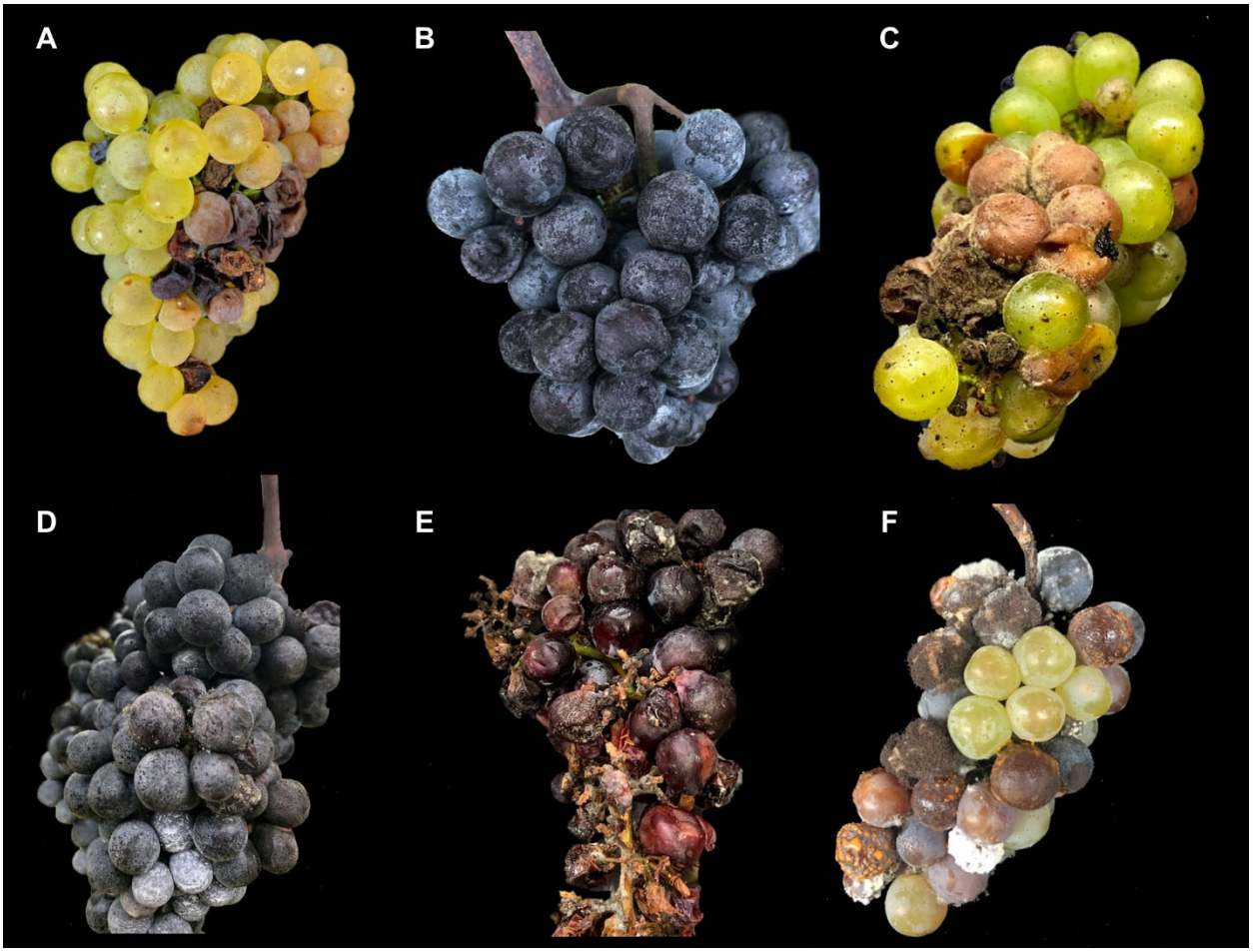

Fig. 2.2. Clusters of wine grapes collected from Mid-Atlantic vineyards with various symptoms of late season bunch rot from which (A) *Aspergillus*; (B) *Colletotrichum*; (C) *Alternaria* and *Botrytis*; (D) *Botrytis*; (E) *Colletotrichum* and *Neopestalotiopsis*; (F) *Aspergillus, Colletotrichum*, and *Pestalotiopsis* spp. were isolated.

2.3.2) Species identification

Seven *Diaporthe* (Phomopsis) isolates were selected for species identification, and were found to belong to three species, *D. eres*, *D. ampelina*, and *D. guangxiensis* (Fig. 2.3). Of the ten *Cladosporium* isolates collected, nine were found to belong to the *C. cladosporioides* species complex, and were found to be *C. cladospoirioides* sensu stricto, *C. pseudocladosporioides*, and *C. perangustum.* One isolate belonged to the *C. herbarum* complex and was identified as *C. allicinum* (Fig. 2.4). Each *Neopestalotiopsis* isolate was identified as *N. rosae,* and a few *Pestalotiopsis* isolates were included that grouped with the outgroup *Pestalotiopsis* sp. (Fig. 2.5). The *Pestalotiopsis* isolates were likely *P. biciliata,* which was recently found in the Mid-Atlantic region (Kepner and Swett 2018). Of the eight *Fusarium* isolates selected for identification, seven were *F. fujikuroi* and one was *F. proliferatum* (Fig. 2.6). All *Alternaria* isolates aligned within section *Alternaria* section Alternata. The sequencing of more loci would be able to elucidate the exact species of the isolates within this section (Fig. 2.7).

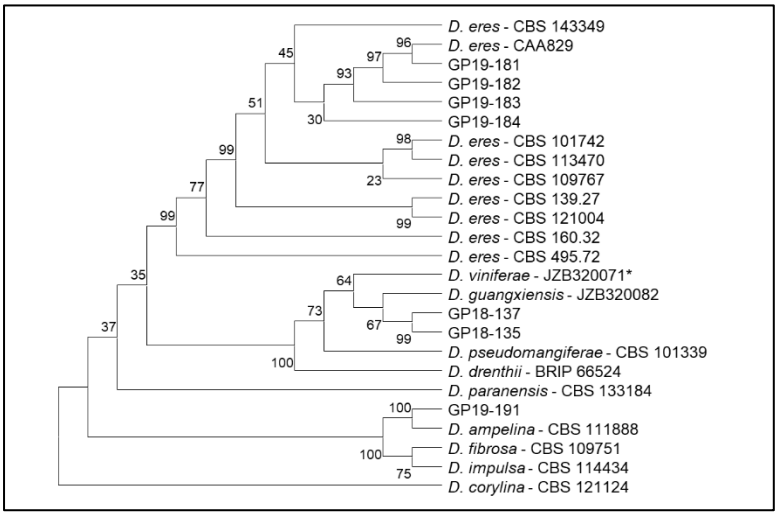

Fig. 2.3. The unrooted maximum parsimony tree of the translation elongation factor-1 (*tef1*) and β-tubulin regions of *Diaporthe* spp. along with those of isolates collected from Mid-Atlantic vineyards.

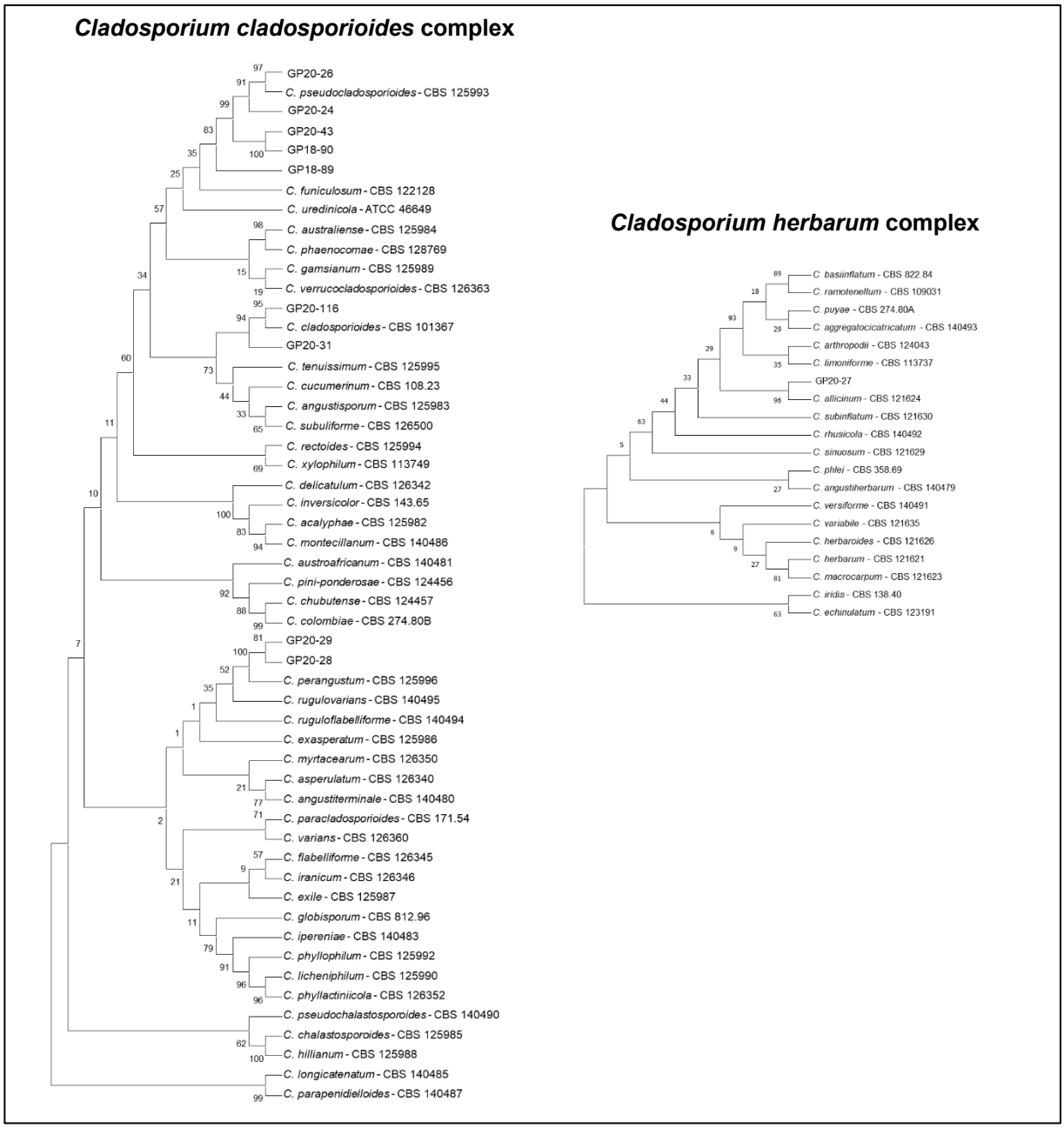

Fig. 2.4. Unrooted maximum parsimony trees of concatenated sequences of *tef1* and actin of the *Cladosporium cladosporioides* species complex (left) and the *C. herbarum* species complex (right) along with isolates collected from Mid-Atlantic vineyards.

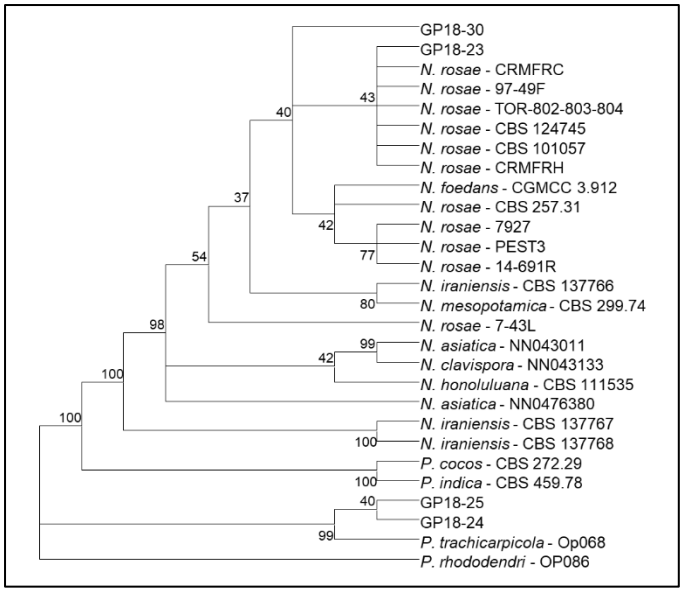

Fig. 2.5. Maximum parsimony tree constructed from concatenated internal transcribed spacer (*ITS*), translation elongation factor-1 (*tef1*), and β-tubulin sequences of *Neopestalotiopsis* spp. and isolates collected from Mid-Atlantic vineyards with *P. rhododendri* as the outgroup.

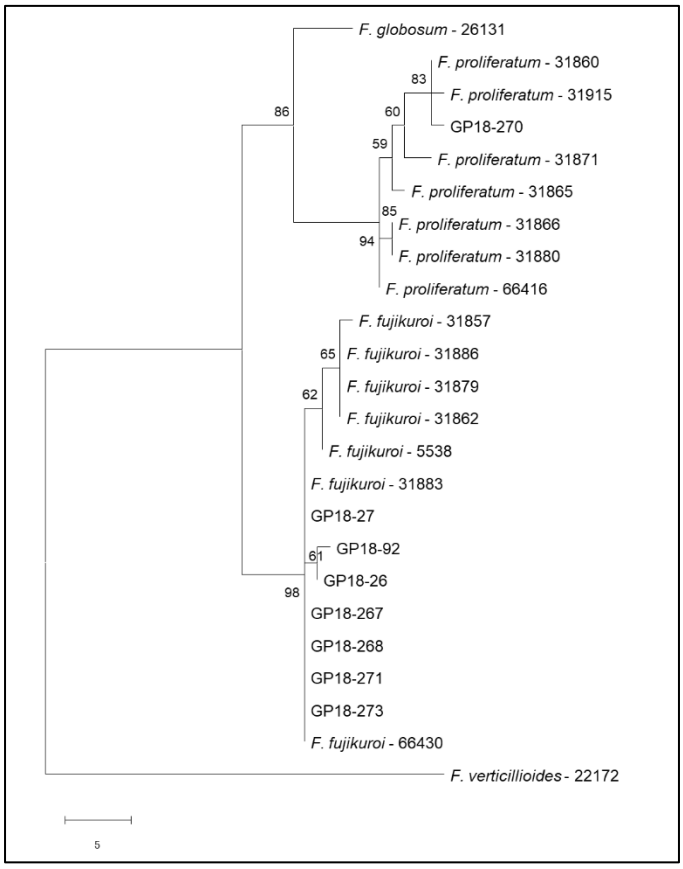

Fig. 2.6. Maximum parsimony tree of the translation elongation factor-1 (*tef1*) sequences of *Fusarium* spp. along with isolates collected from Mid-Atlantic vineyards with *F. verticillioides* as the outgroup.

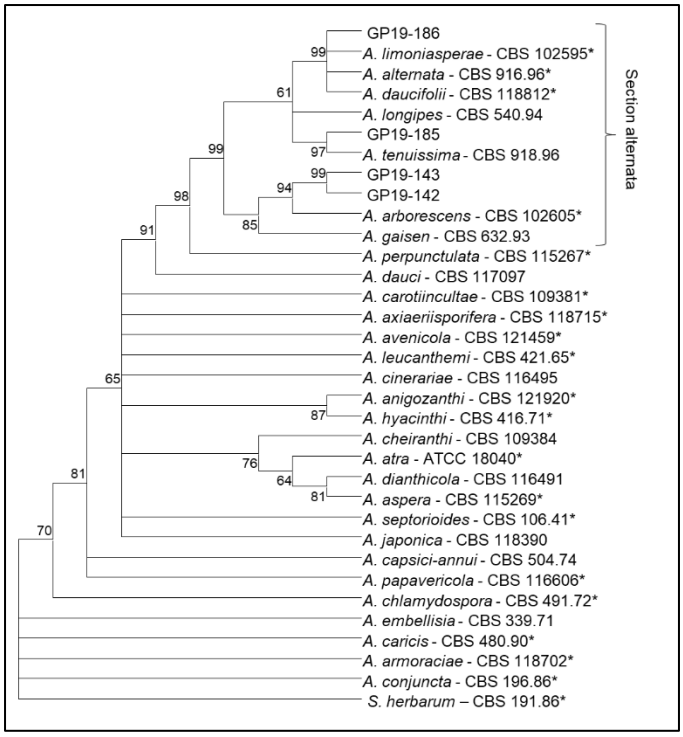

Fig. 2.7. Maximum parsimony tree constructed from concatenated sequences of the translation elongation factor-1 (*tef1*) and RNA polymerase subunit II (*rpb2*) regions of previously described *Alternaria* spp. and isolates collected from Mid-Atlantic vineyards with *Stemphylium herbarum* as the outgroup. Type strains are indicated with an asterisk.

All *Aspergillus* isolates had similar colony morphology on PDA medium, with prolific black sporulation with a prostrate mycelial margin and circular form. Amongst the 56 isolates that were compared in phylogenic analysis of the partial calmodulin gene, there were 347 variable nucleotides out of a total of a length of 634 nucleotides. The analysis revealed all 31 isolates collected from Mid-Atlantic wine grapes to be *A. uvarum* or *A. japonicus*. Five isolates were *A. japonicus* and 26 were *A. uvarum* and there was 77% bootstrap support for this differentiation (Fig. 2.8). Also, all isolates except GP19-60 had the species-delineating single nucleotide polymorphisms (SNPs) proposed by Samson et al. (2014), confirming the identification of the two species. Both species are within the *Aspergillus* uniseriate group and the *A. aculeatus* clade of *Aspergillus* section *Nigri* (Samson et al. 2014).

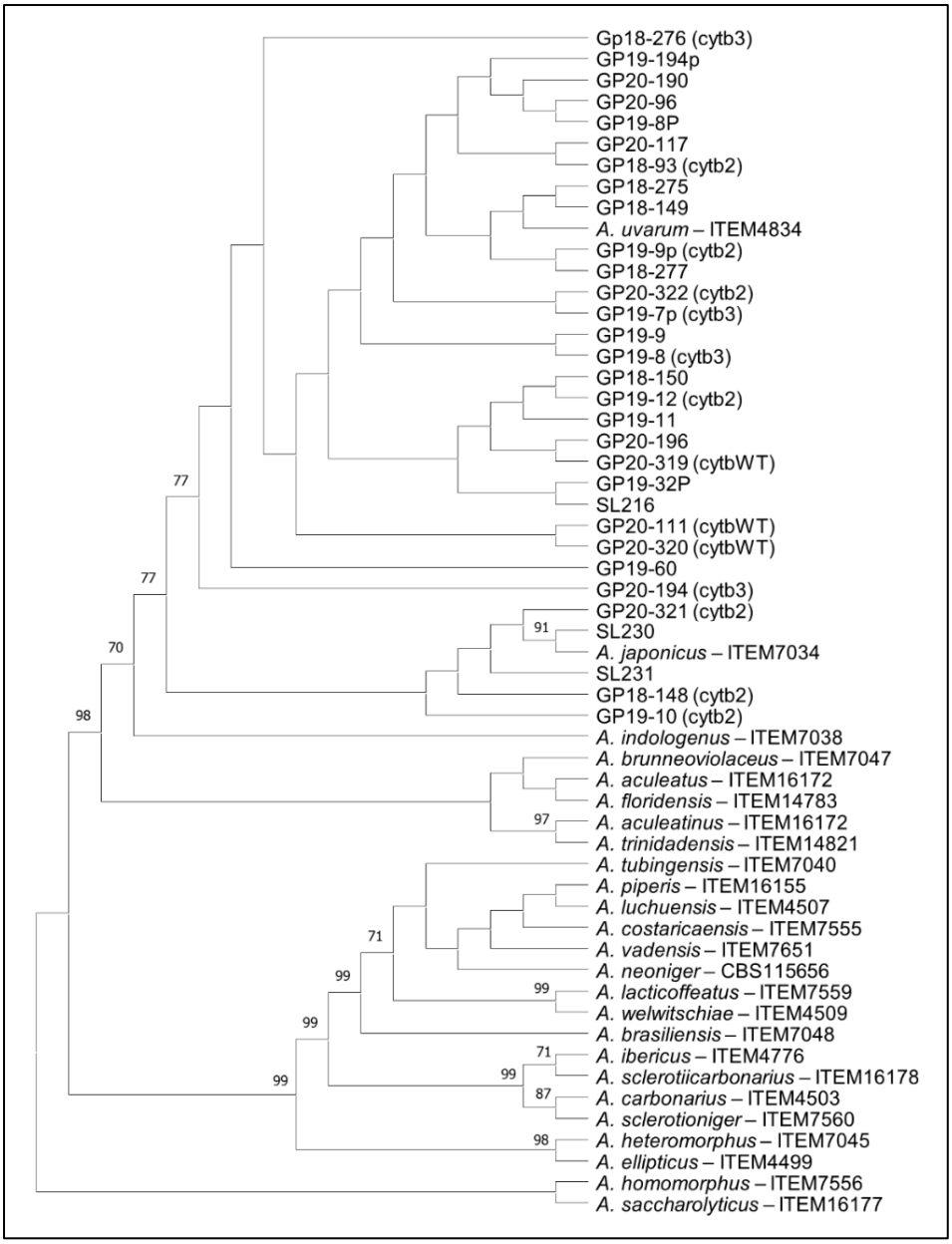

Fig. 2.8. The most parsimonious tree of species within the *Aspergillus* section *Nigri* with isolate names and isolates of *Aspergillus* collected from wine grapes with late season bunch rot symptoms in the Mid-Atlantic United States from this study. Bootstrap support for branches above 70% is indicated. The cytochrome b (*cytb*) genotype is also indicated in parenthesis for some isolates from this study.

Of the 249 Botrytis isolates collected, the *gapdh* region (930 bp) of 57 isolates was amplified and compared to *gapdh* sequences of *B. caroliniana, B. cinerea, B. fragariae, B. mali,* and *B. pseudocinerea* with 7 isolates from blackberry, 7 from black raspberry, 26 from grape, 7 from red raspberry, and 10 from strawberry. All sequences were 100% identical with the *gapdh* of *B. cinerea* isolate B05.10 (GenBank accession CP009819). Compared to the *gapdh* sequences of *B. cinerea*, the other 23 *Botrytis* species included in the phylogenic analysis contained at least 3 nucleotide variations (Fig. 2.9).

Of the *Colletotrichum* isolates (n = 48) collected in this and a previous study, isolates were separated into 8 morphological groups and were molecularly identified as *C. aenigma* (n = 26)*, C. fructicola* (n = 5)*, C. nymphaeae* (n = 7)*,* and *C. fioriniae* (n = 10). Two species, *C. fioriniae* and *C. nymphaeae,* belonged to the *C. acutatum* complex and two species, *C. aenigma* and *C. fructicola* belonged to the *C. gloeosporioides* complex (Fig. 2.10). The identification of *C. aenigma* and *C. fructicola* was not definitive from the sequences of the three loci, but the isolates will be considered as these species due to these two species being previously identified from ripe rot symptomatic grapes in this region (Oliver 2018) and in China (Peng et al. 2013; Yan et al. 2015). Two of the isolates from asymptomatic grape berries were *C. nymphaeae* and one was *C. fioriniae*.

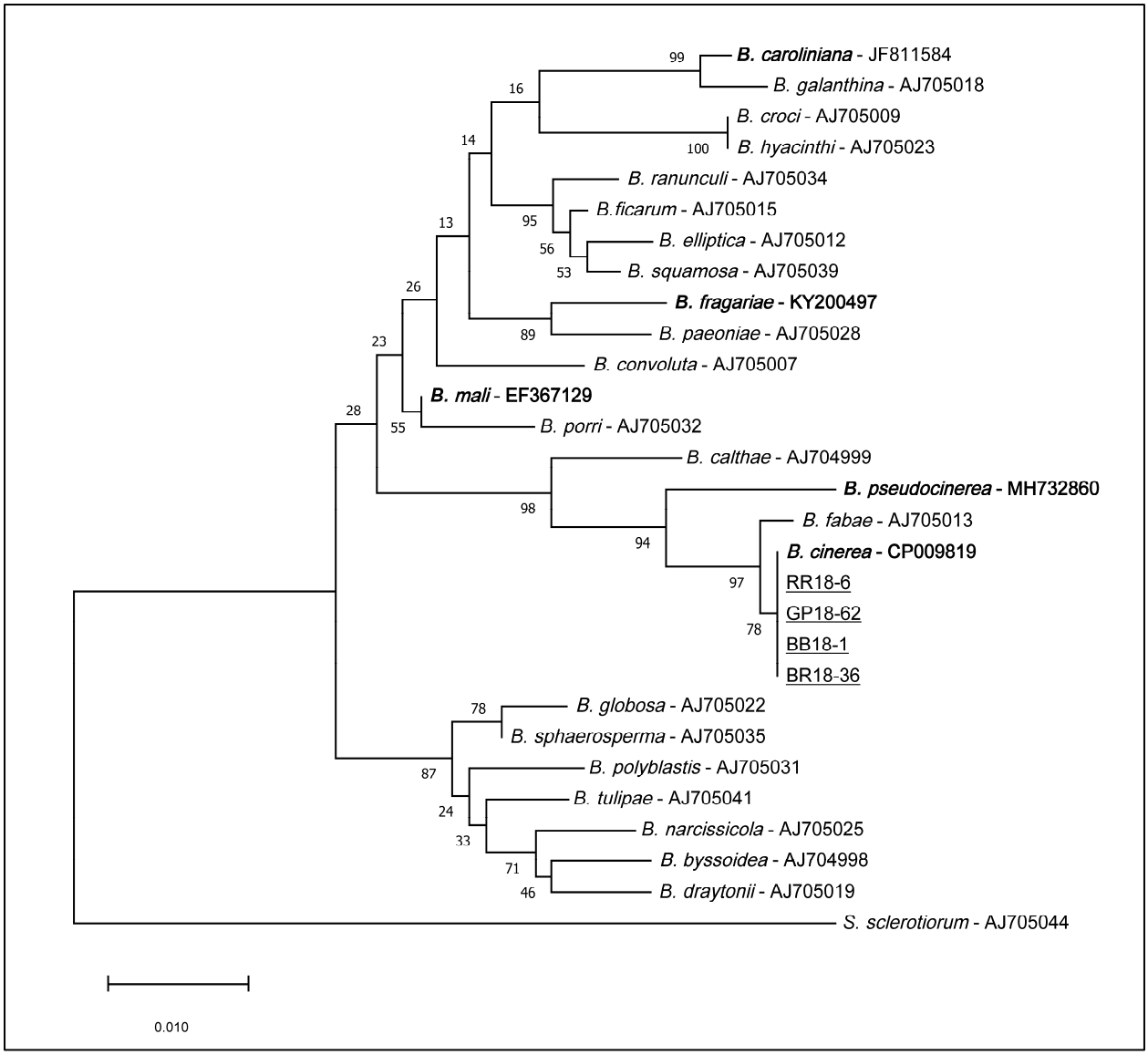

Fig. 2.9. Phylogenic tree based upon the glyceraldehyde-3-phosphate dehydrogenase gene of *Botrytis* spp. including sequences from isolates previously reported in small fruit crops (bold) along with GenBank accession numbers, and four isolates from this study (underlined), with *Sclerotinia sclerotiorum* as the outgroup. The phylogenic tree was constructed with MEGA version X software, and bootstrap frequencies were calculated with 1,000 replicates.

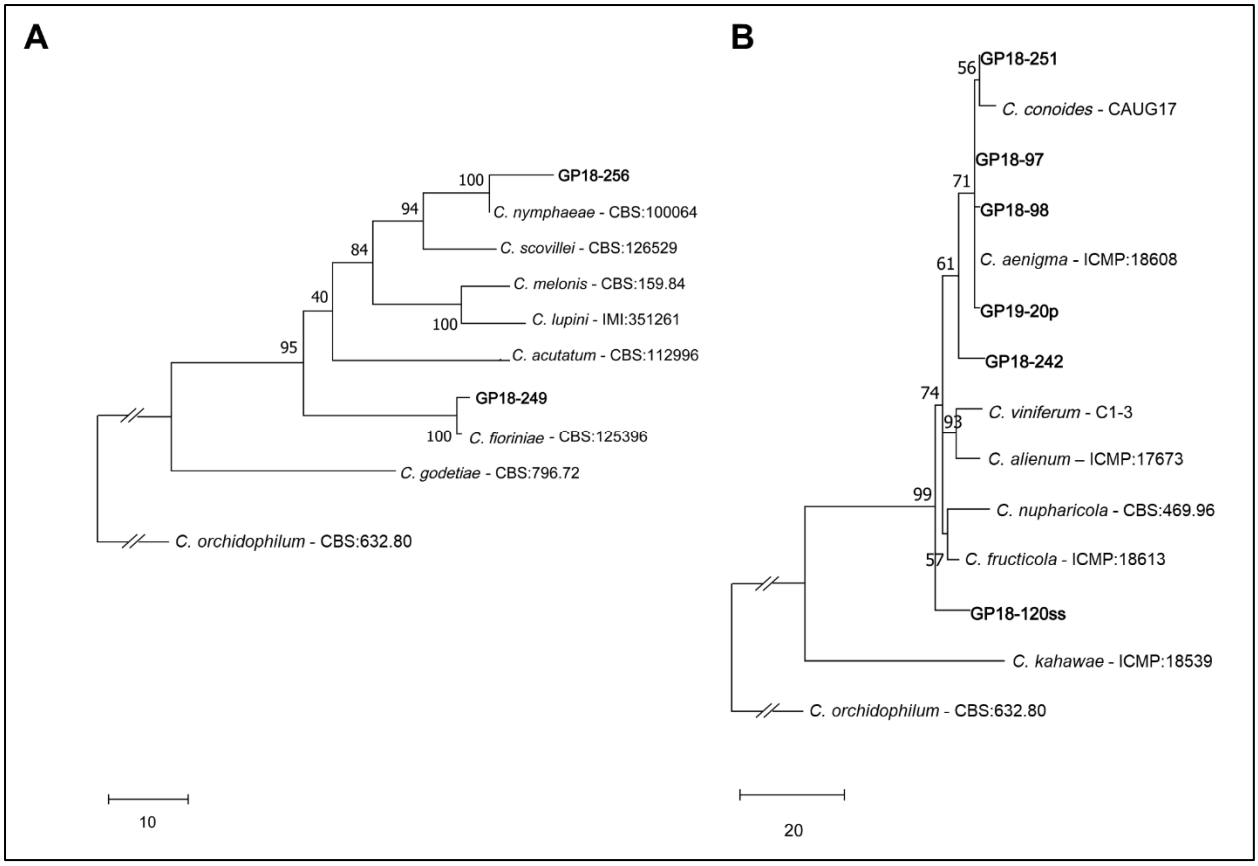

Fig. 2.10. Most parsimonious trees obtained from a heuristic search of concatenated sequences of β-tubulin, *gapdh*, and *chs-1* of *Colletotrichum* spp. collected from grape clusters of Mid-Atlantic vineyards along with ex-type strains within the A) *C. acutatum* species complex and the B) *C. gloeosporioides* species complex with *C. orchidophilum* as the outgroup. The analysis was performed with 1000 bootstrap replications using MEGA software, version X.

2.3.3) In-field pathogenicity of *A. alternata*, *A. uvarum*, *B. cinerea*, and *N. rosae*

The mature fruit of the four cultivars in the trials were evaluated for disease and six different disease symptoms were most common. The causal agents of Alternaria, Aspergillus, and Neopestalotiopsis fruit rots were isolated and morphologically identified as *A. alternata, A. uvarum,* and *N. rosae,* respectively. Alternaria fruit rot appeared as prostrate growth of dense, dark green to dark brown mycelium on the fruit surface (Fig. 2.11A). Clusters with Aspergillus fruit rot had tan to dark brown tufts of conidiophores that could be stained pink or red by the berry skin (Fig. 2.11B). Berries with Aspergillus fruit rot infections also tended to easily detach

from the rachis. Neopestalotiopsis fruit rot appeared as a pure white web of mycelium, at times surrounded by small black bumps (Fig. 2.11C). Three other diseases were immediately identified as Botrytis bunch rot, ripe rot, and powdery mildew. The characterization of each disease except powdery mildew fruit rot was confirmed by isolation and morphological identification of the causal agents. Ripe rot severity was low in both years and powdery mildew was not present in the first year but was very severe in the second year on the foliage and the fruit (data not shown).

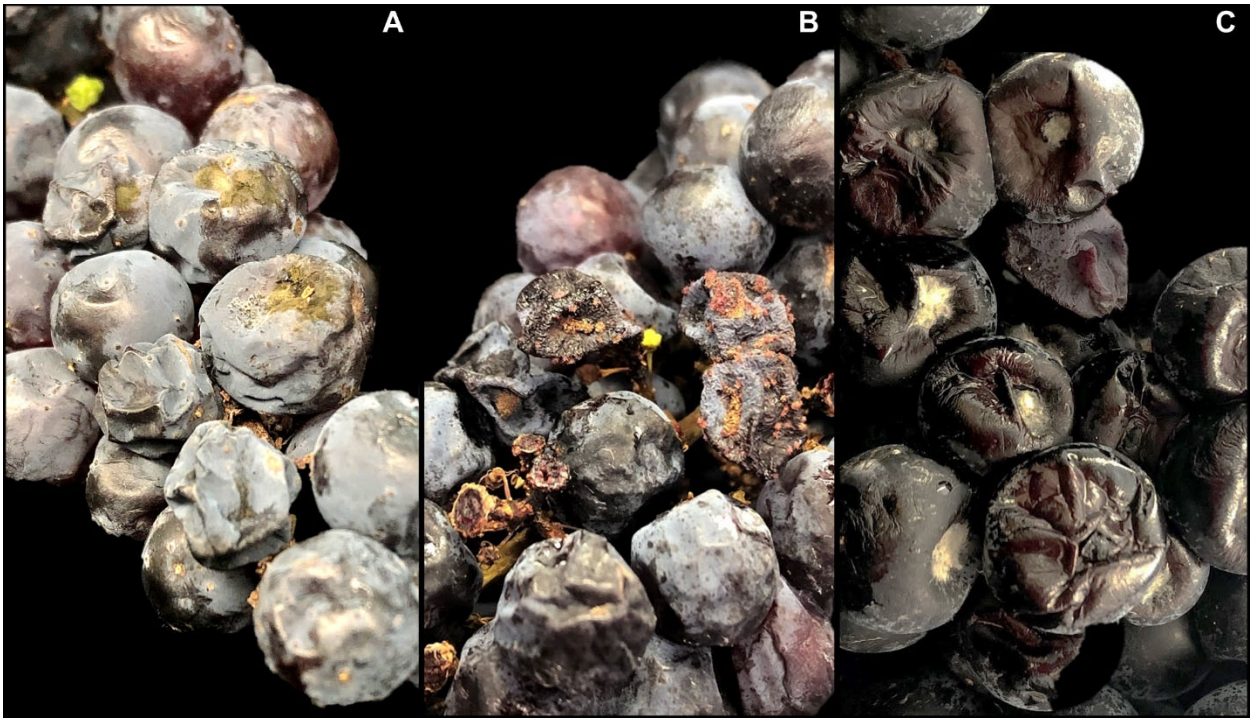

Fig. 2.11. Disease symptoms of (A) Alternaria fruit rot, (B) Aspergillus fruit rot, and (C) Neopestalotiopsis fruit rot from clusters inoculated with *Alternaria alternata, Aspergillus uvarum,* and *Neopestalotiopsis rosae*, respectively. Clusters were sourced from a replicated field trial in Maryland.

In general, all four fruit rotting diseases of interest occurred in the experiment in both years and disease tended to be more severe in 2020 than in 2019 except for *Botrytis* bunch rot. On non-wounded fruit, the primary disease occurring on the clusters was usually associated with

the inoculum. However, it was common for more than one disease to occur on fruit inoculated with a single pathogen, and fungi of different genera could be isolated from them. For example, four different diseases were observed on fruit inoculated with *B. cinerea* in 2020 (Fig. 2.12A-D). The non-wounded water inoculation treatment resulted in relatively little disease severity of either of the four diseases in both years, except for Alternaria and Neopestalotiopsis fruit rot in 2020 (Fig. 2.12A, D). On non-wounded treatments, clusters inoculated with *A. uvarum* at the pre-harvest timing in 2019 and at the veraison timing in 2020 had significantly greater Aspergillus fruit rot severity than the control (Fig. 2.12B). No other inocula caused its associated disease to be significantly greater than the control in either year on non-wounded fruit (Fig. 2.12A-D). Over both seasons, non-wounded Chardonnay clusters tended to have more severe fruit rots than the other cultivars, whereas Chambourcin tended to have the least severe fruit rot on non-wounded clusters (Fig. A1).

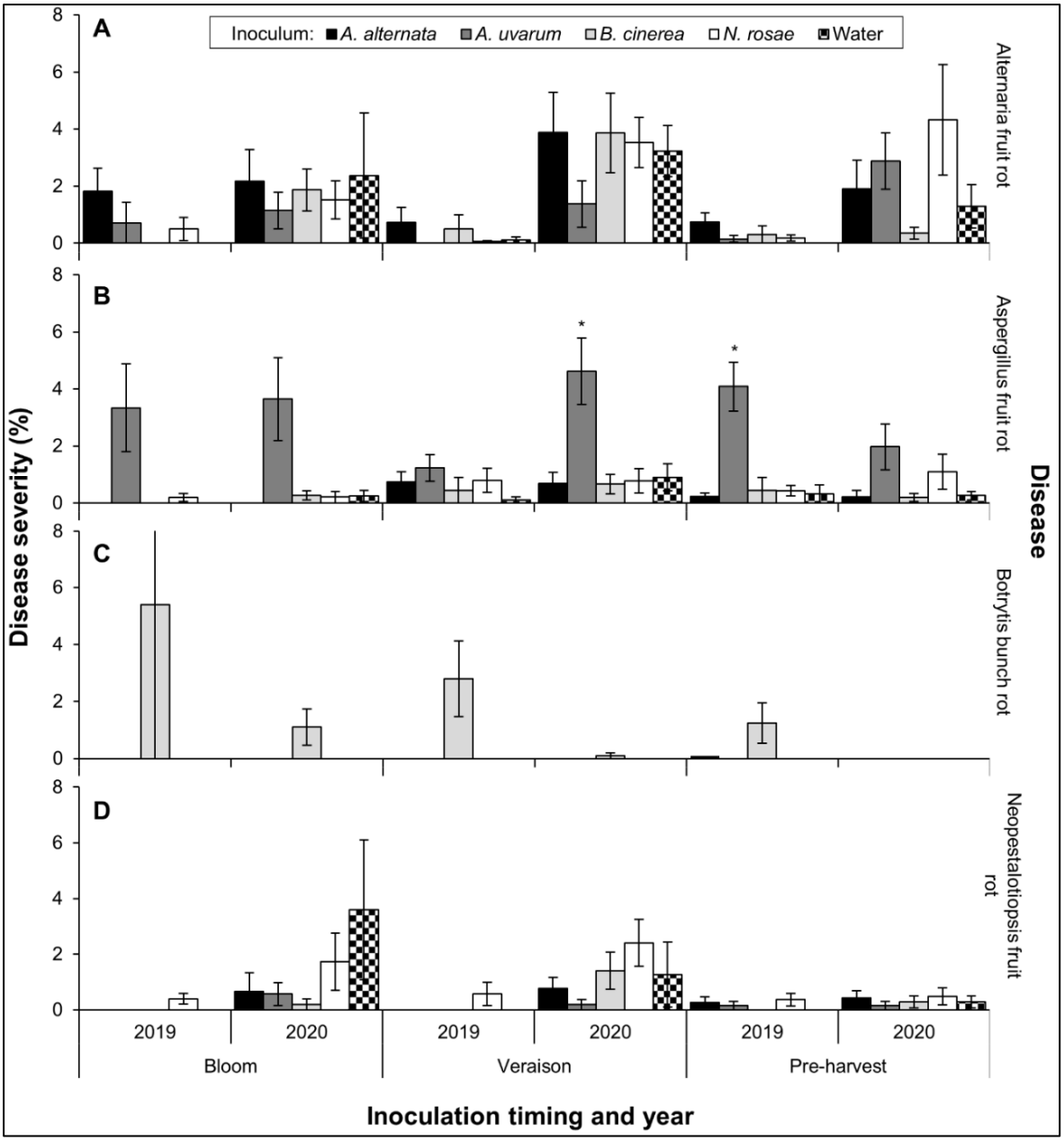

Fig. 2.12. Average severity of (A) Alternaria, (B) Aspergillus, (C) Botrytis, and (D) Neopestalotiopsis fruit rot across non-wounded clusters of four wine grape cultivars inoculated with four fungi and water at bloom, veraison, and pre-harvest in a field trial conducted in 2019 and 2020. One ($p < 0.05$), two ($p < 0.005$), or three ($p < 0.0005$) asterisks indicate that the disease severity was significantly greater than the water-inoculated treatment that was set as the control for the Steel multiple comparisons tests. Each disease/year/inoculation timing combination was evaluated with the Steel multiple comparisons test separately and error bars represent standard error.

Wounded fruit tended to have greater disease severity than non-wounded fruit in both years and it was also common for clusters inoculated with one fungus to exhibit diseases associated with other fungi (Fig. 2.13A-D). For example, compared to the control, significant levels of Aspergillus fruit rot occurred on clusters inoculated with *A. alternata, A. uvarum,* and *N. rosae* in 2019, but only on clusters inoculated with *A. uvarum* in 2020 (Fig. 2.13B). Significantly higher Alternaria fruit rot severity was observed only on fruit inoculated with *A. alternata* in 2019 at the pre-harvest timing (Fig. 2.13A). Also, only clusters inoculated with *B. cinerea* had significant severities of Botrytis bunch rot in both years (Fig. 2.13C), while clusters inoculated with *N. rosae* had significantly higher Neopestalotiopsis fruit rot in 2019 only (Fig. 2.13D). The severity of disease on different wounded cultivars was not consistent between the two years (Fig. A2). In 2019 and 2020, the factors of cultivar, inoculation timing, and wounding had a significant impact on cluster weight, while the inoculum did not. In 2019, there was no interaction between wounding and any other variable on cluster weight, and wounded fruit were found to weigh less than non-wounded fruit. In 2019, there was a significant cultivar*inoculation timing interaction, and Chambourcin inoculated and bagged at veraison and pre-harvest had the highest weight according to a post hoc Tukey's honestly significant difference test (Fig. 2.14). In 2020 there was a significant cultivar*inoculation timing interaction and a significant wounding*inoculation timing interaction, but no interaction between all three factors. Similar to the first year, wounded treatments tended to have lower cluster weights than non-wounded treatments at all three inoculation timings in 2020 (Fig. A3). Further, Cabernet Franc and Merlot clusters inoculated at bloom weighed significantly more than those inoculated at veraison and pre-harvest (Fig. 2.14).

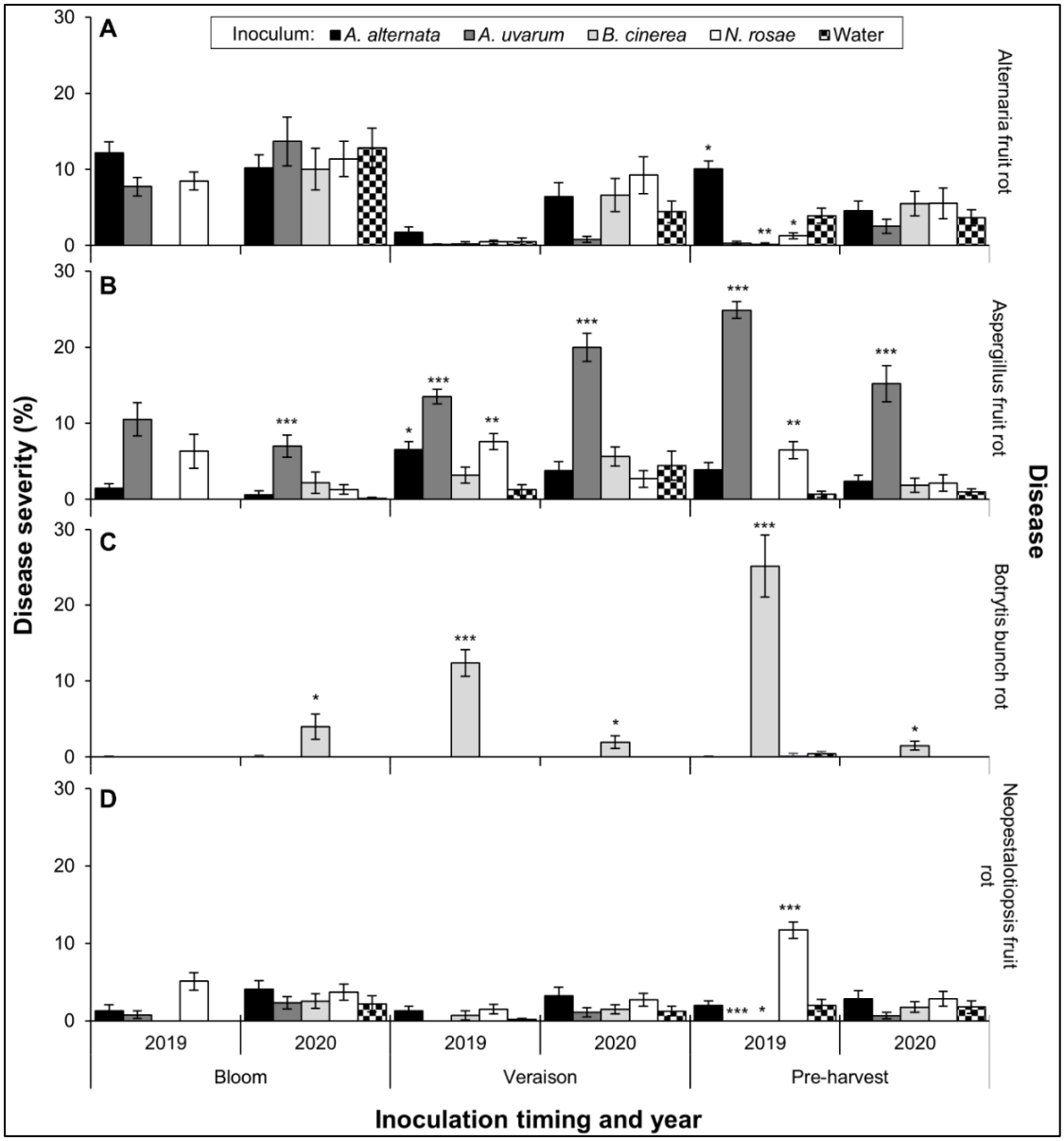

Fig. 2.13. Average severity of (A) Alternaria, (B) Aspergillus, (C) Botrytis, and (D) Neopestalotiopsis fruit rot across wounded clusters of four wine grape cultivars inoculated with four fungi and water at bloom, veraison, and pre-harvest in a field trial conducted in 2019 and 2020. One ($p < 0.05$), two ($p < 0.005$), or three ($p < 0.0005$) asterisks indicate that the disease severity was significantly greater than the water-inoculated treatment that was set as the control for the Steel multiple comparisons tests. Each disease/year/inoculation timing combination was evaluated with the Steel multiple comparisons test separately and error bars represent standard error. The wounded-bloom inoculated treatment was not included for the *B. cinerea* and water inoculum in 2019.

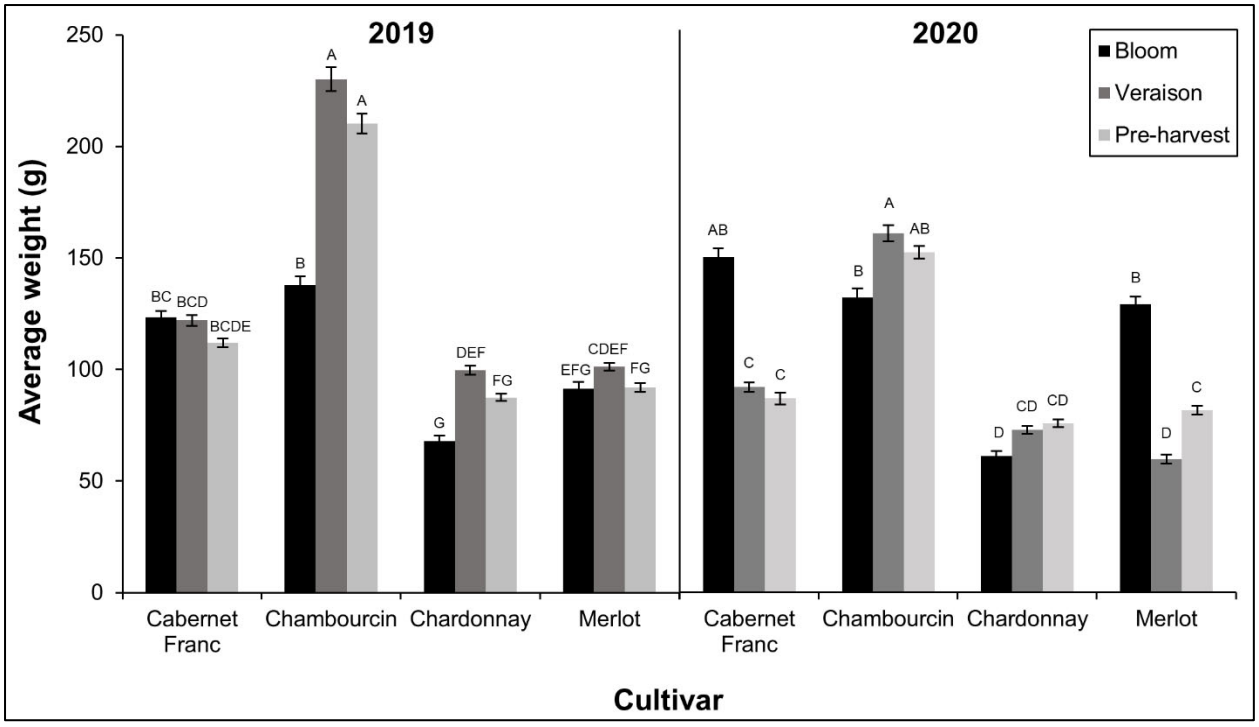

Fig. 2.14. Average cluster weight of four wine grape cultivars in a replicated field trial in 2019 and 2020 that were inoculated with five inocula at the phenological stages of bloom, veraison, and pre-harvest. Error bars represent standard error and bars labeled with different letters are significantly different according to a post hoc Tukey's honestly significant difference test conducted independently for each year.

2.4) Discussion

Each of the 15 fungal genera identified from the Mid-Atlantic isolates collected in this study have been previously associated with LSBR. Each genus has also been demonstrated to be pathogenic on detached fruit except for *Sporobolomyces*, a yeast associated with sour rot of grapes, and *Curvularia* (Barbetti 1980; Jayawardena et al. 2015; Lederer et al. 2013; Lorenzini et al. 2015; Rajput et al. 2020; Rousseaux et al. 2014; Steel et al. 2007). It is important to note that the collection and identification of isolates was limited, and other species within these genera are likely present in Mid-Atlantic vineyards (Kepner and Swett 2018). A more focused study on one of these genera may reveal other species that differ in pathogenicity and fungicide sensitivity.

Furthermore, the limited number of isolates collected from Virginia and Pennsylvania likely did not accurately represent the distribution of fungal species associated with LSBR in these states. Yet, this study effectively demonstrates the most prevalent LSBR-associated fungi in this region (Fig. 2.1).

The most commonly isolated genus was *Botrytis*. Although other species of *Botrytis* have been reported from blackberry, strawberry, and grape (Cosseboom et al. 2018; Dowling et al. 2017; Fernández-Ortuño et al. 2012b; Walker et al. 2011), only *B. cinerea* was identified in this study. A larger selection of isolates may have revealed different species, but *B. cinerea* appears to be the primary causal agent of gray mold in small fruit and grape production in the Mid-Atlantic United States. *B. cinerea* might be favored in vineyards and small fruit farms over other *Botrytis* spp. because it has a broad host range and can infect different adjacently planted crops (Valero-Jiménez et al. 2019). *B. cinerea* was also shown to be more competitive and aggressive than *B. fragariae,* which has only been found on strawberry (Rupp et al. 2017).

Four *Colletotrichum* spp. were identified from isolates collected from both ripe rot symptomatic and asymptomatic grape berries, belonging to the *C. acutatum* and the *C. gloeosporioides* complexes. Both *C. fioriniae* and *C. nymphaeae* were clearly identified by the three genes that were sequenced, however the identification of *C. aenigma* and *C. fructicola* is less certain due to many closely related species within the *C. gloeosporioides* complex (Fig. 2.10) (Weir et al. 2012). However, all four of these species have been previously isolated and identified from ripe rot symptomatic grapes (Oliver 2018; Peng et al. 2013; Yan et al. 2015). The sequencing of multiple other genes for the fungi identified as *C. aenigma* and *C. fructicola* may have resulted in the identification as a different, but very closely related species.

Within the genus *Aspergillus*, *A. japonicus* and *A. uvarum* were identified. The isolates were identified with a phylogenic analysis of the calmodulin gene, similar to Samson et al. (2014). A large majority of isolates were *A. uvarum*, which was previously reported from wine grapes in Slovakia (Mikušová et al. 2010). A smaller percentage of isolates were *A. japonicus,* which has also been reported from wine grapes previously (Kepner and Swett 2018). Interestingly, many species of *Aspergillus* have been isolated from wine grapes in other regions, but only *A. uvarum* and *A. japonicus* have been reported in the Mid-Atlantic (Kepner and Swett 2018; Rousseaux et al. 2014). Despite the apparently low diversity of *Aspergillus* spp. in the Mid-Atlantic, these two species belong to *Aspergillus* section *Nigri,* which was also the predominant section associated with wine grapes in other regions (Rousseaux et al. 2014; Samson et al. 2014; Serra et al. 2006). With a larger sample size, more species may have been isolated in this region, but it is likely that *Aspergillus* section *Nigri* is the primary group associated with wine grapes in the Mid-Atlantic. In addition to causing fruit rot, *A. japonicus* has also been reported to produce ochratoxin A (Abarca et al. 2004; Perrone et al. 2008) and both species have been associated with aspergillosis symptoms in medical patients (Badali et al. 2016).

Within the next most frequently isolated genera, *A. alternata,* has been isolated from grapes, but *N. rosae* has not. *N. rosae* has been reported as a pathogen of eucalyptus (Santos et al. 2020), blueberry (Rodríguez-Gálvez et al. 2020), and strawberry (Baggio et al. 2021; Rebollar-Alviter et al. 2020). Due to the recent subdivision of the genus *Pestalotiopsis* into *Pestalotiopsis, Neopestalotiopsis,* and *Pseudopestalotiopsis* (Maharachchikumbura et al. 2014), it is possible that *N. rosae* has been endemic to Mid-Atlantic grapes for years, but never characterized as this species. Within *Diaporthe,* all three species had been previously identified

from grape (Manawasinghe et al. 2019). Within *Cladosporium*, all four species had been isolated from grape as well, but *C. allicinum* has not yet been tested for pathogenicity (Gao et al. 2019; Hassan et al. 2021). Both Fusarium species were also detected on grapes, but *F. fujikuroi* has not been tested for pathogenicity (Bolton et al. 2016; Lorenzini and Zapparoli 2015). Detached fruit assays are typically used to assess the pathogenicity of fungi associated with grape fruit rots. This has been previously conducted for many of the species identified in this study, but in-field inoculations may reveal more about the pathogenic potential of the more frequently isolated, yet understudied species from this study. Furthermore, the identification of these fungi to the species level allows for accurate reflection on previous literature for further investigation into the causes of LSBR in the Mid-Atlantic.

The pathogenicity of the inocula *A. alternata*, *A. uvarum*, and *N. rosae* in a vineyard setting was tested for the first time in this study. *A. uvarum* was demonstrated to be the most pathogenic of these fungi, at times causing higher disease severity than the well-established pathogen *B. cinerea*. The ability of *A. uvarum* to cause significant disease severity on non-wounded fruit confirms this fungus as a primary pathogen (Fig. 2.12B). *A. alternata, B. cinerea*, and *N. rosae* did not cause significant levels of disease severity on non-wounded fruit. Since *B. cinerea* is a known primary pathogen of grape, these results hint that the environmental conditions may not have been ideal for infection by this fungus. Conditions may have not been ideal for the other inocula as well. During the bloom, veraison, and pre-harvest inoculations, the weather was often very warm and sunny, and the water-based spore suspensions may have quickly dried, not allowing the fungi to infect the fruit.

Bagging was a critical component of the field experiments conducted in this study because the grape ripening season in Maryland often entails high disease pressure and no

fungicides were applied to the clusters during the trials. Bags have been shown to effectively reduce the severity of fruit rotting diseases (Karajeh 2018), and clusters that were protected by bags throughout the season appeared healthier than non-bagged fruit (data not shown). As the bags were placed on the fruit immediately following inoculation, the bags may have also prolonged the wetness duration of the inoculum, increasing the chance for infection (Broome et al. 1995). The bags may have also altered the ambient environment around the clusters throughout the season, providing shade but also perhaps trapping heat. Drain holes on the downward facing side of the bags may have aided in equalizing the temperature inside and outside of the bags. Although the bagging resulted in less than natural development conditions by shading the clusters, non-target disease issues were avoided and conclusions of the pathogenicity of each inocula were not in jeopardy because disease severity was compared relative to control clusters that were bagged in the same manner.

The wounded treatments facilitated infection by the inocula, and higher disease severity was observed on these clusters. On the wounded fruit, *A. uvarum* and *B. cinerea* were found to cause significantly more Aspergillus fruit rot (Fig. 2.13B) and Botrytis bunch rot (Fig. 2.13C) than the water-inoculated control in both years, respectively. Interestingly, both *A. alternata* and *N. rosae* were only found to cause significantly more Alternaria (Fig. 2.13A) or Neopestalotiopsis fruit rot (Fig. 2.13D) than the control in 2019 at the pre-harvest timing, respectively. Also, during the pre-harvest timing in 2019, clusters inoculated with the *A. uvarum* and *B. cinerea* inoculum displayed significantly less Alternaria and Neopestalotiopsis fruit rot than the control (Fig. 2.13A, D). This is likely because these inocula caused very high severities of their respective diseases (Aspergillus fruit rot and Botrytis bunch rot), thereby outcompeting other less aggressive pathogens like *A. alternata* or *N. rosae*. The ability of these four fungi to

cause significant levels of disease on wounded fruit means that these fungi were able to act as secondary pathogens.

Highly severe diseases emerged that were not inoculated with an associated pathogen. For example, there were significant levels of Aspergillus fruit rot on wounded clusters not inoculated with the associated pathogen *A. uvarum* (Fig. 2.13B). There were also high levels of Alternaria fruit rot on wounded clusters inoculated with water (Fig. 2.13A). This was likely the result of native inoculum in the vineyard, with infection aided by the fruit wounding. Other naturally occurring diseases appeared on the fruit such as ripe rot and powdery mildew. Powdery mildew was widespread and very severe in 2020 in all cultivars except Chambourcin. Previous studies have suggested that powdery mildew infection occurring early in the season can cause wounds in the berry cuticle, providing an entry point for secondary fungal pathogens (Gadoury et al. 2003). Although clusters appearing healthy were selected for inoculations, latent or diffuse powdery mildew infections are not visible to the unaided eye (Gadoury et al. 2007). It is therefore possible that the high levels of Alternaria and Neopestalotiopsis fruit rots on water-inoculated clusters in 2020 were secondary infections resulting from the severe powdery mildew epidemic. Interestingly, little to no Botrytis bunch rot was observed on clusters that were not inoculated with the pathogen. The conditions in the field may not have been suitable for Botrytis bunch rot to naturally occur during the two seasons of this study, and little Botrytis bunch rot was observed in other Maryland vineyards during this season (data not shown).

Cultivar was not a factor in the statistical analysis of disease severity, however there may be differences in susceptibility between the cultivars tested. French-American hybrid grapevines (e.g., Chambourcin) tend to be more tolerant to some foliar and fruit rotting diseases than French cultivars (e.g., Cabernet Franc, Chardonnay, and Merlot) (Wilcox et al. 2015). This trend could

be seen on the non-wounded fruit, where the average disease severity on Chambourcin was consistently low compared to the other cultivars (Fig. A1). This was not true on the wounded fruit, for wounding may have allowed the pathogens to overcome varietal resistances (Fig. A2). It is also noteworthy that most isolates (88%) were collected from *V. vinifera* cultivars, as opposed to hybrid cultivars. This could be due to varietal resistance resulting in fewer hybrid clusters being sampled or because a greater proportion of Mid-Atlantic acreage consists of *V. vinifera* cultivars.

The phenological stage of the grape cluster is an important factor for disease infection for Botrytis bunch rot, black rot, and powdery mildew (Gadoury et al. 2003; McClellan and Hewitt 1973; Molitor and Berkelmann-Loehnertz 2011), and this may be an important factor for *A. uvarum* infection as well. In both years, the inoculation of *A. uvarum* at veraison and pre-harvest resulted in significantly more Aspergillus fruit rot than the control (Fig. 2.12; Fig. 2.13). The inoculation timing also had a significant effect on the weight of the clusters; however, this was likely due to the protective bagging rather than the inoculum because the inoculum did not have a significant effect on the weight. The protective bags were placed on the clusters at the point of inoculation and may have protected the fruit from subsequent detrimental effects from the environment and other diseases and pests. For example, clusters bagged and inoculated at bloom in 2020 tended to weigh more than those bagged and inoculated at veraison and pre-harvest (Fig. A3). Bloom-inoculated clusters were protected from external pressures like the severe powdery mildew outbreak in 2020 from bloom until harvest (about four months), while the other clusters were only protected from veraison until harvest (about two months) or from pre-harvest until harvest (about one month). However, bagging at the fragile bloom stage also posed risks and damaged clusters in this trial, at times breaking the inflorescence completely off the grapevine.

This may explain the lower cluster weights observed on bloom bagged clusters in 2019. If all clusters to be inoculated in these trials were bagged at bloom, only to be removed for the inoculation and wounding treatments at veraison and pre-harvest, a clearer difference between inoculation timings may have occurred.

The pathogenicity of understudied fungal species involved in LSBR of wine grapes in the Mid-Atlantic region was assessed. The primary fruit rotting pathogens were found to be *A. uvarum, Botrytis* spp., and *Colletotrichum* spp. while *A. alternata* and *N. rosae* appear to act as secondary pathogens in the Mid-Atlantic. This is the first study confirming the in-field pathogenicity of *A. uvarum,* which caused the most disease when infection occurred during the veraison or pre-harvest stages. For prevention of LSBR in general, the prevention of wounding appears to be a critical first step to controlling the majority of the LSBR diseases. An integrated approach can be taken to reduce fruit rotting diseases by growing disease resistant hybrid cultivars and by preventing fruit wounding from primary pathogens, insects, weather events, and birds. For the primary pathogens, fungicides can be highly effective means of control, although the sensitivity of lesser studied fungi like *A. uvarum* is not well understood, and fungicide resistance is a threat to efficacy, especially with regards to *B. cinerea*.

Chapter 3: Fungicide Sensitivity of Grape Late Season Rot Pathogens

3.1) Introduction

The fungicide sensitivity of the frequently isolated fungi *A. alternata* (Avenot and Michailides 2020; Iacomi-Vasilescu et al. 2004), *B. cinerea* (Adamo 2016), and *Colletotrichum* spp. (Oliver 2016) has been investigated, but not with *A. uvarum* or *A. japonicus*. There are also gaps in the understanding of *Botrytis* fungicide sensitivity, because *Botrytis* populations have acquired resistance to most effective fungicide chemical classes and isolates with multi-fungicide resistance have been found worldwide (Cosseboom et al. 2019; Fan et al. 2017; Fernández-Ortuño et al. 2016; Panebianco et al. 2015; Weber 2011). *Botrytis* species are considered a major threat in many high value cropping systems such as small fruit and wine grapes, causing both pre- and post-harvest gray mold (Dean et al. 2012).

Resistance in *B. cinerea* to most site-specific active ingredients has been associated with mutations at the fungicide target site (Hahn 2014). Mutations in the *β-tubulin* gene, the two-component histidine kinase gene (*bos1*), the cytochrome b gene (*cytb*), the 3-keto reductase gene (*erg27*), and the iron-sulfur protein gene of the succinate dehydrogenase complex (*sdhB*) have been related with resistance to methyl-benzimidazole carbamates (MBCs), dicarboximides (DCs), quinone-outside inhibitors (QoIs), hydroxyanilides (Has), and succinate dehydrogenase inhibitors (SDHIs), respectively. These mutations generally provide cross-resistance between fungicides within the same chemical class, however, SDHIs appear to have incomplete cross-resistance. For example, the mutation H272R in *sdhB* confers resistance to boscalid but not fluopyram, fluxapyroxad, or penthiopyrad, while the mutation P225F confers resistance to all four fungicides (Amiri et al. 2014; Fernández-Ortuño et al. 2017; Hu et al. 2016). To our

knowledge, *B. cinerea* isolates with different *sdhB* genotypes have not been tested for sensitivity to the two novel SDHI fungicides, pydiflumetofen and inpyrfluxam. Pydiflumetofen, a N-methoxy-(phenylethyl)-pyrazole-carboxamide, is labeled for use in grape and other crops targeting *B. cinerea* in the United States. Inpyrfluxam, a pyrazole-4-carboxamide, is not yet registered in the United States but has the potential for use in crops targeting *B. cinerea.*

While multi-fungicide resistance is typically conferred by accumulation of target-site mutations in individual *Botrytis* isolates (Li et al. 2014), it has also been associated with overexpression of the ABC transporter *atrB*, leading to reduced sensitivity to anilinopyrimidine (AP) and phenylpyrrole (PP) fungicides (Kretschmer et al. 2009). The levels of *atrB* overexpression and the resulting resistance to these fungicides can vary based on the mutations in *mrr1* that regulates *atrB* expression. Accordingly, isolates have been classified into two groups, multiple drug resistant 1 (MDR1) and MDR1h. MDR1 isolates contain various missense mutations, while MDR1h isolates all contain a specific mutation, Δ497L/V (Fernández-Ortuño et al. 2015; Leroch et al. 2013). Isolates with a second MDR mechanism, called MDR2, overexpress the major facilitator superfamily gene *mfsm2*. This is caused by rearrangements in the *mfsm2* promotor and leads to reduced sensitivity to AP, DC, HA, and PP fungicides (Kretschmer et al. 2009).

Little is known about the sensitivity of *Aspergillus* and *Neopestalotiopsis* spp. associated with LSBR. *Aspergillus niger* and *Aspergillus flavus* were tested for sensitivity to thiophanate-methyl, tebuconazole, iprodione (Thomidis et al. 2009), boscalid, captan (Serey et al. 2007), and pyraclostrobin (Latorre et al. 2002) using single fungicide concentrations *in vitro* or on detached fruit. Because certain *Aspergillus* spp. can be both plant and human pathogens, fungicide resistance development is a high concern. Recently, demethylation inhibitor (DMI) resistant

isolates of *A. fumigatus* were isolated from human and plant hosts, indicating that fungicides applied for agricultural purposes could cause off-target resistance selection (Verweij et al. 2009). Other studies suggested that *Pestalotiopsis* spp. were sensitive to carbendazim and iprodione (Saju et al. 2011), but carbendazim-resistant isolates have recently been found (Yong et al. 2014). To address these knowledge gaps, the fungicide sensitivity of *Aspergillus, Botrytis,* and *Neopestalotiopsis* to important fungicides was investigated using multiple techniques.

3.2) Materials and Methods

3.2.1) Discriminatory dosage sensitivity to site specific fungicides

A discriminatory dosage mycelial growth assay developed by Fernández-Ortuño et al. (2014) was used to test each *Botrytis* isolate for resistance to the following fungicides using previously established doses: boscalid (75 µg/ml), cyprodinil (4 µg/ml), fenhexamid (50 µg/ml), fludioxonil (0.5 µg/ml), iprodione (10 µg/ml), isofetamid (5 µg/ml), penthiopyrad (5 µg/ml), pyraclostrobin (10 µg/ml), and thiophanate-methyl (100 µg/ml) (Cosseboom et al. 2019). Also, two other SDHIs, pydiflumetofen and benzovindiflupyr were included at a concentration of 5 µg/ml, based on the fact that EC_{50} values of sensitive *B. cinerea* isolates are comparable for SDHIs including penthiopyrad, isofetamid, pydiflumetofen, and benzovindiflupyr (Table 3.1) (Amiri et al. 2014; Fernández-Ortuño et al. 2017; Hu et al. 2016; Zuniga et al. 2020). The formulated products Miravis (pydiflumetofen; Syngenta Crop Protection, Basel, Switzerland), Aprovia (benzovindiflupyr; Syngenta Crop Protection), Endura (boscalid; BASF Crop Protection, Research Triangle Park, NC), Vangard (cyprodinil; Syngenta Crop Protection), Elevate (fenhexamid; Arysta Lifescience, Cary, NC), Scholar SC (fludioxonil; Syngenta Crop Protection), Rovral (iprodione; FMC, Philadelphia, PA), Kenja 400 (isofetamid; ISK

Biosciences, Concord, OH), Fontelis (penthiopyrad; Corteva Agriscience, Wilmington, DE), Cabrio (pyraclostrobin; BASF Crop Protection), and Topsin M (thiophanate-methyl; United Phosphorous Inc., King of Prussia, PA) were used for the resistance phenotyping.

The fungicides were mixed with the following media after autoclaving and cooling to 55 °C: cyprodinil with Czapek-Dox agar; fenhexamid, fludioxonil, iprodione, pyraclostrobin (plus 100 µg/ml salicyl hydroxamic acid), and thiophanate-methyl with malt extract agar (MEA); and pydiflumetofen, benzovindiflupyr, boscalid, isofetamid, and penthiopyrad with yeast bacto acetate agar (YBA) (Stammler and Speakman 2006; Weber and Hahn 2011). Also, a positive control was included with non-amended Czapek-Dox agar. One milliliter of each fungicide-amended medium was pipetted into 15 mm diameter wells of 24-well plates. After each isolate was revived from storage on PDA for three to four days at room temperature, mycelium was plated onto each well of the plates using a sterilized toothpick. After incubation for five days at 22 °C, the plates were visually evaluated for the presence Which or absence (S) of mycelial growth (Fernández-Ortuño et al. 2014).

3.2.2) Fungicide target gene mutations

B. cinerea isolates sensitive and resistant to the DC (n = 11), HA (n = 6), MBC (n = 9), QoI (n = 5), and SDHI (n = 19) chemical classes were screened for mutations in fungicide target genes. DNA was extracted as described above and the following target genes were amplified with PCR using previously described primers and thermocycling protocols (Table A1): *sdhB* for the SDHI fungicides pydiflumetofen, benzovindiflupyr, boscalid, isofetamid, and penthiopyrad, the partial β-tubulin gene for the MBC thiophanate-methyl, *cytb* for the QoI pyraclostrobin, and *bos1* for the DC iprodione. A new reverse primer (erg27end2) for *erg27* for the HA fenhexamid was developed to pair with the previously published forward primer erg27beg and thermocycling

protocol due to difficulty with the reverse primer erg27end (Table A1). Nine isolates that were identified as R to fludioxonil according to the mycelial growth assay were screened for the MDR1 or MDR1h genotypes. Four primers were used to amplify and sequence the *atrB* transcription factor *mrr1,* and a consensus of the four sequences for each isolate was compared to *mrr1* sequences of the non-MDR *B. cinerea* isolates B05.10 and T4 (GenBank accession numbers CP009809 and FQ790263, respectively). Additionally, a non-MDR *B. cinerea* group S isolate 5d5 (Hu et al. 2019) was included for the comparison of *mrr1* amino acid variations. Fifty isolates were also screened for a sequence rearrangement in *mfsm2* that results in the MDR2 phenotype using a previously described protocol (Kretschmer et al. 2009).

To investigate the genetic basis of *Aspergillus* sensitivity to azoxystrobin, the partial cytochrome b gene was sequenced. A cytochrome b sequence of *Aspergillus tubingensis* (GenBank accession LC545447) was used as a template sequence for primer design. Primers AspCytF8 and AspCytR9 were designed to amplify a 1027 bp region of cytochrome b (Table A1). The same reagent mixture as described above was used for amplification of the cytochrome b target with these two primers. The thermocycling conditions were 95 °C for 3 min, 35 cycles of 95 °C for 30 s, 55 °C for 30 s, and 72 °C for 60 s, and 72 °C for 5 min. The amplicons were then purified and sanger sequenced as described above and submitted to GenBank (Table A2). Then, the coding region was translated and compared between each isolate for amino acid variations.

3.2.3) EC_{50} sensitivity to site specific fungicides

Thirteen isolates of *Botrytis* with different *sdhB* genotypes were chosen for sensitivity analysis using serial dilutions of the active ingredients benzovindiflupyr (Aprovia), inpyrfluxam (Indiflin; Valent BioSciences, Libertyville, IL), and pydiflumetofen (Miravis) to determine the effective concentration that inhibits mycelial growth by 50% (EC_{50}) compared to the control. *B. cinerea*

has previously been tested for EC_{50} sensitivity to benzovindiflupyr (Hu et al. 2016) and was included as a relative comparison. Isolate genotypes included: three isolates of each wild-type, H272R, H272Y, and P225F, and one isolate with N230I genotype. Petri dishes (90 mm diameter) were amended with 0.003, 0.03, 0.1, 0.3, 1.0, 10, and 100 µg/ml pydiflumetofen and inpyrfluxam, and 0.05, 0.1., 0.5, 1.0, and 10 µg/ml benzovindiflupyr mixed with PDA that had cooled to 55 °C. Non-amended PDA plates were compared to fungicide-amended plates as controls. PDA plugs (10 mm diameter) from freshly growing mycelia of each isolate were placed face-down onto the center of each medium described above. After incubation at 22 °C in the dark for three days, the diameter of mycelial growth (minus the diameter of inoculation mycelial plug) was measured for the three replicates of each fungicide-concentration combination. The percent relative growth for each concentration was calculated as the relative mycelial growth on each fungicide concentration compared to the control. This experiment was conducted once.

The five isolates of *A. uvarum* and *N. rosae* that were identified above and used as inoculum were tested for their sensitivity to azoxystrobin (Abound Flowable; Syngenta Crop Protection, Basel, Switzerland), boscalid (Endura; BASF Crop Protection, Research Triangle Park, NC) and difenoconazole (Inspire; Syngenta Crop Protection). Serial dilutions of the fungicides mixed with PDA were used to determine the effective concentration that inhibits mycelial growth by 50% (EC_{50}). The media were autoclaved and cooled to 55 °C before the fungicide was mixed into the media in a laminar flow hood. Azoxystrobin was amended at the concentrations of 0.01, 0.1, 0.3, 1, 3, 10, and 100 µg/ml, boscalid at the concentrations of 0.1, 1, 3, 10, 30, and 100 µg/ml, and difenoconazole at the concentrations of 0.01, 0.03, 0.3, 1, 3, 10, and 100 µg/ml. A 25 mm^2 agar plug of each isolate was transferred to the center of three plates of each concentration for all fungicides and three plates of non-amended PDA. The plates were

then incubated at 22 °C until mycelial growth on non-amended plates reached at least 80% of the diameter of the 100 mm Petri dishes. At this point, the diameter of mycelial growth on each concentration was measured in two perpendicular directions using digital calipers. This experiment was conducted twice.

Because a broad range in sensitivity was observed with azoxystrobin, the sensitivity of more isolates was evaluated with a new method. A random selection of 12 *A. uvarum* isolates to azoxystrobin (Abound flowable, Syngenta Crop Protection, Greensboro, NC) was evaluated with a 96-well SmartReader96 photometer (Accuris USA, Edison, NJ) similar to a previous study (Stammler and Speakman 2006). First, flat-bottom 96-well plates were prepared with multiple concentrations of the active ingredient in a liquid medium by adding 50 µl of 2X concentrated YBA medium (20 g yeast extract, 20 g of Bacto peptone, and 40 g of sodium acetate in 1-liter deionized water) to each well. Then, 25 µl of a 4X concentrated azoxystrobin solution was added to each well. Lastly, 25 µl of a 4X concentration of spore suspension was added to each well. The final concentration of the spore suspensions was 1 x 10^4 conidia/ml, and the final azoxystrobin concentrations were 0, 0.01, 0.03, 0.1, 0.3, 1, 3, 10, 30, and 100 µg/ml. Each isolate's spore suspension was added to three wells for every azoxystrobin concentration that was included in the assay and three wells per concentration were aliquoted with 25 µl sterile deionized water instead of the spore suspension as a negative control. The final volume in each well was 100 µl, and the plates were gently vortexed to mix the YBA medium, spore suspension, and fungicide in each well. The plates were then incubated at 22 °C in the dark for two days before the plates were analyzed with the photometer at the 405 nm filter setting.

3.2.4) Detached fruit sensitivity assays

For *B. cinerea,* a detached fruit assay was conducted to verify that the mycelial growth assay was applicable for identifying field-relevant fungicide resistant isolates in grape. Fifteen isolates from blackberry, grape, and strawberry identified as S and R to each chemical class were revived by recovering a filter paper culture stock from cold storage and plating onto a fresh plate of PDA. The plates were incubated at 22 °C in the dark for one week followed by one week under constant fluorescent light to induce sporulation. The following genotypes identified in the S and R isolates were included in the assay: E198A in β-tubulin, I365N and I365S in *bos1*, G143A in *cytb*, F412I and F412S in *erg27*, MDR1h in *mrr1*, and P225F, H272R, and H272Y in *sdhB*. Isolates sensitive to each chemical class with wild-type genotypes were also included. Spore suspensions were made by flooding sporulating plates with sterile water, rubbing the conidiophores with sterile forceps, quantifying with a hemocytometer, then diluting to 1 x 10^5 conidia per ml (Amiri et al. 2018).

Store-bought, Ruby seedless grapes were cut from their rachises with pedicels attached and surface sterilized in 1% sodium hypochlorite for 1 minute, then rinsed with sterile deionized water. After drying, groups of grapes were treated with the fungicides Cabrio (119 µg a.i./ml), Elevate (599 µg a.i./ml), Endura (235 µg a.i./ml), Rovral (1249 µg a.i./ml), Scholar SC (262 µg a.i./ml), Topsin M (1258 µg a.i./ml), and Vangard (393 µg a.i./ml) by misting with an atomizer until runoff. After drying, the grapes were wounded with a sterile toothpick by inserting to a depth of one centimeter. For each treatment, 20 µl of spore suspension was then pipetted into the wound of 12 grapes. Also, positive and negative control groups were included and were misted with water instead of fungicide. The positive control group was inoculated with *B. cinerea*, while 20 µl of sterile deionized water was pipetted into the wound of the negative control group. The

inoculated grapes were placed on test tube racks inside of enclosed plastic boxes containing moist paper towels. After incubating at 22 °C in ambient diurnal lighting for six days, the lesion diameter was measured for each fruit. This experiment was conducted twice independently.

Other detached grape assays were conducted to evaluate the effect of different amino acid variations in the cytochrome b gene of *Aspergillus* inoculum on azoxystrobin efficacy. Two *A. uvarum* isolates per genotype were selected for inoculum with GP19-12 and GP18-93 as the "AUcytb2" inoculum, GP20-310 and GP20-111 as "AUcytbWT", and GP19-8 and GP18-276 as "AUcytb3", and two *A. japonicus* isolates, GP18-148 and GP19-10, called "AJcytb2" were selected. Spore suspensions at a concentration of 1 x 10^6 conidia per ml were prepared for each isolate and the two suspensions per genotype were mixed. Then ripe, seedless red table grapes were surface sterilized with 1% sodium hypochlorite for one minute, rinsed with sterile deionized water, and allowed to dry. The fruit were wounded with a sterile toothpick, and half were dipped in an azoxystrobin (Abound Flowable) solution at a concentration of 499 µg azoxystrobin per ml and half were dipped in sterile deionized water for two minutes. After drying, ten fruit per genotype and fungicide treatment were inoculated with 15 µl of spore suspension pipetted directly into the wound. Also, ten fruit were not inoculated as a control. The fruit were then incubated in the dark at 22 °C for four days. After this time, the diameter of lesions on the fruit was measured. This experiment was conducted three times.

3.2.5) Molecular docking

The ability of azoxystrobin to bind to the cytochrome b complex with newly discovered amino acid variations was evaluated in silico with the AutoDockTools software V1.5.7 (The Scripps Research Institute, La Jolla, CA). First, models of these cytochrome b complex variants were created using I-TASSER, a web-based protein modeling software that predicts the form of

proteins using amino acid sequences and previous structural models (Roy et al. 2010). The amino acid sequences of the cytochrome b variants were submitted to I-TASSER, and the closest matching model was downloaded (Table A5). The model of azoxystrobin was sourced from the Research Collaboratory for Structural Bioinformatics database (https://www.rcsb.org/ligand/AZO). The cytochrome b complex models were loaded into AutoDockTools as the "macromolecule", and the azoxystrobin model was loaded as the "ligand".

Before docking, various steps were taken to prepare the molecules and ensure accuracy. First, any water molecules and heteroatoms were removed from the macromolecule. The macromolecule was also checked for any missing atoms and was repaired if necessary. Then, polar hydrogens and Kollman charges were added to the macromolecule, and Gasteiger charges were added to the ligand. The number of torsions, or rotatable bonds, on the ligand was automatically set at 8 by the software. Then, the grid box was set to encapsulate the binding pocket of azoxystrobin on the cytochrome b complex at a size of 40 X 40 X 40 Å (Esser et al. 2004). The grid box did not allow the ligand to bind outside of the box confines. Docking was run with 50 Lamarckian genetic algorithm runs, a population size of 300, and 250,000 evaluations (Meng et al. 2011; Ren et al. 2020). The 50 genetic algorithm runs that were conducted for each macromolecule variant were screened for docking that matched the description by Esser et al. (2004), and any other hydrogen bonds between the ligand and macromolecule were noted. The docked ligand-macromolecule conformations with the lowest binding energy were visualized using PyMOL V2.5.1 (Schrödinger Inc., New York, NY).

3.2.6) Statistical analysis

All statistical analyses in this project were conducted using the software JMP Pro 14.1 (SAS Institute, Cary, NC). For *B. cinerea* isolates characterized as either S or R, a generalized linear model with a logit link function was used to evaluate the effect of the active ingredient and crop on the frequency of resistance with active ingredient and crop regarded as fixed effects. Each isolate was also characterized according to the number of chemical classes that it was resistant to (CCR). A Kruskal-Wallis test was used to compare the median CCR value of isolates from the five different crops. This was followed with a post hoc, Bonferroni corrected Wilcoxon test to test for significant differences between the five crops. For the detached fruit assay, the mean lesion diameters of the different treatments within each active ingredient were compared with a nonparametric Steel method multiple comparisons test. The wild-type or sensitive isolate to each fungicide was considered the control. This was done for both trials separately. For the sensitivity testing of pydiflumetofen and inpyrfluxam, the EC_{50} values were calculated by regressing the percent relative growth against the $\log_{10}$ of the fungicide concentration. The square root-transformed means of EC_{50} values of isolates with the wild-type, H272R, H272Y, and P225F genotypes were compared with an ANOVA followed by a post hoc Tukey's honestly significant difference test. The EC_{50} values of the isolate with the N230I genotype was not included in the statistical analysis because only one isolate was tested.

From the photometer testing of *Aspergillus*, the values for each isolate and concentration were corrected by subtracting the values of the control wells. Then, the concentration at which the fungal growth was inhibited by 50% (EC_{50}) was derived via probit analysis (Grabke and Stammler 2015). This was conducted twice for every isolate, and then the EC_{50} values were averaged between the two tests for each isolate before statistical comparisons. The effect of the

genotype on the mean EC_{50} values was compared with ANOVA, and this was followed with a Tukey's HSD test for multiple comparisons. From the detached fruit assays with *Aspergillus*, the lesion diameter data was compared between the fixed effects of genotype, fungicide (treated or non-treated), an interaction between genotype and fungicide, and the random effect of the assay number. A post hoc Tukey's HSD test was conducted for multiple comparisons ($\alpha = 0.05$). The percent inhibition by the fungicide treatments was also calculated from lesion diameters of the treated and non-treated fruit. The percent inhibition was compared between treatments in a similar fashion to the lesion diameter data, but genotype was the only effect.

3.3) Results

3.3.1) Discriminatory dosage sensitivity to site specific fungicides

All 249 *Botrytis* isolates were tested for resistance to eleven active ingredients resulting in the following frequencies of resistant isolates: 92% to pyraclostrobin, 86% to cyprodinil, 71% to thiophanate-methyl, 48% to fenhexamid, 47% to iprodione, 26% to boscalid, 11% to fludioxonil, 8% to penthiopyrad, 7% to benzovindiflupyr, 4% to pydiflumetofen, and 4% to isofetamid. Variations in resistance frequency were found in all crop-active ingredient combinations (Fig. 3.1). According to a generalized linear model, both active ingredient ($DF = 10$, $\chi^2 = 929.21$, $p < 0.0001$) and crop ($DF = 4$, $\chi^2 = 29.65$, $p < 0.0001$) had significant effects on frequency of resistance. In the same model, a significant interaction was observed between active ingredient and crop ($DF = 40$, $\chi^2 = 146.58$, $p < 0.0001$).

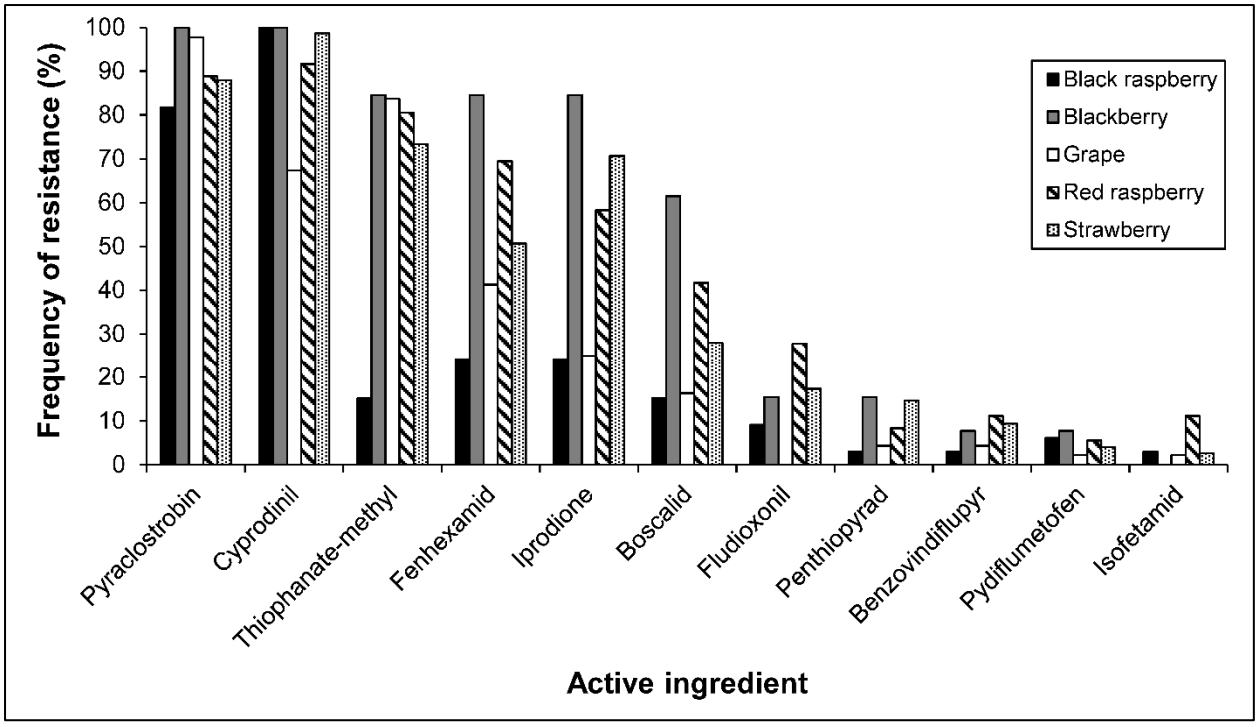

Fig. 3.1. Frequencies of resistance to eleven active ingredients in *Botrytis cinerea* isolates collected from black raspberry (n=33), blackberry (n=13), grape (n=92), red raspberry (n=36), and strawberry (n=75) in Maryland and Pennsylvania from 2014 to 2019 that were evaluated with a mycelial growth assay.

The fungicides tested in the mycelial growth assay represented seven distinct chemical classes, and the isolates were summarized according to the number of chemical classes to which they were resistant (nCCR; Fig. 3.2). Eight isolates were 0CCR, 19 were 1CCR, 37 were 2CCR, 54 were 3CCR, 60 were 4CCR, 47 were 5CCR, 33 were 6CCR, and 7 were 7CCR. The 7CCR isolates were from three strawberry and two red raspberry farms in 2015 and 2019. The 0CCR isolates were collected from blackberry, black raspberry, red raspberry, and strawberry, but not from grape. The median CCR values of isolates from blackberry (6), red raspberry (5), and strawberry (5) was statistically higher ($\alpha = 0.01$) than grape (3), which was higher than black raspberry (2).

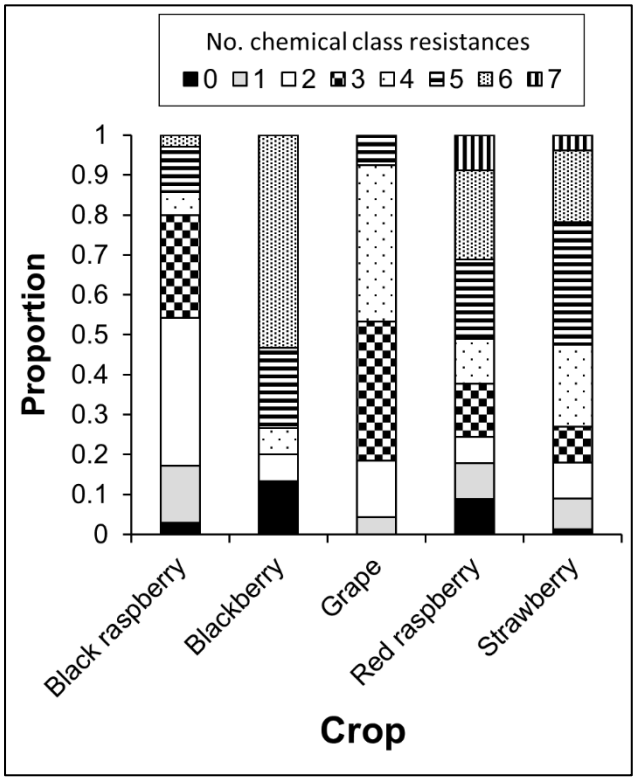

Fig. 3.2. Proportion of *Botrytis cinerea* isolates collected 2014 to 2019 from blackberry (n=13), red raspberry (n=36), strawberry (n=75), grape (n=92), and black raspberry (n=33), resistant to 0, 1, 2, 3, 4, 5, 6, or 7 distinct chemical classes.

3.3.2) Fungicide target gene mutations

Various previously reported mutations were found within each corresponding target gene from a selection of isolates characterized as resistant in the mycelial growth assay: E198A in β-tubulin, I365N/S, Q369P, and N373S in *bos1*, G143A in *cytb*, P238S, N369D, and F412I/S in *erg27*, and P225F and H272R/Y in *sdhB*. It is noteworthy that target genes of isolates characterized as S or R in the bioassay contained sequences that matched the resistance phenotype for 42 of 50 isolates. Five isolates that had the H272R mutation were characterized as S to boscalid, and retesting revealed two of the five to be R to boscalid. Also, three isolates initially characterized as R to fludioxonil contained no mutations in *mrr1* and retesting revealed that they were S to fludioxonil.

The *mrr1* and *mfsm2* gene sequences were used to identify MDR1 and MDR2 isolates, respectively. The *mrr1* sequences of the six MDR1 or MDR1h isolates were compared to fungicide sensitive *B. cinerea* reference isolates (T4 and B05.10), and contained many same-sense and missense mutations including 18 bp and 21 bp insertions, indicating they belonged to group S of *B. cinerea* (Leroch et al. 2013). One of these six isolates contained a 3-bp deletion at codon 497 (Δ497L/V) and was identified as MDR1h, while the other five were identified as MDR1. A total of 12 amino acid variations were found in *mrr1* from MDR1 and MDR1h isolates (Fig. 3.3). All these variations have been previous reported except T509A and G721Y (Fernández-Ortuño et al. 2015). It is also noteworthy that the comparison in Fig. 3.3 was made based on a *Botrytis* group S isolate 5d5 sensitive to fludioxonil, in which *mrr1* amino acid positions are shifted from sensu stricto *B. cinerea* (e.g., isolate B05.10) due to insertions and deletions within this gene. For instance, the mutation Δ497L/V in relation to B05.10 is identical with Δ508L/V in relation to isolate 5d5 (Fig. 3.3). Amino acid substitutions in relation to the sequence of *B. cinerea* isolate B05.10 are listed in the appendix (Table A6).

An allele-specific PCR was used to identify isolates as either MDR2 (2273 bp) or non-MDR2 (1625 bp) based on amplicon size. Out of the 50 isolates tested, all revealed approximately 1600 bp amplicons, the expected length of non-MDR2 isolates (data not shown).

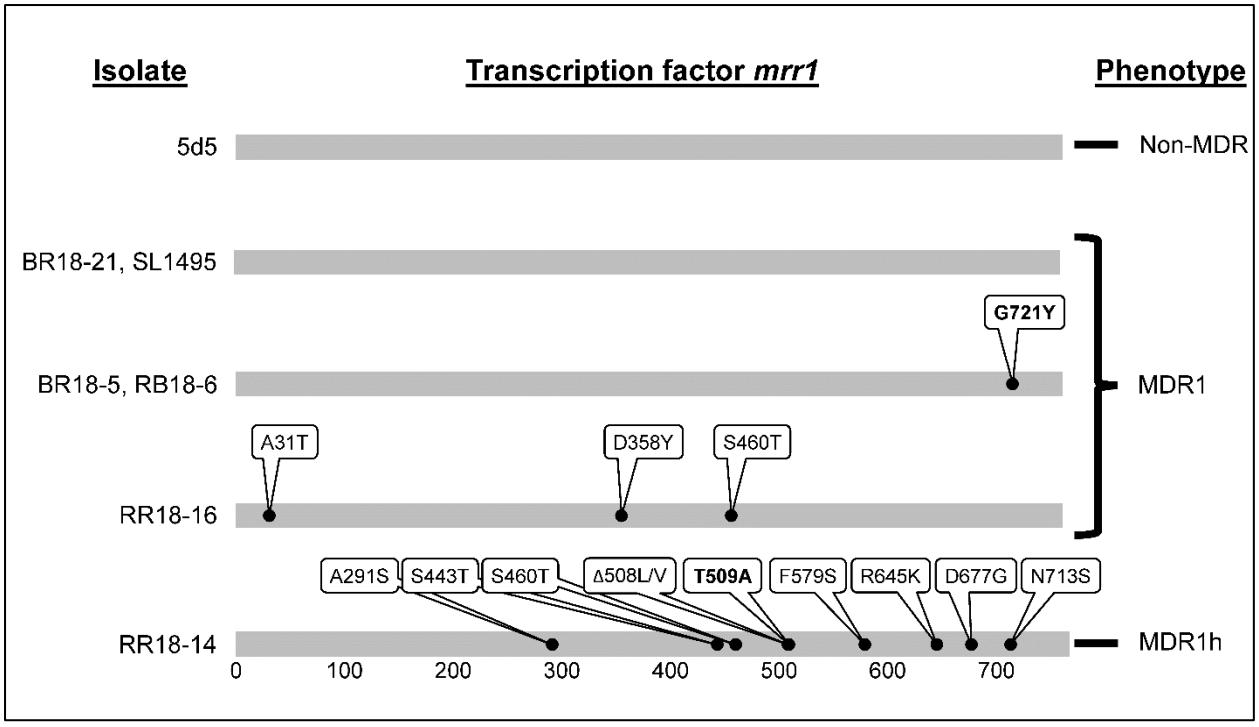

Fig. 3.3. Amino acid variations of the fludioxonil-resistance related *atrB* transcription factor *mrr1* between one non-multidrug resistance (MDR), five MDR1, and one MDR1h *Botrytis cinerea* isolates in relation to the non-MDR isolate 5d5 (Hu et al. 2019). Variations in bold (T509 and G721Y) have not been reported previously.

3.3.3) EC_{50} sensitivity to site specific fungicides

Multiple concentrations of the SDHI fungicides pydiflumetofen, benzovindiflupyr, and inpyrfluxam resulted in varying sensitivity of isolates with different *sdhB* genotypes (Table 3.1). The EC_{50} values varied from isolate to isolate and from genotype to genotype. Wild-type isolates were found to have the lowest mean EC_{50} values (most sensitive) for both active ingredients. Isolates with the H272Y genotype had the highest mean EC_{50} values (least sensitive) to pydiflumetofen, and isolates with the P225F genotype had the highest mean EC_{50} values to inpyrfluxam. An ANOVA revealed that the isolate genotype had a significant effect on the EC_{50} values for both pydiflumetofen ($DF = 3$, $F = 10.115$, $p = 0.004$) and inpyrfluxam ($DF = 3$, $F = 12.962$, $p = 0.002$).

Table 3.1. Effective concentration of pydiflumetofen, benzovindiflupyr, inpyrfluxam that inhibits 50% mycelial growth (EC_{50}; µg/ml) values of *Botrytis cinerea* isolates with different *sdhB* genotypes

		Inpyrfluxam		Pydiflumetofen		Benzovindiflupyr
SdhB Genotype	Isolate name	EC_{50}	Mean EC_{50}[z]	EC_{50}	Mean EC_{50}	EC_{50}
Wild-type	Mod5	1.52	1.01 c	0.71	0.42 b	0.26
	Gik1	1.01		0.28		-[y]
	Flor5	0.51		0.26		-
H272R	GP18-182	0.54	0.67 bc	1.00	0.81 b	0.44
	GP18-51	0.87		0.46		-
	GP18-81	0.60		0.97		-
H272Y	GP18-165	46.06	23.20 a	6.09	149.75 a	5.18
	Gik20	9.80		250.90		-
	Mod20	13.75		192.27		-
P225F	GP18-204	73.86	48.76 ab	92.59	38.83 a	-
	FL12-355	4.49		3.73		-
	GP18-205	67.94		20.17		1.16
N230I	FL12-255	0.90		0.92		-

[z] Values in the same column with matching letters are not statistically different according to a post hoc Tukey's honest significant difference test (α = 0.05).

[y] "-" = not tested.

Five isolates of *A. uvarum* and *N. rosae* were tested for their sensitivity to the fungicides azoxystrobin, boscalid and difenoconazole. All *N. rosae* isolates were insensitive to boscalid and azoxystrobin (EC_{50} > 100 µg/ml) but sensitivity to difenoconazole ranged from 0.30 to 5.06 µg/ml (Table 3.2). Sensitivity of *A. uvarum* isolates ranged 0.63 to >100 µg/ml for azoxystrobin, 0.59 to 4.73 µg/ml for boscalid, and 0.18 to 1.12 µg/ml for difenoconazole.

Table 3.2. Range and mean of EC_{50} values (µg/ml) for five isolates of *Aspergillus uvarum* and five isolates of *Neopestalotiopsis rosae* tested for sensitivity to azoxystrobin, boscalid, and difenoconazole in two separate trials

	A. uvarum		***N. rosae***	
Fungicide	**Range**	**Mean ± SE**	**Range**	**Mean ± SE**
Azoxystrobin	0.63 - >100	NC[z]	>100	NC[z]
Boscalid	0.59 - 4.73	2.51 ± 0.53	>100	NC[z]
Difenoconazole	0.18 - 1.12	0.62 ± 0.10	0.30 - 5.06	1.81 ± 0.61

[z] NC = Not calculated. All or some isolates had higher EC_{50} values than could be measured (above 100 µg/ml); therefore, standard error (SE) was not calculated.

A photometer was used to determine the *Aspergillus* mycelial growth of fungicide amended wells compared to a control, and calculations were conducted to determine the EC_{50}. After observing wide variations in EC_{50} values between isolates, the partial cytochrome b gene was sequenced for 11 *A. uvarum* and three *A. japonicus* isolates. Amino acid variations were then compared between the isolates, with the *A. tubingensis* amino acid sequence as the template. Within *A. uvarum,* three isolates were found to have identical amino acid sequences to the template, four had two mutations, S108A and A194V, and four had three mutations, S108A, A194V, and F129L. The three *A. japonicus* isolates had two mutations, S108A and A194V. The isolates with no mutations are herein regarded as cytbWT, those with two mutations as cytb2, and three mutations as cytb3 (Fig. 2.8). Cytb3 isolates had significantly higher EC_{50} values compared to the cytb2 and cytbWT genotypes. Based on the average EC_{50} values from each genotype, the cytb3 genotype EC_{50} values were 9X higher than the cytb2 genotype and 19X higher than the cytbWT genotype (Table 3.3). The four cyb3 isolates were each collected from a different vineyard, with three vineyards in Maryland and one in Pennsylvania.

Table 3.3. The dose of azoxystrobin that inhibited *Aspergillus uvarum* growth by 50% compared to the control (EC_{50}) that was tested using a photometer in two assays. The genotype average ± standard error (SE) values followed by a different letter were significantly different according to a Tukey's HSD test.

Isolate	Mutations	Genotype name	Assay 1	Assay 2	Average	Genotype average ± SE
GP20-111	None	CytbWT	0.12	0.11	0.11	0.28 ± 0.14 b
GP20-319			0.04	0.01	0.02	
GP20-320			0.54	0.89	0.71	
GP18-93	S108A/A194V	Cytb2	0.12	1.65	0.89	0.58 ± 0.20 b
GP19-9p			0.06	0.75	0.41	
GP19-12			0.97	0.16	0.56	
GP20-322			0.88	0.06	0.47	
GP18-276	S108A, F129L, A194V	Cytb3	6.10	NA[z]	6.10	5.36 ± 0.61 a
GP19-7p			7.84	5.62	6.73	
GP19-8			4.10	NA	4.10	
GP20-194			3.72	5.27	4.50	

[z] This isolate was only tested once

3.3.4) Detached fruit sensitivity assays

A selection of isolates from blackberry, grape, and strawberry with different fungicide resistance phenotypes and genotypes were inoculated into grapes that had been exposed to fungicide treatment. Field rates of each fungicide effectively controlled the wild-type/S isolates but not the mutant/R isolates (Fig. 3.4). Between the two experiments, a few (8%) grapes not treated with a fungicide and not inoculated developed gray mold lesions, while all non-treated grapes that were inoculated with *B. cinerea* developed lesions. Different mutations within the same target gene, such as P225F, H272R, and H272Y in *sdhB*, did not have an effect on the size of the lesions. All mutant/R isolates had statistically higher mean lesion diameters than the wild-type/S isolates for each fungicide and each trial ($p < 0.01$).

With *Aspergillus,* there was a significant difference in lesion diameters between the fungicide and inoculum genotype treatments ($P < 0.001$) (Fig. 3.5A), while there was no difference between the three experiments ($P = 0.333$). Of the non-treated berries, the AUcytb2, AJcytb2, and the AUcytb3 inocula treatments resulted in significantly larger lesion diameters than the AUcytbWT treatment, indicating that the AucytbWT inoculum less aggressively colonized the fruit. There was no difference in lesion diameters between treated and non-treated berries for the AUcytb3 inoculum, but significant differences for the other three inocula. This was reflected in the percent inhibition analysis, where the AUcytb3 inoculum had the lowest percent inhibition, and the AUcytbWT inoculum was the most inhibited (Fig. 3.5B).

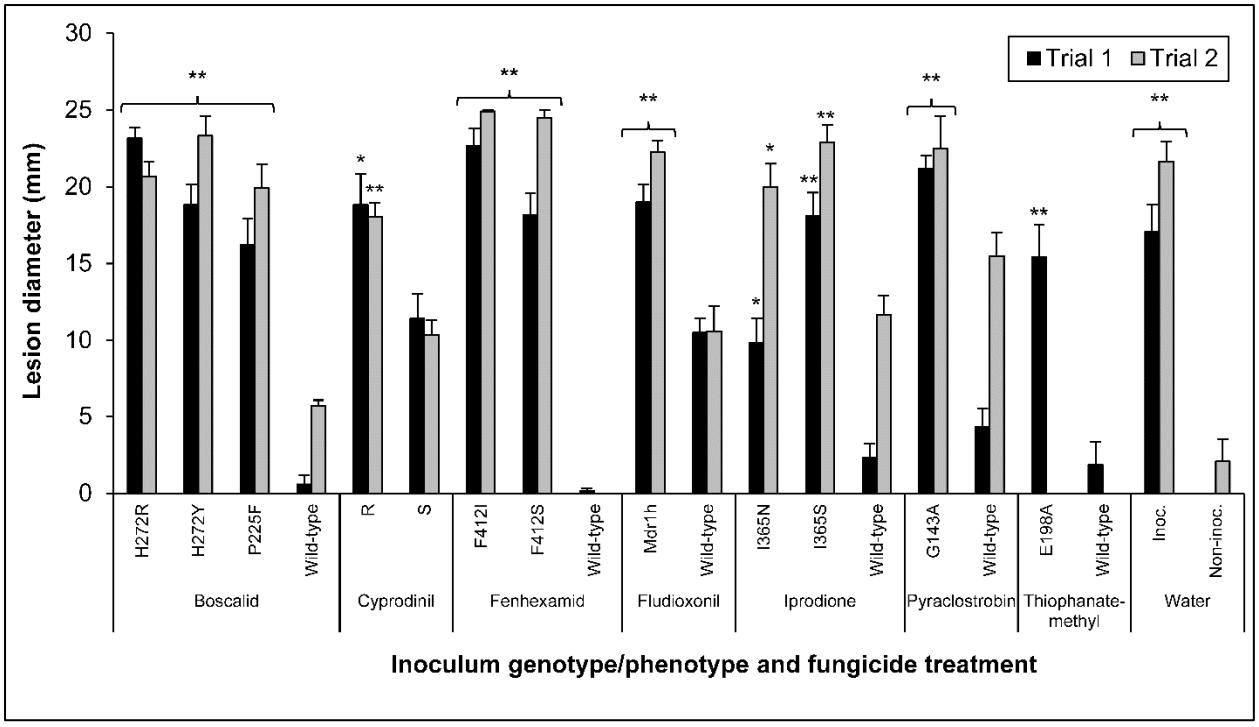

Fig. 3.4. Average lesion diameter of grapes inoculated with fifteen *Botrytis cinerea* isolates from blackberry, grape, and strawberry with various fungicide resistance genotypes/phenotypes after being treated with fungicides. Error bars represent standard error. No data was collected with thiophanate-methyl for trial 2. Significant differences between lesion diameter of mutant/R/inoculated and the wild-type/S/non-inoculated treatments for each fungicide treatment are indicated with "*" ($p < 0.01$) or "**" ($p < 0.001$) according to a Steel multiple comparisons test.

3.3.1) Molecular docking

The cytochrome b complex models for each variant displayed the location of each mutation (Fig. 3.6). The F129L mutation took place on the C helix, the A194V mutation on the E helix, and the S108A mutation near the quinone reduction (Qi) site as described by (Esser et al. 2004). The ability of the fungicide azoxystrobin to dock to the Qo binding cavity of cytochrome b complex was evaluated with 50 genetic algorithm runs for each variant of the macromolecule. On average, the shift in energy during docking was significantly greater ($P < 0.001$) for cytbWT (-4.44 ± 0.09 kcal/mol) than cytb2 (-3.17 ± 0.26 kcal/mol) and cytb3 (-2.68 ± 0.32 kcal/mol), indicating that

the system was most stable with the cytbWT variant. Of the top five most stable conformations, hydrogen bonds were observed between azoxystrobin and E273, M125, and M122 of cytbWT, E273 and M125 of cytb2, and A126 and M122 of cytb3 (Table A7; Fig. 3.6). The bonding of azoxystrobin with E273 matched that observed in x-ray crystallography by Esser et al. (2004).

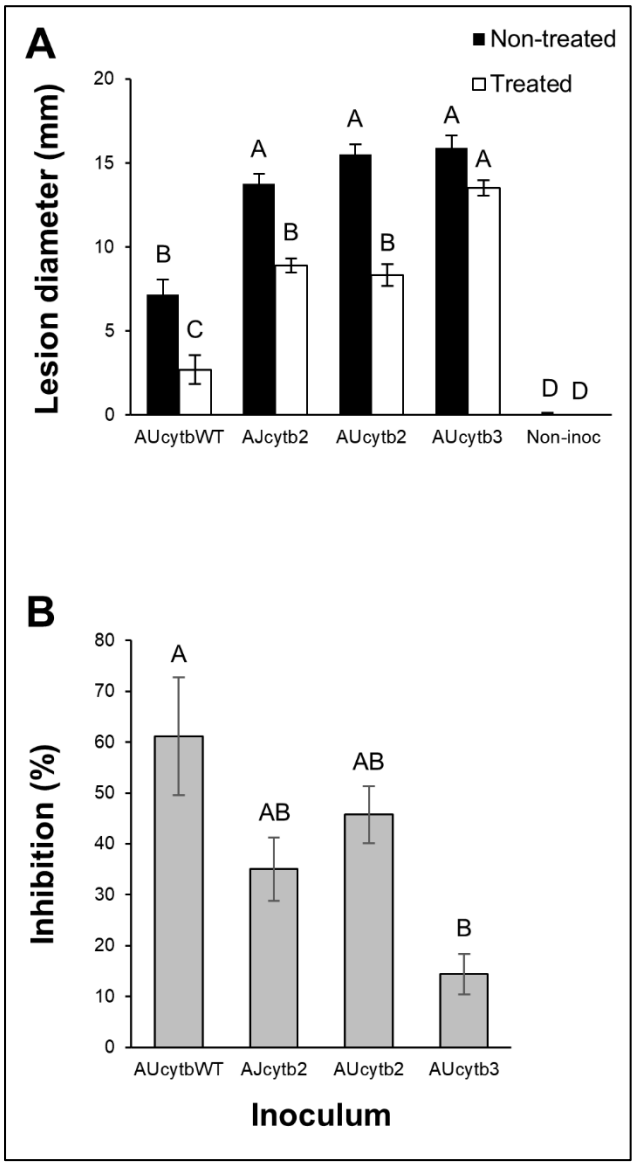

Fig. 3.5. Combined results of A) lesion diameters (mm) from three detached grape assays that were wounded and inoculated or not inoculated with three cytochrome b genotypes of *Aspergillus uvarum,* AUcytbWT, AUcytb2, and AUcytb3, and one genotype of *A. japonicus,* AJcytb2 that were either treated or non-treated with the fungicide azoxystrobin, and B) percent inhibition of lesion diameter between the treated and non-treated fruit for each genotype and species. Columns with different letters are significantly different according to a Tukey's HSD test and error bars are the standard error of the mean.

3.4) Discussion

This was the first study to conduct baseline sensitivity testing of *N. rosae* and *A. uvarum* to azoxystrobin, boscalid, and difenoconazole. These fungicides were chosen because they represent three important chemical classes of fungicides (QoIs, SDHIs, and DMIs) that are already used for control of other grape bunch rots. The *N. rosae* isolates in this study were found to be insensitive to boscalid and azoxystrobin, however more isolates may need to be tested along with molecular analyses to determine if this insensitivity is intrinsic or acquired. Only one other study has begun to assess the fungicide sensitivity of this species. Rebollar-Alviter (2020) found *N. rosae* isolates were sensitive to field rates of captan, fludioxonil + cyprodinil, difenoconazole, prochloraz, and iprodione *in vitro*. Prior research on *A. uvarum* is also limited, but five *A. uvarum* isolates were found to have similar sensitivities to closely related fungi within *Aspergillus* section *Nigri* tested for sensitivity to the clinically used demethylation inhibitors itraconazole and voriconazole (Badali et al. 2016). Also, three out of five isolates of *A. uvarum* were insensitive to azoxystrobin (Table 3.2).

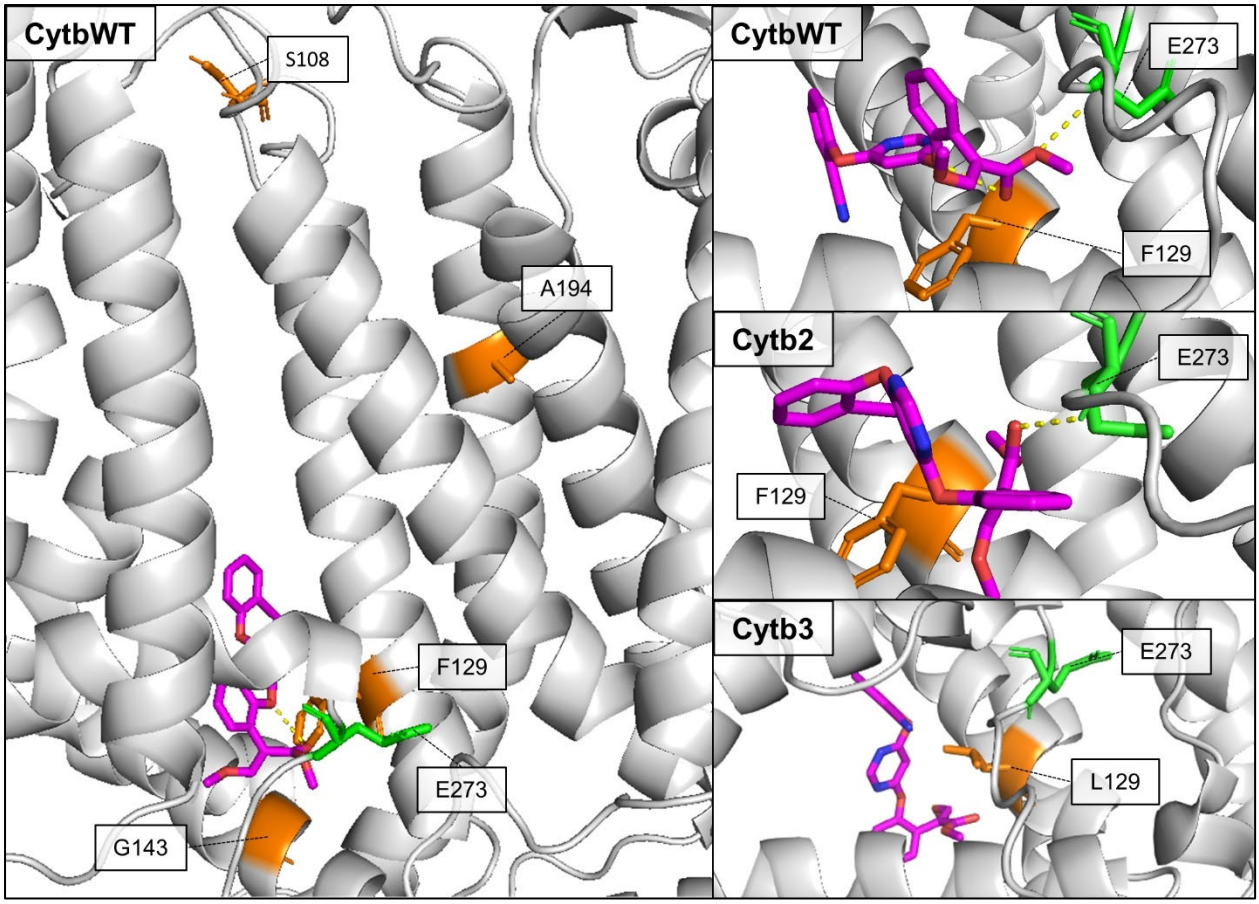

Fig. 3.6. Fungicide docking simulations of the fungicide azoxystrobin (pink) on three variants of the cytochrome b complex with the binding target residue in green and residues of potential interest in orange with hydrogen bonds between azoxystrobin and the macromolecule indicated with yellow dotted lines.

Due to the pathogenicity of *A. uvarum,* and the wide-ranging sensitivity to azoxystrobin, follow up investigations were conducted. Of a selection of isolates chosen for cytochrome b sequencing, three genotypes were identified. The wildtype designation “cytbWT” was given to the isolates with amino acid sequences that matched a previously published *A. tubingensis* isolate, WU-2223L (Yoshioka et al. 2020). This was accepted as the wildtype because WU-2223L was collected in 1960, which was before the introduction of quinone outside inhibitor fungicides. *A. tubingensis* is also in section *Nigri* of *Aspergillus* and is therefore closely related to the species identified in this study (Fig. 2.8). Due to this relatedness, the recently published

draft genome of WU-2223L may be a useful resource for future investigations of *A. uvarum* or *A. japonicus* (Yoshioka et al. 2020). The other two genotypes were cytb2, with S108A and A194V, and cytb3 with S108A, A194V, and F129L. Only the cytb2 genotype was observed with the *A. japonicus* isolates, but it is possible that other genotypes could have been observed if more *A. japonicus* isolates were collected and sequenced. This was the first time that this gene had been sequenced from these two species, and the F129L and A194V have been previously discovered in *Aspergillus flavus,* while the S108A substitution has not been reported in any fungus to our knowledge (Albakri et al. 2021; Ali et al. 2021). The F129L mutation has been associated with QoI resistance in many fungi, while A194V has not been broadly reported or cited as altering sensitivity to QoI fungicides (Fernández-Ortuño et al. 2008).

Isolates of both species and the three cytochrome b genotypes were found to vary in their sensitivity to azoxystrobin *in vitro* and in detached fruit assays (Table 3.3; Fig. 3.5). Similar results were observed in both tests, with cytbWT being the most sensitive, followed by cytb2 and cytb3. The cytochrome b sequence appeared to have a greater impact on the sensitivity to azoxystrobin than the species, as both AUcytb2 and AJcytb2 had similar sensitivities to azoxystrobin (Fig. 3.5). The difference between the three genotypes was more drastic in the photometer plate testing than the detached fruit assays, with the cytb3 isolates having much higher EC_{50} values than the other isolates (Table 3.3). This photometer technique has been previously used for assessing *Botrytis cinerea* sensitivity to QoI fungicides (Grabke and Stammler 2015). In the detached fruit assays, each inoculum was able to cause fruit rot, even when treated with the fungicide (Fig. 3.5). The berries in these assays were wounded, inoculated, and incubated in ideal conditions for this disease, and greater control of the cytbWT and ctytb2 inocula with a QoI fungicide would have likely occurred if the fruit were not wounded. One

more notable aspect was that the cytbWT isolates tended to grow slower than the other genotypes on artificial growing media and caused smaller lesions on the detached fruit than the other isolates.

The mutations in the cytochrome b gene resulted in different amino acid sequences and may have altered the ability of QoI fungicides to bind and inhibit the function of the critical cytochrome b complex (Esser et al. 2004). At position 129, the substitution of phenylalanine with leucine, replaced one hydrophobic amino acid with another, but leucine does not have an aromatic ring like phenylalanine (Fig. 3.6). Aromatic rings tend to provide stability to tertiary structures (Burley and Petsko 1985), and the absence may have altered the shape of the binding pocket, not allowing azoxystrobin to easily bind (Cao et al. 2005). With A194V, these two amino acids (Alanine and Valine) are very similar in structure with hydrophobic side chains, differing by only an alkyl group. At position 108, serine has a polar side chain and was substituted with alanine, which has a hydrophobic side chain. Therefore, this mutation likely caused more of a conformational shift in the protein structure than the mutation at position 194. In addition to the type of amino acid substitution, the location of the substitution on the enzyme is likely also critical to the effect of the mutation (Cao et al. 2005). For example, positions 129 and 143 are locations of two widely reported resistance-conferring mutations and are located inside of the binding pocket (Fig. 3.6) (Fernández-Ortuño et al. 2008). Therefore, it is apparent that mutations at these sites could cause major changes to the efficacy of the fungicide. On the other hand, positions 108 and 194 are not as close to the binding pocket, and substitutions at these sites may not have as large of an effect (Cao et al. 2005). Despite the distance from the binding picket, there did appear to be an effect of the two mutations at 108 and 194 on the binding energy during

the molecular docking, and the difference in sensitivity of the fungus between cytbWT and cytb2, and is likely due to S108A, rather than A194V (Fig. 3.6; Table 3.3).

For *Botrytis*, the mycelial growth assay was an effective and efficient way to characterize the resistance profile of many isolates. The resistance frequencies to each active ingredient were similar to previous studies (Cosseboom et al. 2019; Fernández-Ortuño et al. 2014), with high frequencies of resistance to cyprodinil, fenhexamid, iprodione, pyraclostrobin, and thiophanate-methyl (Fig. 3.1). Fernández-Ortuño et al. (2014) demonstrated that this mycelial growth assay was capable of identifying *B. cinerea* isolates with field-relevant resistance by conducting a detached strawberry assay. A detached grape assay conducted in this study demonstrated that the same discriminatory doses in the mycelial growth assay were also useful for identifying isolates with field-relevant resistance in grape cropping systems. For example, the boscalid R isolates with genotypes P225F, H272R, and H272Y all had an average lesion diameter of at least 15 mm while the boscalid S isolate with wild-type *sdhB* gene had an average lesion diameter less than 6 mm for both trials. Despite the fact that a few fungicides such as cyprodinil and fludioxonil did not seem to provide adequate control for fruit inoculated with S isolates, significant differences in lesion size were observed between S and R isolates across all fungicide treatments (Fig. 3.4). The assays were conducted under optimal conditions for disease infection using detached and wounded berries, which could explain such reduced control efficacy.

The mycelial growth assay was an effective and mostly accurate tool for quickly characterizing fungicide resistance, with initial testing revealing that 8 out of 50 resistance genotypes from target gene sequences did not align with the resistance phenotypes observed in the mycelial growth assay. After utilizing the mycelial growth assay to re-evaluate the eight isolates with discrepancies, it was concluded that the resistance phenotype of five isolates were

initially characterized incorrectly. These discrepancies may have occurred due to the qualitative and visual evaluation method used for the mycelial growth assay. Although careful considerations of each discriminatory dose were made when developing the mycelial growth assay, a single discriminatory dose can make delineating S from R isolates difficult for fungicides such as boscalid, cyprodinil, iprodione, and fludioxonil (Fernández-Ortuño et al. 2014). Weber and Hahn (2011) demonstrated the quantitative nature of cyprodinil, iprodione, and fludioxonil resistance, while resistance to boscalid, pyraclostrobin, and thiophanate-methyl appeared to be more qualitative. This is likely due to the genetic mechanism responsible for each resistance phenotype. The level of resistance to boscalid can vary between isolates that have the same *sdhB* genotype and is also dependent on which mutation has occurred in the *sdhB* gene (Grabke and Stammler 2015; Veloukas et al. 2013).

Various genotypes were observed in *B. cinerea* genes that have been associated with fungicide resistance. All mutations in β-tubulin, *bos1, cytb, erg27,* and *sdhB* have been previously reported (Amiri and Peres 2014; Chen et al. 2016; Fernández-Ortuño et al. 2016; Hahn 2014), and all but three isolates with these mutations were found to be resistant in the mycelial growth assay. Some mutations were more common than others. Out of 19 *sdhB* sequences of different isolates, 16 had H272R, 2 had P225F, and 1 had H272Y. The genotype H272R was by far the most prevalent from this small selection of sequences and this mutation generally only confers field-relevant resistance to boscalid and not the other SDHIs (Hu et al. 2016). A few isolates with different *sdhB* genotypes had varying sensitivities to the two recently released SDHIs, pydiflumetofen and inpyrfluxam, and the effect of the mutation on the EC_{50} value was found to be statistically significant for both fungicides. Their different chemical structures may impact the way that these fungicides interact with the *sdhB* target site of *B.*

cinerea and the level of fungicide resistance that could be gained from mutations in *sdhB* (Hu et al. 2016). SDHIs have been placed into different chemical groups (inpyrfluxam and benzovindiflupyr are pyrazole-4-carbamates); however, this does not appear to help predict SDHI efficacy against *Botrytis* with different *sdhB* genotypes (Fernández-Ortuño et al. 2017; Hu et al. 2016).

In this study, PDA was used for the sensitivity (EC_{50}) testing of SDHIs, while YBA was used for resistance phenotyping using single discriminatory dosages. The use of YBA with a serial dilution method for sensitivity testing was initially attempted; however, mycelial growth on this medium was limited for all treatments including the non-amended plates, and the diametric measurements could not be used to calculate accurate EC_{50} values. YBA has been used for sensitivity testing using a microtiter method (Stammler and Speakman 2006) and for resistance phenotyping using discriminatory doses (Fernández-Ortuño et al. 2014; Weber and Hahn 2011). However, others had issues using YBA in serial dilution or spiral gradient-based methods for SDHI sensitivity testing and opted for PDA (Amiri et al. 2014; Fernández-Ortuño et al. 2017). When PDA is used for sensitivity testing of *B. cinerea* to SDHIs, it appears to yield higher EC_{50} values than YBA, but relative comparisons between *sdhB* genotypes can be made. For example, *B. cinerea* sensitivity to benzovindiflupyr in this study was higher than in a previous study that used YBA in the microtiter method, however, similar relationships were observed between different *sdhB* mutants (Hu et al. 2016).

With regards to MDR genotypes, six isolates were found to be R to fludioxonil. Of these, five were classified as MDR1 and one as MDR1h according to their *mrr1* genotypes. To our knowledge, this is the first report of MDR1 isolates from red raspberry and black raspberry and MDR1h isolates from red raspberry. MDR1 isolates have been previously isolated from

blackberry, strawberry, and grape, and MDR1h have been isolated from grape and blackberry (Fernández-Ortuño et al. 2015; Leroch et al. 2013). The six MDR1/MDR1h isolates contained two insertions in *mrr1*, which is the signature of a unique clade called *B. cinerea* group S (Leroch et al. 2013). When compared to *B. cinerea* isolates B05.10 and T4, these MDR1/MDR1h isolates contained previously reported amino acid variations that have been associated with the MDR1 phenotype: D354Y, M432T, I443L, F568S, R634K, N666G, and G702S (Fernández-Ortuño et al. 2015). Interestingly, two of these MDR1 isolates had the same *mrr1* genotype as the non-MDR *B. cinerea* group S isolate 5d5 (Fig. 3.3). A recent study demonstrated that the *atrB* overexpression that leads to fludioxonil resistance (indicative of MDR1 phenotype) is not always caused by mutations in *mrr1* in *B. fragariae* (Hu et al. 2019). Further investigation is needed to understand if the same phenomenon may be responsible for the fludioxonil resistance that occurred in these isolates. A selection of isolates was also screened for the MDR2 genotype, but none were found. The distribution of MDR2 appears to vary by region, as it was more common in French than German vineyards (Kretschmer et al. 2009; Mernke et al. 2011).

Different levels of fungicide resistance were found in each crop, with a higher median CCR value found in blackberry, red raspberry, and strawberry than in grape and black raspberry. There are many factors that can result in higher overall fungicide resistance frequencies in one crop versus another, such as crop susceptibility, and chemical and cultural practices that can be influenced by the crop value. Strawberries are an example of a high selection pressure cropping system due to the highly susceptible crop, intensive fungicide spray programs in the nurseries and fruit production fields, and annual re-planting (Oliveira et al. 2017). Other factors unique to Mid-Atlantic small fruit and grape production may also affect the frequencies of resistance

observed. Growing for the u-pick market might favor use of resistance-prone site-specific fungicides that are low in toxicity and have short re-entry intervals. Also, multiple small fruit are typically grown in close proximity on the same farm. This has the potential to allow resistant subpopulations to drift between the adjacently planted crops (Amiri et al. 2018). Despite the differences between the cropping systems, fungicide resistance appears to be a significant issue in each crop tested, and resistance management strategies such as rotation or tank-mixing and the use of spray decision support systems should be implemented wherever fungicides are applied (Amiri et al. 2019; Cordova et al. 2017).

This study revealed the current fungicide resistance profile of *B. cinerea* in the Mid-Atlantic, and that only two site-specific chemical classes (PPs and SDHIs) of fungicides showed low frequency of resistance (≤ 12%). Due to this, small fruit and wine grape growers have few effective fungicide rotation options since fungicides are typically applied multiple times per season to achieve adequate gray mold control. Resistance is not an issue with multisite products like captan, thiram, and biological control materials; however, these products are generally not as effective as site-specific fungicides. The future efficacy of PPs and SDHIs depends on the reduction of selection pressure by reducing the number of site-specific fungicide applications per season and minimizing the amount of *B. cinerea* entering and surviving in production fields (Cordova et al. 2017; Oliveira et al. 2018). This is clearly a challenge, as resistant isolates of *B. cinerea* can be easily transferred with planting stock and can be blown from crop to crop due to *B. cinerea's* wide host range (Jarvis 1962; Oliveira et al. 2017). Results from this study validated the usefulness of a previously developed bioassay for resistance detection in *B. cinerea* from grape and broadened the knowledge of the impact of various *sdhB* mutations on the efficacy of new SDHI fungicides.

The *Aspergillus* and azoxystrobin sensitivity results appear to demonstrate the selection of resistance to QoI fungicides in *Aspergillus* populations in vineyards, which is interesting because growers in the Mid-Atlantic do not typically apply fungicides for the prevention of *Aspergillus* fruit rot. This represents off-target resistance selection, which has been raised as a possible phenomenon in DMI resistance with the human pathogen *A. fumigatus* (Verweij et al. 2009). Azoxystrobin and other QoI fungicides are used to control many fungal diseases in agriculture and can be highly effective. It is apparent that the fungicides applied in a field induce a selection pressure on all sensitive fungi that are exposed, not just the target organism. One issue is that QoI fungicides are also present in many pre-mixture fungicide formulations, and excess non-target selection in more threatening pathogens (e.g., *Colletotrichum* spp.) could occur when the QoI fungicide in the mixture is not effective against the target (e.g., *Botrytis cinerea*). Due to these implications, resistance management strategies are of high importance for the prevention of resistance selection in both the target and non-target pathogens in the environment and field.

Chapter 4: A SYBR Green qPCR Method for Detecting and Quantifying Spores of *Colletotrichum acutatum* and *C. gloeosporioides* Species Complexes Causing Ripe Rot of Grape

4.1) Introduction

Species of *Colletotrichum* are significant pathogens to many important crops, and two species complexes, the *Colletotrichum acutatum* and the *C. gloeosporioides* complexes, can be especially pathogenic on a variety of fruit crops such as apple, grape, peach, blueberry, and strawberry (Dowling et al. 2020). In wine grapes, both complexes cause the ripe rot disease, with symptoms rapidly progressing just before harvest. Ripe rot control is critical because a low severity of ripe rot can cause off flavors and reduce the quality of wine produced from infected grapes (Meunier and Steel 2009). *Colletotrichum* spp. have been shown to overwinter in vineyards and to infect flower and fruit tissues (Samuelian et al. 2012). However, the multiple species of *Colletotrichum* differ in pathogenicity and fungicide sensitivity (Greer et al. 2011). Further understanding of the presence and prevalence of different *Colletotrichum* spp. in a vineyard using spore traps can provide insight for improved management efforts as it has with grape powdery mildew (Thiessen et al. 2017).

Ripe rot is caused by at least 12 *Colletotrichum* species, the most prevalent belonging to either the *C. acutatum* or *C. gloeosporioides* complexes (Echeverrigaray et al. 2019; Lei et al. 2016; Oliver 2018; Pan et al. 2016; Yan et al. 2015; Yokosawa et al. 2020). *C. perseae, C. viniferum, C. hebeiense, C. conoides, C. aenigma, C. fructicola, C. kahawae,* and *C. gloeosporioides* sensu stricto belong to the *C. gloeosporioides* complex, while *C. fioriniae, C.*

nymphaeae belong to the *C. acutatum* complex. *C. cliviicola* and *C. capsici* are not in either complex and have not been reported on grape in North America (Jayawardena et al. 2016). The most prevalent species appear to vary by region, but the *C. acutatum* complex (predominantly *C. fioriniae*) was the most prevalent in the Mid-Atlantic U.S., and species within this complex may be more pathogenic to grapes than those of *C. gloeosporioides* complex (Greer et al. 2011; Oliver 2018).

The life cycle of ripe rot may be complicated due to the many fungal species involved; however, it is known that *C. acutatum* can overwinter on mummified bunches and woody tissues (Samuelian et al. 2012). *Colletotrichum* spp. have a wide host range and have been isolated from many groundcover and tree species that inhabit and surround vineyards in the Eastern U.S. (Martin and Peter 2021). *Colletotrichum* conidia disseminate primarily via rain splash, but some species may also produce ascospores that disseminate through wind (Madden 1993). Ascospores are not readily produced by *C. acutatum* complex spp. but can be produced by *C. gloeosporioides* complex spp. (Sutton and Shane 1983). Conidia of *Colletotrichum* spp. have also been able to infect grape inflorescences and cluster tissues from bloom until harvest (Oliver 2016; 2018; Samuelian et al. 2014). Once initial infection occurs, *Colletotrichum* can produce secondary conidia and remain latent post-infection (Oliver 2018). However, it is unclear how much inoculum is naturally present in a vineyard throughout the season.

Spore traps can be used to detect pathogens for many purposes, including disease warning systems and epidemiological studies (Thiessen et al. 2017). Fungi that disseminate aerially can be trapped using volumetric methods that can quantify the density of inoculum in the atmosphere (Quesada et al. 2018; Thiessen et al. 2016). Water dispersed fungi are generally trapped via passive methods such as funnel type traps, microscope slides, or petri dishes placed

throughout a field (Eskalen and Gubler 2001; Martin and Peter 2021). In vineyards, airborne spores of *Erysiphe necator* have been trapped by volumetric samplers placed outside of the canopy that impacted spores onto a sampling surface (Thiessen et al. 2016). Vaseline-coated microscope slides have been attached to grape cordons used to trap water dispersed spores of *Phaeomoniella* and *Phaeoacremonium* (Eskalen and Gubler 2001).

Spore presence on traps can be quantified using in vitro, microscopy, and molecular based methods, and quantitative real-time PCR (qPCR) has become the standard method for spore quantification in recent years (Mahaffee and Stoll 2016). In vitro and microscope methods may not be accurate or effective for all fungal species and may be very time consuming. Molecular based methods have the potential to be more specific to a desired genotype and qPCR can be used to accurately quantify the amount of DNA on a spore trap. The DNA quantity can be used to estimate the number of spores on each spore trap (Martin and Peter 2021; Quesada et al. 2018). TaqMan qPCR has been used to detect and quantify *C. acutatum* and *C. gloeosporioides* inoculum in infected grape berries, and strawberry leaves and fruit, and in apple orchards (Debode et al. 2009; Garrido et al. 2009; Martin and Peter 2021; Samuelian et al. 2011). SYBR Green qPCR may be more cost-effective than TaqMan assays, therefore more suitable for large scale spore trapping applications. Further, previous methodologies used primers targeting the internal transcribed spacer (*ITS*) region, which has a high copy number and allows for detection of low DNA quantities (Debode et al. 2009). However, multi-copy rRNA regions such as *ITS*, can vary in copy number between different strains and species (Debode et al. 2009; Longo et al. 2013), therefore some studies have opted to target single-copy genes such as β-tubulin (Pouzoulet et al. 2013). Due to the multiple species of *Colletotrichum* that are present in vineyards, a single-copy gene would be a preferred target for spore trapping applications.

The inoculum dispersal of *Colletotrichum* spp. in vineyards has not yet been assessed, and a spore-trapping method for tracking and quantifying inoculum of this pathogen will further elucidate its life cycle. As there are multiple species of *Colletotrichum* that cause ripe rot and may behave differently, the ability to quantify different genotypes is necessary. QPCR has been demonstrated as a reliable and genotype-specific method and could serve as an effective tool for this purpose. Therefore, the objectives of this study were to create a qPCR-based spore trapping method for accurately and specifically quantifying DNA and conidia of fungi in the *C. acutatum* and *C. gloeosporioides* species complexes. This method will be a useful tool for increasing the epidemiological understanding of *Colletotrichum* spp. in grape production and could be utilized for other contexts where the study of *C. acutatum* and *C. gloeosporioides* complexes is needed.

4.2) Materials and Methods

4.2.1) Primer design and specificity

Several candidate primer pairs were designed for use in qPCR to quantify the number of spores of *Colletotrichum* spp. within either the *C. acutatum* or *C. gloeosporioides* complexes on spore traps. Primers were created using the online software Benchling (www.benchling.com) with reference sequences of β-tubulin*, ITS,* and *gapdh* of *Colletotrichum* spp. that were previously associated with ripe rot (Table A2). Primers were designed to amplify an 80-200 bp region and to only bind to DNA of *C. acutatum* or *C. gloeosporioides* complex species. These primers and *C. acutatum* complex specific primers developed in a previous study were initially tested in PCR for specificity to either DNA of an isolate from the *C. acutatum* complex or an isolate from the *C. gloeosporioides* complex (Debode et al. 2009; Samuelian et al. 2011). Satisfactory primers were then tested for specificity with DNA of fungi commonly isolated from grapes in Mid-

Atlantic vineyards including *C. aenigma, C. fioriniae, C. fructicola, C. nymphaeae, Alternaria* sp., *Aspergillus* sp., *Botrytis* sp., *Nigrospora* sp., *Cladosporium* sp., *Phomopsis* sp., *Penicillium* sp., *Fusarium* sp., and *Pestalotiopsis* sp.

The DNA of each species was amplified through PCR using three different primer pairs. Each PCR was conducted with a total volume of 20 µl with 1x PerfeCTa SYBR Green FastMix (Quantabio, Beverly, MA), 0.25 µM of each primer, and 2 µl DNA template (10 ng/µl). The first PCR utilized universal primers (i.e. ITS1/ITS4) that amplified the *ITS* region as described above. The second used primers designed to only amplify the target sequence of *C. acutatum* complex species, and the third with primers designed to only amplify the target sequence of *C. gloeosporioides* complex species. Thermocycling conditions for the second and third PCR reactions were 95 °C for 3 min followed by 35 cycles of 95 °C for 20 s, 58 °C for 20 s, and 72 °C for 20 s, then a final extension step of 72 °C for 5 min. This was followed by electrophoresis on a SYBR Safe DNA (Invitrogen) stained, 1% agarose gel at 100 volts for 40 minutes. Primers were considered suitable for continued testing if single bands of expected length were observed only for the desired *Colletotrichum* spp. This test was conducted with the successful primer pairs twice. The ability of the successful primer pairs to distinguish between the two *Colletotrichum* species complexes was also tested on the DNA extracted from all 48 *Colletotrichum* isolates evaluated in this study.

4.2.2) Standard curve

The DNA templates extracted from mycelia of four isolates identified as *C. fioriniae, C. nymphaeae, C. aenigma,* and *C. fructicola* was quantified using a Qubit fluorometer (Thermo Fisher Scientific Inc., Waltham, MA) and diluted to 10 ng/µl with pure water. A standard curve was then created for the candidate primer pairs specific to either the *C. acutatum* (with the *C.*

fioriniae and *C. nymphaeae* DNA templates) or *C. gloeosporioides* (with the *C. aenigma* and *C. fructicola* DNA templates) complexes in qPCR by creating six, 1:10 serial dilutions of the DNA templates. Each dilution of the DNA template was replicated three times. The qPCR was conducted with the same reaction mixture in the previous paragraph in a BioRad CFX 96 instrument with a thermocycling protocol of 95 °C for 3 min, 45 cycles of 95 °C for 20 sec, 58 °C for 20 sec, and 72 °C for 20 sec, followed by a melt curve from 65 to 95 °C with a 5 sec hold and 1 °C per cycle. The threshold for the calculation of the quantification cycle (Cq) value was automatically set by the Bio-Rad CFX 96 instrument. The log gDNA template concentrations were regressed against the Cq values to create the standard curve. Primer pairs were deemed suitable for the spore trap analysis if the efficiency of the standard curve was between 90 and 110% and if the R-square value was above 0.98 (Quesada et al. 2018).

4.2.3) Sensitivity assay and spore calculation

The sensitivity of the assay was tested by extracting DNA from known quantities of spores. First, *C. fioriniae* and *C. aenigma* were grown on quarter-strength PDA and incubated in the dark at 25 °C for one week. Conidia were suspended by repeatedly pipetting 1 ml of sterile deionized water on the sporulating plates of each species. The spore suspension concentrations were calculated using a hemocytometer and were diluted to $1x10^7$ conidia/ml and then conidia of both species and water as a control were pipetted onto 20 x 20 mm areas on the surface of Vaseline coated microscope slides, a previously described spore trap (Eskalen and Gubler 2001). The spore suspension and water droplets were then allowed to dry overnight before extraction of DNA.

For the DNA extraction, a sterile cotton swab was used to scrape the Vaseline from the 20 x 20 mm area of the microscope slide. The tip of the cotton swab was cut off and placed into the PowerBead tube of the DNeasy PowerLyzer PowerSoil DNA Extraction Kit (Qiagen, Hilden,

Germany), except that the 0.1 mm glass beads were replaced with 2.4 mm diameter metal beads. A FastPrep 24 (MP Biomedicals, Irvine, CA) instrument was used for the homogenization step of the extraction for 3 rounds of 45 seconds at 5 m/s with 5 minutes of rest between rounds. The remainder of the DNA extraction was conducted according to the kit manufacturer's instructions. Serial dilutions of the DNA extracted from the *C. fioriniae* and *C. aenigma* conidia were created with dilutions ranging from DNA representing $1x10^7$ to 10 conidia and $5x10^6$ to 5 conidia in two separate reactions. Triplicates of each extraction and the extraction control was amplified in qPCR as described above and a standard curve was created. The limit of detection (LOD) was defined as the least amount of conidia that could be consistently amplified. The limit of quantification (LOQ) was defined as the least amount of conidia that amplified with coefficient of variation below 25% (Kralik and Ricchi 2017).

4.3) Results

4.3.1) Primer specificity

The β-tubulin, *gapdh*, and *ITS* regions were evaluated for their use as targets for *C. acutatum* and *C. gloeosporioides* complex-specific primers, and primers targeting the β-tubulin gene were the most successful for the *C. acutatum* (BtubAcuf/BtubAcuGlor) and the *C. gloeosporioides* complexes (BtubGlof/BtubAcuGlor) (Table A1). The *C. acutatum* complex specific primers created a 142 bp amplicon and the *C. gloeosporioides* complex specific primers created a 138 bp amplicon (Fig. A4). These primers only amplified the target region of the desired species, while the universal ITS1/4 primers amplified all DNA templates (Fig. 4.1). The complex-specific primers were also able to successfully characterize all 48 isolates tested in this study according to their *Colletotrichum* species complex in standard PCR (data not shown). These results aligned

with the multilocus identification of a selection of isolates from each morphological group. The primers targeting the *ITS* region created in this study and a previous study revealed more vivid bands than those targeting the β-tubulin under ultraviolet light, but faint bands occurred with DNA from non-target fungi (data not shown).

4.3.2) Standard curve and assay sensitivity

The standard curves revealed that both the *C. acutatum* and *C. gloeosporioides* specific primers were able to amplify the partial β-tubulin gene of the target species with an acceptable efficiency (between 90 and 110%) and low variance ($r^2 > 0.98$) with mycelial DNA of all four species (Fig. 4.2) and conidial DNA from *C. fioriniae* and *C. aenigma* (Fig. 4.3). The LOD with the *C. acutatum* complex specific primers was determined to be 50 *C. fioriniae* conidia per spore trap. The LOD with the *C. gloeosporioides* specific primers was determined to be 100 *C. aenigma* conidia per spore trap (Fig. 4.3). The melt curve peak of *C. fioriniae* DNA was 80-81 °C with the *C. acutatum* specific primers and was 81-82 °C with the *C. gloeosporioides* specific primers and *C. aenigma* DNA.

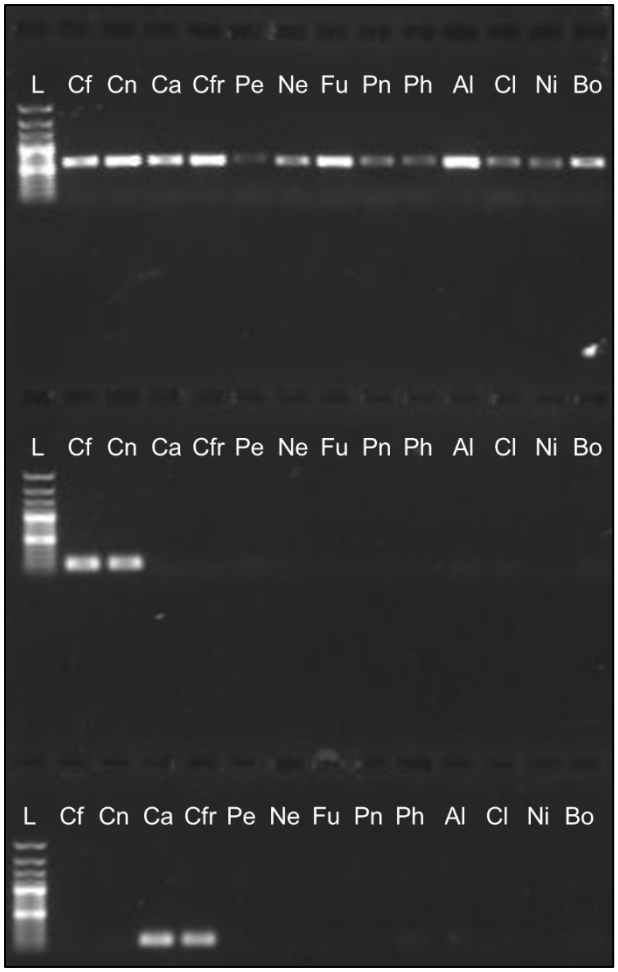

Fig. 4.1. Photograph of a 1% agarose gel with three sets of PCR products amplified with primers ITS1/4 (top row), BtubAcuF/BtubAcuGlor (middle), and BtubGloF/BtubAcuGlor (bottom row) with a 100 bp plus ladder (L). Cf = *Colletotrichum fioriniae,* Cn = *C. nymphaeae*, Ca = *C. aenigma,* Cfr = *C. fructicola*, Pe = *Pestalotiopsis* sp., Ne = *Neopestalotiopsis* sp., Fu = *Fusarium* sp., Pn = *Penicillium* sp., Ph = *Phomopsis* sp., Al = *Alternaria* sp., Cl = *Cladosporium* sp., Ni = *Nigrospora* sp., and Bo = *Botrytis* sp.

4.4) Discussion

An effective method for detecting and quantifying spores of *Colletotrichum* spp. was developed in this study. Furthermore, the primers in this study were created to selectively target *Colletotrichum* spp. at the complex level, rather than the species level. Ten out of twelve *Colletotrichum* spp. that cause ripe rot are within the two complexes tested in this study (Echeverrigaray et al. 2019; Lei et al. 2016; Oliver 2018; Pan et al. 2016; Yan et al. 2015; Yokosawa et al. 2020), therefore our primers should apply to *Colletotrichum* spp. from other vineyards, and possibly other crops where the two complexes are of concern such as apples or strawberries (Dowling et al. 2020).

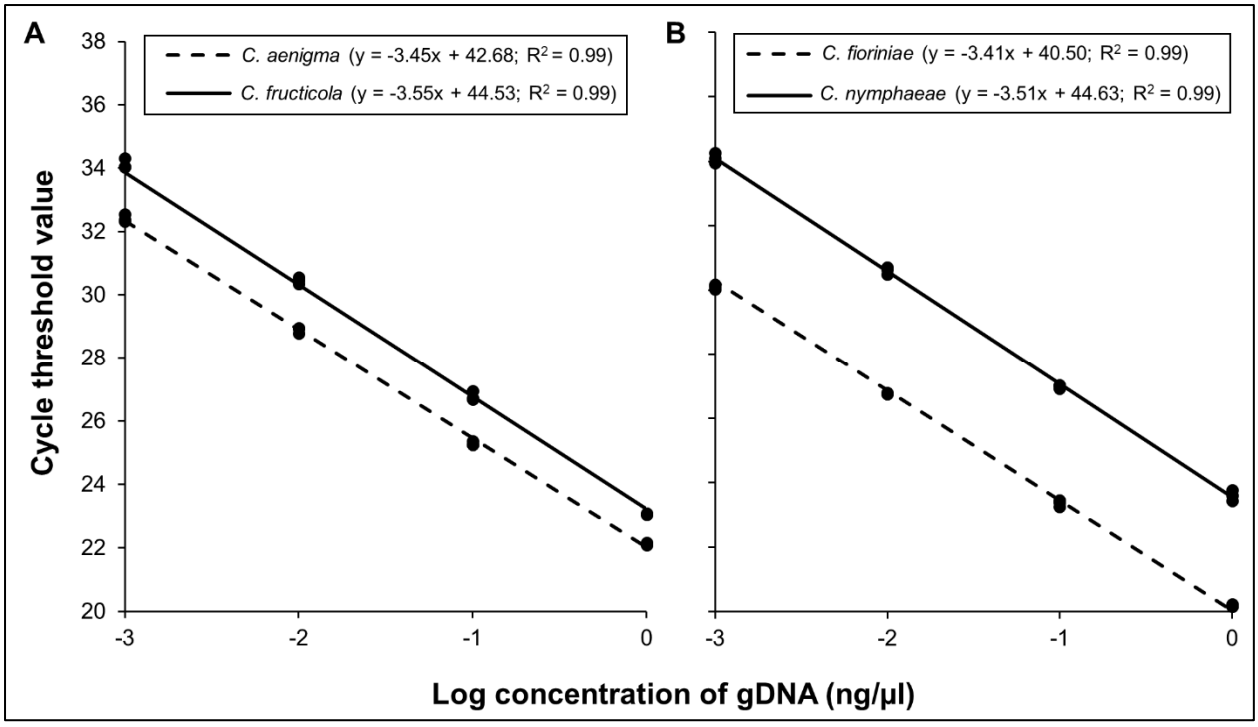

Fig. 4.2. Standard curve of serial dilutions of gDNA extracted from mycelium of (a) two *Colletotrichum gloeosporioides* complex species (*C. aenigma* and *C. fructicola*) in qPCR with *C. gloeosporioides*-specific primers BtubGlof/BtubAcuGloR and (b) two *C. acutatum* complex spp. (*C. fioriniae* and *C. nymphaeae*) in qPCR with *C. acutatum* complex-specific primers BtubAcuf/BtubAcuGlor.

The assay used primers targeting the β-tubulin gene of *Colletotrichum* spp. within two commonly occurring species complexes and did not detect other common fungi associated with asymptomatic and fruit rot symptomatic grape berries in Mid-Atlantic vineyards (Cosseboom and Hu 2021c). All fungal genera screened in this study have also been previously identified on grapes in other regions of the world; therefore, this assay will likely be applicable in other vineyards (Barbetti 1980; Jayawardena et al. 2015; Rousseaux et al. 2014; Steel et al. 2007). This study also utilized a SYBR Green qPCR method which can be less specific than the TaqMan method, both of which have been used in spore trapping applications (Martin and Peter 2021; Quesada et al. 2018). On the other hand, β-tubulin appeared to be an appropriate target for the

SYBR Green method, as primers targeting the *ITS* region were not sufficiently specific. This may be due to the highly conserved nature of the *ITS* region. SYBR Green technology may also be more desirable than TaqMan for long term or large-scale spore trapping applications due to lower cost reagents. Furthermore, the single-copy nature of β-tubulin was more desirable than the multi-copy *ITS* region, since this assay targets two *Colletotrichum* species complexes that contain many species which may vary in *ITS* copy number (Pouzoulet et al. 2013). This will allow the accurate use of this assay for other grape regions where different species within the two complexes have been reported as causing ripe rot (Jayawardena et al. 2016; Lei et al. 2016).

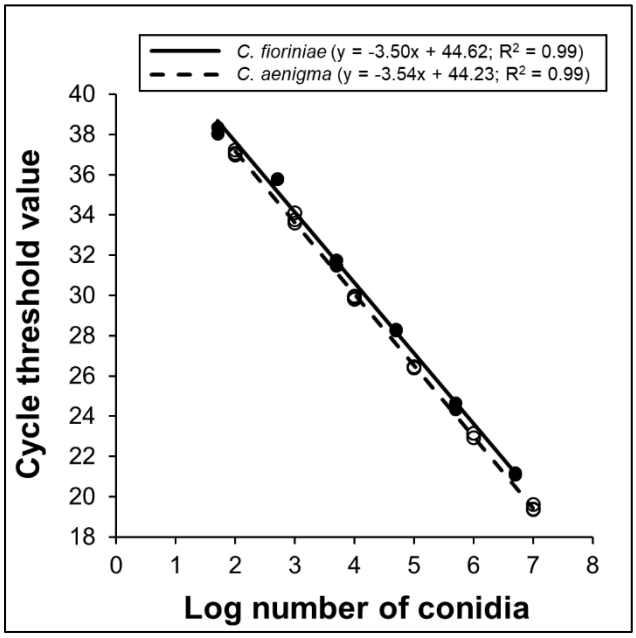

Fig. 4.3. Standard curve of serial dilutions of gDNA extracted from *Colletotrichum* conidia placed onto Vaseline-coated microscope slides. *C. fioriniae* was amplified with *C. acutatum* complex specific primers BtubAcuf/BtubAcuGlor and *C. aenigma* was amplified with *C. gloeosporioides* specific primers BtubGlof/BtubacuGlor.

The primers developed in this study had an acceptable sensitivity and were found to detect as low as 50 conidia of *C. fioriniae* with the *C. acutatum* complex specific primers, and as low as 100 conidia of *C. aenigma* with the *C. gloeosporioides* complex specific primers. A previous study has developed both a SYBR Green and a TaqMan assay for the detection of the

C. acutatum complex and targeted the *ITS* region and found that their SYBR Green assay was more sensitive but chose to continue with the TaqMan assay due to specificity concerns (Debode et al. 2009). Their assay could reliably detect as low as 25 conidia. The *ITS* region has also been the target for spore quantification of other fungi due to the high copy number per genome, resulting in highly sensitive assays (Primiano et al. 2021; Schweigkofler et al. 2004; Thiessen et al. 2017). However, *Colletotrichum* spp. typically produce large quantities of conidia in natural and agricultural settings with most spore traps in non-sprayed forests and apple orchards detecting over 1000 *C. acutatum* conidia (median no. conidia > 1000; Martin and Peter 2020). Therefore, the SYBR Green assay from this study should easily detect and quantify *Colletotrichum acutatum* and *gloeosporioides* species complexes in spore trapping applications.

Due to the sensitivity and specificity of the spore quantification protocol developed in this study, it should be applicable for spore trapping detection and quantification of the two detrimental *Colletotrichum* species complexes found causing ripe rot worldwide (Greer et al. 2011; Oliver 2018). Furthermore, the primers could also be utilized in standard PCR as a simple *C. acutatum* or *C. gloeosporioides* species complex identification tool. The understudied etiology of the ripe rot disease warrants further investigation, and a reliable, yet sensitive spore quantification method would be a valuable assay for the study of the epidemiology and potentially disease prediction of ripe rot and other diseases caused by these two *Colletotrichum* species complexes.

Chapter 5: Ontogenic Susceptibility of Grape Clusters to Ripe Rot, caused by the *Colletotrichum acutatum* and *C. gloeosporioides* Species Complexes

5.1) Introduction

Ripe rot of grape is a destructive fruit rot caused by species within the genus of *Colletotrichum* with an understudied etiology and epidemiology. It is a fruit disease that typically occurs and progresses rapidly during the pre-harvest stage, occurring in regions with a warm and wet ripening season, such as the Mid-Atlantic U.S. (Oliver 2018), southeastern Australia (Melksham et al. 2002), and southern China (Yan et al. 2015). Ripe rot is caused by at least 13 *Colletotrichum* species, with the most prevalent belonging to either the *C. acutatum* or *C. gloeosporioides* complexes (Echeverrigaray et al. 2019; Lei et al. 2016; Oliver 2018; Pan et al. 2016; Yan et al. 2015; Yokosawa et al. 2020). Prior studies have greatly enhanced the ability to control this disease, however devastating ripe rot outbreaks continue to occur in the Mid-Atlantic and other regions (Oliver 2016; Samuelian et al. 2014).

Fungicides are the primary tool used to manage ripe rot, and multiple sprays per season are typically applied for ripe rot and other fruit rots of concern (Greer et al. 2011). However, the timing of fungicide applications for ripe rot control is complicated by the lengthy growing season (up to 6 months), limited effective fungicides (Dowling et al. 2020), as well as the potential for late season fungicide applications to interfere with winemaking (Gava et al. 2021). In addition, the popularity of growing highly susceptible French cultivars such as Chardonnay, Merlot, and

Cabernet Sauvignon may have further contributed to the frequent outbreaks of ripe rot in the Mid-Atlantic and other growing regions (Shiraishi et al. 2007).

Phenological stages of grape clusters can vary in their susceptibility to important fungal and oomycete diseases. Ontogenic resistance is a critical component of the etiology of multiple grape fruit rotting diseases including downy mildew (*Plasmopara viticola*), powdery mildew (*Erysiphe necator*), black rot (*Guignardia bidwellii*), and Botrytis bunch rot (*Botrytis cinerea*) (Gadoury et al. 2003; Kennelly et al. 2007; McClellan and Hewitt 1973; Molitor and Berkelmann-Loehnertz 2011; Petit et al. 2010), with the bloom stage being particularly susceptible. For instance, grape clusters developed severe powdery mildew symptoms only if they were inoculated with *Erysiphe necator* from a few days pre-bloom to two to three weeks post-bloom (Gadoury et al. 2003). The discovery and understanding of ontogenic resistance to these diseases has allowed for a reduced number of fungicide applications per season.

Currently, there is little information on the susceptibility of grape phenological stages to ripe rot, making more targeted and effective fungicide applications impossible. A few studies have demonstrated the ability of *Colletotrichum* spp. to cause latent infections, being isolated from naturally inoculated, asymptomatic grape clusters at bloom (BBCH 65), veraison (BBCH 83), pre-harvest (BBCH 85), and harvest (BBCH 89) stages (Lorenz et al. 1995; Steel et al. 2007). Furthermore, one study found that a fungicide application at the bloom stage significantly reduced the incidence of latent infection; however, the severity of ripe rot symptoms at harvest was not reported (Samuelian et al. 2014). A similar study also artificially inoculated clusters at various phenological stages, but low severities of ripe rot were observed from each treatment at the harvest stage (Oliver 2016). It remains unclear which factors are required for activating latent

ripe rot infections, or whether grape cluster ontogeny plays a role, especially in the high ripe rot severities that have been observed in Mid-Atlantic vineyards.

Recent studies have started to uncover the life cycle and inoculum sources of *Colletotrichum* spp. in vineyards. *Colletotrichum* spp. can overwinter on dormant grape tissues and on common plant species that surround Mid-Atlantic vineyards (Martin and Peter 2021; Samuelian et al. 2012); therefore, initial inoculum is likely present in the early season. Spore traps have been used as an inoculum detection method to understand the presence and biology of pathogens, and real-time quantitative PCR (qPCR) has been used in conjunction with spore traps to quantify inoculum (Thiessen et al. 2016). The dispersal of *Colletotrichum* spp. in vineyards has not yet been assessed, but species within the *C. acutatum* complex tend to produce water-dispersed conidia, while species within the *C. gloeosporioides* complex can also produce airborne ascospores (which can also be aided by rain) (Madden 1993; Sutton and Shane 1983). QPCR has been used to detect and quantify *C. acutatum* colonization in infected grape tissues (Samuelian et al. 2011), but spore trapping methods have not been used to quantify spores of *Colletotrichum* in vineyards.

In this study, the epidemiology and etiology of ripe rot was investigated under both field and lab settings, with the goals of i) investigating the susceptibility of grape clusters at various phenological stages to ripe rot in vineyards, ii) isolating and identifying *Colletotrichum* from ripe rot symptomatic grapes, iii) quantifying inoculum of the *C. acutatum* and *C. gloeosporioides* species complexes throughout the season with spore traps, and iv) tracking weather variables. Insights from this study may provide improved understanding of timing of ripe rot infection and development, which in turn would identify critical control points and avoid unnecessary chemical input.

5.2) Materials and methods

5.2.1) Bagging timing and evaluation of ripe rot severity

In two vineyards and three cultivars, six individual trials were conducted from 2019 to 2021. These trials involved cluster bagging to expose phenological cluster stages to naturally occurring *Colletotrichum* inoculum and environmental conditions. The two vineyards were a commercial vineyard (SMT) in Burkittsville, Maryland, and a research vineyard at the Wye Research & Education Center (Wye REC) of University of Maryland in Queenstown, Maryland. Specifically, two adjacent rows of Cabernet Sauvignon planted in 2014 and Merlot planted in 2013 with a history of severe ripe rot (Hu and Cosseboom 2019) were used for the trials at SMT in 2019 and 2020, and only the row of Cabernet Sauvignon was used for the 2021 trial (Fig. 5.1). At the Wye REC, 6, 3-yr-old rows of Cabernet Franc were used for the trial in 2021. During each of the six trials, randomly selected clusters were covered with commercially available paper bags for grape production (Shijiazhuang Yishun Package Machine Co., Shijiazhuang, Hebei Province, China) at the phenological stages of bloom (BBCH 65), bb-size (BBCH 71), pea-size (BBCH 75), berry touch (BBCH 79), veraison (BBCH 83), and pre-harvest (BBCH 85) (Lorenz et al. 1995). Thirty clusters were included per bagging treatment for the Cabernet Sauvignon and Merlot SMT trials in 2019, and 20 clusters per treatment were included in the other four trials. The paper bags (20 x 30 cm) were white with a water-resistant wax coating, an attached wire-tie at the opening, and a ventilation hole at one side of the lower end. The bags were applied by slipping over the clusters, closing the top of the bag around the peduncle, and securing the bag by wrapping the peduncle with the wire-tie. In order to control for the potential effect of the bags on disease occurrence, 'inverse' treatments were included in the four trials in 2020 and 2021, where 100 grape clusters

were bagged at bloom, followed by removal of 20 bags at the phenological stages of bb-size, pea-size, berry touch, veraison, and pre-harvest, respectively. Once the bags were removed, the peduncles were tagged with a colored ribbon unique to each bag removal time point (Fig. A5). At full ripeness (BBCH 89), the ribbon-tagged and bagged clusters were harvested, weighed, and analyzed for ripe rot severity, including 20 clusters that had never been bagged. There were a total of 12 treatments consisting of grape clusters exposed or protected during various time periods from bloom to harvest.

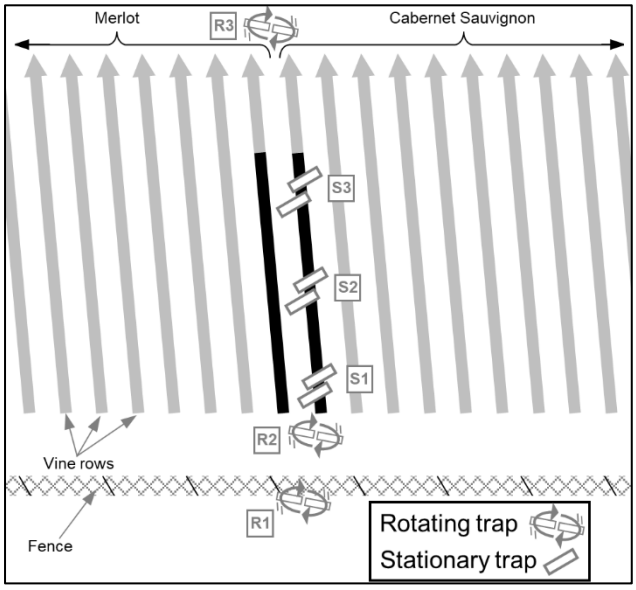

Fig. 5.1. Locations of rotating and stationary spore traps placed in the SMT vineyard in 2019 and 2020 with grapes that were bagged at different phenological stages indicated in black.

Disease severity was a visual estimation of the percentage of berries per cluster exhibiting ripe rot symptoms (Gadoury et al. 2003), and the evaluation was conducted with the evaluator blind to the bagging treatment to reduce bias. The severity of any other non-ripe rot cluster issues, such as diseases caused by *B. cinerea* and *Alternaria* spp. were also noted similarly. A small number of bags fell off or were torn during the season, resulting in variable numbers of clusters evaluated for disease severity and weight per treatment (Table A8). Both

vineyards were trained to a vertical-shoot-positioned trellis system and no fungicides were applied to the canopy or fruit zone for the duration of each trial that had known efficacy against *Colletotrichum* spp. The bagging timing and harvesting was conducted at different dates for each cultivar because they matured at different rates (Table A8).

5.2.2) Spore trap deployment and analysis in qPCR

Prior to bloom in 2019 and 2020, six spore traps were placed in the SMT vineyard including three rotating-arm type spore traps designed to capture airborne spores (Quesada et al. 2018), and three stationary spore traps designed to capture water or rain dispersed spores (Eskalen and Gubler 2001). Two of the rotating-arm traps, R2 and R3, were placed just outside of the canopy at both ends of the vine rows, and trap R1 was attached to a fence 15 m from the nearest grapevine. The stationary traps, S1, S2, and S3, were attached to the trunks of vines at three locations in the experimental area (Fig. 5.1). Both types of traps utilized two standard glass microscope slides with one side coated with a thin film of Vaseline. The Vaseline-coated side was placed on the leading edge of the rotating-arm traps and was on the upward side of the stationary traps. The microscope slides were replaced every 7 to 11 days from bloom until harvest and were stored at -20 °C until analysis. The batteries in the rotating spore traps were replaced every two to three weeks.

DNA was extracted from a 20 x 20 mm area of each Vaseline-coated microscope slide that was exposed during the field trial using the DNeasy Powersoil Powerlyzer Kit (Qiagen, Hilden, Germany) according to Cosseboom and Hu (2021a). The eluted DNA from each spore trap slide was stored at -20 °C as a different sample. Then, the quantity of gDNA belonging to the *C. acutatum* or *C. gloeosporioides* species complexes in each sample was evaluated in qPCR as described previously (Cosseboom and Hu 2021a).

Each qPCR reaction contained a total volume of 20 µl with 1x PerfeCTa SYBR Green FastMix (Quantabio, Beverly, MA), 7 µl purified water, 0.25 µM of each primer, and 2 µl DNA template. DNA of each complex was quantified in two separate reactions with the first reaction containing *C. acutatum* complex specific primers BtubAcuF/BtubAcuGloR and the second containing the *C. gloeosporioides* complex specific primers BtubGloF/BtubAcuGloR (Table A1). Three biological replicates were included per sample, the negative control, and the standard curve for each plate. The standard curve consisted of serial dilutions of DNA extracted from either $1x10^6$ *C. fioriniae* (*C. acutatum* complex) or $1x10^6$ *C. aenigma* (*C. gloeosporioides* complex) conidia and was used to ensure that the PCR reaction was efficient (90-110%) with low variance (>0.98) between replicates and to estimate the number of *C. acutatum* or *C. gloeosporioides* complex conidia in each sample. The negative control were reactions containing the elution from a DNA extraction conducted on an unused spore trap.

The qPCR assay was conducted with a BioRad CFX 96 (Hercules, CA) instrument with a thermocycling protocol of 95 °C for 3 min, 40 cycles of 95 °C for 20 sec, 58 °C for 20 sec, and 72 °C for 20 sec, followed by a melt curve from 65 to 95 °C with a 5 sec hold and 1 °C per cycle. The cycle threshold was automatically set by the BioRad CFX 96 instrument. The log number of spores on each trap was estimated with an equation from a linear regression of the log quantities of conidia in each standard curve sample against their respective quantification cycle (Cq) values. Samples with Cq values beyond the limit of quantification of (50 spores with the *C. acutatum* complex primers and 100 spores with the *C. gloeosporioides* complex specific primers; approximately 37 cycles) were unreliable and were considered to contain DNA of 0 conidia. The melt curve peaks for each reaction were also evaluated for assurance that the DNA amplified

during the reaction was the target for which the primers were designed (Cosseboom and Hu 2021a).

5.2.3) Fungal isolate collection and identification

After clusters from the bagging trials were weighed and evaluated for ripe rot severity, up to ten clusters exhibiting ripe rot symptoms from each treatment were set aside for fungal isolation. If visible sporulation was observed, a sterile loop was used to transfer the conidia to a plate of potato dextrose agar (PDA). If no sporulation was observed, the berries were surface sterilized in 1% sodium hypochlorite for 60 seconds and then rinsed in sterile deionized water. Then, berry skin was excised and transferred to a plate of PDA. The plates were incubated at 25 °C for three days, and then no more than two colonies resembling *Colletotrichum* spp. from each plate were transferred to a fresh plate of PDA. These isolates were placed into different groups based on a visual assessment of colony morphology, and a selection of isolates from each morphology group were selected for molecular identification from the 2019, 2020, and 2021 field trials.

DNA was extracted from these isolates according to Chi et al. (2009), and β-tubulin (*tub2*), chitin synthase 1 (*chs-1*), and glyceraldehyde-3-phosphate dehydrogenase (*gapdh*), were amplified with PCR with the primers Btub2fd and Btub4rd, CHS-79F and CHS-345R, and Gdf and Gdr, respectively. The amplicons were Sanger Sequenced by Genewiz inc., and BLAST was used to identify which *Colletotrichum* species complex the isolates belonged to. For isolates identified as belonging to the *C. gloeosporioides* complex, an additional genomic region, the Apn2 to MAT1-2-1 intergenic region (*Ap-MAT*), was amplified and sequenced in the same manner with primers CgDL_F6 and CgMAT1_F2 (Table A1). Reference sequences of *Colletotrichum* species in each relevant species complex were acquired via GenBank, and the

sequences used to identify the isolates collected in this study were deposited in GenBank (Table A2).

The sequences were aligned for each gene, trimmed to the same length, and concatenated. Then, Maximum Parsimony analysis was performed using MegaX software to obtain most parsimonious trees with Tree Bisection Reconnection branch swapping and 1000 random sequence additions. Up to 5000 trees were kept and the robustness of the tree was evaluated by 1000 bootstrap replications. This was conducted for each *Colletotrichum* species complex individually.

5.2.4) Weather monitoring

An Atmos 41 weather station (Meter Group Inc., Pullman, WA) at both locations was used to track rainfall and temperature throughout each season, and Phytos 31 leaf wetness sensors (Meter Group Inc.) were added in 2020 and 2021. In the SMT vineyard, the Atmos 41 station was located at the same location as rotating spore trap R2 and three leaf wetness sensors were placed in the lower canopy of the Merlot vines in the same row as the bagging trials within 10 m of the Atmos 41 station. At the Wye REC vineyard, the weather station and four leaf wetness sensors were located in a vineyard 200 m from the bagging trial vine rows. The leaf wetness sensors were in the lower canopies of Vidal Blanc and Chambourcin vines. Leaf wetness data above 450 were considered wet according to the manufacturer's instructions. Weather data was summarized by day with total rainfall, total leaf wetness duration, and average temperature.

5.2.5) Statistical analysis

Statistical analyses were conducted using the software JMP 14.0 (SAS Institute, Cary, NC). The effect of the bagging timing variable on the severity of ripe rot and cluster weight from the field trials were evaluated in two separate analyses. The disease severity data was square root

transformed to fit the ANOVA assumptions of homogenous variance and normally distributed residuals. If any variables were significant, post-hoc analysis was conducted with a Tukey's HSD test. This was done for each of the six trials individually. A similar analysis was conducted on the black rot and downy mildew severity observed in two trials in 2020. For the spore trap data, the log number of spores was compared between the spore trap type (rotating and stationary) and the *Colletotrichum* species complex-specific primers (*C. acutatum* complex and *C. gloeosporioides* complex) and an interaction between the two variables was evaluated for the 2019 and 2020 seasons separately. If any variables were significant, a post-hoc Student's t-test or a Tukey's HSD test was performed.

5.3) Results

5.3.1) Disease severity and weight evaluation

In each trial, ripe rot occurred naturally and was prevalent on non-bagged clusters in the experimental plots. The general disease symptoms appeared as clusters with rough berry skin that may have been slightly shriveled (Fig. A5). Orange sporulation could also be observed on the skin surface occasionally. Ripe rot was observed at each bagging timing in each trial, except for the Merlot clusters in 2020 that were bagged at BB-size (BBCH 71) (Fig. 5.2). The highest average ripe rot severity tended to be observed on treatments where the clusters were exposed after veraison (treatments 6-11) compared to the treatments where the clusters were protected by bags during veraison (treatments 1-5; 12). Furthermore, the ripe rot severity of treatments 6-11 were statistically higher than the other treatments in all the trials with three outliers (i.e. treatments 6 and 12 for Merlot in 2020 and treatment 5 for Cabernet Franc in 2021) across all 62 treatments combined. In a similar pattern, but with a lesser extent, clusters that were only

exposed from pre-harvest to harvest (treatment 12) tended to have higher ripe rot severity than those that were only exposed during the early season. For example, treatment 12 was statistically higher than treatments 2-4 for Merlot in 2020 and Cabernet Sauvignon in 2021. It is also noteworthy that there were no significant differences observed between treatments 1-5 in any of the trials expect for treatment 5 for Cabernet Franc trial in 2021 (Fig. 5.2).

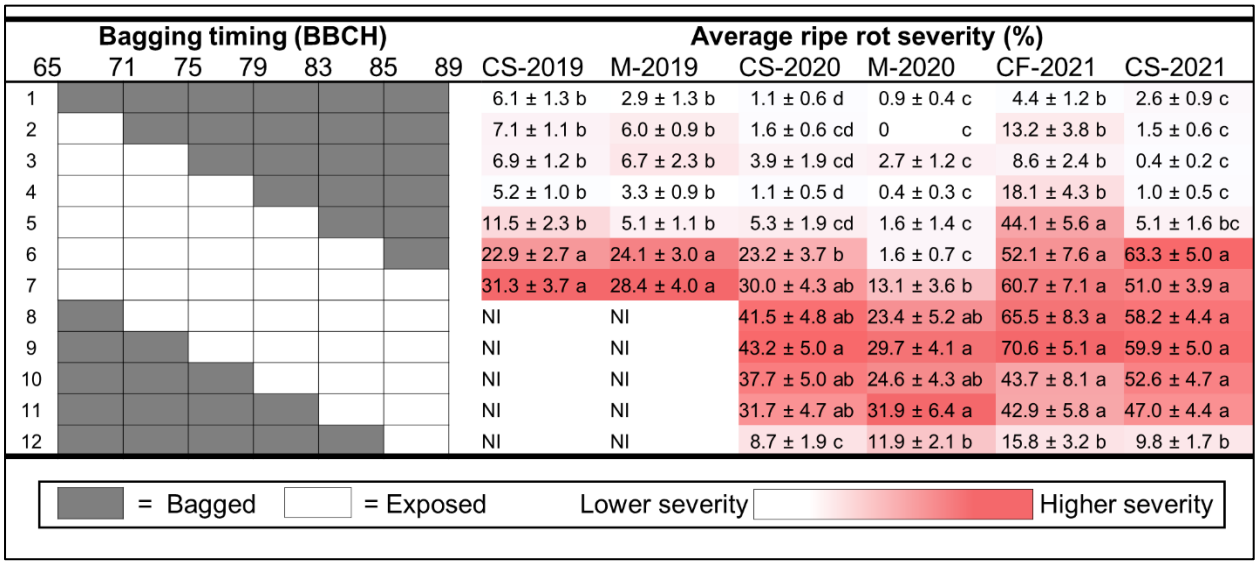

Fig. 5.2. Average ripe rot severity (%) ± standard error of the mean from six trials conducted with the cultivars Cabernet Franc (CF), Cabernet Sauvignon (CS), and Merlot (M) with grape clusters protected by bags at different phenological stages starting at bloom (BBCH 85) and ending at full ripeness (BBCH 89). The effect of bagging timing was evaluated on the square root transformed ripe rot severity for each trial separately with ANOVA followed by a post hoc Tukey's HSD test. Ripe rot severity values followed by a different letter are significantly different. Bag removal treatments were not included (NI) in 2019.

All fruit clusters that were evaluated for ripe rot severity were also evaluated for their weight. Clusters that were bagged for a majority of the season tended to weigh more than those that were exposed throughout the season, with the average cluster weight of the non-bagged treatment being the nearly the lightest out of the treatments in most of the trials (Fig. 5.3). Statistical differences in cluster weight between the bagging treatments was observed in each

trial except for Cabernet Sauvignon in 2019, yet the trend in cluster weights was similar to Merlot in the same season.

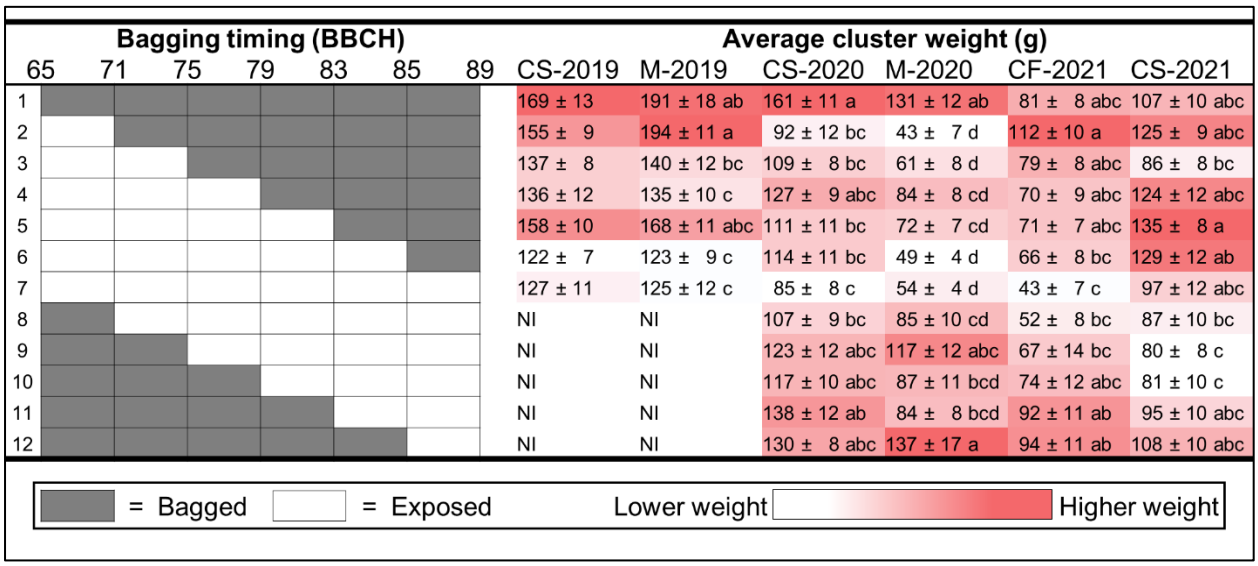

Fig. 5.3. Average grape cluster weights ± standard error of the mean from six trials conducted with the cultivars Cabernet Franc (CF), Cabernet Sauvignon (CS), and Merlot (M) with grape clusters protected by bags at different phenological stages starting at bloom (BBCH 85) and ending at full ripeness (BBCH 89). The effect of bagging timing was evaluated on the cluster weights for each trial separately with ANOVA followed by a post hoc Tukey's HSD test. Weight values followed by a different letter are significantly different. Bag removal treatments were not included (NI) in 2019.

5.3.2) Isolate collection and identification

Colletotrichum spp. were collected from ripe rot symptomatic clusters with 57 isolates from the Wye REC vineyard in 2021 and 155, 137, and 68 isolates were collected from the SMT vineyard in 2019, 2020, and 2021, respectively. Of the three cultivars sampled in this study, 63, 227, and 138 isolates were collected from Cabernet Sauvignon, Merlot, and Cabernet Franc, respectively. The BLAST search of the genomic regions sequenced from 51 isolates representing different cultural morphologies revealed that all isolates belonged to either the *C. acutatum* or the *C. gloeosporioides* species complexes. The multilocus phylogenic analysis was conducted on the

sequences of each complex separately, and two distinct groups were most closely related to *C. fioriniae* and *C. nymphaeae* in the *C. acutatum* complex (Fig. A6). In the *C. gloeosporioides* complex, four distinct groups were identified to be most closely related with *C. aenigma, C. fructicola*, *C. siamense,* and *C. temperatum* (Fig. A7).

The phylogenic analysis of the representative isolates from each morphological group mentioned above was used to infer the identity all isolates collected in this study. As a result, 257 (61.6%), 82 (19.7%), 55 (13.2%), 21 (5.0%), 1 (0.2%), and 1 (0.2%) isolates were identified as *C. fioriniae, C. nymphaeae, C. aenigma, C. fructicola*, *C. siamense,* and *C. temperatum* from all vineyards and years, respectively. *C. fioriniae* was the most prevalent species collected in each trial (Fig. 5.4). Due to the prevalence of this species and *C. nymphaeae,* the *C. acutatum* complex was more prevalent than the *C. gloeosporioides* complex, consisting of 81.3% of isolates collected. Further, the *C. acutatum* complex was isolated more frequently than the *C. gloeosporioides* complex from each bagging treatment, but the *C. gloeosporioides* complex was isolated with increased frequency from bagging treatments where the clusters were exposed in the early season (Fig. A8). The less commonly isolated species *C. fructicola* and *C. siamense* were only isolated from the SMT vineyard, while *C. temperatum* was only isolated from the Wye REC vineyard. *C. siamense* and *C. temperatum* were rare, with only one isolate of each being collected and *C. temperatum* has never been previously associated with ripe rot of grape.

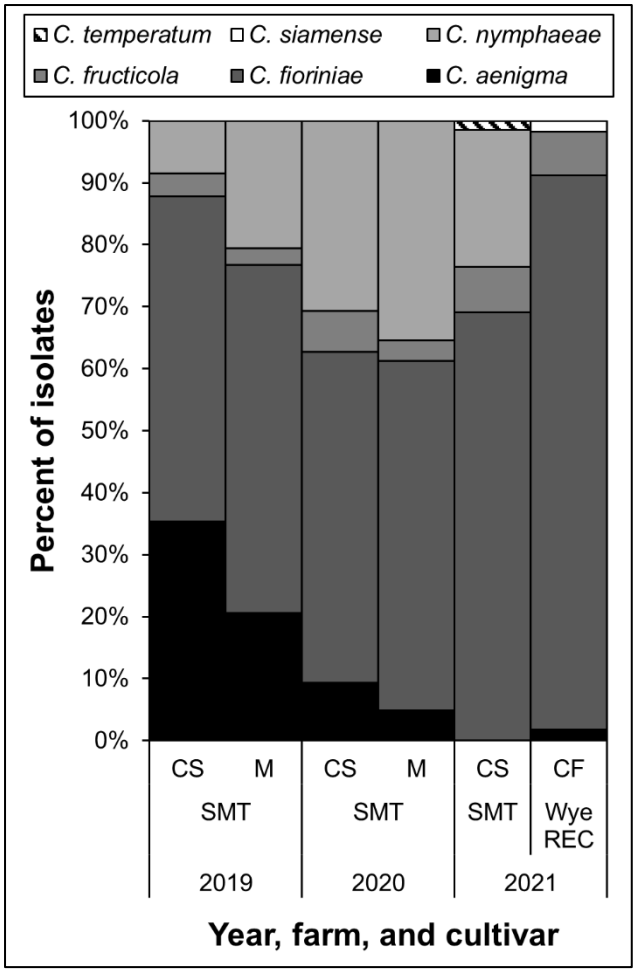

Fig. 5.4. Frequency of *Colletotrichum* spp. isolated from clusters exhibiting ripe rot symptoms from bagging trials conducted at the SMT vineyard in 2019 with Cabernet Sauvignon (CS; n = 82) and Merlot (M; n = 73), the SMT vineyard in 2020 with CS (n = 75) and M (n = 62), the SMT vineyard in 2021 with CS (n = 68), and the Wye REC vineyard in 2021 with Cabernet Franc (CF; n = 57).

5.3.3) Quantification of *C. acutatum* and *C. gloeosporioides* complex spores on spore traps

All spore trap samples were processed using qPCR and both DNA of the *C. acutatum* and *C. gloeosporioides* complexes were detected in both years. *C. gloeosporioides* was detected in the early season (May in 2019 and June in 2020) and late season (September and October in 2019 and October in 2020), but not in the middle of either season. *C. acutatum* was detected in every month of both seasons (from bloom to harvest stage), but not in June or July of 2019 (Table 5.1). The standard curve was used to calculate the number of conidia from the quantity of DNA measured in the qPCR assay. In both 2019 and 2020, *Colletotrichum* species complex and trap

type had a significant effect on conidia abundance, and in 2020, there was a significant interaction between these two variables. Two separate post hoc analyses were conducted for the 2019 data, finding that significantly more *C. acutatum* spores than *C. gloeosporioides* were detected on both spore trap types ($p = 0.015$), and that the stationary traps detected more of both complexes than rotating traps ($p = 0.048$). A similar trend occurred in 2020 (Table 5.1), but the post hoc test conducted on the significantly interacting variables ($p = 0.026$) found that the number of *C. acutatum* conidia on stationary traps was significantly higher than *C. gloeosporioides* on stationary traps and both complexes on rotating traps. DNA of both complexes were also detected on the rotating trap (R3) placed 15 m from the nearest grapevine (Fig. 5.1; Table 5.1).

5.3.4) Weather monitoring

Weather stations in the vineyards monitored temperature and rainfall for the duration of the bagging field trials and spore trap collection in all three years and leaf wetness sensors were installed in the latter two years. Rainfall was observed in every month of the bagging trials except for October at the SMT vineyard in 2021 (Fig. 5.5). The ripening period of 2021 at SMT experienced very little rainfall, with less than 5 mm after 1 July until harvest. At the SMT vineyard, the most rainfall occurred during July (170 mm), June (189 mm), and June (124 mm) in 2019, 2020, and 2021, respectively, and in August (172 mm) at the Wye REC vineyard in 2021. Beyond rainfall, dew events were very frequent, resulting in multiple hours of leaf wetness on most days. The month with the highest average leaf wetness per day was August for the SMT vineyard in 2020, September for the SMT vineyard in 2021, and October for the Wye REC vineyard in 2021. July was the hottest month during each season and in each vineyard with the average temperature between 24.7 to 26.5 ºC.

Table 5.1. The total number of *Colletotrichum acutatum* and *C. gloeosporioides* species complex conidia quantified by month from three rotating (R1, R2, and R3) and three stationary spore traps (S1, S2, and S3) that were each placed at different locations in the SMT vineyard. The number of conidia was inferred from the quantity of *C. acutatum* or *C. gloeosporioides* complex gDNA present on each spore trap

			***C. acutatum* complex**				***C. gloeosporioides* complex**			
Trap Type	**Year**	**Date collected**	**Trap 1**	**Trap 2**	**Trap 3**	**Total**	**Trap 1**	**Trap 2**	**Trap 3**	**Total**
Rotating	2019	May	260	959	-[a]	1219	109	-	-	109
		Jun	-	-	-	-	-	-	-	-
		Jul	-	-	-	-	-	-	-	-
		Aug	1058	433	4756	6246	-	-	-	-
		Sep	163	-	724	887	-	-	-	-
		Oct	-	-	-	-	-	-	-	-
		Total	1481	1392	5480	8352	109	-	-	109
	2020	Jun	-	1748	-	1748	-	-	-	-
		Jul	-	407	-	407	-	-	-	-
		Aug	-	-	-	-	-	-	-	-
		Sep	1198	-	-	1198	-	-	-	-
		Oct	3379	-	-	3379	104	-	-	104
		Total	4577	2156	-	6733	104	-	-	104
Stationary	2019	May	-	863	NA[b]	863	-	403	NA	403
		Jun	-	-	NA	-	-	-	NA	-
		Jul	-	-	-	-	-	-	-	-
		Aug	-	1184	985	2170	-	-	-	-
		Sep	-	4714	-	4714	-	203	-	203
		Oct	55364	9354	-	64718	1451	766	190	2406
		Total	55364	16115	985	72465	1451	1371	190	3011
	2020	Jun	917	-	-	917	283	-	-	283
		Jul	-	-	-	-	-	-	-	-
		Aug	1208	-	-	1208	-	-	-	-
		Sep	1558	1144	3200	5902	-	-	-	-
		Oct	3399	3253	4716	11368	168	-	180	348
		Total	7083	4398	7915	19396	451	-	180	631

[a] No conidia detected.

[b] The upper-stationary traps were not deployed from 5/17/2019 to 6/28/2019.

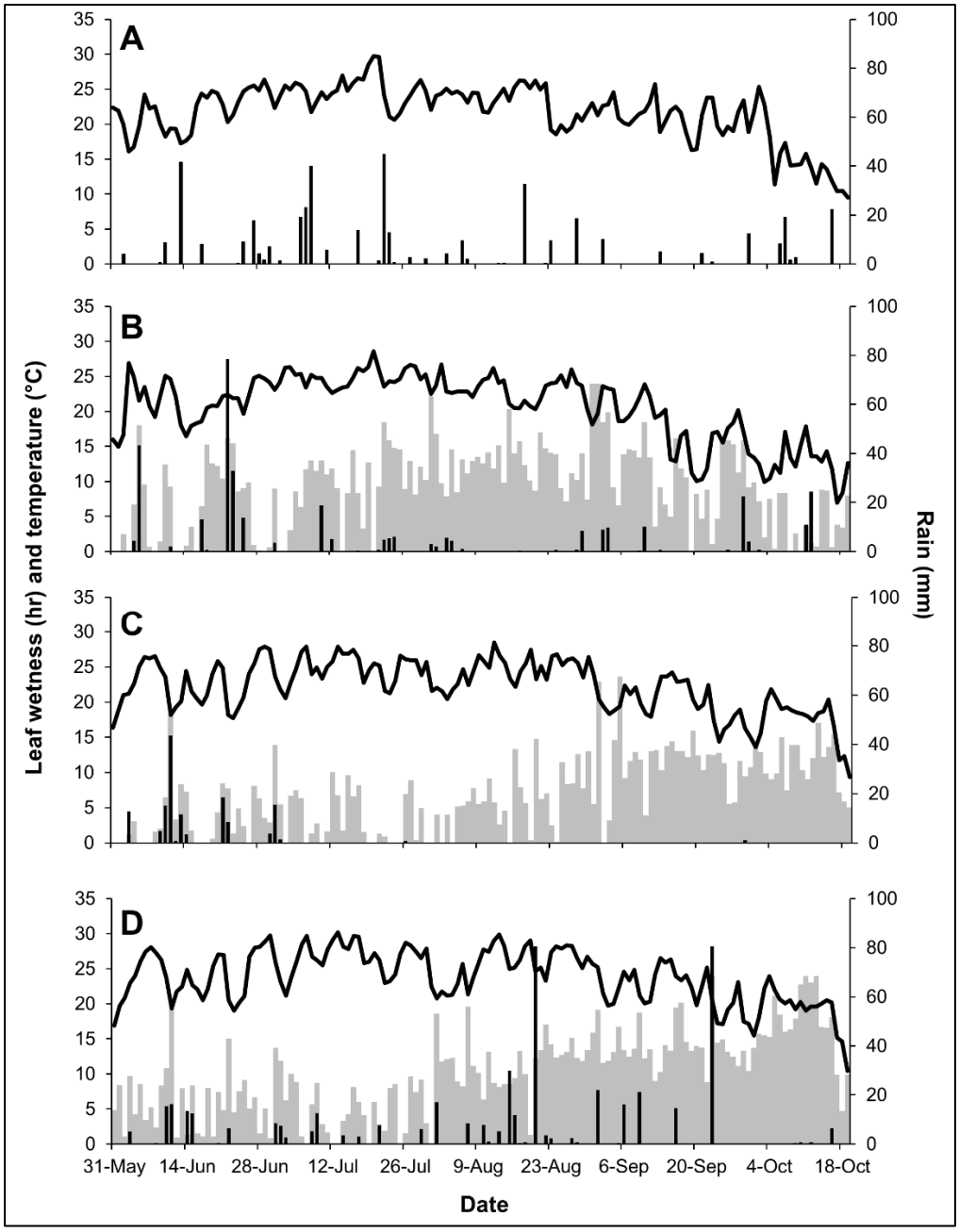

Fig. 5.5. Total rainfall (black columns), total leaf wetness duration (gray columns), and average temperature (black line) per day in the SMT vineyard in A) 2019, B) 2020, and C) 2021, and D) in the Wye REC vineyard in 2021. Leaf wetness data was not available from the SMT vineyard in 2019.

5.4) Discussion

The investigation of the ripe rot pathogen identity, inoculum, weather monitoring, and ontogenic susceptibility have revealed valuable insights into the etiology and epidemiology of ripe rot. The cumulative evidence suggests that the late season, from veraison to harvest, is the most susceptible window for ripe rot development. First, severe ripe rot outbreaks occurred on non-bagged clusters that were exposed (non-bagged) for the entirety of the season for each trial. Other treatments with clusters exposed during only the latter part of the season also had the high severities of ripe rot (Fig. 5.2), suggesting an important dynamic occurred during the latter part of the season which caused the clusters of these treatments to have higher disease severities. This occurred over multiple seasons, in two Mid-Atlantic vineyards, and with three wine grape cultivars. Previous studies have primarily investigated the severity of latent infection caused by inoculation at different phenological stages in greenhouse and field conditions, while this study investigated the severity of ripe rot symptoms on clusters (Oliver 2016; Samuelian et al. 2014). The severe symptoms on clusters with late season exposure could be explained by the species and concentration of inoculum, environmental conditions, or ontogenic susceptibility.

Multiple species of *Colletotrichum* were isolated from ripe rot symptomatic grapes and were similar to those found in nearby Virginia and in other grape growing regions where ripe rot is a significant disease (Greer et al. 2011; Oliver 2018). *C. fioriniae* was the predominant species collected in the trials and was also very prevalent in other vineyards and apple orchards in the Mid-Atlantic region (Martin and Peter 2021; Oliver 2018). Due to this, *C. fioriniae* is a significant threat to grape production in this region. Interestingly, this pathogen was not identified in ripe rot investigations in China (Lei et al. 2016; Peng et al. 2013). Additionally, to the best of our knowledge, the present study reported *C. temperatum* and *C. siamense* associated

with ripe rot of grape in the world and North America for the first time, respectively. Only one isolate of each were collected, but further investigation into the identity and pathogenicity of *C. temperatum* would be of interest due to the limited information on this species. It has only been reported on stems and rotten fruit of *Vaccinium macrocarpon* from New Jersey and New York (Doyle et al. 2013), which indicates that it may be endemic to the eastern United States. Furthermore, the phylogeny of this fungus has not been thoroughly examined, with only two of the four loci used for *C. gloeosporioides* complex identification available (Table A2).

Each isolate collected in this study belonged to either the *C. acutatum* or the *C. gloeosporioides* species complex, with the *C. acutatum* complex being more frequent. The proportion of these two species complexes associated with ripe rot appears to vary by vineyard (Fig. 5.4), region, and possibly cultivar (Greer et al. 2011; Lei et al. 2016). The higher frequency of the *C. acutatum* complex was also reflected in the spore trapping, where more spores of *C. acutatum* complex were quantified than the *C. gloeosporioides* complex (Table 5.1). The proportion of the two species complexes varied by the treatment, but there was no clear relationship between this proportion and the severity of ripe rot at each bagging timing (Fig. A8). The *C. acutatum* species complex was the most prevalent for each cultivar and each trial (data not shown). Therefore, the two species complexes appeared to interact with the different developmental stages of the clusters in a similar way, with only the clusters exposed in the late season developing severe ripe rot. Additionally, both complexes have been demonstrated to be pathogenic on grape (Greer et al. 2011).

This was the first study to investigate the presence of *Colletotrichum* spores in a vineyard. Spore traps detected both *C. acutatum* and *C. gloeosporioides* complex DNA throughout the 2019 and 2020 seasons, and the DNA was assumed to be from conidial spores.

Both the *C. acutatum* and *C. gloeosporioides* complexes produce water-dispersed conidia, while only the *C. gloeosporioides* complex has been observed producing wind dispersed ascospores in the field (Madden 1993; Sutton and Shane 1983). Stationary traps placed below the fruit zone tended to detect more DNA than rotating traps that were placed outside of the canopy (Table 5.1), which suggests that a majority of inoculum builds and spreads via rain from within the vineyard and is therefore likely made up of primarily conidia. Although *Colletotrichum* DNA was more frequently detected on the stationary traps than the rotating traps, most traps of both types had either no DNA or were below the detection threshold (Table 5.1). Alternatively, a stationary funnel type trap might have been able to collect more spores and be more successful at spore detection because spores in rainwater could have splashed off the slides. Funnel type traps have been used successfully for *C. acutatum* complex monitoring and detected much higher spore quantities than the traps used in this study (Martin and Peter 2021). The spore trap data demonstrated that inoculum of *Colletotrichum* were present throughout the two seasons at the SMT vineyard. Considering the presence of inoculum, in addition to the *Colletotrichum* infection-conducive environmental factors, it stands to reason that ripe rot pressure is constant in the early, middle, and late season during these trials.

Colletotrichum DNA concentration appeared to be variable by the season timing but increased in concentration toward the end of the season as ripe rot symptoms appeared (Fig. 5.2; Table 5.1). *Colletotrichum* overwintering in grapevine tissues and other vineyard groundcover flora likely contributed to the presence of inoculum beginning in the early season and throughout the season (Martin and Peter 2021; Samuelian et al. 2012). Furthermore, the detection of inoculum on the rotating spore trap at the fence location (trap R1) indicates that *Colletotrichum* spores were spreading into and out of the vineyard throughout the season (Table 5.1). Clusters

exposed during only the early season may have had latent infections from this inoculum, but these latent infections alone did not result in clusters with high ripe rot severity (Fig. 5.2). A previous study demonstrated that *Colletotrichum* can be isolated from latently infected, asymptomatic clusters (Steel et al. 2007). Our preliminary trials in a greenhouse also found that inoculation at bloom resulted in latent infections, but did not result in severe ripe rot symptoms, while inoculation at the pre-harvest did (data not shown). The increase in inoculum concentration observed toward the end of both seasons was likely due to the heavy sporulation from ripe rot symptomatic clusters (the first symptoms were typically observed shortly after veraison, or full color change). The month of august, synchronous with the veraison stage (Table A8), appeared to be a 'transitional month' from resistance to susceptibility to ripe rot (Fig. 5.2), yet there were no more spores detected this month than in May or June (Table 5.1).

As with other plant pathogens, environmental variables such as temperature, humidity, and leaf wetness are critical for *Colletotrichum* infection (Steel et al. 2007; Wilson 1990). The environmental conditions were conducive for infection throughout the season, with days commonly having average temperatures between 20 to 30 °C and greater than 10 hours of leaf wetness (Fig. 5.5). Rain contributed to leaf wetness, but daily dew events appeared to result in most of the leaf wetness that was observed. In a controlled environment, *C. acutatum* infection of grape berries did not occur at relative humidity below 50% and was greatest at 87% and was also able to infect grape berries between 20 to 35 °C (Steel et al. 2007). A previous study found that a similar temperature range was critical for strawberry infection by *C. acutatum,* and that a leaf wetness duration longer than 13 hours resulted in the greatest incidence of infection (Wilson 1990). With the presence of inoculum throughout the season, these environmental conditions likely resulted in multiple infection events throughout the season.

Paper bagging of developing grape clusters has been demonstrated as a tool that physically prevents infection and reduces disease severity on grapes (Karajeh 2018). Bags were effective this study for reducing ripe rot, likely by excluding the pathogen and reduce exposure to excess wetness, which is critical for *Colletotrichum* infection (Wilson 1990). Clusters that were bagged the entire season had statistically the lowest severity of ripe rot [similar in severity to clusters in vine rows outside of the trial that were treated with an intensive spray program (data not shown)], while the non-bagged treatment in the trials had very high ripe rot severity. Cluster bagging also had a beneficial effect for reducing diseases besides ripe rot and increased cluster weight (Fig. 5.3; Fig. A9). The most notable was the severe black rot (*Guignardia bidwellii)* and downy mildew (*Plasmopara viticola*) outbreak that occurred on Cabernet Sauvignon and Merlot clusters that were exposed during the early part of the season in 2020. Shortly after bloom, many berries were exhibiting black rot symptoms, with greater severity on Merlot clusters. Also, sporulation of *P. viticola* was observed on the peduncles. At harvest, these diseases had progressed, resulting in hard, shriveled berries with necrotic peduncles. Clusters that were protected by bags from bloom to pea-size (treatments 1, 9-12) had very little black rot and downy mildew issues, while clusters exposed during this period had very severe symptoms (Fig. A9). This trend agrees with prior studies on grape black rot and downy mildew, which have suggested that the bloom stage is most susceptible (Kennelly et al. 2007; Molitor and Berkelmann-Loehnertz 2011). As these black rot and downy mildew results concur with previous studies, the bags appeared to function as an appropriate and effective pathogen-exclusion tool for the investigation of ripe rot etiology, which was the focus of this study (Fig. A9). Other diseases were also observed including Alternaria fruit rot, Aspergillus fruit rot, Botrytis bunch rot, and sour rot, but these diseases were rare and usually not severe (data not

shown). Cluster bagging can be an effective fruit rot management strategy and can reduce fungicide inputs (Karajeh 2018), but implementation of bags in a commercial setting may not be financially practical.

The data collected in this study suggests that the age of the cluster is a major factor in its susceptibility to ripe rot. Despite the presence of inoculum (of multiple species) (Fig. 5.4, Table 5.1), and the infection-conducive environmental conditions throughout the seasons (Fig. 5.5), the host only appeared to be susceptible to infection that led to severe ripe rot development after veraison (Fig. 5.2). Clusters exposed from veraison to harvest (treatments 6 to 11) generally had higher ripe rot severity than those that were only exposed from pre-harvest to harvest (treatment 12). The pre-harvest stage is likely very susceptible, but the disease did not have enough time to extensively develop on the clusters that were only exposed after pre-harvest (treatment 12). Overall, the susceptibility of the pre-harvest stage was observed with the sometimes significantly higher severity than the treatments 2 to 5 (Fig. 5.2). Age related, or ontogenic resistance of the grape host to diseases has been known for diseases such as black rot, downy mildew, powdery mildew, and Botrytis bunch rot (Gadoury et al. 2003; McClellan and Hewitt 1973; Molitor and Berkelmann-Loehnertz 2011; Petit et al. 2010). This is the first study to observe an ontogenic susceptibility relationship with ripe rot. Due to the consistent results observed during repetition of this trial over multiple seasons, vineyards, and cultivars in the Mid-Atlantic U.S., this relationship may apply to ripe rot epidemics in other grape growing regions. Yet, this will need to be confirmed, since variations in climate has been shown to influence ontogenic resistance to grape downy mildew (Kennelly et al. 2007).

Due to these findings, late season fungicide applications for ripe rot could be an effective management method. In a fungicide efficacy trial in 2018, lower ripe rot severities were

observed on plots treated with effective fungicides in the late season compared to the early season (Hu and Cosseboom 2019). This was observed again during two randomized fungicide efficacy trials in 2021 at two Maryland vineyards, where plots not treated with ripe rot-effective fungicides resulted in an average of 10.0% and 55.9% ripe rot severity, while plots treated with multiple applications of captan after veraison resulted in an average of 5.1% and 14.5% ripe rot severity, respectively (M. J. Hu, unpublished data). This will need further testing and confirmation; yet late season fungicide applications may be restricted in some regions (Samuelian et al. 2014). Olive, blueberry, and strawberry also appear to show a similar yet more gradual increase in susceptibility to *Colletotrichum* fruit rotting diseases as they mature (Moral et al. 2008; Verma et al. 2007; Wilson 1990). Due to this, the earlier stages of these crops may still be susceptible enough to warrant a protective fungicide application, but perhaps not with grapes, as the ontogenic resistance in grapes to other diseases has been significant enough to make the phenological stage of the cluster an important consideration in disease management (Molitor and Berkelmann-Loehnertz 2011). As few studies have investigated different fungicide regimes for ripe rot, investigations considering the ontogenic susceptibility and conducive environmental conditions have the potential to increase the ability to prevent ripe rot with reduced chemical input. Additionally, further histological and biochemical investigations into the interactions between *Colletotrichum* spp. and the grape host during different phenological stages are needed to understand the ontogenic relationship observed in this study.

Chapter 6: Predicting Ripe Rot of Grape, caused by *Colletotrichum fioriniae,* with Leaf Wetness, Temperature, and the Crop Growth Stage

6.1) Introduction

Ripe rot is a devastating disease of wine grapes (*Vitis* spp.) caused by *Colletotrichum* spp. with the potential to cause large losses with average severities in untreated plots up to 67% and 37% in the Mid-Atlantic US and Northeast China, respectively (Cosseboom and Hu 2022; Ji et al. 2021). The conditions that favor ripe rot are still unclear, making timely and effective control difficult. Thus, it is common to spray fungicides from bloom to harvest for the prevention of this disease in vineyards with high disease pressure. The first difficulty is that many species have been associated with the disease, which may differ in fungicide sensitivity and pathogenicity (Dowling et al. 2020). *C. fioriniae* in the *C. acutatum* species complex was the most prevalent species reported in the Mid-Atlantic US and the *C. acutatum* complex was also found to be the most prevalent in the NSW Australia growing region (Cosseboom and Hu 2022; Greer et al. 2011; Oliver 2018). However, the *C. gloeosporioides* complex was more prevalent in Brazil and China (Echeverrigaray et al. 2019; Lei et al. 2016; Yan et al. 2015). Ripe rot appears to be region or climate specific, with only one recent report from the large wine growing region of Italy and none from California or France (Zapparata et al. 2017). This indicates that environmental conditions play a large role in the infection and development of this disease, and these conditions have begun to be investigated (Steel et al. 2012; Steel et al. 2011).

Although studies have confirmed the ability of *Colletotrichum* to cause quiescent infections at high incidence during early grape developmental stages (Greer et al. 2014; Steel et al. 2012), these infections may remain latent and not lead to ripe rot symptoms (Cosseboom and

Hu 2022; Oliver 2016). Alternatively, late season grape developmental stages may be more susceptible to infection that leads to disease. A recent study found that grapes exposed to natural inoculum in the late season developed more severe ripe rot than those that were exposed before veraison, indicating that grapes may have ontogenic susceptibility to ripe rot (Cosseboom and Hu 2022). A significant ontogenic relationship to disease susceptibility has also been demonstrated for other grape fruit rotting diseases, such as black rot (*Guignardia bidwellii),* downy mildew (*Plasmopara viticola*), and powdery mildew (*Erysiphe necator*) (Gadoury et al. 2003; Hoffman et al. 2002; Kennelly et al. 2007), and therefore may be an important factor for predicting ripe rot epidemics.

Recently, a mechanistic model was created for ripe rot, compiling research from previous publications (Ji et al. 2021). This model accounts for many variables including wetness duration (LWD), temperature, inoculum quantity, infection rate, infection severity, overwintering inoculum, and berry and leaf surface area. The studies that the previous model was based on evaluated the severity of latent infection (the percentage of berries from which *Colletotrichum* could be isolated) rather than the severity of disease symptoms (the percentage of berries with ripe rot symptoms) (Greer et al. 2014; Ji et al. 2021; Steel et al. 2012). It also assumed that early season infections could remain latent and cause ripe rot in the late season, which may not be accurate due to the ontogenic susceptibility to this disease (Cosseboom and Hu 2022).

Disease prediction models have been developed for the prediction of other *C. acutatum* complex-associated diseases such as anthracnose fruit rot of strawberry or blueberry (Miles et al. 2013; Wilson 1990). The Wilson (1990) model has been successfully implemented in disease warning systems in strawberry, and trials found that plots treated with fungicides according to the model received less applications than traditional calendar-based spray programs while

maintaining an acceptable level of control (Hu et al. 2020; MacKenzie and Peres 2012). With wine grapes, there is little tolerance for ripe rot, with as little as three percent ripe rot severity able to cause off flavors in wine (Meunier and Steel 2009).

Various methods for empirically modeling plant diseases generally fall into two categories of supervised machine learning: regression and classification (Sperschneider 2020). Both categories consist of similar techniques, such as decision tree (DT), random forest (RF), support vector machine (SVM), neural network (NN), logistic regression (LGR) (classification only), and linear regression (regression only) (Shahoveisi et al. 2022). The regression category requires a continuous response variable, while the classification category requires a categorical, typically binary, response variable. A few recent studies have found that some lesser utilized methods, such as NN or DT were able to create more accurate models than the more traditional methods of LNR and LGR (Shahoveisi et al. 2022; Sperschneider 2020).

Due to continued severe outbreaks of ripe rot and the recent developments in ripe rot epidemiology, the objectives of this study were to i) assess the severity and incidence of ripe rot from grapes inoculated at the bloom and pre-harvest stages with *C. fioriniae* at various temperature and LWD treatments during inoculation, ii) develop environmental risk prediction models from these data sets using multiple machine learning methods, iii) model the ontogenic susceptibility of grape to ripe rot, and iv) select candidate models for future validation by testing for their ability to accurately predict the severity of past ripe rot epidemics.

6.2) Materials and Methods

6.2.1) Isolates and inoculum

Three isolates of *C. fioriniae* that were collected from ripe rot symptomatic fruit from Maryland vineyards and identified in a previous study were used as inoculum (Cosseboom and Hu 2022). For the preparation of spore suspensions, the isolates were revived from storage and plated on quarter-strength potato dextrose agar ($^{1/4}$ PDA). This medium consisted of 10 g PDA (Thermo Scientific, Waltham, MA) and 15 g agar (Thermo Scientific) per liter. These plates were incubated for one week at 25 °C under constant fluorescent light to induce sporulation. Then each plate was flooded with sterile deionized water and the spores were liberated with a cell spreader before pouring through sterile, double-layered cheesecloth. The filtrate from each conidial suspension was mixed and the concentration of conidia was counted using a hemacytometer and diluted to 1 x 10^6 conidia per milliliter.

6.2.2) Detached fruit assays

Ripe (Brix average 22%) wine grapes of the cultivar Merlot were harvested from a Maryland vineyard in September 2019 and individual berries were detached from the grape cluster with the pedicels attached. This vineyard was part of a previous study which was not sprayed with fungicides effective against *Colletotrichum* during the growing season (Cosseboom and Hy 2021). Berries were rinsed in a 1% sodium hypochlorite solution for one minute, followed by rinsing in sterile deionized water. After drying, the berries were submerged in the *C. fioriniae* spore suspension solution for two minutes. Immediately after the submersion period, six groups of 30 berries were placed on paper towels in front of a box fan for 20 minutes for drying. This treatment was considered to experience zero hours of LWD. The remainder of berries were separated into groups of 30 and evenly spaced on plastic-wrapped test tube racks and were

covered and sealed with a second layer of plastic wrap to maintain moisture on the surface of the berries. These racks of berries, including racks of the "0-hr" dried berries, were placed in a larger plastic box, and then placed in incubators set at 12, 16, 18, 22, 26, or 30 °C. After 4, 8, 12, 16, 20, and 24 hours, one rack was removed from each incubator, and the plastic film was removed from each rack and the berries were dried as described above. After the 24-hour period, the plastic boxes containing the racks of berries from each treatment were incubated at 22 °C for three to four weeks, and berries exhibiting ripe rot symptoms were counted and discarded throughout this period. This experiment was conducted again, but with the cultivar Cabernet Sauvignon, harvested in October 2019. The susceptibility of Merlot and Cabernet Sauvignon were previously found to be comparable (Cosseboom and Hu 2022).

6.2.3) Greenhouse trials

250 grafted grapevine transplants of cultivar Cabernet Sauvignon 47.1, rootstock 101-14.1, were potted in plastic pots (7.2 L) with potting mix (Sun Gro Horticulture Professional Growing Mix, Agawam, MA) and were grown in a greenhouse at the University of Maryland, College Park in April 2019. Each grapevine was trained on three vertical 120 cm bamboo stakes. In late May of the same year, vegetative growth of the vines reached the top of the stakes and inflorescences on the grapevines reached full bloom. At this time, a fresh *C. fioriniae* spore suspension, prepared with the same isolates and concentration as described above, was added to a plastic spray bottle, which was used to inoculate each inflorescence by misting with the suspension until runoff. Six groups of plants containing about five inoculated inflorescences each were immediately set in front of two box fans to dry, and these clusters were considered as experiencing zero hours of LWD. Immediately after inoculating the other inflorescences, plastic bags were sealed around the peduncle of each inoculated inflorescence to maintain surface moisture. The inoculated

grapes that were immediately dried and those that were bagged were transferred to plant growth chambers set at 12, 16, 18, 22, 26 or 30 °C. After 4, 8, 12, 16, 20, and 24 hours, a group of grapevines with about five bagged inflorescences were temporarily removed from each growth chamber, followed by removing the plastic bags to dry the inflorescences as mentioned above. Also, a water-control was included by misting five clusters with sterile water, bagging as mentioned above, and incubating at 22 °C for 24 hours. After the final LWD treatment (24 hours) was dried, all grapevines were returned to the greenhouse and maintained until berry maturation. Vegetative growth was pruned as necessary, drip lines were used for irrigation, and no fungicides were applied to the grapevines during this time.

To roughly assess the success of the bloom inoculation, one pea-sized green berry was removed from 222 vines three weeks after inoculation. Each berry was surface sterilized in 1% sodium hypochlorite for one minute and rinsed in sterile deionized water. Then two pieces of each berry were transferred to a petri dish containing PDA, and the plates were incubated at room temperature for seven days. Fungal colonies growing from the berries were visually identified as either the inoculum (*C. fioriniae*) or as other fungi according to the unique color of *C. fioriniae* that matched the inoculum (Khodadi et al. 2020). When berries were fully mature (Brix approximately 23%) on the potted grapevines, ripe rot severity was assessed as the symptoms occurred on the clusters by dividing the number of berries on a cluster exhibiting ripe rot symptoms by the total number of berries on each cluster. The potted grapevines were then maintained as described above until winter, when the plants were overwintered in an unheated shade house.

The same potted grapevines were used for the following two years for two trials (GH1 and GH2) in which clusters were inoculated at the pre-harvest stage, rather than bloom. The pre-

harvest stage was determined as an intermediate stage between veraison (color change) and harvest, and where berry sugar levels were increasing (brix approximately 19%). Five temperature treatments, 12, 17, 22, 27, and 32 °C, and five LWD treatments, 0, 6, 12, 18, and 24 h, were included in these trials. Water controls were also included in the pre-harvest-inoculated trials as in the bloom-inoculated trial. The severity of ripe rot following inoculation was recorded as described for the bloom-inoculated trial.

6.2.4) Environmental risk model development

The continuous disease severity data from the GH1 and GH2 trials was transformed into binary, incidence, for evaluation using classification methods (Shahoveisi et al. 2022). The transformation was conducted data by considering any clusters with greater than or equal to 3% ripe rot severity as "1" and less than 3% as "0". This was done because the data was highly skewed towards severities between 0 to 15% and small severities of ripe rot are detrimental. 3% ripe rot severity was demonstrated to cause off flavors and discoloration in wine (Meunier and Steel 2009). From the detached fruit assays (DF1 and DF2), the ripe rot incidence data regarded a berry with or without ripe rot symptoms as "1" or "0", respectively. The incidence data from GH1, GH2, and the combined greenhouse trials (GH1+2), and the DF1, DF2, and the combined detached fruit trials (DF1+2) were analyzed separately with JMP Pro software (Version 15.2.0, SAS Institute Inc., Cary, NC).

Five supervised-learning classification techniques, ANN, RF, DT, SVM, and LGR were used to create ripe rot incidence prediction models based on the independent variables of temperature and LWD during inoculation. Each berry in the detached fruit assays was considered an individual (1259 and 1249 berries for the first and second trials, respectively), and each cluster in the pre-harvest greenhouse trials was considered as an individual for the analyses (132

and 157 clusters for the first and second trials, respectively), with the incidence as the dependent variable. The models were trained and validated with K fold cross validation for the greenhouse trials (K = 5) and the detached fruit trials (K = 10) (Hoffmann et al. 2019).

Two sets of parameters were input to each model, and analysis was conducted for GH1, GH2, GH1+2, DF1, DF2, and DF1+2, separately. The first parameter set was LWD and temperature for the SVM, DT, RF, and NN methods. For the second set, polynomial and quadratic combinations of LWD and temperature to the third degree (i.e., LWD, temperature, LWD^2, $temperature^2$, LWD^3, and $temperature^3$) were used for logistic regression models with ridge (LGRr) or LASSO (LGRl) regularization through the generalized regression function in JMP (Bulger et al. 1987; Wilson et al. 1990). Regularization was used to reduce overfitting and improve accuracy of the logistic regression by either shrinking the effect of parameters that caused excess variation (ridge) or removing parameters (LASSO). Regularization has been found to be advantageous over stepwise predictor selection methods in regression for minimizing prediction error (Dalla Lana et al. 2021; Hastie et al. 2009).

For each analysis method, various hyperparameters were tuned to increase accuracy, while limiting overfitting by choosing the hyperparameter settings that resulted in the highest AUC (Area Under Curve) value of the ROC (Receiver Operating Characteristic) curve and the lowest misclassification rate of the validation dataset (Hoffmann et al. 2019). For LGRr and LGRl, the minimum penalty was set at 0.0001, 0.01, 0.1, or 0.5, which adjusted the strength of the shrinkage in the regularization (Hastie et al. 2009). For the ANN, a single hidden layer with 3 neurons was used with the tanh activation function and the learning rate was set at 0.1, 0.5 or 0.7 (Shahoveisi et al. 2022). The DT was conducted according to the default settings in JMP with K fold cross validation with no additional splitting or pruning. The RF is an algorithm that uses

many decision trees, and the number of trees was set at either 10 or 100, with 10 minimum splits and 50 maximum splits per tree. Since K fold cross validation was not available for this method, 10% of the data was used as the validation set. The SVM was conducted with the cost value set at 1 or 100, regression loss (ε) set at 0.5 or 1, and a radial basis function (RBF) kernel was utilized with a numerical tolerance of 0.0001 (Shahoveisi et al. 2022). In all, six environmental risk models for each trial and combination of trials were selected for further analysis from the classification methods: LGRr, LGRl, NN, DT, RF, and SVM.

The output of these models was an environmental risk probability. The metrics of accuracy, recall, and AUC were calculated to analyze how well the models could predict the ripe rot incidence of the "test" datasets. The DF1 models used the ripe rot incidence of DF2 as the test dataset and the DF2 models used the ripe rot incidence of DF1 as the test dataset, and likewise for the GH1 and GH2 models. A default cutoff value of 0.5 was selected for calculation of classification accuracy and recall, and prediction probabilities above this value were categorized as "1" for positive (P; for predicted ripe rot incidence) or less than this value as "0" for negative (N; no predicted ripe rot incidence) for each row in the dataset (Esposito et al. 2021; Jain et al. 2000). The ability of each of these models to correctly (T or true) or incorrectly (F or false) classify data as positive (P) or negative (N) was first evaluated with the accuracy, or the true positives (TP) plus true negatives (TN) over all predictions. Models with accuracy values closer to 100% were better at correctly classifying the data. Secondly, the sensitivity, or recall, is the proportion of TP out of the TP plus false negatives (FN). Models with higher recall values had fewer false negatives. Lastly, a more general measure of model fitness, called AUC (area under curve), was calculated from a plot using calculations from both the recall and specificity to

create a Receiver-Operator-Characteristic (ROC) curve (Bradley 1997). The AUC, accuracy, and recall were then compared between the environmental risk models created in this study.

6.2.5) Phenological susceptibility model development

Due to evidence of ontogenic susceptibility of grape to ripe rot (Cosseboom and Hu 2022), a model was created to predict ripe rot susceptibility based off the phenological stage. The ripe rot severity data from five bagging trials from Cosseboom and Hu (2022) were utilized, excluding the Merlot 2020 trial due to complications with other diseases. Briefly, each trial consisted of bagging grape clusters at different phenological stages to expose them to natural environmental conditions and inoculum for different durations of a season. Ripe rot severity was then evaluated at full maturity. The average ripe rot severity from treatments one through seven from Cosseboom and Hu (2022) were utilized each of the five trials.

A calculation was conducted to transform the severity data from these treatments into susceptibility values for each phenological stage (Table A9). First, the severity of each treatment was subtracted from the following treatment (e.g., treatment 2 – treatment 1, treatment 3 – treatment 2, etc.) to determine the amount that ripe rot severity changed between the bagging treatments. Then the severity of treatment 1 was considered the baseline susceptibility, and the values calculated above were added to each subsequent value to determine the relative change in susceptibility between the stages. Then, these susceptibility values were normalized between trials by rescaling the highest average value per trial as 1, and the lowest value per trial as 0 (Table A9). The susceptibility values represented the stages of bloom to bb-size (BBCH 66-71), bb-size to pea-size (BBCH –2 - 75), pea-size to berry touch (BBCH 76 – 79), berry touch to veraison (BBCH 80 – 83), veraison to pre-harvest (BBCH 84 – 85), and pre-harvest to harvest (BBCH 86 – 89), respectively (Lorenz et al. 1995). These stages were given ordinal “stage code”

labels of 1 through 6, respectively, and their relationship to the susceptibility values was determined by fitting a sigmoid curve to the data using the Fit Curve function in JMP.

6.2.6) Ripe rot model testing

The outputs of the environmental risk models were multiplied by the output of the phenological susceptibility model to derive the predicted ripe rot disease risk. An evaluation of each ripe rot model's accuracy for predicting past ripe rot epidemics was conducted. Ripe rot severity and incidence data from 45 epidemics in two sites over three years were utilized, including data from clusters that were either bagged or exposed for different durations (Table 6.1). Each epidemic took place on grapevines that were not sprayed with fungicides that affect ripe rot from bloom to harvest. Forty-three of these epidemics (SMT 2019, SMT 2020, SMT 2021, and Wye 2021) were reported previously (Cosseboom and Hu 2022). Two are reported for the first time in this study (Wye 2019 and Wye 2020) and each epidemic consisted of an evaluation of ripe rot severity and incidence from 14 to 78 clusters, respectively (Table 6.1). Relative humidity and ambient temperature data were also collected from weather stations at each site at 5 to 15-minute intervals from the bloom stage to harvest. Since every weather station did not provide LWD data, high relative humidity was used as a proxy for LWD, with relative humidity above 90% considered wet for all sites (Beruski et al. 2019). If a gap in LWD less than four hours occurred, then LWD continued to accumulate after the gap (Hu et al. 2020). Each day in which infection was predicted (prediction probability above a certain threshold) by the models was considered an infection event. Infection event thresholds from 0.3 to 0.75 were utilized. Linear regressions were conducted on the number of infection events against the mean ripe rot severity from each epidemic for each model and threshold separately.

To determine the potential for models created in this study to reduce the number of fungicide applications for ripe rot per season, each model was virtually evaluated for the number of fungicide applications that would be triggered by model-predicted infection events in the same six trials that were utilized above. A fungicide application was triggered whenever the prediction probability crossed the infection event thresholds mentioned above. However, no applications could be triggered within ten days of each other. The number of applications triggered for each trial was summarized as the average number of fungicide sprays per season.

6.1) Results

6.1.1) Disease incidence

The ability of *C. fioriniae* to infect grape clusters under different temperature and LWD conditions was evaluated on grape clusters at the bloom and preharvest stages, and on detached grapes at the pre-harvest to harvest stage. The clusters in the bloom-inoculated trial developed ripe rot, but at low severities (Fig. A10), and control clusters misted with water for the inoculation did not produce any ripe rot. The symptoms started to emerge at the pre-harvest stage and the highest severity out of any treatment was less than 10%. There was also no clear trend in ripe rot severity of these clusters based on the temperature and LWD. Infection from the bloom-inoculation was verified on pea-sized fruit. These berries were harvested and plated on PDA, and 43 of 222 (19.4%) grape berries yielded colonies of *C. fioriniae*, indicating that they were latently infected, while the three berries from water-inoculated control clusters did not yield any fungal growth. Due to the limited sampling, this likely did not reflect the true infection incidence.

Table 6.1. Mean severity ± standard error of the mean (SE) of ripe rot epidemics included in the model testing analysis that consisted of bagging or not bagging clusters to limit exposure of clusters to natural inoculum and weather conditions. Exposure values are phenological growth stages according to the BBCH scale described by Lorenz et al (1995)

Trial	Cultivar	Treatment[z]	Exposure	No. clusters evaluated	Mean severity ± SE (%)
SMV 2019	Cabernet Sauvignon	1	>65	17	6.1 ± 1.3
		2	>65 to 71	27	7.1 ± 1.1
		3	>65 to 75	31	6.9 ± 1.2
		4	>65 to 79	29	5.2 ± 1.0
		5	>65 to 83	28	11.5 ± 2.3
		6	>65 to 85	29	22.9 ± 2.7
		7	>65 to 89	28	31.3 ± 3.7
SMV 2020	Cabernet Sauvignon	1	>65	20	1.1 ± 0.6
		2	>65 to 71	20	1.6 ± 0.6
		3	>65 to 75	19	3.9 ± 1.9
		4	>65 to 79	19	1.1 ± 0.5
		5	>65 to 83	20	5.3 ± 1.9
		6	>65 to 85	20	23.2 ± 3.7
		7	>65 to 89	20	30.0 ± 4.3
		8	>65; 71 to 89	20	41.5 ± 4.8
		9	>65; 75 to 89	18	43.2 ± 5.0
		10	>65; 79 to 89	17	37.7 ± 5.0
		11	>65; 83 to 89	14	31.7 ± 4.7
		12	>65; 85 to 89	19	8.7 ± 1.9
SMV 2021	Cabernet Sauvignon	1	>65	20	2.6 ± 0.9
		2	>65 to 71	20	1.5 ± 0.6
		3	>65 to 75	18	0.4 ± 0.2
		4	>65 to 79	20	1.0 ± 0.5
		5	>65 to 83	20	5.1 ± 1.6
		6	>65 to 85	20	63.3 ± 5.0
		7	>65 to 89	20	51.0 ± 3.9
		8	>65; 71 to 89	20	58.2 ± 4.4
		9	>65; 75 to 89	20	59.9 ± 5.0
		10	>65; 79 to 89	19	52.6 ± 4.7
		11	>65; 83 to 89	17	47.0 ± 4.4
		12	>65; 85 to 89	20	9.8 ± 1.7
Wye 2019	Chardonnay	NA	>65 to 89	78	5.8 ± 1.1
Wye 2020	Merlot	NA	>65 to 89	39	49.4 ± 4.1
Wye 2021	Cabernet Franc	1	>65	15	4.4 ± 1.2
		2	>65 to 71	19	13.2 ± 3.8
		3	>65 to 75	17	8.6 ± 2.4
		4	>65 to 79	20	18.1 ± 4.3
		5	>65 to 85[y]	19	44.1 ± 5.6
		6	>65 to 85	18	52.1 ± 7.6
		7	>65 to 89	19	60.7 ± 7.1
		8	>65; 71 to 89	13	65.5 ± 8.3
		9	>65; 75 to 89	18	70.6 ± 5.1
		10	>65; 79 to 89	15	43.7 ± 8.1
		11	>65; 83 to 89	17	42.9 ± 5.8
		12	>65; 85 to 89	17	15.8 ± 3.2

[z] Treatment number is according to Cosseboom and Hu (2022), NA = Data is from this study/no treatment number.
[y] According to the dates of bagging, this treatment was actually exposed until early veraison rather than berry touch as stated in Cosseboom and Hu (2022).

In general, clusters of greenhouse-grown grapes inoculated during the pre-harvest stage (trials GH1 and GH2) developed much higher severities of ripe rot than clusters inoculated at the bloom stage (Fig. 6.1; Fig. A10). Ripe rot severity ranged from 0 to 100% on inoculated clusters. Similar trends were observed between the GH1 and GH2 trials, with longer LWD and the 27 °C inoculation temperature resulting in the most severe ripe rot. However, there was variation between the two trials, with the GH1 having higher incidences of ripe rot than GH2. For example, the 24-hour LWD treatment resulted in 100% incidence in GH1 with every temperature except 12 °C, whereas only the 27 °C treatment reached 100% incidence in GH2 (Fig. 6.1). The two detached fruit assays (DF1 and DF2) revealed similar results to those observed in the GH1 and GH2 (Fig. 6.2). The highest disease incidences observed in both DF1 and DF2 occurred on the 26 °C inoculation temperature treatments, however incidence didn't reach 100% in any treatment. Further, the highest incidence occurred on grapes in these two trials with a LWD of 20 hours. Other diseases such as Botrytis and Phomopsis fruit rot commonly occurred and were removed from the detached fruit assays.

6.1.2) Environmental risk models

Due to the low ripe rot severity observed in the bloom-inoculated greenhouse trial, this trial was not repeated, and classification analysis was not conducted on the data. The DF trials didn't have 100% ripe rot incidence in any treatment, which meant that the maximum predicted risk was generally lower than the GH models. The multiple predictive models from the detached fruit and greenhouse trials varied in AUC, recall, and accuracy (Table 6.2). The models created from the GH trial ripe rot incidence were generally better able to correctly classify the incidence than the DF models, with the fitness metrics were generally higher for the GH trials than the DF trials. However, the incidence was counted differently in the GH trials than the DF trials. While the

accuracy values did not vary widely between trials/models, the recall and AUC values varied more widely. The highest recall and AUC values were observed in the GH2 models, indicating few false negatives. The JMP formula scripts for each environmental risk model created in this study were included in a Git Hub repository (https://github.com/smallfruitUMD/Ripe_Rot_Models).

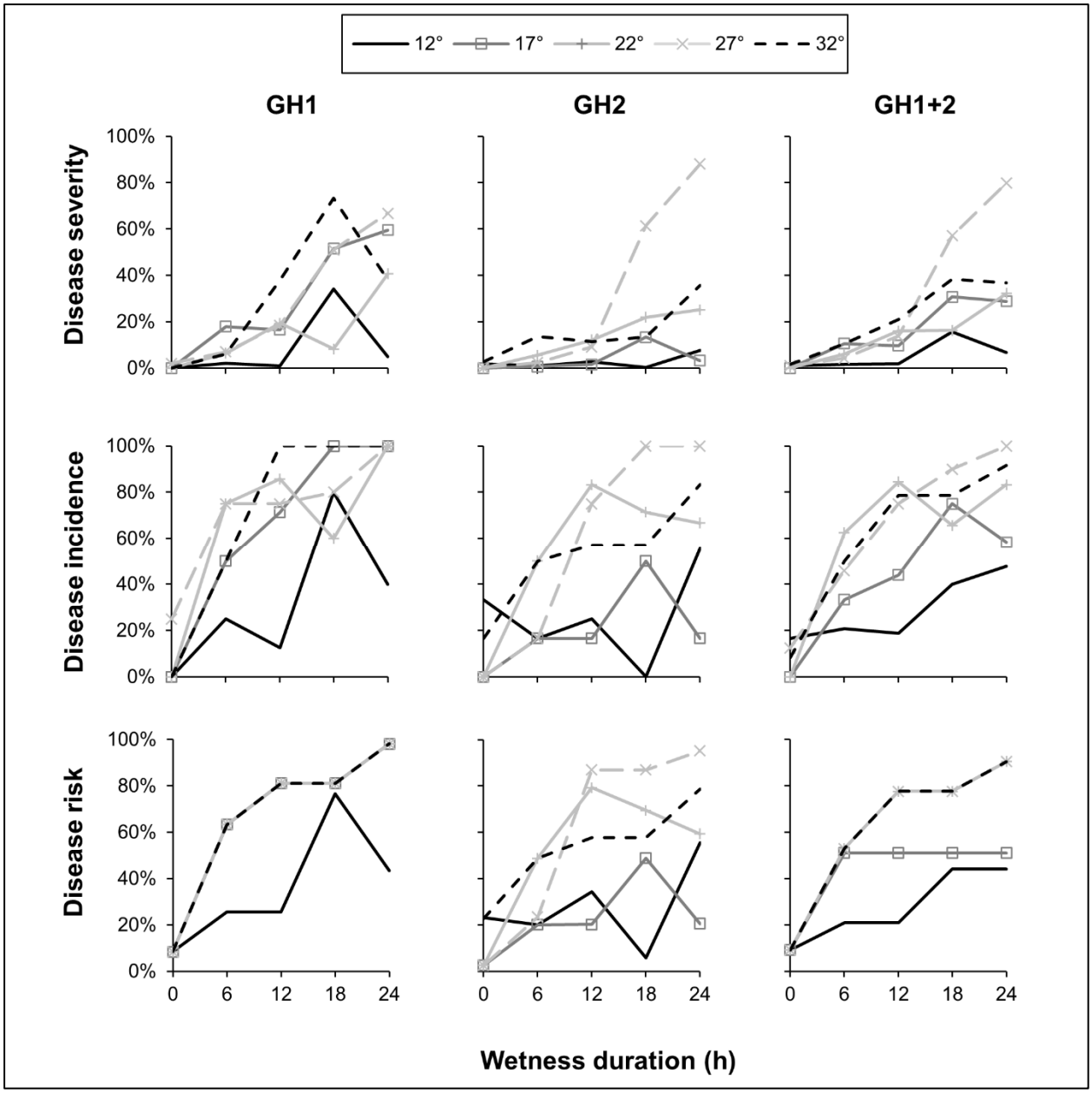

Fig. 6.1. The severity (top) and incidence (middle) of ripe rot disease on mature grape clusters of potted grapevines in two greenhouse trials (GH) that were inoculated with *C. fioriniae* at the pre-harvest stage under multiple wetness duration and temperature conditions and disease risk (bottom) from the top environmental risk models that were created with the decision tree method from the incidence data of each trial.

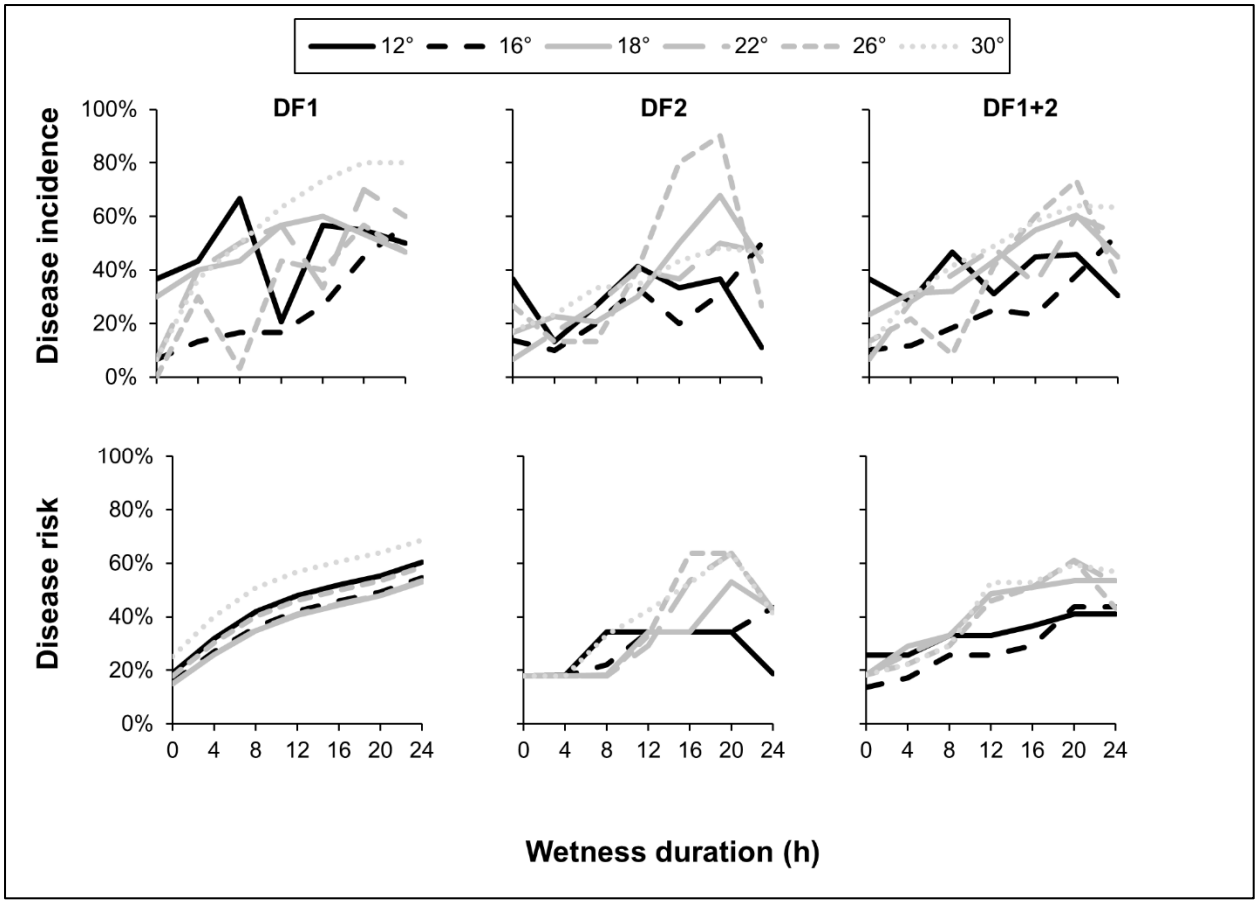

Fig. 6.2. The incidence (top) of ripe rot disease on mature grape berries that were inoculated under multiple wetness duration and temperature conditions in two detached fruit assay (DF) trials and the disease risk (bottom) of the top environmental risk models under these conditions for each trial. The models were created with logistic regression with ridge regularization, a neural network, and a random forest for the DF1, DF2, and combined DF1+2 trials, respectively.

Table 6.2. Fitness of the environmental risk models created from detached fruit (DF) and greenhouse (GH) trials on the test datasets from the trials and ripe rot risk model testing scores at an optimal infection event threshold. The infection event analysis was a correlation of predicted infection events from temperature, wetness duration, and phenological growth stage data from vineyards against the severity of ripe rot that actually occurred. The predicted number of applications is the average number of fungicide applications (apps.) for ripe rot per season that would be triggered by each ripe rot risk model if implemented in a warning system

			Validation fitness metrics[y]			Infection event analysis			Model-triggered fungicide apps.
Trial	**Method[z]**	**Parameters**	**Accuracy**	**Recall**	**AUC**	**Threshold**	**R^2**	**Equation**	**Avg. apps. per season**
DF1	DT		0.60	0.34	0.61	0.40	0.69	y = 1.11x + 7.46	4.7
	LGR	LASSO, Min. penalty = 0.1	0.62	0.21	0.63	0.30	0.73	y = 0.98x + 5.80	4.7
	LGR	Ridge, Min. penalty = 0.01	0.62	0.21	0.63	0.35	0.76	y = 1.17x + 6.40	4.7
	NN	Learning rate = 0.5	0.61	0.19	0.62	0.30	0.71	y = 0.96x + 5.99	4.8
	RF	100 trees	0.62	0.23	0.62	0.35	0.69	y = 0.96x + 6.17	5.0
	SVM	Cost = 100, ε = 1	0.59	0.28	0.58	0.40	0.73	y = 1.06x + 5.97	4.7
DF2	DT		0.59	0.09	0.65	0.35	0.63	y = 3.53x + 11.42	2.5
	LGR	LASSO, Min. penalty = 0.1	0.59	0.03	0.67	0.30	0.76	y = 1.57x + 7.47	4.0
	LGR	Ridge, Min. penalty = 0.0001	0.61	0.12	0.63	0.30	0.76	y = 1.36x + 6.30	4.3
	NN	Learning rate = 0.7	0.61	0.16	0.65	0.45	0.81	y = 3.72x + 7.53	3.0
	RF	100 trees	0.58	0.06	0.66	0.30	0.76	y = 1.43x + 6.69	4.3
	SMV	Cost = 1, ε = 1	0.59	0.11	0.53	0.35	0.74	y = 3.16x + 8.08	2.8
DF1+2	DT		NA	NA	NA	0.35	0.67	y = 1.17x + 7.26	4.7
	LGR	LASSO, Min. penalty =0.1	NA	NA	NA	0.30	0.73	y = 1.13x + 6.14	4.7
	LGR	Ridge, Min. penalty = 0.0001	NA	NA	NA	0.30	0.77	y = 1.26x + 6.47	4.5
	NN	Learning rate = 0.7	NA	NA	NA	0.40	0.72	y = 1.87x + 7.37	3.5
	RF	100 trees	NA	NA	NA	0.35	0.81	y = 1.67x + 6.57	4.2
	SVM	Cost = 100, ε = 0.5	NA	NA	NA	0.30	0.62	y = 1.19x + 8.00	4.5
GH1	DT		0.62	0.59	0.74	0.65	0.79	y = 1.54x + 6.90	4.2
	LGR	LASSO, Min. penalty =0.0001	0.67	0.60	0.78	0.60	0.79	y = 1.32x + 5.23	4.7
	LGR	Ridge, Min. penalty = 0.1	0.63	0.64	0.79	0.55	0.77	y = 1.53x + 6.28	4.2
	NN	Learning rate =0.5	0.67	0.60	0.77	0.60	0.75	y = 1.14x + 6.05	4.7
	RF	100 trees	0.66	0.56	0.73	0.45	0.74	y = 1.16x + 5.94	4.7
	SVM	Cost = 1, ε = 0.5	0.66	0.57	0.74	0.70	0.78	y = 1.37x + 5.28	4.5
GH2	DT		0.65	0.84	0.75	0.65	0.85	y = 3.18x + 7.77	2.5
	LGR	LASSO, Min. penalty = 0.1	0.66	0.91	0.87	0.40	0.78	y = 1.56x + 6.36	4.2
	LGR	Ridge, Min. penalty =0.0001	0.70	0.90	0.87	0.45	0.80	y = 1.81x + 7.37	3.7
	NN	Learning rate = 0.7	0.63	0.88	0.76	0.70	0.84	y = 2.60x + 7.39	3.0
	RF	100 trees	0.66	0.89	0.83	0.40	0.83	y = 2.63x + 7.52	3.2
	SVM	Cost = 1, ε = 0.5	0.66	0.89	0.82	0.60	0.83	y = 2.10x + 6.99	3.3
GH1+2	DT		NA	NA	NA	0.60	0.85	y = 2.77x + 7.14	3.0
	LGR	LASSO, Min. penalty =0.01	NA	NA	NA	0.55	0.79	y = 1.63x + 5.71	4.3
	LGR	Ridge, Min. penalty = 0.01	NA	NA	NA	0.55	0.79	y = 1.56x + 5.82	4.3
	NN	Learning rate = 0.1	NA	NA	NA	0.60	0.77	y = 1.82x + 6.81	4.0
	RF	100 trees	NA	NA	NA	0.55	0.80	y = 1.71x + 6.79	3.8
	SVM	Cost = 1, ε = 1	NA	NA	NA	0.55	0.81	y = 1.71x + 6.10	3.8

[z] Statistical method to derive the environmental risk model: DT = decision tree; LGR = logistic regression; NN = neural network; RF = random forest; SVM = support vector machine.

[y] Models were trained with ripe rot incidence data from a trial, and were tested for their ability to correctly classify incidence data of a separate trial (i.e., the DF1-DT model was tested on the DF2 incidence data). This model testing could not be performed for the DF1+2 and GH1+2 models (NA = not applicable).

6.1.3) Phenological susceptibility model

Based off this study, the bloom stage appeared to be more resistant to latent disease than the pre-harvest stage. The same trend was observed from the ripe rot epidemics observed by Cosseboom and Hu (2022) (Fig. 6.3). Utilizing data from five trials from this prior study, the relationship of the phenological growth stage to susceptibility was described best with a sigmoid curve. The "Gompertz 4P" function fit the curve with the highest coefficient of determination of 0.971 and is written as:

$$Susceptibility = LA + (UA - LA) * \text{Exp}\left(-\text{Exp}\left(-GR * (stage\ code - IP)\right)\right)$$

Where *LA* is the lower asymptote of 0.043, *UA* is the upper asymptote of 0.974, *GR* is the growth rate of 2.567, *stage code* is the number given to the phenological growth stages (1 through 6), and *IP* is the inflection point of 4.331 (Fig. 6.3). According to the susceptibility model, the pre-bloom to berry touch stages (BBCH <65 to 79; *stage codes* 1 to 3) had a susceptibility score of 0.043, berry touch to veraison (BBCH 79 to 83; *stage code* 4) had 0.133, veraison to pre-harvest (BBCH 83 to 85; *stage code* 5) had 0.821, and pre-harvest to harvest (BBCH 85 to 89; *stage code* 6) had 0.961.

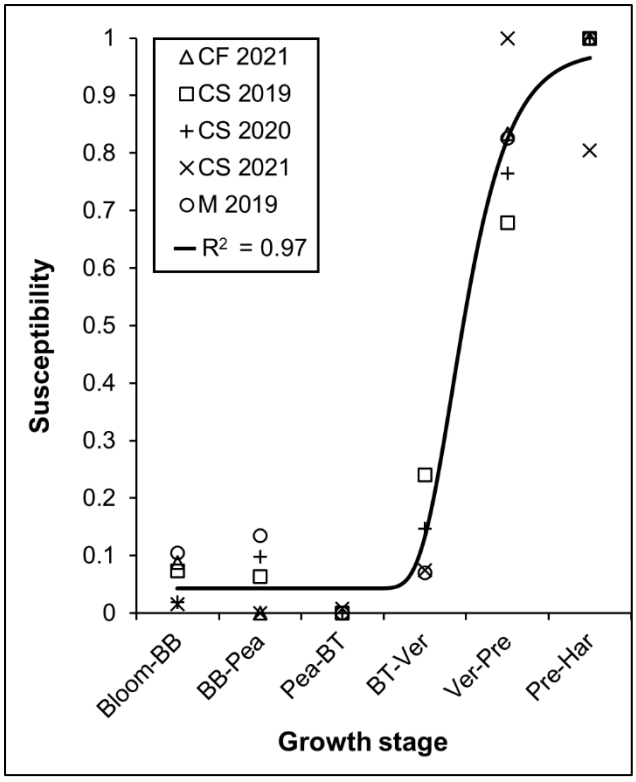

Fig. 6.3. The susceptibility of grape clusters at the phenological growth stages of bloom to BB-size (BB), BB to pea-size (Pea), Pea to berry touch (BT), BT to veraison (Ver), Ver to pre-harvest (Pre), and Pre to harvest (Har) of clusters from five field trials with a fitted Gompertz curve.

6.1.4) Model testing

The predicted values from the environmental risk models were multiplied by the phenological susceptibility model output to acquire the ripe rot disease risk probability. Each disease risk model created in this study was evaluated for how well it could predict the severity of previous ripe rot epidemics by regressing the number of predicted infection events against the average ripe rot severity (Fig. 6.4). Modifying the threshold for determining an infection event affected the accuracy of prediction of ripe rot severity, and an optimal threshold was selected for each model based on the R^2 value (Table A10). For example, at the thresholds of 0.3, 0.5, and 0.7, the NN model from DF2 had coefficient of determinations of 0.66, 0.73, and 0, respectively. At the threshold of 0.7, the model did not predict any infection events (Table A10). The three models with the highest coefficient of determination were the DT model from GH2 (R^2 = 0.85 at a threshold of 0.65), the DT model from the combined GH trials (R^2 = 0.85 at a threshold of 0.6),

and the NN model from GH2 (R^2 = 0.84 at a threshold of 0.7). Of the detached fruit assays, the NN model from DF2 produced the best model (R^2 = 0.81 at a threshold of 0.45) (Fig. 6.4; Table 6.2).

Other metrics such as the slope and y-intercept of the regression line were used to evaluate the utility of the models. The GH2-DT model had a slope of approximately 3.2, meaning that the predicted ripe rot severity rose by 3.2% after each predicted infection event. A higher slope, or fewer predicted infection events per epidemic, also triggered fewer fungicide applications in the virtual ripe rot warning systems evaluated in this study. In this testing, each of the four best models triggered about 3 fungicide applications per season at the respective thresholds mentioned above, and the top model, GH2-DT, triggered an average of 2.5 applications per season. In general, the models with the highest R^2 values also had the highest slopes and triggered the fewest average fungicide applications per season. The best models also had y-intercepts close to 0 (Table 6.2).

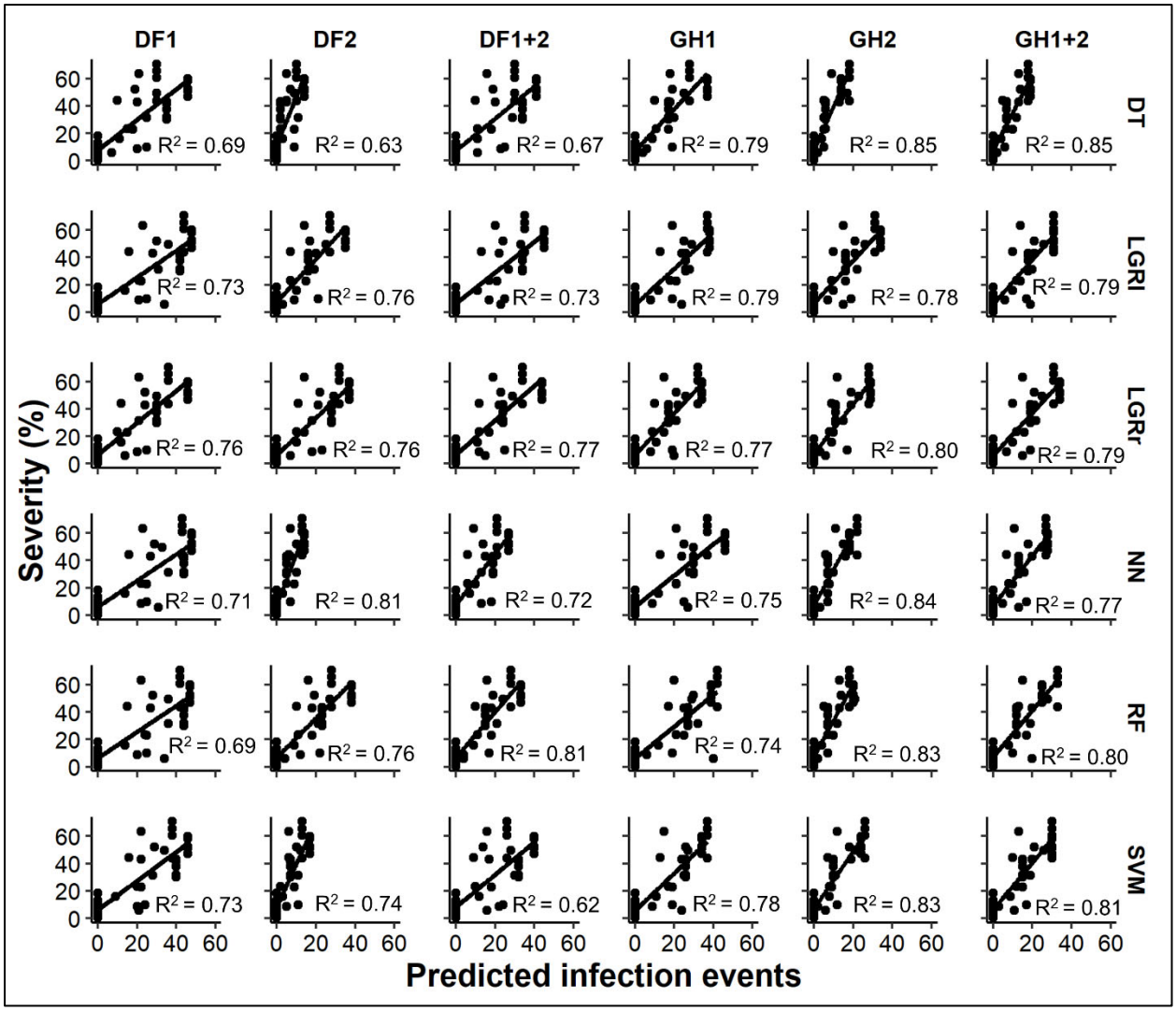

Fig. 6.4. Linear regressions of predicted number of ripe rot infection events against the ripe rot severity from 45 ripe rot epidemics. Infection events were predicted with models with optimized thresholds created from phenological susceptibility and environmental risk factors based on detached fruit (DF) and greenhouse (GH) trials, and the classification methods of the decision tree (DT), logistic regression with ridge (LGRr) or LASSO regularization (LGRl), neural network (NN), random forest (RF), or support vector machine (SVM).

6.2) Discussion

In this study, multiple ripe rot prediction models were created and screened for accuracy and applicability for testing in a ripe rot disease warning system. The ripe rot prediction models consist of two components, an environmental risk component and a phenological stage risk

component. Although a ripe rot model was recently published (Ji et al. 2021), it is missing the potentially important factor of ontogenic susceptibility of the grapevine host to ripe rot. This was a recent discovery and was incorporated into the models described in this study (Cosseboom and Hu 2022). In fact, the results of the bloom-inoculated and pre-harvest-inoculated greenhouse trials supports the results of Cosseboom and Hu (2022) that suggests that grape clusters become more susceptible as they mature. Under optimal environmental conditions during inoculation, the bloom-inoculated trial resulted in very low severities of ripe rot (Fig. A10), while the pre-harvest-inoculated trials resulted in high severities of ripe rot (Fig. 6.1). After disease severity and incidence was collected during the bloom-inoculated trial, the clusters were left on the vines, wounded with a toothpick, and overhead misters were turned on at regular intervals to increase disease pressure. After these efforts, ripe rot severity increased (data not shown), but not near the levels observed when the clusters were inoculated at the pre-harvest stage. Furthermore, the infection of the bloom-inoculated clusters was confirmed by plating surface-sterilized berries on PDA. Interestingly, most of these infections appeared to remain latent, and did not lead to severe ripe rot at harvest. Other studies have also noted that *Colletotrichum* can infect grape clusters at high incidences at various phenological stages, but these studies did not report whether these early-season infections resulted in ripe rot symptoms (Steel et al. 2007, 2012).

The susceptibility of grape clusters was best described with a sigmoidal curve (Fig. 6.3), where susceptibility drastically increased between the berry touch and veraison stages and remained very high until harvest. The data used for this susceptibility calculation was from field trials that were naturally inoculated with the ripe rot pathogen (Cosseboom and Hu 2022). The presence of inoculum throughout the seasons in these trials and ripe rot conducive weather conditions provided evidence that the late-season phenological stages were truly more

susceptible than the early-season stages. This is an important component of the models in this study because optimal environmental conditions occurring before veraison (during a ripe rot resistant phenological stage) would result in low disease risk prediction probabilities. The resistant phenological stages from bloom to berry touch account for over half of the duration of a grape growing season, and therefore likely do not warrant protection from fungicides for ripe rot. This could be confirmed through fungicide efficacy trials.

The environmental risk component was created by modeling the effect of temperature and LWD on ripe rot incidence based on detached fruit assay and greenhouse assay results. For both types of assays, there was variability between and within experiments, and some treatments did not result in expected results from both detached fruit and greenhouse trials (Fig. 6.1; Fig. 6.2). Wine grapes from local vineyards were used for the detached fruit assays, which complicated the trials because they were at times previously infected with other diseases like sour rot, Phomopsis fruit rot, or even ripe rot. Fruit with any other diseases were removed from the trials. With the pre-harvest inoculated greenhouse assays, the ripeness of individual clusters was variable at the time of inoculation, appearing to affect the severity of disease. Due to greenhouse conditions being excessively hot, some clusters stopped maturing early, with some berries never reaching full color change. Thus, the variation between trials and treatments would likely be reduced with increased sample size and better greenhouse conditions. Despite this, similar trends in ripe rot incidence with regards to temperature and LWD took place across all trials. As a result of careful modeling and selection, the best models created in this study were able to accurately predict the severity of real-world ripe rot epidemics (Table 6.2).

K-fold validation was used to split the data sets into validation and training sets during the model training. Hyperparameters were tuned for each of the classification methods and the

models with the greatest ability to correctly classify their validation sets were selected for further testing. It is important to note that both the training and validation datasets are from the same experiment(s) and are subject to bias from the conditions in the experiment(s). Therefore, the models should be verified with test data from outside of the experiments (Hoffmann et al. 2019). This was the purpose of evaluating the ability of the models to correctly classify the "test" datasets, containing data from trials not used in the training of the models. This model testing found that the GH2 models tended to have higher recall and AUC values than the models created from the other trials. Recall, a measure of false negative classifications, may be an important metric for disease risk models, because failing to report a real infection event could result in a missed fungicide application and higher disease severity. However, this testing could not be conducted with the models created from the combined trials, and the testing was subject to the bias of greenhouse or laboratory experimental conditions. Therefore a second model testing with past weather data and ripe rot epidemics from real vineyards was conducted (Ji et al. 2021) (Fig. 6.4; Table 6.2).

From the correlation of the infection events and ripe rot severity from previous epidemics, it was possible to choose candidate models for a ripe rot warning system for preventative fungicide applications. The correlations provided helpful statistics, such as the coefficient of determination (R^2), slope, and y-intercept. In this context, an ideal regression would have reported a R^2 of 1, a high slope (but less than 100), and a y-intercept of 0. A high R^2, such as 0.85, which was observed with the DT model from the GH2 trial, meant that the experimental model was able to closely predict the severities observed in field trials. For the application of a ripe rot warning system, a higher slope value would be preferred, since a higher slope results in less predicted infection events, thereby triggering less fungicide applications

(Table 6.2). This also meant that every infection event predicted a large increase in ripe rot severity, such as an increase of 3.2% ripe rot per infection event with the GH2-DT model. Lastly, a y-intercept close to 0 is an indicator that a model is accurate at the extreme lower end, where 0 predicted infection events should result in 0% ripe rot severity (Fig. 6.4; Table 6.2).

The models were also evaluated for the number of fungicides they would have triggered if they were used in a ripe rot warning system. The best model, the GH2-DT model, triggered an average of 2.5 applications per season, based on weather data from three years in two Mid-Atlantic vineyards. As expected, models with higher slopes in the correlation analysis also triggered fewer applications per season (Table 6.2). The infection event threshold played a key role in the number of sprays triggered per season, with lower thresholds resulting in more triggered sprays (Table A10). For the use of any of these models in a disease warning system, the infection event threshold will be a critical consideration, as it affects not only the number of triggered sprays, but also the accuracy (R^2) of the model (Table 6.2).

The next step for model testing would involve implementation in multiple fungicide efficacy trials. In the 2021 season, two preliminary trials were conducted with the DF2-NN model. This was the best model from the detached fruit assay models in terms of its validation metrics and correlation statistics (Table 6.2). In both field trials, the efficacy of the model-based applications (0.45 threshold) was compared to 12-day interval applications with the fungicide captan. From the ripe rot severities at harvest, the model-based treatment appeared to be as effective as the 12-day interval treatment, while resulting in two fewer sprays at one trial and an equal number of sprays in the other trial (data not shown). Further testing of this and the top GH models from this study would be needed to fully validate and determine the best candidate model for broader-scale implementation.

In this study, multiple models were created and virtually evaluated with ripe rot epidemic data from previous field trials. A few models may be acceptable candidates for further testing such as DF2-NN, GH2-NN, GH2-DT, or GH1+2-DT. Each of these models resulted in similar R^2 values, slopes, and average numbers of predicted fungicide applications, but the GH2-DT was slightly better. The empirical basis and phenological susceptibility component of the models in this study sets these models apart from a previously published model (Ji et al. 2021). When our environmental risk models were virtually deployed in a ripe rot warning system without consideration for phenological susceptibility, over three extra sprays per season were triggered for every model on average (data not shown). In vineyards, multiple pathogens pose a threat to grape production in addition to *Colletotrichum,* and fungicides may provide protection from other pathogens during the early season. Later in the season, ripe rot conducive weather conditions might also be conducive for other pathogens, which may be simultaneously controlled with a fungicide with broad spectrum activity. In conclusion, the models created and tested in this study demonstrated the ability to accurately predict ripe rot utilizing the growth stage, LWD, and temperature which may be useful for the improved control of ripe rot with reduced fungicide inputs.

Summary

The highly destructive group of diseases, the late season bunch rots (LSBR), was investigated in Mid-Atlantic wine grape vineyards by identifying the fungi associated with LSBR, determining which fungi were problematic primary pathogens, evaluating the fungicide sensitivity of the primary pathogens, and investigating the epidemiology of one of the most destructive LSBR, ripe rot. The isolate collection and species identification provided an estimation of the most prevalent fungi associated with LSBR in the Mid-Atlantic, providing a foundation for further investigations. Within the most frequently isolated genera, the in-field pathogenicity of *A. uvarum*, *A. alternata,* and *N. rosae* was investigated with *B. cinerea* as a positive control. Over two replications of the experiment, *A. uvarum* acted as a primary pathogen, able to cause disease on non-wounded fruit when inoculated at veraison and pre-harvest. The fungicide sensitivity of *A. uvarum* and *B. cinerea* was investigated, and fungicide resistance was detected in both fungi. Resistance was linked to mutations in target genes and the relevance of the resistance was confirmed with detached grape experiments. Field experiments demonstrated that grapes become much more susceptible after the beginning of the veraison stage, indicating that the late season is critical for ripe rot management. Next, greenhouse and laboratory assays found a significant relationship between wetness duration and temperature and ripe rot incidence. Candidate ripe rot prediction models were created from these trials based on the cluster growth stage, leaf wetness, and temperature. The results from the experiments in this dissertation may allow vineyard managers to better control LSBR diseases with the reduction of ineffective or unnecessary fungicide applications and may improve application timing. As the research was primarily

conducted with Mid-Atlantic LSBR-associated fungi, vineyard production practices, and climate, the results and conclusions may or may not apply to other grape growing regions.

Appendices

Table A1. Primers used for PCR amplification and sequencing

Primer name	Gene	Primer sequence (5'-3')	Reference
Act512F	Actin	ATGTGCAAGGCCGGTTTCGC	Weir et al. 2012
Act783R	Actin	TACGAGTCCTTCTGGCCCAT	Weir et al. 2012
CgDL_F6	*Ap-MAT*	AGTGGAGGTGCGGGACGTT	Rojas et al. 2010
CgMAT1_F2	*Ap-MAT*	TGATGTATCCCGACTACCG	Rojas et al. 2010
BF1	*Bos1*	TACCGATCGAAAAACCCAAC	Ma et al. 2007
BF2	*Bos1*	CAACGTTATGGCACAAAATCTCA	Ma et al. 2007
BF3	*Bos1*	GGTCGGAACTGATGGAACTC	Ma et al. 2007
BF4	*Bos1*	GCAAACCGTATGATCATGGA	Ma et al. 2007
BF5	*Bos1*	TCCCGTTATTCATGTCAGCTT	Ma et al. 2007
BR1	*Bos1*	TGGGCTGGTCTCTCAATCTT	Ma et al. 2007
BR2	*Bos1*	AAGTTTCTGGCCATGGTGTTCA	Ma et al. 2007
BR3	*Bos1*	CGCGGTAAGTGAGGTCTAGG	Ma et al. 2007
BR4	*Bos1*	AGCTCGATTCTCCAAAGCAG	Ma et al. 2007
BR5	*Bos1*	AAGTACTCGCAGTCGGTGGT	Ma et al. 2007
Cmd5	Calmodulin	CCGAGTACAAGGAGGCCTTC	Hong et al. 2005
Cmd6	Calmodulin	CCGATAGAGGTCATAACGTGG	Salah et al. 2019
Chs-345r	*Chs-1*	TGGAAGAACCATCTGTGAGAGTTG	Carbone and Kohn 1999
Chs-79f	*Chs-1*	TGGGGCAAGGATGCTTGGAAGAAG	Carbone and Kohn 1999
AspCytF8	*Cytb*	ACACAGTAGAAATTTGTCCTAACTC	Chapter 3
AspCytR9	*Cytb*	ATGATAGATTCACCACAACCAGCTA	Chapter 3
Qo13ext	*Cytb*	GGTATAACCCGACGGGGTTATAGAATAG	Fernández-Ortuño et al. 2012a
Qo14ext	*Cytb*	AACCATCTCCATCCACCATACCTACAAA	Fernández-Ortuño et al. 2012a
Erg27beg	*Erg27*	TGGGATTACCACCATGGGAGACAAGTG	Fillinger et al. 2008
Erg27end2	*Erg27*	CAATGGTTCCGCATTTCTTTGCCTCC	Cosseboom and Hu 2021b
G3pdhfor+	*Gapdh*	ATTGACATCGTCGCTGTCAACGA	Staats et al. 2005
G3pdhrev+	*Gapdh*	ACCCCACTCGTTGTCGTACCA	Staats et al. 2005
Gdf	*Gapdh*	GCCGTCAACGACCCCTTCATTGA	Templeton et al. 1992
Gdr	*Gapdh*	GGGTGGAGTCGTACTTGAGCATGT	Templeton et al. 1992
ITS1	*ITS*	TCCGTAGGTGAACCTGCGG	White et al. 1990
ITS4	*ITS*	TCCTCCGCTTATTGATATGC	White et al. 1990
Mfsm2-pfor	*Mfsm2*	TAGCCAATGGATCCTACG	Kretschmer et al. 2009
Mfsm2-prev	*Mfsm2*	CGAGATGGATGCCATTTCAGAG	Kretschmer et al. 2009
Mrr1-atg	*Mrr1*	TCAACATCATGAATCCAACAGTC	Kretschmer et al. 2009
TF1-4	*Mrr1*	GGATAGGGTATTGCGTAGATCG	Kretschmer et al. 2009
TF1-2-new	*Mrr1*	CTATCCGATCGACCGGTA	Leroch et al. 2013
TF1-3-new	*Mrr1*	TGCTGTGACGAGCATGAC	Leroch et al. 2013
Frpb2-7cr	*Rpb2*	CCCATRGCTTGYTTRCCCAT	Liu et al. 1999
Rpb2-5f2	*Rpb2*	GGGGWGAYCAGAAGAAGGC	Sung et al. 2007
IpBcBeg	*SdhB*	CCACTCCTCCATAATGGCTGCTCTCCGC	Leroux et al. 2010
IpBcEnd	*SdhB*	CTCATCAAGCCCCCTCATTGATATC	Leroux et al. 2010
728f	*Tef1*	CATCGAGAAGTTCGAGAAGG	Carbone and Kohn 1999
EF2	*Tef1*	GGARGTACCAGTSATCATGTT	O'Donnell and Cigelnik 1997
TEF1	*Tef1*	ATGGGTAAGGAGGACAAGAC	O'Donnell et al. 1998
TEF1	*Tef1*	GGAAGTACCAGTGATCATGTT	O'Donnell et al. 1998
TubF1	β-tubulin	GCTTTTGATCTCCAAGATCCG	Banno et al. 2008
TubR1	β-tubulin	CTGGTCAAAGGAGCAAATCC	Banno et al. 2008
BT2A	β-tubulin	GGTAACCAAATCGGTGCTGCTTTC	Glass and Donaldson 1995
BT2B	β-tubulin	ACCCTCAGTGTAGTGACCCTTGGC	Glass and Donaldson 1995
BtubAcuf	β-tubulin	GGAAACATTCCGCTGACCAT	Cosseboom and Hu 2021a
BtubAcuGlor	β-tubulin	AGCACCAATCTGGTTACCCTGT	Cosseboom and Hu 2021a
BtubGlof	β-tubulin	TGGATTGTTTTGCTGACTGC	Cosseboom and Hu 2021a
Btub2fd	β-tubulin	GTBCACCTYCARACCGGYCARTG	Woudenberg et al. 2009
Btub4rd	β-tubulin	CCRGAYTGRCCRAARACRAAGTTGTC	Woudenberg et al. 2009

Table A2. GenBank accession numbers of the genomic regions actin, Apn2 to MAT1-2-1 intergenic region (Ap-MAT), calmodulin (CAM), chitin synthase 1 (CHS-1), glyceraldehyde-3-phosphate dehydrogenase (GAPDH), internal transcribed spacer (ITS), RNA polymerase subunit II (RPB2), translation elongation factor-1 (TEF1), and β-tubulin (TUB2) of various fungi utilized for phylogenic analysis, with type strains indicated with an asterisk and isolates collected in this study in bold

Species	Isolate name	Actin	Ap-MAT	CAM	CHS-1	GAPDH	ITS	RPB2	TEF1	TUB2
Alternaria alternata	CBS 916.96*	-	-	-	-	-	AF347031	KC584375	-	-
Alternaria anigozanthi	CBS 121920*	-	-	-	-	-	KC584180	KC584376	-	-
Alternaria arborescens	CBS 102605*	-	-	-	-	-	AF347033	KC584377	-	-
Alternaria armoraciae	CBS 118702*	-	-	-	-	-	KC584182	KC584379	-	-
Alternaria aspera	CBS 115269*	-	-	-	-	-	KC584242	KC584474	-	-
Alternaria atra	ATCC 18040*	-	-	-	-	-	AF229486	KC584475	-	-
Alternaria avenicola	CBS 121459*	-	-	-	-	-	KC584183	KC584380	-	-
Alternaria axiaeriisporifera	CBS 118715*	-	-	-	-	-	KC584184	KC584381	-	-
Alternaria capsici-annui	CBS 504.74	-	-	-	-	-	KC584187	KC584385	-	-
Alternaria caricis	CBS 480.90*	-	-	-	-	-	AY278839	KC584467	-	-
Alternaria carotiincultae	CBS 109381*	-	-	-	-	-	KC584188	KC584386	-	-
Alternaria cheiranthi	CBS 109384	-	-	-	-	-	AF229457	KC584387	-	-
Alternaria chlamydospora	CBS 491.72*	-	-	-	-	-	KC584189	KC584388	-	-
Alternaria cinerariae	CBS 116495	-	-	-	-	-	KC584190	KC584389	-	-
Alternaria conjuncta	CBS 196.86*	-	-	-	-	-	FJ266475	KC584390	-	-
Alternaria dauci	CBS 117097	-	-	-	-	-	KC584192	KC584392	-	-
Alternaria daucifolii	CBS 118812*	-	-	-	-	-	KC584193	KC584393	-	-
Alternaria dianthicola	CBS 116491	-	-	-	-	-	KC584194	KC584394	-	-
Alternaria embellisia	CBS 339.71	-	-	-	-	-	KC584230	KC584449	-	-
Alternaria gaisen	CBS 632.93	-	-	-	-	-	KC584197	KC584399	-	-
Alternaria hyacinthi	CBS 416.71*	-	-	-	-	-	KC584233	KC584457	-	-
Alternaria japonica	CBS 118390	-	-	-	-	-	KC584201	KC584405	-	-
Alternaria leucanthemi	CBS 421.65*	-	-	-	-	-	KC584240	KC584472	-	-
Alternaria limoniasperae	CBS 102595*	-	-	-	-	-	FJ266476	KC584408	-	-
Alternaria longipes	CBS 540.94	-	-	-	-	-	AY278835	KC584409	-	-
Alternaria papavericola	CBS 116606*	-	-	-	-	-	FJ357310	KC584446	-	-
Alternaria perpunctulata	CBS 115267*	-	-	-	-	-	KC584210	KC584418	-	-
Alternaria septorioides	CBS 106.41*	-	-	-	-	-	KC584216	KC584427	-	-
Alternaria tenuissima	CBS 918.96	-	-	-	-	-	AF347032	KC584435	-	-
Aspergillus aculeatinus	ITEM 16172*	-	-	EU159241	-	-	-	-	-	-
Aspergillus aculeatus	ITEM 7046*	-	-	EF661148	-	-	-	-	-	-
Aspergillus brasiliensis	ITEM 7048*	-	-	FN594543	-	-	-	-	-	-
Aspergillus brunneoviolaceus	ITEM 7047*	-	-	EF661147	-	-	-	-	-	-
Aspergillus carbonarius	ITEM 4503*	-	-	EF661167	-	-	-	-	-	-
Aspergillus costaricaensis	ITEM 7555*	-	-	FN594545	-	-	-	-	-	-
Aspergillus ellipticus	ITEM 4499*	-	-	EF661170	-	-	-	-	-	-
Aspergillus floridensis	ITEM 14783*	-	-	HE984429	-	-	-	-	-	-
Aspergillus heteromorphus	ITEM 7045*	-	-	EF661169	-	-	-	-	-	-
Aspergillus homomorphus	ITEM 7556*	-	-	FN594549	-	-	-	-	-	-
Aspergillus ibericus	ITEM 4776*	-	-	EF661163	-	-	-	-	-	-
Aspergillus indologenus	ITEM 7038*	-	-	AM419750	-	-	-	-	-	-
Aspergillus japonicus	**GP18-148**	-	-	ON377027	-	-	-	-	-	-
Aspergillus japonicus	**GP19-10**	-	-	ON377032	-	-	-	-	-	-
Aspergillus japonicus	**GP20-321**	-	-	ON377015	-	-	-	-	-	-
Aspergillus japonicus	ITEM 7034*	-	-	FN594551	-	-	-	-	-	-
Aspergillus japonicus	**SL230**	-	-	ON377041	-	-	-	-	-	-
Aspergillus japonicus	**SL231**	-	-	ON377038	-	-	-	-	-	-
Aspergillus lacticoffeatus	ITEM 7559*	-	-	EU163270	-	-	-	-	-	-
Aspergillus luchuensis	ITEM 4507*	-	-	JX500071	-	-	-	-	-	-
Aspergillus neoniger	CBS115656*	-	-	FJ491700	-	-	-	-	-	-
Aspergillus piperis	ITEM 16155*	-	-	EU163267	-	-	-	-	-	-
Aspergillus saccharolyticus	ITEM 16177*	-	-	HM853554	-	-	-	-	-	-
Aspergillus sclerotiicarbonarious	ITEM 16178*	-	-	EU159235	-	-	-	-	-	-
Aspergillus sclerotioniger	ITEM 7560*	-	-	FN594557	-	-	-	-	-	-
Aspergillus trinidadensis	ITEM 14821*	-	-	HE984434	-	-	-	-	-	-
Aspergillus tubingensis	ITEM 7040*	-	-	EF661151	-	-	-	-	-	-
Aspergillus uvarum	**GP18-149**	-	-	ON377039	-	-	-	-	-	-
Aspergillus uvarum	**GP18-150**	-	-	ON377019	-	-	-	-	-	-
Aspergillus uvarum	**GP18-275**	-	-	ON377016	-	-	-	-	-	-
Aspergillus uvarum	**Gp18-276**	-	-	ON377011	-	-	-	-	-	-
Aspergillus uvarum	**GP18-277**	-	-	ON377040	-	-	-	-	-	-
Aspergillus uvarum	**GP18-93**	-	-	ON377029	-	-	-	-	-	-
Aspergillus uvarum	**GP19-11**	-	-	ON377031	-	-	-	-	-	-
Aspergillus uvarum	**GP19-12**	-	-	ON377023	-	-	-	-	-	-
Aspergillus uvarum	**GP19-194P**	-	-	ON377012	-	-	-	-	-	-
Aspergillus uvarum	**GP19-32P**	-	-	ON377026	-	-	-	-	-	-
Aspergillus uvarum	**GP19-60**	-	-	ON377034	-	-	-	-	-	-
Aspergillus uvarum	**GP19-7P**	-	-	ON377030	-	-	-	-	-	-
Aspergillus uvarum	**GP19-8**	-	-	ON377033	-	-	-	-	-	-
Aspergillus uvarum	**GP19-8P**	-	-	ON377022	-	-	-	-	-	-
Aspergillus uvarum	**GP19-9**	-	-	ON377021	-	-	-	-	-	-
Aspergillus uvarum	**GP19-9P**	-	-	ON377025	-	-	-	-	-	-
Aspergillus uvarum	**GP20-111**	-	-	ON377013	-	-	-	-	-	-
Aspergillus uvarum	**GP20-117**	-	-	ON377017	-	-	-	-	-	-
Aspergillus uvarum	**GP20-190**	-	-	ON377018	-	-	-	-	-	-
Aspergillus uvarum	**GP20-194**	-	-	ON377035	-	-	-	-	-	-
Aspergillus uvarum	**GP20-196**	-	-	ON377028	-	-	-	-	-	-

Aspergillus uvarum	**GP20-319**	-	-	ON377036	-	-	-	-	-	-
Aspergillus uvarum	**GP20-320**	-	-	ON377014	-	-	-	-	-	-
Aspergillus uvarum	**GP20-322**	-	-	ON377024	-	-	-	-	-	-
Aspergillus uvarum	**GP20-96**	-	-	ON377020	-	-	-	-	-	-
Aspergillus uvarum	ITEM 4834*	-	-	AM745755	-	-	-	-	-	-
Aspergillus uvarum	**SL216**	-	-	ON377037	-	-	-	-	-	-
Aspergillus vadensis	ITEM 7651*	-	-	FN594560	-	-	-	-	-	-
Aspergillus welwitschiae	ITEM 4509*	-	-	KC480196	-	-	-	-	-	-
Botrytis byssoidea	MUCL94	-	-	-	-	AJ704998	-	-	-	-
Botrytis calthae	CBS175.63	-	-	-	-	AJ704999	-	-	-	-
Botrytis caroliniana	CB15	-	-	-	-	JF811584	-	-	-	-
Botrytis cinerea	B05.10*	-	-	-	-	CP009819	-	-	-	-
Botrytis convoluta	9801	-	-	-	-	AJ705007	-	-	-	-
Botrytis croci	MUCL436	-	-	-	-	AJ705009	-	-	-	-
Botrytis draytonii	9701	-	-	-	-	AJ705019	-	-	-	-
Botrytis elliptica	BE9714	-	-	-	-	AJ705012	-	-	-	-
Botrytis fabae	CBS109.57	-	-	-	-	AJ705013	-	-	-	-
Botrytis ficarum	CBS176.63	-	-	-	-	AJ705015	-	-	-	-
Botrytis fragariae	SP30	-	-	-	-	KY200497	-	-	-	-
Botrytis galanthina	MUCL435	-	-	-	-	AJ705018	-	-	-	-
Botrytis globosa	MUCL444	-	-	-	-	AJ705022	-	-	-	-
Botrytis hyacinthi	1	-	-	-	-	AJ705023	-	-	-	-
Botrytis mali	BPI412756	-	-	-	-	EF367129	-	-	-	-
Botrytis narcissicola	MUCL18857	-	-	-	-	AJ705025	-	-	-	-
Botrytis paeoniae	MUCL16084	-	-	-	-	AJ705028	-	-	-	-
Botrytis polyblastis	MUCL21492	-	-	-	-	AJ705031	-	-	-	-
Botrytis porri	MUCL3234	-	-	-	-	AJ705032	-	-	-	-
Botrytis pseudocinerea	Bp-362	-	-	-	-	MH732860	-	-	-	-
Botrytis ranunculi	CBS178.63	-	-	-	-	AJ705034	-	-	-	-
Botrytis sclerotiorum	484	-	-	-	-	AJ705044	-	-	-	-
Botrytis sphaerosperma	MUCL21481	-	-	-	-	AJ705035	-	-	-	-
Botrytis squamosa	PRI026	-	-	-	-	AJ705039	-	-	-	-
Botrytis tulipae	BT9830	-	-	-	-	AJ705041	-	-	-	-
Cladosporium acalyphae	CBS 125982	HM148481	-	-	-	-	HM147994	-	HM148235	-
Cladosporium aciculare	CBS 140488	KT600607	-	-	-	-	KT600411	-	KT600509	-
Cladosporium aggregatocicatricatum	CBS 140493	KT600645	-	-	-	-	KT600448	-	KT600547	-
Cladosporium allicinum	CBS 121624	EF679502	-	-	-	-	EF679350	-	EF679425	-
Cladosporium angustiherbarum	CBS 140479	KT600574	-	-	-	-	KT600378	-	KT600475	-
Cladosporium angustisporum	CBS 125983	HM148482	-	-	-	-	HM147995	-	HM148236	-
Cladosporium angustiterminale	CBS 140480	KT600575	-	-	-	-	KT600379	-	KT600476	-
Cladosporium aphidis	CBS 132182	JN906998	-	-	-	-	JN906978	-	JN906985	-
Cladosporium arthropodii	CBS 124043	JN906998	-	-	-	-	JN906979	-	JN906985	-
Cladosporium asperulatum	CBS 126340	HM148485	-	-	-	-	HM147998	-	HM148239	-
Cladosporium australiense	CBS 125984	HM148486	-	-	-	-	HM147999	-	HM148240	-
Cladosporium austroafricanum	CBS 140481	KT600577	-	-	-	-	KT600381	-	KT600478	-
Cladosporium austrohemisphaericum	CBS 140482	KT600578	-	-	-	-	KT600382	-	KT600479	-
Cladosporium basiinflatum	CBS 822.84	HM148487	-	-	-	-	HM148000	-	HM148241	-
Cladosporium chalastosporoides	CBS 125985	HM148488	-	-	-	-	HM148001	-	HM148242	-
Cladosporium chubutense	CBS 124457	FJ936165	-	-	-	-	FJ936158	-	FJ936161	-
Cladosporium cladosporioides	CBS 101367	HM148489	-	-	-	-	HM148002	-	HM148243	-
Cladosporium colombiae	CBS 274.80B	FJ936166	-	-	-	-	FJ936159	-	FJ936163	-
Cladosporium cucumerinum	CBS 108.23	HM148557	-	-	-	-	HM148068	-	HM148312	-
Cladosporium delicatulum	CBS 126342	HM148568	-	-	-	-	HM148079	-	HM148323	-
Cladosporium dominicanum	CBS 119415	EF101368	-	-	-	-	DQ780353	-	JN906986	-
Cladosporium echinulatum	CBS 123191	JN906999	-	-	-	-	JN906980	-	JN906987	-
Cladosporium exasperatum	CBS 125986	HM148579	-	-	-	-	HM148090	-	HM148334	-
Cladosporium exile	CBS 125987	HM148580	-	-	-	-	HM148091	-	HM148335	-
Cladosporium flabelliforme	CBS 126345	HM148581	-	-	-	-	HM148092	-	HM148336	-
Cladosporium funiculosum	CBS 122128	HM148582	-	-	-	-	HM148093	-	HM148337	-
Cladosporium fusiforme	CBS 119414	EF101372	-	-	-	-	DQ780388	-	JN906988	-
Cladosporium gamsianum	CBS 125989	HM148584	-	-	-	-	HM148095	-	HM148339	-
Cladosporium globisporum	CBS 812.96	HM148585	-	-	-	-	HM148096	-	HM148340	-
Cladosporium halotolerans	CBS 119416	EF101397	-	-	-	-	DQ780364	-	JN906989	-
Cladosporium herbaroides	CBS 121626	EF679509	-	-	-	-	EF679357	-	EF679432	-
Cladosporium herbarum	CBS 121621	EF679516	-	-	-	-	EF679363	-	EF679440	-
Cladosporium hillianum	CBS 125988	HM148586	-	-	-	-	HM148097	-	HM148341	-
Cladosporium inversicolor	CBS 143.65	HM148589	-	-	-	-	HM148100	-	HM148344	-
Cladosporium iperenia	CBS 140483	KT600589	-	-	-	-	KT600394	-	KT600491	-
Cladosporium iranicum	CBS 126346	HM148599	-	-	-	-	HM148110	-	HM148354	-
Cladosporium iridis	CBS 138.40	EF679523	-	-	-	-	EF679370	-	EF679447	-
Cladosporium langeronii	CBS 189.54	EF101357	-	-	-	-	DQ780379	-	JN906990	-
Cladosporium licheniphilum	CBS 125990	HM148600	-	-	-	-	HM148111	-	HM148355	-
Cladosporium limoniforme	CBS 113737	KT600591	-	-	-	-	KT600396	-	KT600493	-
Cladosporium longicatenatum	CBS 140485	KT600598	-	-	-	-	KT600403	-	KT600500	-
Cladosporium longissimum	CBS 300.96	EF101385	-	-	-	-	DQ780352	-	EU570259	-
Cladosporium macrocarpum	CBS 121623	EF679529	-	-	-	-	EF679375	-	EF679453	-
Cladosporium montecillanum	CBS 140486	KT600602	-	-	-	-	KT600406	-	KT600504	-
Cladosporium myrtacearum	CBS 126350	HM148606	-	-	-	-	HM148117	-	HM148361	-
Cladosporium paracladosporioides	CBS 171.54	HM148609	-	-	-	-	HM148120	-	HM148364	-
Cladosporium parapenidielloides	CBS 140487	KT600606	-	-	-	-	KT600410	-	KT600508	-
Cladosporium penidielloides	CBS 140489	KT600608	-	-	-	-	KT600412	-	KT600510	-

Cladosporium perangustum	CBS 125996	HM148610	-	-	-	-	HM148121	-	HM148365	-
Cladosporium phaenocomae	CBS 128769	JF499881	-	-	-	-	JF499837	-	JF499875	-
Cladosporium phlei	CBS 358.69	JN907000	-	-	-	-	JN906981	-	JN906991	-
Cladosporium phyllactiniicola	CBS 126352	HM148639	-	-	-	-	HM148150	-	HM148394	-
Cladosporium phyllophilum	CBS 125992	HM148643	-	-	-	-	HM148154	-	HM148398	-
Cladosporium pini-ponderosae	CBS 124456	FJ936167	-	-	-	-	FJ936160	-	FJ936164	-
Cladosporium pseudochalastosporoides	CBS 140490	KT600611	-	-	-	-	KT600415	-	KT600513	-
Cladosporium pseudocladosporioides	CBS 125993	HM148647	-	-	-	-	HM148158	-	HM148402	-
Cladosporium psychrotolerans	CBS 119412	EF101365	-	-	-	-	DQ780386	-	JN906992	-
Cladosporium puyae	CBS 274.80A	KT600614	-	-	-	-	KT600418	-	KT600516	-
Cladosporium ramotenellum	CBS 109031	KT600615	-	-	-	-	KT600419	-	KT600517	-
Cladosporium rectoides	CBS 125994	HM148683	-	-	-	-	HM148193	-	HM148438	-
Cladosporium rhusicola	CBS 140492	KT600637	-	-	-	-	KT600440	-	KT600539	-
Cladosporium ruguloflabelliforme	CBS 140494	KT600655	-	-	-	-	KT600458	-	KT600557	-
Cladosporium rugulovarians	CBS 140495	KT600656	-	-	-	-	KT600459	-	KT600558	-
Cladosporium salinae	CBS 119413	EF101390	-	-	-	-	DQ780374	-	JN906993	-
Cladosporium sinuosum	CBS 121629	EF679540	-	-	-	-	EF679386	-	EF679464	-
Cladosporium sphaerospermum	CBS 102045	EF101378	-	-	-	-	DQ780351	-	EU570262	-
Cladosporium subinflatum	CBS 121630	EF679543	-	-	-	-	EF679389	-	EF679467	-
Cladosporium subuliforme	CBS 126500	HM148686	-	-	-	-	HM148196	-	HM148441	-
Cladosporium tenuissimum	CBS 125995	HM148687	-	-	-	-	HM148197	-	HM148442	-
Cladosporium uredinicola	ATCC 46649	HM148712	-	-	-	-	AY251071	-	HM148467	-
Cladosporium variabile	CBS 121635	EF679556	-	-	-	-	EF679402	-	EF679480	-
Cladosporium varians	CBS 126360	HM148713	-	-	-	-	HM148222	-	HM148468	-
Cladosporium velox	CBS 119417	EF101388	-	-	-	-	DQ780361	-	JN906995	-
Cladosporium verrucocladosporioides	CBS 126363	HM148717	-	-	-	-	HM148226	-	HM148472	-
Cladosporium versiforme	CBS 140491	KT600613	-	-	-	-	KT600417	-	KT600515	-
Cladosporium xylophilum	CBS 113749	HM148719	-	-	-	-	HM148228	-	HM148474	-
Colletotrichum acutatum	CBS 112996*	-	- [a]	-	JQ005797	JQ948677	-	-	-	JQ005860
Colletotrichum acutatum	CBS:112996	-	-	-	JQ005797	JQ948677	JQ005776	-	-	JQ005860
Colletotrichum aenigma	**GP19-105**	-	OL982489	-	OL982426	OL982445	-	-	-	OL982464
Colletotrichum aenigma	**GP19-113**	-	OL982488	-	OL982427	OL982446	-	-	-	OL982465
Colletotrichum aenigma	**GP19-114**	-	OL982487	-	OL982428	OL982447	-	-	-	OL982466
Colletotrichum aenigma	**GP19-46**	-	OL982493	-	OL982422	OL982441	-	-	-	OL982460
Colletotrichum aenigma	**GP19-52**	-	OL982492	-	OL982423	OL982442	-	-	-	OL982461
Colletotrichum aenigma	**GP19-75**	-	OL982491	-	OL982424	OL982443	-	-	-	OL982462
Colletotrichum aenigma	**GP19-76**	-	OL982490	-	OL982425	OL982444	-	-	-	OL982463
Colletotrichum aenigma	**GP20-145**	-	OL982486	-	OL982429	OL982448	-	-	-	OL982467
Colletotrichum aenigma	**GP20-150**	-	OL982485	-	OL982431	OL982449	-	-	-	OL982469
Colletotrichum aenigma	**GP21-66**	-	OL982477	-	OL982420	OL982439	-	-	-	OL982458
Colletotrichum aenigma	ICMP 18608*	-	KM360143	-	JX009774	JX010044	-	-	-	JX010389
Colletotrichum aenigma	ICMP:18608	-	-	-	JX009774	JX010044	JX010244	-	-	JX010389
Colletotrichum alatae	ICMP 17919*	-	KC888932	-	JX009837	JX009990	-	-	-	JX010383
Colletotrichum alienum	ICMP 12071*	-	KM360144	-	JX009882	JX010028	-	-	-	JX010411
Colletotrichum alienum	ICMP:17673	-	-	-	JX009754	JX010018	JX010217	-	-	JX010385
Colletotrichum aotearoa	ICMP 18537*	-	KC888930	-	JX009853	JX010005	-	-	-	JX010420
Colletotrichum asianum	ICMP 18580*	-	FR718814	-	JX009867	JX010053	-	-	-	JX010406
Colletotrichum camelliae	LS-19*									
Colletotrichum capsici	CBS:120709	-	-	-	-	-	EF683603	-	-	EF683602
Colletotrichum chrysophilum	CMM4268*	-	KX094325	-	KX094083	KX094183	-	-	-	KX094285
Colletotrichum chrysophilum	CMM4363	-	KX094323	-	KX094071	KX094180	-	-	-	KX094283
Colletotrichum clidemiae	ICMP 18658*	-	KC888929	-	JX009877	JX009989	-	-	-	JX010438
Colletotrichum cliviicola	CSSK4	-	-	-	GQ856722	GQ856756	GQ485607	-	-	GQ849440
Colletotrichum conoides	CAUG17	-	-	-	KP890156	KP890163	KP890169	-	-	KP890174
Colletotrichum conoides	CAUG17*	-	-	-	KP890156	KP890162	-	-	-	KP890174
Colletotrichum cordylinicola	ICMP 18579*	-	JQ899274	-	JX009864	JX009975	-	-	-	JX010440
Colletotrichum fioriniae	CBS 125396	-	-	-	JQ948960	JQ948629	-	-	-	JQ949950
Colletotrichum fioriniae	CBS:125396	-	-	-	JQ948960	JQ948629	JQ948299	-	-	JQ949950
Colletotrichum fioriniae	**GP19-104**	-	-	-	OL982324	OL982366	-	-	-	OL982398
Colletotrichum fioriniae	**GP19-146**	-	-	-	OL982328	OL982367	-	-	-	OL982399
Colletotrichum fioriniae	**GP20-127**	-	-	-	OL982331	OL982376	-	-	-	OL982408
Colletotrichum fioriniae	**GP20-128**	-	-	-	OL982332	OL982375	-	-	-	OL982407
Colletotrichum fioriniae	**GP20-139**	-	-	-	OL982335	OL982374	-	-	-	OL982406
Colletotrichum fioriniae	**GP20-176**	-	-	-	OL982340	OL982373	-	-	-	OL982405
Colletotrichum fioriniae	**GP20-181**	-	-	-	OL982342	OL982372	-	-	-	OL982404
Colletotrichum fioriniae	**GP20-228**	-	-	-	OL982344	OL982371	-	-	-	OL982403
Colletotrichum fioriniae	**GP20-252**	-	-	-	OL982347	OL982370	-	-	-	OL982402
Colletotrichum fioriniae	**GP21-27**	-	-	-	OL982354	OL982361	-	-	-	OL982393
Colletotrichum fioriniae	**GP21-59**	-	-	-	OL982355	OL982360	-	-	-	OL982392
Colletotrichum fructicola	**GP19-39**	-	OL982494	-	OL982421	OL982440	-	-	-	OL982459
Colletotrichum fructicola	**GP20-241**	-	OL982484	-	OL982430	OL982451	-	-	-	OL982468
Colletotrichum fructicola	**GP20-242**	-	OL982483	-	OL982432	OL982452	-	-	-	OL982470
Colletotrichum fructicola	**GP20-243**	-	OL982482	-	OL982433	OL982453	-	-	-	OL982471
Colletotrichum fructicola	**GP21-171**	-	OL982479	-	OL982434	OL982454	-	-	-	OL982474
Colletotrichum fructicola	**GP21-185**	-	OL982478	-	OL982435	OL982455	-	-	-	OL982476
Colletotrichum fructicola	**GP21-64**	-	OL982480	-	OL982436	OL982456	-	-	-	OL982473
Colletotrichum fructicola	ICMP 18581*	-	JQ807838	-	JX009866	JX010033	-	-	-	JX010405
Colletotrichum fructicola	ICMP:18613	-	-	-	JX009772	JX009998	JX010167	-	-	JX010388
Colletotrichum fructicola	Y5	-	MZ724633	-	MZ724653	MZ724658	-	-	-	MZ724648
Colletotrichum fructivorum	Coll1414*	-	JX145300	-	-	-	-	-	-	JX145196
Colletotrichum gloeosporioides	CBS 112999*	-	JQ807843	-	JQ005326	JQ005239	-	-	-	JQ005587

Colletotrichum gloeosporioides	ICMP:17821	-	-	-	JX009818	JX010056	JX010152	-	-	JX010445
Colletotrichum godetiae	CBS 796.72	-	-	-	JQ949068	JQ948738	-	-	-	JQ950058
Colletotrichum godetiae	CBS:796.72	-	-	-	JQ949068	JQ948738	JQ948407	-	-	JQ950058
Colletotrichum hebeiense	JZB330024	-	KF377573	-	-	KF377505	-	-	-	-
Colletotrichum hebeiense	JZB330028	-	-	-	KF289008	KF377495	KF156863	-	-	KF288975
Colletotrichum henanense	CGMCC 3.17354*	-	KJ954524	-	-	KJ954810	-	-	-	KJ955257
Colletotrichum horii	ICMP 10492*	-	JQ807840	-	JX009752	GQ329681	-	-	-	JX010450
Colletotrichum jiangxiense	CHMCC 3.17890	-	KU251730	-	KU251941	KU252047	-	-	-	KU252202
Colletotrichum kahawae	ICMP 17816*	-	JQ894579	-	JX009813	JX010012	-	-	-	JX010444
Colletotrichum kahawae subsp. ciggaro	ICMP:18539	-	-	-	JX009800	JX009966	JX010230	-	-	JX010434
Colletotrichum lupini	IMI 351261	-	-	-	JQ948838	JQ948507	-	-	-	JQ949828
Colletotrichum lupini	IMI:351261	-	-	-	JQ948838	JQ948507	JQ948177	-	-	JQ949828
Colletotrichum melonis	CBS 159.84*	-	-	-	JQ948855	JQ948524	-	-	-	JQ949845
Colletotrichum melonis	CBS:159.84	-	-	-	JQ948855	JQ948524	JQ948194	-	-	JQ949845
Colletotrichum musae	ICMP 19119*	-	KC888926	-	JX009896	JX010050	-	-	-	HQ596280
Colletotrichum noveboracense	ACFK109*	-	MN640564	-	-	MN640567	-	-	-	MN640569
Colletotrichum nupharicola	CBS469.96	-	-	-	JX009834	JX009936	JX010189	-	-	JX010397
Colletotrichum nymphaeae	CBS 100064	-	-	-	JQ948885	JQ948554	-	-	-	JQ949875
Colletotrichum nymphaeae	CBS:100064	-	-	-	JQ948885	JQ948554	JQ948224	-	-	JQ949875
Colletotrichum nymphaeae	**GP19-130**	-	-	-	OL982325	OL982364	-	-	-	OL982396
Colletotrichum nymphaeae	**GP19-132**	-	-	-	OL982326	OL982368	-	-	-	OL982400
Colletotrichum nymphaeae	**GP19-138**	-	-	-	OL982327	OL982363	-	-	-	OL982395
Colletotrichum nymphaeae	**GP19-154**	-	-	-	OL982329	OL982362	-	-	-	OL982394
Colletotrichum nymphaeae	**GP19-160**	-	-	-	OL982330	OL982369	-	-	-	OL982401
Colletotrichum nymphaeae	**GP20-135**	-	-	-	OL982333	OL982387	-	-	-	OL982419
Colletotrichum nymphaeae	**GP20-138**	-	-	-	OL982334	OL982382	-	-	-	OL982414
Colletotrichum nymphaeae	**GP20-144**	-	-	-	OL982336	OL982385	-	-	-	OL982417
Colletotrichum nymphaeae	**GP20-154**	-	-	-	OL982337	OL982381	-	-	-	OL982413
Colletotrichum nymphaeae	**GP20-157**	-	-	-	OL982338	OL982380	-	-	-	OL982412
Colletotrichum nymphaeae	**GP20-158**	-	-	-	OL982339	OL982379	-	-	-	OL982411
Colletotrichum nymphaeae	**GP20-179**	-	-	-	OL982341	OL982365	-	-	-	OL982397
Colletotrichum nymphaeae	**GP20-186**	-	-	-	OL982343	OL982378	-	-	-	OL982410
Colletotrichum nymphaeae	**GP20-248**	-	-	-	OL982345	OL982384	-	-	-	OL982416
Colletotrichum nymphaeae	**GP20-249**	-	-	-	OL982346	OL982386	-	-	-	OL982418
Colletotrichum nymphaeae	**GP20-267**	-	-	-	OL982348	OL982383	-	-	-	OL982415
Colletotrichum nymphaeae	**GP20-268**	-	-	-	OL982349	OL982377	-	-	-	OL982409
Colletotrichum nymphaeae	**GP21-135**	-	-	-	OL982350	OL982359	-	-	-	OL982391
Colletotrichum nymphaeae	**GP21-170**	-	-	-	OL982351	OL982358	-	-	-	OL982390
Colletotrichum nymphaeae	**GP21-175**	-	-	-	OL982352	OL982357	-	-	-	OL982389
Colletotrichum nymphaeae	**GP21-178**	-	-	-	OL982353	OL982356	-	-	-	OL982388
Colletotrichum orchidophilum	CBS 632.80*	-	-	-	JQ948812	JQ948481	-	-	-	JQ949802
Colletotrichum orchidophilum	CBS:632.80	-	-	-	JQ948812	JQ948481	JQ948151	-	-	JQ949802
Colletotrichum perseae	CBS 141365	-	KX620177	-	-	KX620242	-	-	-	KX620341
Colletotrichum perseae	GA039	-	-	-	-	KX620236	KX620302	-	-	KX620335
Colletotrichum psidii	ICMP 19120*	-	KC888931	-	JX009901	JX009967	-	-	-	JX010443
Colletotrichum queenslandicum	ICMP 1778*	-	KC888928	-	JX009899	JX009934	-	-	-	JX010414
Colletotrichum salsolae	ICMP 19051*	-	KC888925	-	JX009863	JX009916	-	-	-	JX010403
Colletotrichum scovillei	CBS 126529*	-	-	-	JQ948928	JQ948597	-	-	-	JQ949918
Colletotrichum scovillei	CBS:126529	-	-	-	JQ948928	JQ948597	JQ948267	-	-	JQ949918
Colletotrichum siamense	**GP21-9**	-	OL982481	-	OL982437	OL982450	-	-	-	OL982472
Colletotrichum siamense	ICMP 18578*	-	JQ899289	-	JX009865	JX009924	-	-	-	JX010404
Colletotrichum temperatum	Coll883*	-	JX145298	-	-	-	-	-	-	JX145211
Colletotrichum temperatum	**GP21-177**	-	OL982495	-	OL982438	OL982457	-	-	-	OL982475
Colletotrichum theobromicola	ICMP 18649*	-	KC790726	-	JX009869	JX010006	-	-	-	JX010447
Colletotrichum ti	ICMP 4832*	-	KM360146	-	JX009898	JX009952	-	-	-	JX010442
Colletotrichum tropicale	ICMP 18653*	-	KC790728	-	JX009870	JX010007	-	-	-	JX010407
Colletotrichum viniferum	C1-3	-	-	-	-	KF377469	KF156840	-	-	KF288965
Colletotrichum wuxiense	CGMCC 3.17894*	-	KU251722	-	KU251939	KU252045	-	-	-	KU252200
Colletotrichum xanthorrhoeae	ICMP 17903*	-	KC790689	-	JX009823	JX009927	-	-	-	JX010448
Diaporthe ampelina	CBS 111888	-	-	KC343258	-	-	KC343016	-	KC343742	KC343984
Diaporthe corylina	CBS 121124	-	-	KC343246	-	-	KC343004	-	KC343730	KC343972
Diaporthe eres	CAA829	-	-	MK883832	-	-	MK792306	-	MK828077	MK837928
Diaporthe eres	CBS 101742	-	-	KC343315	-	-	KC343073	-	KC343799	KC344041
Diaporthe eres	CBS 109767	-	-	KC343801	-	-	KC343075	-	KC344043	KC343559
Diaporthe eres	CBS 113470	-	-	KC343388	-	-	KC343146	-	KC343872	KC344114
Diaporthe eres	CBS 121004	-	-	KC343376	-	-	KC343134	-	KC343860	KC344102
Diaporthe eres	CBS 139.27	-	-	KC343289	-	-	KC343047	-	KC343773	KC344015
Diaporthe eres	CBS 143349	-	-	MG281712	-	-	MG281017	-	MG281538	MG281190
Diaporthe eres	CBS 160.32	-	-	KC343465	-	-	KC343228	-	KC343954	KC344196
Diaporthe eres	CBS 495.72	-	-	KC343249	-	-	KC343007	-	KC343733	KC343975
Diaporthe fibrosa	CBS 109751	-	-	KC343341	-	-	KC343099	-	KC343825	KC344067
Diaporthe guangxiensis	JZB320082	-	-	MK736715	-	-	MK335760	-	MK523557	MK500156
Diaporthe impula	CBS 114434	-	-	KC343363	-	-	KC343121	-	KC343847	KC344089
Diaporthe paranensis	CBS 133184	-	-	KC343413	-	-	KC343171	-	KC343897	KC344139
Diaporthe pseudomangiferae	CBS 101339	-	-	KC343423	-	-	KC343181	-	KC343907	KC344149
Diaporthe viniferae	JZB320071*	-	-	MK500119	-	-	MK341551	-	MK500107	MK500112
Fusarium fujikuroi	5538	-	-	-	-	-	-	-	MN193860.1	-
Fusarium fujikuroi	31857	-	-	-	-	-	-	-	KX656178.1	-
Fusarium fujikuroi	31862	-	-	-	-	-	-	-	KX656179.1	-
Fusarium fujikuroi	31879	-	-	-	-	-	-	-	KX656180.1	-
Fusarium fujikuroi	31883	-	-	-	-	-	-	-	KX656181.1	-

Fusarium fujikuroi	31886	-	-	-	-	-	-	-	KX656182.1	-
Fusarium fujikuroi	66430	-	-	-	-	-	-	-	KX656192.1	-
Fusarium globosum	26131	-	-	-	-	-	-	-	KF466417.1	-
Fusarium proliferatum	31860	-	-	-	-	-	-	-	KX656208.1	-
Fusarium proliferatum	31865	-	-	-	-	-	-	-	KX656209.1	-
Fusarium proliferatum	31866	-	-	-	-	-	-	-	KX656210.1	-
Fusarium proliferatum	31871	-	-	-	-	-	-	-	KX656212.1	-
Fusarium proliferatum	31880	-	-	-	-	-	-	-	MH398167.1	-
Fusarium proliferatum	31915	-	-	-	-	-	-	-	KX656213.1	-
Fusarium proliferatum	66416	-	-	-	-	-	-	-	KX656214.1	-
Fusarium verticillioides	22172	-	-	-	-	-	-	-	MW402146.1	-
Neopestalotiopsis asiatica	NN0476380	-	-	-	-	-	JX398983	-	JX399049	JX399018
Neopestalotiopsis clavispora	NN043011	-	-	-	-	-	JX398978	-	JX399044	JX399013
Neopestalotiopsis clavispora	NN043133	-	-	-	-	-	JX398979	-	JX399045	JX399014
Neopestalotiopsis rosae	TOR-802-803-804	-	-	-	-	-	KU096879	-	KU096881	KU096880
Neopestalotiopsis foedans	CGMCC 3.912	-	-	-	-	-	JX398987	-	JX399053	JX399022
Neopestalotiopsis honoluluana	CBS 111535	-	-	-	-	-	KM199363	-	KM199546	KM199461
Neopestalotiopsis iraniensis	CBS 137767	-	-	-	-	-	KM074045	-	KM074053	KM074056
Neopestalotiopsis iraniensis	CBS 137768	-	-	-	-	-	KM074048	-	KM074051	KM074057
*Neopestalotiopsis javaensis***	CBS 257.31	-	-	-	-	-	KM199357	-	KM199543	KM199437
Neopestalotiopsis mesopotamica	CBS 137766	-	-	-	-	-	KM074047	-	KM074054	KM074058
Neopestalotiopsis mesopotamica	CBS 299.74	-	-	-	-	-	KM199361	-	KM199541	KM199435
Neopestalotiopsis rosae	7927	-	-	-	-	-	KY271740	-	KY271093	KY271094
Neopestalotiopsis rosae	14-691R	-	-	-	-	-	MK895142	-	MK903334	MK903338
Neopestalotiopsis rosae	97-49F	-	-	-	-	-	MK895141	-	MK903333	MK903337
Neopestalotiopsis rosae	CBS 101057	-	-	-	-	-	KM199359	-	KM199523	KM199429
Neopestalotiopsis rosae	CBS 124745	-	-	-	-	-	KM199360	-	KM199524	KM199430
Neopestalotiopsis rosae	CRMFRC	-	-	-	-	-	MN385718	-	MN268532	MN268529
Neopestalotiopsis rosae	CRMFRH	-	-	-	-	-	MN385719	-	MN268533	MN268530
Neopestalotiopsis rosae	PEST3	-	-	-	-	-	KY688075	-	KY688074	KY688073
Neopestalotiopsis sPestalotiopsis	7-43L	-	-	-	-	-	MK895144	-	MK903336	MK903340
Pestalotiopsis cocos	CBS 272.29	-	-	-	-	-	KM199378	-	KM199553	KM199467
Pestalotiopsis indica	CBS 459.78	-	-	-	-	-	KM199381	-	KM199560	KM199470
Pestalotiopsis rhododendri	OP086	-	-	-	-	-	KC537804	-	KC537811	KC537818
Pestalotiopsis trachicarpicola	Op068	-	-	-	-	-	JQ845947	-	JQ845946	JQ845945
Stemphylium herbarum	CBS 191.86*	-	-	-	-	-	KC584239	KC584471	-	-

Table A3. Timing of wounding, inoculation, and harvest of grape clusters of four cultivars that were inoculated with *Alternaria alternata*, *Aspergillus uvarum*, *Botrytis cinerea* and Neopestalotiopsis rosae in 2019 and 2020

Cultivar	**Inoculation timing**	**2019**			**2020**		
		Inoculation	**Wounding**	**Harvest**	**Inoculation**	**Wounding**	**Harvest**
Chardonnay	Bloom	23 May	23 Aug	17 Sep	10 Jun	28 Aug	11 Sep
	Veraison	25 Jul	25 Jul	17 Sep	14 Aug	14 Aug	11 Sep
	Pre-harvest	23 Aug	23 Aug	17 Sep	28 Aug	28 Aug	11 Sep
Chambourcin	Bloom	6 Jun	20 Sep	15 Oct	10 Jun	11 Sep	8 Oct
	Veraison	9 Aug	9 Aug	15 Oct	18 Aug	18 Aug	8 Oct
	Pre-harvest	20 Sep	20 Sep	15 Oct	11 Sep	11 Sep	8 Oct
Cabernet Franc	Bloom	30 May	20 Sep	15 Oct	10 Jun	11 Sep	1 Oct
	Veraison	9 Aug	9 Aug	15 Oct	18 Aug	18 Aug	1 Oct
	Pre-harvest	20 Sep	20 Sep	15 Oct	11 Sep	11 Sep	1 Oct
Merlot	Bloom	30 May	13 Sep	1 Oct	10 Jun	11 Sep	1 Oct
	Veraison	9 Aug	9 Aug	1 Oct	18 Aug	18 Aug	1 Oct
	Pre-harvest	13 Sep	13 Sep	1 Oct	11 Sep	11 Sep	1 Oct

Table A4. Frequency (%) of berries from which fungal genera were isolated from asymptomatic Cabernet Sauvignon berries collected from a commercial Maryland vineyard in 2020

	Collection date										
Genus	**21-May**	**19-Jun**	**7-Jul**	**23-Jul**	**1-Aug**	**17-Aug**	**8-Sep**	**15-Sep**	**25-Sep**	**9-Oct**	**14-Oct**
Alternaria	40	100	100	80	100	50	100	75	50	100	50
Aureobasidium	0	0	0	40	60	0	0	0	0	0	0
Botrytis	0	0	40	0	0	50	0	0	0	0	0
Cladosporium	0	0	0	80	60	0	50	75	100	25	75
Colletotrichum	0	0	0	0	0	0	0	0	75	75	50
Fusarium	60	100	60	20	0	75	25	25	0	25	0
Guignardia	0	0	0	0	20	0	0	0	0	0	0
Neopestalotiopsis	0	0	0	0	0	25	0	50	75	75	100
Nigrospora	0	20	40	0	0	25	0	0	25	50	0
Penicillium	20	20	20	0	0	25	0	0	25	25	25
Pestalotiopsis	0	0	20	20	20	25	100	0	0	100	0
Phomopsis	0	0	0	0	0	25	50	0	0	50	0

Table A5. Amino acid sequences of cytochrome b variants of *Aspergillus uvarum*, with variable codons in bold

Genotype
CytbWT
MRMLKSHPLLKMVNSYMMDSPQPANMSYLWNFGSLLAMCLGMQMVTGVTLAMHYTPSVLEAFNSVEHIMRDVN NGWLVRYLHANTASAFFFLVYLHMGRGLYYGSYK**S**PRTLTWAMGTVMTMVMMATA**F**LGYVLPYGQMSLWGAT VITNTMSAMPWMGQDMVEFMWGGFSVNNATLNRFFALHFLLPFVLAAL**A**LMHLMAMHDTVGSGNPLGMSGNYD RLPFAPYFMFKDLVTIFIFFIVLSMFVFFMPNALGDSENYVMANPMQTPPAIVPEWYLLPFYAILRSMPNKLLGVMAM FSAILALMVMPITDLSKLRGVQFRPLSKVAFYIFVANFLVLMQMGAKHVETPFIELGQISTVLYFAHFFVMVPVVSTIE NSLVELATKK
Cytb2
MRMLKSHPLLKMVNSYMMDSPQPANMSYLWNFGSLLAMCLGMQMVTGVTLAMHYTPSVLEAFNSVEHIMRDVN NGWLVRYLHANTASAFFFLVYLHMGRGLYYGSYK**A**PRTLTWAMGTVMTMVMMATA**F**LGYVLPYGQMSLWGAT VITNTMSAMPWMGQDMVEFMWGGFSVNNATLNRFFALHFLLPFVLAAL**V**LMHLMAMHDTVGSGNPLGMSGNYD RLPFAPYFMFKDLVTIFIFFIVLSMFVFFMPNALGDSENYVMANPMQTPPAIVPEWYLLPFYAILRSMPNKLLGVMAM FSAILALMVMPITDLSKLRGVQFRPLSKVAFYIFVANFLVLMQMGAKHVETPFIELGQISTVLYFAHFFVMVPVVSTIE NSLVELATKK
Cytb3
MRMLKSHPLLKMVNSYMMDSPQPANMSYLWNFGSLLAMCLGMQMVTGVTLAMHYTPSVLEAFNSVEHIMRDVN NGWLVRYLHANTASAFFFLVYLHMGRGLYYGSYK**A**PRTLTWAMGTVMTMVMMATA**L**LGYVLPYGQMSLWGAT VITNTMSAMPWMGQDMVEFMWGGFSVNNATLNRFFALHFLLPFVLAAL**V**LMHLMAMHDTVGSGNPLGMSGNYD RLPFAPYFMFKDLVTIFIFFIVLSMFVFFMPNALGDSENYVMANPMQTPPAIVPEWYLLPFYAILRSMPNKLLGVMAM FSAILALMVMPITDLSKLRGVQFRPLSKVAFYIFVANFLVLMQMGAKHVETPFIELGQISTVLYFAHFFVMVPVVSTIE NSLVELATKK

Table A6. Amino acid variations in *mrr1* of 8 *Botrytis* isolates with fludioxonil sensitive isolate B05.10 as the reference sequence

Species	***B. cinerea***	***B. cinerea* group S**						
Isolate name	**B05.10 (reference)**	**5d5**	**SL1495**	**RR18-16**	**RR18-14**	**BR18-5**	**BR18-21**	**RB18-6**
Fludioxonil resistance phenotype	**Sensitive**	**Sensitive**	**Resistant**	**Resistant**	**Resistant**	**Resistant**	**Resistant**	**Resistant**
Variations	None			A33T				
		Y119D	-[z]	-	-	-	-	-
		N164T	-	-	-	-	-	-
		I228T	-	-	-	-	-	-
		P258S	-	-	-	-	-	-
		V287A	-	-	V287S	-	-	-
		A289S	-	-	-	-	-	-
		N312Q	-	-	-	-	-	-
		T352A	-	-	-	-	-	-
			-	**D354Y**	-	-	-	-
		Q381K	-	-	-	-	-	-
		Q382E	-	-	-	-	-	-
		V392I	-	-	-	-	-	-
		M431I	-	-	-	-	-	-
		M432S	-	-	M432T	-	-	-
		S437T	-	-	-	-	-	-
		I443L[y]	-	-	-	-	-	-
		I445F	-	-	-	-	-	-
		T449S	-			-	-	-
		I492V	-	-	-	-	-	-
		L497V	-	-	**Δ497L/V**	-	-	-
		A498T	-	-	-	-	-	-
		G499C	-	-	-	-	-	-
		Y510F	-	-	-	-	-	-
		C511S	-	-	-	-	-	-
		I513V	-	-	-	-	-	-
		V524A	-	-	-	-	-	-
					F568S			
		V579A	-	-	-	-	-	-
		E601G	-	-	-	-	-	-
		G602S	-	-	-	-	-	-
		R627K	-	-	-	-	-	-
					R634K			
		R656L	-	-	-	-	-	-
		N666D	-	-	**N666G**	-	-	-
		A668G	-	-	-	-	-	-
		G670E	-	-	-	-	-	-
		C671F	-	-	-	-	-	-
		C682R	-	-	-	-	-	-
		S684P	-	-	-	-	-	-
		G702N	-	-	G702S	-	-	-
		G710C	-	-	-	G710Y	-	G710Y
		C744G	-	-	-	-	-	-

[z] "-" = variation is identical to the one listed under the same row of isolate 5d5.

[y] Variations in bold have been previously reported by Fernández-Ortuño et al. 2015.

Table A7. Binding energy, root mean square deviation (RMSD), and hydrogen bonds observed when docking azoxystrobin to three variations of the cytochrome b complex macromolecule of *Aspergillus uvarum* with 50 genetic algorithm runs per variant

Macromolecule	Mutations	Rank	Sub-rank	Run	Binding energy	Cluster RMSD	Reference RMSD	Hydrogen bonds
CytbWT	Wildtype	1	1	48	-6.28	0.00	114.36	E273
		2	1	10	-5.80	0.00	117.39	
		2	2	28	-5.00	1.73	117.21	
		3	1	18	-5.42	0.00	114.79	
		4	1	37	-5.23	0.00	118.73	M125
		4	2	44	-5.19	1.88	119.19	M122; M125
		4	3	43	-4.72	1.94	118.71	
		4	4	50	-4.45	1.65	118.97	
		4	5	33	-4.07	1.96	117.77	
		5	1	21	-5.12	0.00	117.33	
		5	2	41	-4.82	1.71	117.60	
		5	3	46	-4.44	1.96	119.93	
		5	4	6	-4.35	1.95	118.43	
		6	1	32	-5.05	0.00	118.11	
		6	2	14	-4.87	1.98	118.07	
		6	3	23	-4.11	1.46	119.15	
		7	1	16	-4.88	0.00	119.19	M122
		7	2	8	-4.84	1.29	118.78	
		7	3	45	-3.49	1.87	120.41	
		7	4	7	-2.94	1.88	120.27	
		8	1	38	-4.86	0.00	119.04	
		8	2	34	-3.94	1.84	120.22	
		9	1	29	-4.86	0.00	117.88	
		9	2	5	-4.24	1.84	119.00	
		9	3	35	-4.01	1.46	118.53	
		10	1	9	-4.83	0.00	117.92	
		10	2	11	-4.77	1.69	118.77	
		10	3	3	-4.12	1.23	118.56	
		11	1	12	-4.69	0.00	119.46	
		11	2	20	-4.64	1.99	118.72	
		11	3	4	-3.95	1.85	119.01	
		12	1	2	-4.63	0.00	119.15	M122
		13	1	1	-4.51	0.00	120.18	
		14	1	19	-4.51	0.00	119.56	
		14	2	40	-4.49	1.43	119.22	
		14	3	26	-4.36	1.40	119.50	
		14	4	39	-4.04	1.94	120.00	
		15	1	15	-4.46	0.00	119.82	
		16	1	36	-4.33	0.00	119.57	
		17	1	42	-4.19	0.00	119.19	
		17	2	49	-4.01	1.60	119.02	
		18	1	31	-4.17	0.00	118.01	
		19	1	13	-4.06	0.00	120.24	
		19	2	17	-3.79	1.64	119.35	
		19	3	27	-3.71	1.79	120.14	M122
		20	1	47	-3.93	0.00	121.29	
		20	2	30	-3.40	1.37	120.59	
		21	1	25	-3.86	0.00	118.49	
		21	2	22	-3.59	1.93	118.43	
		22	1	24	-3.78	0.00	118.85	
Cytb2	S108A; A194V	1	1	50	-7.23	0.00	115.23	E273; M125
		1	2	13	-6.93	0.73	115.58	E273; M125
		1	3	49	-6.87	1.52	115.11	M125
		1	4	31	-5.48	1.45	114.63	E273
		1	5	25	-5.42	1.13	115.65	M125

		1	6	3	-4.90	1.37	114.86	M125; E273
		1	7	9	-4.25	0.73	114.88	
		1	8	45	-3.59	1.53	115.57	E273
		1	9	2	-3.04	1.13	114.50	
		2	1	8	-5.60	0.00	113.15	E273
		2	2	23	-4.90	1.46	113.18	M139
		2	3	40	-3.47	1.49	113.81	E273
		3	1	27	-4.83	0.00	116.90	
		3	2	22	-4.62	1.30	117.17	
		3	3	35	-4.55	1.62	116.23	
		3	4	11	-4.36	1.35	116.44	
		3	5	4	-1.90	1.91	116.90	
		3	6	16	-1.31	1.72	116.38	
		4	1	29	-4.10	0.00	119.95	
		4	2	44	0.20	1.92	119.81	
		4	3	48	0.74	2.00	118.61	
		5	1	1	-4.02	0.00	119.57	
		5	2	18	-3.41	1.81	120.65	
		5	3	10	-3.26	1.47	120.45	M125
		5	4	37	-3.08	1.68	120.15	
		5	5	36	-2.56	1.75	120.33	M125
		5	6	20	-2.21	1.96	120.02	
		6	1	43	-3.96	0.00	114.97	
		7	1	32	-3.95	0.00	116.80	
		7	2	15	-3.94	1.51	116.16	M125
		7	3	24	-0.68	1.25	116.74	
		8	1	6	-3.95	0.00	113.27	
		9	1	42	-3.91	0.00	117.95	
		10	1	5	-3.86	0.00	116.94	
		10	2	34	-1.09	1.89	118.15	
		11	1	12	-3.35	0.00	113.25	
		12	1	46	-3.07	0.00	114.11	
		12	2	28	-2.69	1.41	114.22	
		13	1	41	-2.92	0.00	118.18	
		14	1	17	-2.66	0.00	118.76	
		15	1	19	-2.66	0.00	114.93	E273
		16	1	26	-2.48	0.00	116.58	
		17	1	33	-2.33	0.00	121.24	
		18	1	47	-2.08	0.00	117.78	
		19	1	30	-1.62	0.00	113.38	E273
		20	1	14	-1.03	0.00	115.61	
		21	1	38	-0.57	0.00	117.19	M125
		22	1	7	-0.42	0.00	114.49	
		23	1	21	-0.38	0.00	116.19	
		24	1	39	0.06	0.00	116.14	M125
Cytb3	S108A; F129L; A194V	1	1	50	-6.24	0.00	119.52	
		1	2	46	-5.52	1.39	119.89	A126
		1	3	19	-5.17	1.73	119.56	M122
		1	4	20	-4.23	1.74	120.40	A126
		1	5	2	-3.79	1.83	120.75	
		1	6	41	-3.40	1.86	120.64	
		2	1	9	-5.91	0.00	119.94	
		2	2	45	-4.40	1.86	119.94	
		2	3	44	-3.83	1.85	120.14	
		2	4	34	-3.57	1.97	120.78	
		3	1	39	-4.77	0.00	121.28	
		3	2	15	-3.96	1.98	120.55	
		3	3	37	-3.46	1.91	121.63	
		4	1	16	-4.46	0.00	121.63	
		4	2	7	-3.97	1.45	121.69	
		5	1	24	-4.39	0.00	120.59	
		6	1	33	-4.32	0.00	112.99	A254

	7	1	4	-4.28	0.00	119.45	
	7	2	26	-3.88	1.65	120.18	
	7	3	17	-3.22	1.72	120.43	
	8	1	30	-4.26	0.00	115.16	A254; L252
	8	2	32	-3.99	1.38	114.83	A254; Y275
	9	1	36	-4.07	0.00	119.09	
	9	2	43	-2.51	1.68	119.75	
	9	3	11	-2.45	1.94	119.42	
	10	1	18	-4.07	0.00	121.14	
	11	1	47	-3.89	0.00	121.47	
	12	1	40	-3.81	0.00	116.58	
	12	2	25	-2.64	0.70	116.55	
	12	3	31	1.32	1.85	116.30	E273
	12	4	1	2.46	1.90	116.01	E273
	13	1	8	-3.62	0.00	120.87	
	13	2	10	-3.32	1.96	121.13	
	14	1	12	-3.41	0.00	121.20	M122
	15	1	3	-2.83	0.00	122.00	
	16	1	38	-2.66	0.00	120.54	
	17	1	35	-2.20	0.00	117.01	
	17	2	29	-1.11	1.52	116.87	
	17	3	14	-0.28	1.36	116.95	
	18	1	49	-2.05	0.00	119.61	
	19	1	42	-1.51	0.00	112.66	A254
	19	2	21	-0.56	1.90	112.54	A254
	19	3	5	3.69	1.97	113.59	G253
	20	1	28	-1.49	0.00	119.88	
	21	1	27	-1.22	0.00	118.82	
	22	1	6	-0.76	0.00	114.51	V271
	23	1	48	-0.22	0.00	115.64	
	24	1	23	-0.03	0.00	118.13	
	25	1	13	0.73	0.00	111.44	
	26	1	22	3.49	0.00	116.53	M139

Table A8. Field trial treatments and dates of the addition and removal of wax-paper bags on clusters of *Vitis vinifera* cultivars Cabernet Franc (CF), Cabernet Sauvignon (CS), and Merlot (M) at different phenological stages on trials conducted from 2019-2021, and the number of clusters evaluated at harvest

		Phenological stage		Date		
Year	**Trt.**	**Bag added**	**Bag removed**	**Bag added**	**Bag removed**	**No. clusters evaluated**
2019	1	Bloom	Harvest	31 May	30 Sep (M); 10 Oct (CS)	18 (M); 17 (CS)
	2	BB-size	Harvest	14 Jun	30 Sep (M); 10 Oct (CS)	27 (M); 27 (CS)
	3	Pea-size	Harvest	28 Jun	30 Sep (M); 10 Oct (CS)	29 (M); 31 (CS)
	4	Berry touch	Harvest	19 Jul	30 Sep (M); 10 Oct (CS)	29 (M); 29 (CS)
	5	Veraison	Harvest	6 Aug	30 Sep (M); 10 Oct (CS)	29 (M); 28 (CS)
	6	Pre-harvest	Harvest	9 Sep (M); 19 Sep (CS)	30 Sep (M); 10 Oct (CS)	30 (M); 29 (CS)
	7	Non-bagged	Non-bagged	Non-bagged	Non-bagged	29 (M); 28 (CS)
	8	Bloom	BB-size	NI[a]	NI	NI
	9	Bloom	Pea-size	NI	NI	NI
	10	Bloom	Berry touch	NI	NI	NI
	11	Bloom	Veraison	NI	NI	NI
	12	Bloom	Pre-harvest	NI	NI	NI
2020	1	Bloom	Harvest	11 Jun	1 Oct (M); 14 Oct (CS)	19 (M); 20 (CS)
	2	BB-size	Harvest	29 Jun	1 Oct (M); 14 Oct (CS)	17 (M); 20 (CS)
	3	Pea-size	Harvest	15 Jul	1 Oct (M); 14 Oct (CS)	17 (M); 19 (CS)
	4	Berry touch	Harvest	1 Aug	1 Oct (M); 14 Oct (CS)	19 (M); 19 (CS)
	5	Veraison	Harvest	17 Aug	1 Oct (M); 14 Oct (CS)	16 (M); 20 (CS)
	6	Pre-harvest	Harvest	8 Sep (M); 15 Sep (CS)	1 Oct (M); 14 Oct (CS)	19 (M); 20 (CS)
	7	Non-bagged	Non-bagged	Non-bagged	Non-bagged	20 (M); 20 (CS)
	8	Bloom	BB-size	11 Jun	29 Jun	20 (M); 20 (CS)
	9	Bloom	Pea-size	11 Jun	15 Jul	18 (M); 18 (CS)
	10	Bloom	Berry touch	11 Jun	1 Aug	19 (M); 17 (CS)
	11	Bloom	Veraison	11 Jun	6 Aug (M); 17 Aug (CS)	14 (M); 14 (CS)
	12	Bloom	Pre-harvest	11 Jun	9 Sep (M); 19 Sep (CS)	18 (M); 19 (CS)
2021	1	Bloom	Harvest	9 Jun (CF); 10 Jun (CS)	15 Sep (CF); 11 Oct (CS)	20 (CF); 20 (CS)
	2	BB-size	Harvest	21 Jun (CF); 24 Jun (CS)	15 Sep (CF); 11 Oct (CS)	19 (CF); 20 (CS)
	3	Pea-size	Harvest	9 Jul (CF); 12 Jul (CS)	15 Sep (CF); 11 Oct (CS)	19 (CF); 18 (CS)
	4	Berry touch	Harvest	29 Jul (CF); 3 Aug (CS)	15 Sep (CF); 11 Oct (CS)	20 (CF); 20 (CS)
	5	Veraison	Harvest	19 Aug (CF); 25 Aug (CS)	15 Sep (CF); 11 Oct (CS)	20 (CF); 20 (CS)
	6	Pre-harvest	Harvest	2 Sep (CF); 17 Sep (CS)	15 Sep (CF); 11 Oct (CS)	20 (CF); 20 (CS)
	7	Non-bagged	Non-bagged	Non-bagged	Non-bagged	20 (CF); 20 (CS)
	8	Bloom	BB-size	9 Jun (CF); 10 Jun (CS)	21 Jun (CF); 24 Jun (CS)	16 (CF); 20 (CS)
	9	Bloom	Pea-size	9 Jun (CF); 10 Jun (CS)	9 Jul (CF); 12 Jul (CS)	19 (CF); 20 (CS)
	10	Bloom	Berry touch	9 Jun (CF); 10 Jun (CS)	29 Jul (CF); 3 Aug (CS)	18 (CF); 19 (CS)
	11	Bloom	Veraison	9 Jun (CF); 10 Jun (CS)	19 Aug (CF); 25 Aug (CS)	19 (CF); 17 (CS)
	12	Bloom	Pre-harvest	9 Jun (CF); 10 Jun (CS)	2 Sep (CF); 17 Sep (CS)	18 (CF); 20 (CS)

[a] "NI" = Treatment not included.

Table A9. Calculation of susceptibility to ripe rot according to data from five trials that consisted of excluding the pathogen *Colletotrichum* with paper bags during different phenological stages with the cultivars Cabernet Franc (CF), Cabernet Sauvignon (CS), and Merlot (M). The susceptibility values were normalized between each trial for the modeling of ripe rot susceptibility according to each phenological stage

Row	Treatment/calculation steps	CF 2021	CS 2020	CS 2021	CS 2019	M 2019
	Ripe rot severity data[z]					
1	Bagged bloom to harvest	4.4	1.1	2.6	6.1	2.9
2	Bagged BB-size to harvest	13.2	1.6	1.5	7.1	6.0
3	Bagged pea-size to harvest	8.6	3.9	0.4	6.9	6.7
4	Bagged berry touch to harvest	18.1	1.1	1.0	5.2	3.3
5	Bagged veraison to harvest	44.1	5.3	5.1	11.5	5.1
6	Bagged pre-harvest to harvest	52.1	23.2	63.3	22.9	24.1
7	Non-bagged	60.7	30.0	51.0	31.3	28.4
	Susceptibility calculation					
8	Row 2 - 1	8.8	0.5	-1.1	1.1	3.1
9	Row 3 - 2	-4.6	2.3	-1.0	-0.2	0.8
10	Row 4 - 3	NA[y]	-2.8	0.5	-1.7	-3.4
11	Row 5 - 4	NA	4.2	4.2	6.3	1.8
12	Row 6 - 5	43.5	17.9	58.2	11.4	19.0
13	Row 7 - 6	8.7	6.8	-12.3	8.4	4.4
14	Row 8	8.8	0.5	-1.1	1.1	3.1
15	Row 8 + 9	4.2	2.8	-2.1	0.8	3.8
16	Row 9 + 10	NA	0.0	-1.6	-0.9	0.5
17	Row 10 + 11	NA	4.2	2.6	5.4	2.2
18	Row 11 + 12	47.7	22.1	60.7	16.8	21.2
19	Row 12 + 13	56.3	28.9	48.5	25.2	25.6
	Susceptibility normalized					
20	Row 14 to 19: smallest = 0, largest = 1; Bloom to BB-size	0.09	0.02	0.02	0.07	0.10
21	Row 14 to 19: smallest = 0, largest = 1; BB-size to pea-size	0.00	0.10	0.00	0.06	0.13
22	Row 14 to 19: smallest = 0, largest = 1; Pea-size to berry touch	NA	0.00	0.01	0.00	0.00
23	Row 14 to 19: smallest = 0, largest = 1; Berry touch to veraison	NA	0.15	0.07	0.24	0.07
24	Row 14 to 19: smallest = 0, largest = 1; Veraison to pre-harvest	0.83	0.77	1.00	0.68	0.83
25	Row 14 to 19: smallest = 0, largest = 1; Pre-harvest to harvest	1.00	1.00	0.80	1.00	1.00

[z] This data was previously published by Cosseboom and Hu (2022).

[y] Treatment four (row 4) was removed from the CF 2021 trial, due to incorrect bagging timing.

Table A10. Coefficients of determination (R^2) from testing environmental risk models created from detached fruit (DF) and greenhouse (GH) trials with linear regression of the predicted number of ripe rot infection events in a season against the ripe rot severity observed at harvest from 45 ripe rot epidemics, and the average number of fungicide applications per season that would be triggered by each model if implemented in a ripe rot warning system. Each model was evaluated with infection event thresholds from 0.3 to 0.75, and the R^2 and average applications per season of the optimal thresholds are outlined

		R^2										Avg. applications per season									
Trial	**Model[z]**	**0.3**	**0.35**	**0.4**	**0.45**	**0.5**	**0.55**	**0.6**	**0.65**	**0.7**	**0.75**	**0.3**	**0.35**	**0.4**	**0.45**	**0.5**	**0.55**	**0.6**	**0.65**	**0.7**	**0.75**
DF1	DT	0.65	0.65	0.69	0.54	0.42	0.36	NA	NA	NA	NA	5.0	4.7	4.7	3.8	2.5	1.8	NA	NA	NA	NA
	LGRl	0.73	0.72	0.52	0.41	0.27	0.10	0.01	NA	NA	NA	4.7	4.5	3.0	2.7	1.3	0.8	0.3	NA	NA	NA
	LGRr	0.72	0.76	0.59	0.38	0.31	0.15	0.02	0.01	NA	NA	4.8	4.7	3.0	2.5	1.5	0.8	0.5	0.2	NA	NA
	NN	0.71	0.70	0.68	0.60	0.51	0.34	0.38	0.28	0.28	NA	4.8	4.7	4.7	3.2	2.8	1.0	0.7	0.2	0.2	NA
	RF	0.69	0.69	0.67	0.44	0.41	0.33	0.22	NA	NA	NA	5.0	5.0	4.7	3.3	2.5	2.2	1.3	NA	NA	NA
	SVM	0.71	0.73	0.73	0.71	0.64	0.63	0.51	0.46	0.39	0.19	5.0	4.7	4.7	4.7	4.3	4.3	3.5	1.7	1.2	0.5
DF2	DT	0.58	0.63	0.57	0.53	0.41	0.41	0.54	0.54	0.13	0.13	3.3	2.5	2.3	2.3	1.2	1.2	0.7	0.7	0.2	0.2
	LGRl	0.76	0.58	0.31	0.15	NA	NA	NA	NA	NA	NA	4.0	2.8	1.0	0.5	NA	NA	NA	NA	NA	NA
	LGRr	0.76	0.70	0.67	0.37	0.21	0.08	0.13	0.13	0.13	0.13	4.3	3.5	3.3	2.0	1.0	0.5	0.2	0.2	0.2	0.2
	NN	0.66	0.77	0.75	0.81	0.73	0.26	0.28	NA	NA	NA	4.0	3.0	3.0	3.0	3.0	1.0	0.8	NA	NA	NA
	RF	0.76	0.63	0.53	0.48	0.13	NA	NA	NA	NA	NA	4.3	3.2	2.2	1.2	0.2	NA	NA	NA	NA	NA
	SVM	0.75	0.74	0.63	0.61	0.63	0.60	0.62	0.60	0.33	0.16	3.2	2.8	2.7	2.5	2.3	2.3	2.3	2.0	1.0	0.5
DF1+2	DT	0.63	0.67	0.63	0.63	0.28	NA	NA	NA	NA	NA	4.7	4.7	3.2	3.2	1.0	NA	NA	NA	NA	NA
	LGRl	0.73	0.69	0.58	0.22	0.16	NA	NA	NA	NA	NA	4.7	3.8	2.8	1.0	0.5	NA	NA	NA	NA	NA
	LGRr	0.77	0.70	0.51	0.48	0.22	0.15	NA	NA	NA	NA	4.5	3.5	2.8	2.2	1.0	0.5	NA	NA	NA	NA
	NN	0.71	0.70	0.72	0.45	0.40	0.46	NA	NA	NA	NA	4.5	4.3	3.5	2.5	1.5	0.3	NA	NA	NA	NA
	RF	0.72	0.81	0.63	0.42	0.31	0.16	NA	NA	NA	NA	4.5	4.2	3.2	2.5	1.8	0.3	NA	NA	NA	NA
	SVM	0.62	0.56	0.53	0.49	0.47	0.46	0.31	0.40	0.03	0.03	4.5	3.8	2.7	2.7	2.5	2.5	1.2	1.2	0.2	0.2
GH1	DT	0.74	0.74	0.74	0.74	0.74	0.76	0.76	0.79	0.52	0.51	4.7	4.7	4.7	4.7	4.7	4.3	4.3	4.2	2.8	2.8
	LGRl	0.72	0.73	0.73	0.74	0.74	0.77	0.79	0.62	0.52	0.51	5.0	5.0	5.0	5.0	4.8	4.8	4.7	4.0	3.2	2.5
	LGRr	0.67	0.70	0.72	0.73	0.76	0.77	0.55	0.48	0.22	0.23	5.0	5.0	5.0	5.0	4.7	4.2	3.3	2.7	1.0	1.0
	NN	0.72	0.72	0.72	0.73	0.73	0.74	0.75	0.65	0.48	0.49	5.0	5.0	5.0	4.8	4.8	4.8	4.7	4.2	3.2	3.0
	RF	0.74	0.74	0.74	0.74	0.73	0.52	0.51	0.51	0.53	0.49	4.7	4.7	4.7	4.7	4.5	3.2	2.2	2.2	2.2	2.0
	SVM	0.72	0.73	0.74	0.74	0.75	0.75	0.76	0.78	0.78	0.38	5.0	5.0	5.0	5.0	5.0	4.8	4.8	4.7	4.5	2.0
GH2	DT	0.79	0.79	0.79	0.80	0.83	0.85	0.85	0.85	0.48	0.39	4.3	3.8	3.8	3.5	3.2	3.0	2.5	2.5	1.2	0.7
	LGRl	0.74	0.77	0.78	0.74	0.57	0.39	0.24	0.16	0.16	0.03	5.0	4.7	4.2	3.3	2.7	2.0	1.3	0.5	0.5	0.2
	LGRr	0.74	0.75	0.79	0.80	0.60	0.48	0.17	0.16	0.16	0.03	5.0	4.8	4.5	3.7	2.8	2.0	1.2	0.5	0.5	0.2
	NN	0.75	0.77	0.80	0.79	0.80	0.82	0.83	0.83	0.84	0.82	5.0	4.5	4.3	4.2	4.2	3.8	3.5	3.2	3.0	2.7
	RF	0.79	0.79	0.83	0.60	0.62	0.52	0.52	0.03	NA	NA	4.0	3.5	3.2	2.2	2.0	0.8	0.8	0.2	NA	NA
	SVM	0.73	0.77	0.79	0.79	0.79	0.83	0.83	0.80	0.63	0.38	4.8	4.5	4.5	4.3	4.0	3.7	3.3	3.2	2.2	0.7
GH1+2	DT	0.74	0.74	0.74	0.70	0.83	0.85	0.85	0.44	0.44	0.15	4.7	4.7	4.7	4.2	3.3	3.0	3.0	1.7	1.7	0.5
	LGRl	0.72	0.74	0.74	0.76	0.77	0.79	0.73	0.50	0.28	0.16	5.0	5.0	5.0	4.8	4.5	4.3	3.7	2.3	1.3	0.7
	LGRr	0.72	0.72	0.73	0.76	0.78	0.79	0.72	0.50	0.34	0.23	5.0	5.0	5.0	4.8	4.7	4.3	3.3	2.7	1.7	0.8
	NN	0.67	0.69	0.71	0.73	0.76	0.76	0.77	0.61	0.48	0.39	5.0	5.0	5.0	4.8	4.8	4.5	4.0	2.2	1.2	0.5
	RF	0.75	0.81	0.81	0.79	0.79	0.80	0.38	0.37	NA	NA	4.5	4.3	4.3	4.3	3.8	3.8	1.5	1.5	NA	NA
	SVM	0.76	0.77	0.79	0.78	0.79	0.81	0.79	0.72	0.44	0.34	5.0	4.8	4.7	4.5	4.3	3.8	3.7	3.3	1.8	0.8

[z] Statistical method to derive the environmental risk model: DT = decision tree; LGRl = logistic regression with LASSO regularization, LGRr = logistic regression with ridge regularization; NN = neural network; RF = random forest; SVM = support vector machine.
[y] NA = No infection events predicted, and no fungicide sprays triggered.

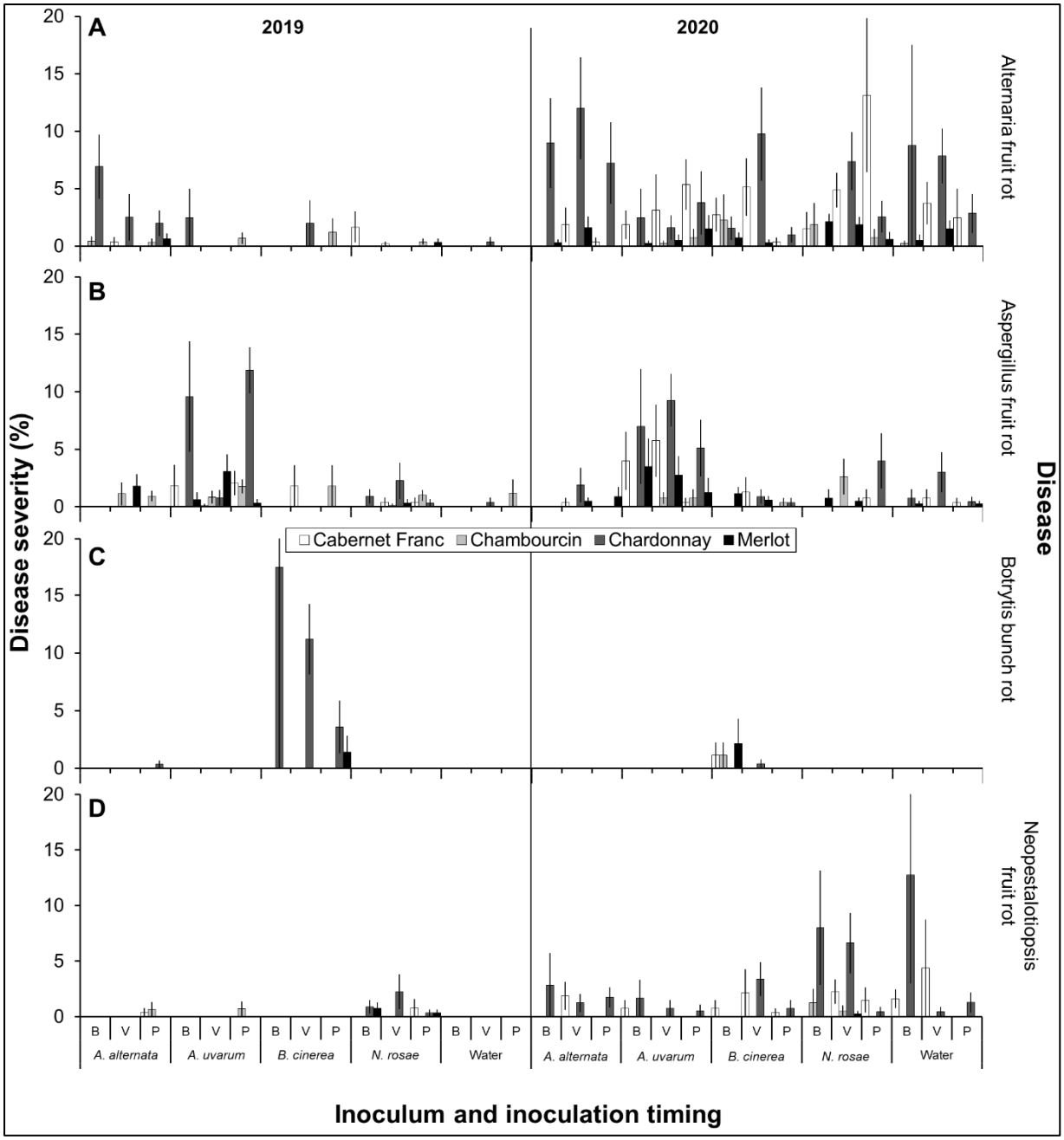

Fig. A1. Average severity of (A) Alternaria, (B) Aspergillus, (C) Botrytis, and (D) Neopestalotiopsis fruit rot on non-wounded clusters of four wine grape cultivars inoculated with four fungi and water at bloom (B), veraison (V), and pre-harvest (P) in a field trial conducted in 2019 and 2020. Error bars represent standard error.

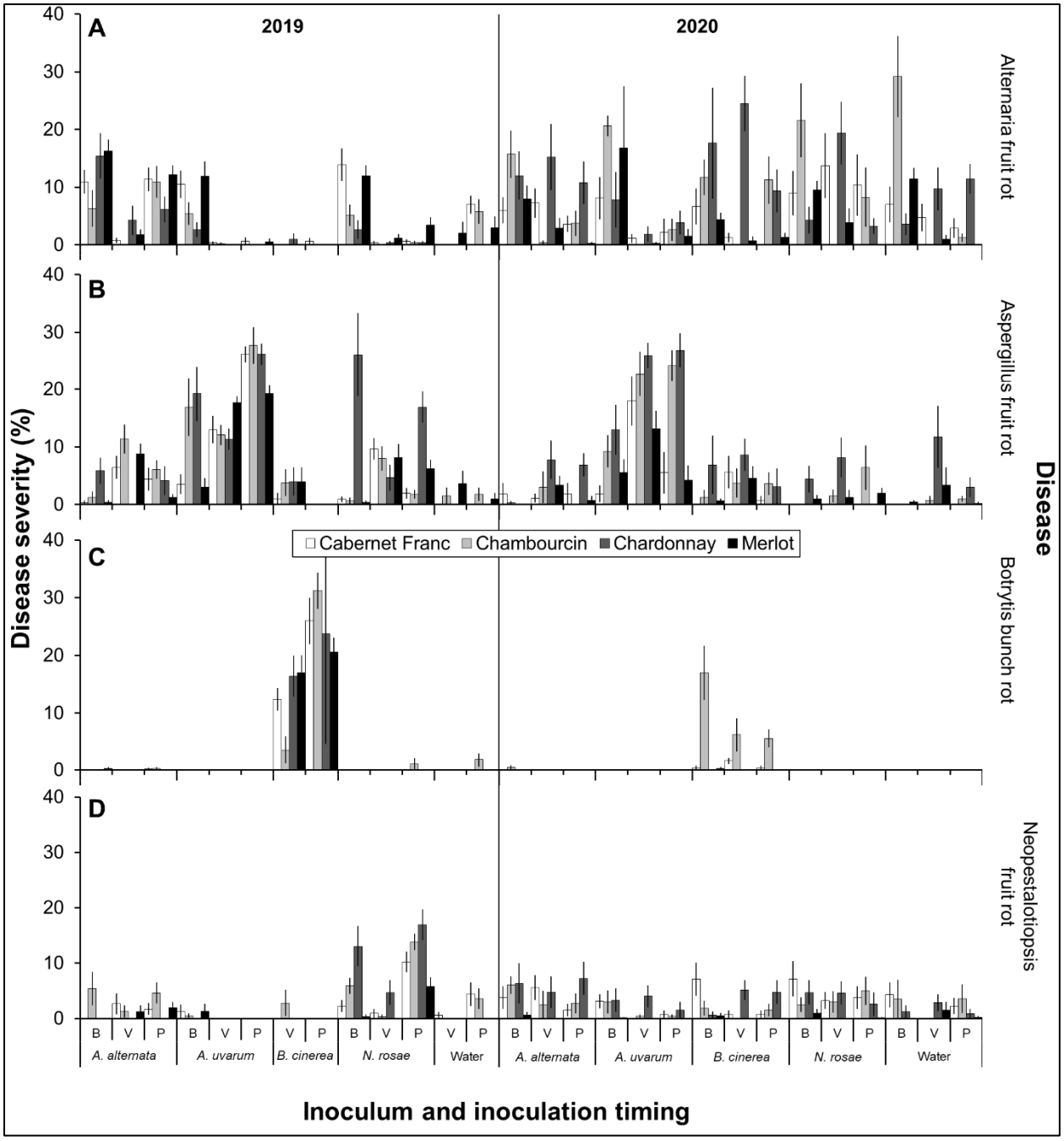

Fig. A2. Average severity of (A) Alternaria, (B) Aspergillus, (C) Botrytis, and (D) Neopestalotiopsis fruit rot on wounded clusters of four wine grape cultivars inoculated with four fungi and water at bloom (B), veraison (V), and pre-harvest (P) in a field trial conducted in 2019 and 2020. Error bars represent standard error. The wounded-bloom inoculated treatment was not included for the *B. cinerea* and water inoculum in 2019.

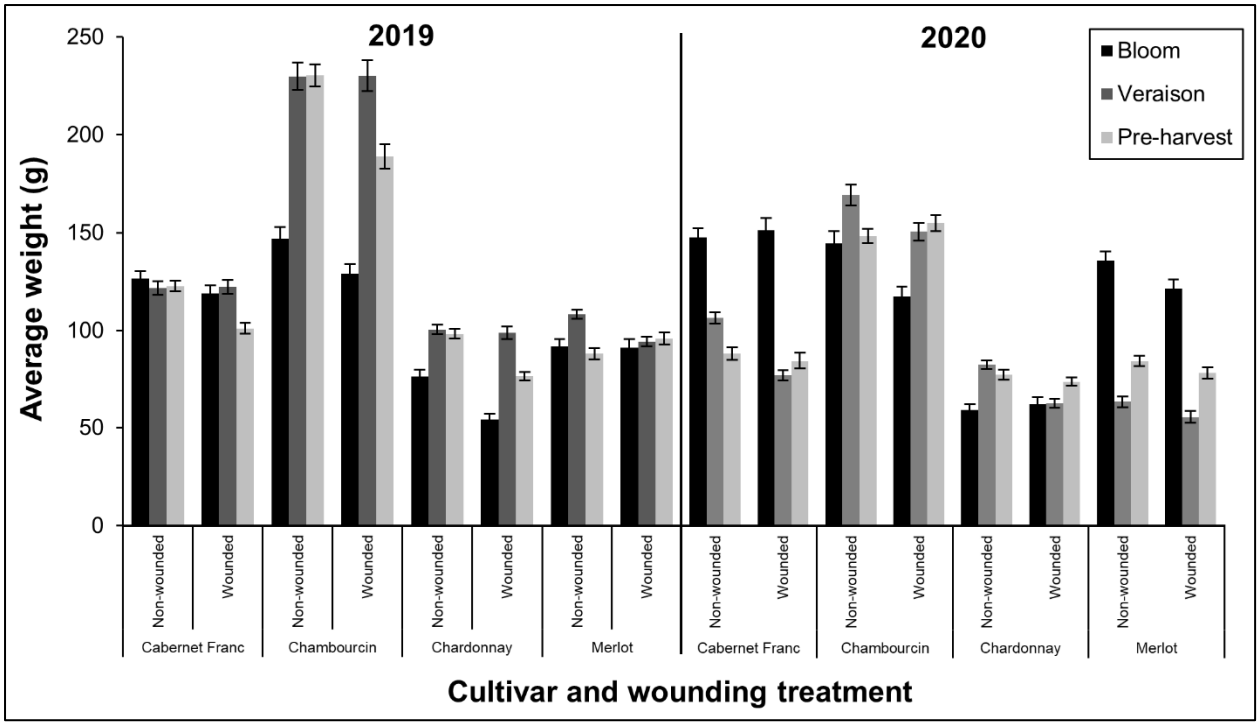

Fig. A3. Average cluster weight of four wine grape cultivars in a replicated field trial in 2019 and 2020 that were either wounded or non-wounded and inoculated with five inocula at the phenological stages of bloom, veraison, and pre-harvest. Error bars represent standard error.

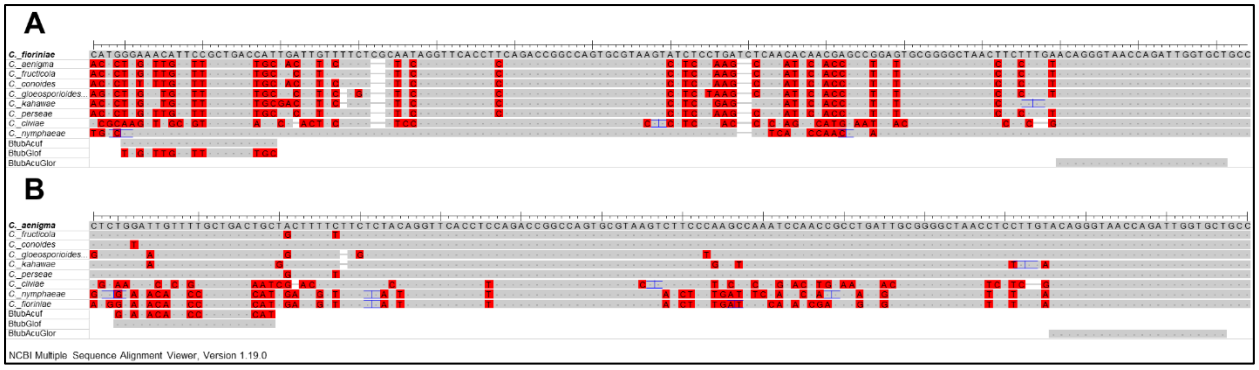

Fig. A4. The alignment of the β-tubulin gene of *Colletotrichum* spp. within the *C. acutatum* species complex (*C. fioriniae* and *C. nymphaeae*), the *C. gloeosporioides* complex (*C. aenigma*, *C. fructicola*, *C. conoides*, *C. gloeosporioides*, *C. kahawae*, and *C. perseae*), and *C. cliviae* (*C. cliviicola*) with *C. acutatum* complex specific forward primer BtubAcuf, *C. gloeosporioides* complex specific forward primer BtubGlof, and the non-specific reverse primer BtubAcuGlor with either A) *C. fioriniae* or B) *C. aenigma* as the template sequence.

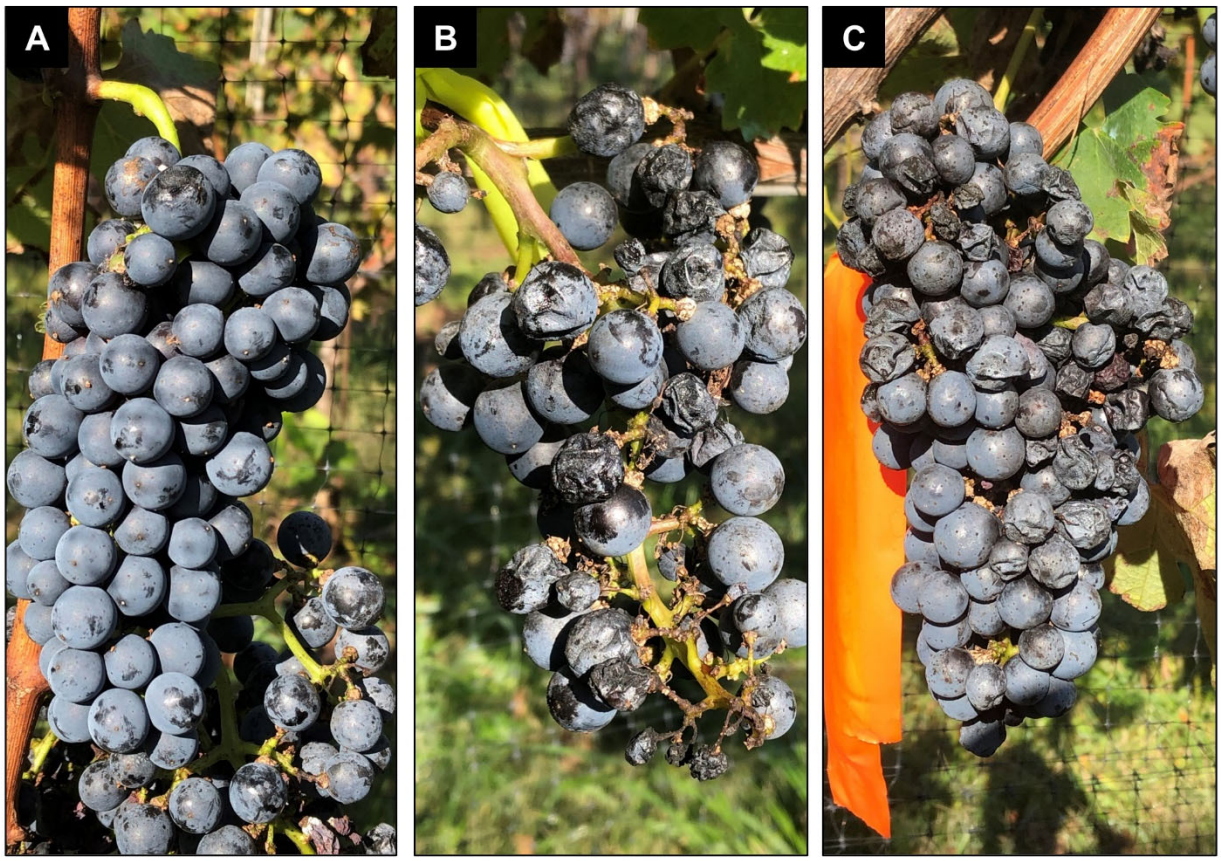

Fig. A5. Grape clusters that were either covered with a bag A) from bloom to harvest, B) bloom to berry touch, or C) bloom to veraison.

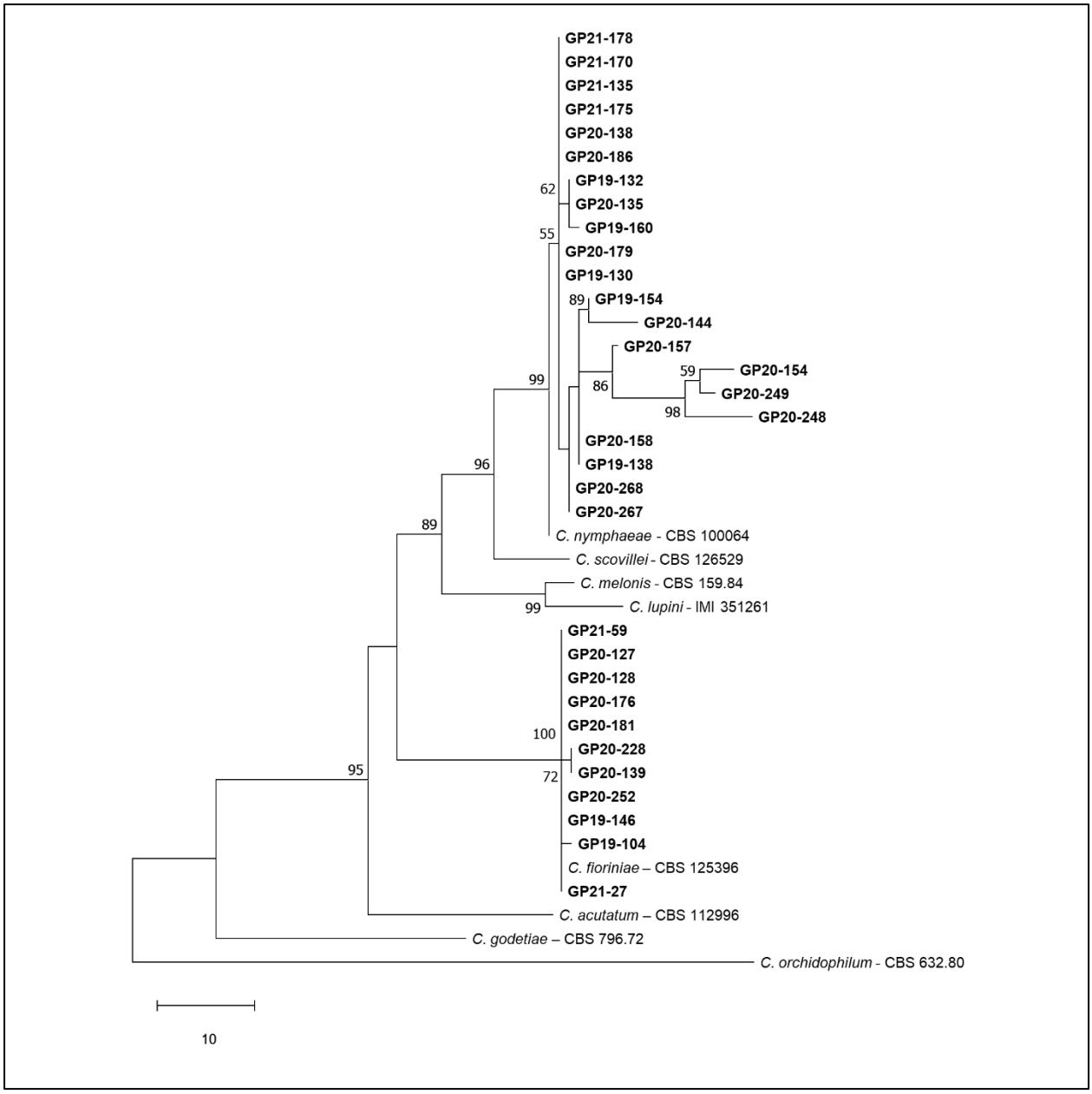

Fig. A6. Rooted maximum parsimony tree of concatenated β-tubulin, chitin synthase-1, and glyceraldehyde-3-phosphate dehydrogenase sequences of fungi within the *Colletotrichum acutatum* species complex (ex-type strain names are followed by an asterisk) with reference strains and isolates collected from vineyard trials from 2019 to 2021 in bold with *C. orchidophilum* as the outgroup.

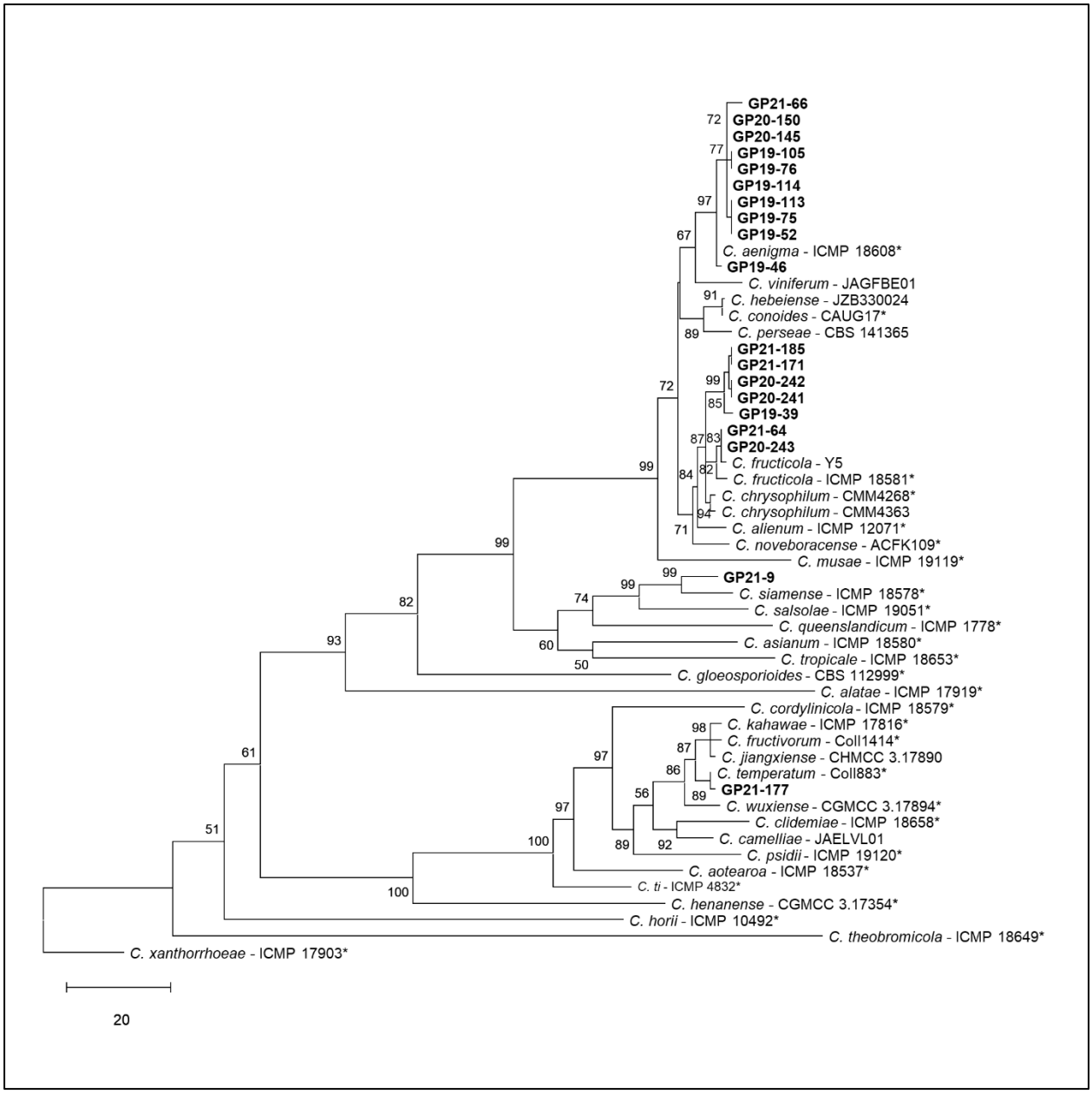

Fig. A7. Rooted maximum parsimony tree of concatenated β-tubulin, chitin synthase-1, glyceraldehyde-3-phosphate dehydrogenase, and the Apn2 to MAT1-2-1 intergenic region sequences of fungi within the *Colletotrichum gloeosporioides* species complex (ex-type strain names are followed by an asterisk) with reference strains and isolates collected from vineyard trials from 2019 to 2021 in bold with *C. xanthorrhoeae* as the outgroup.

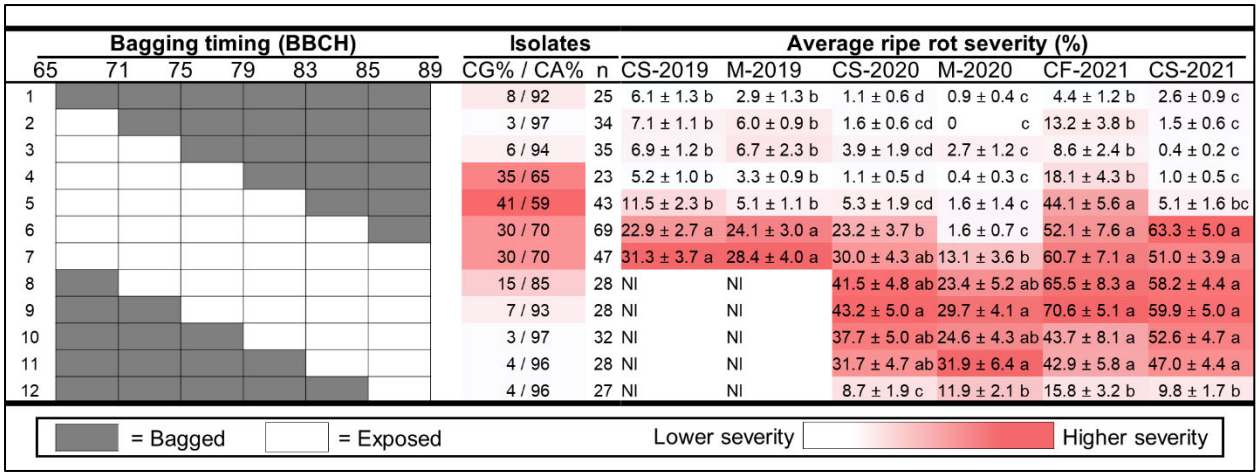

Fig. A8. Frequency of *Colletotrichum acutatum* (CA) and *C. gloeosporioides* (CG) species complexes isolated from grape clusters that were bagged for various periods of cluster development from six separate trials and number (n) of isolates from each bagging treatment and average ripe rot severity (%) ± standard error of the mean from six trials conducted with the cultivars Cabernet Franc (CF), Cabernet Sauvignon (CS), and Merlot (M). The effect of bagging timing was evaluated on the square root transformed ripe rot severity for each trial separately with ANOVA followed by a post hoc Tukey's HSD test. Ripe rot severity values followed by a different letter are significantly different. Bag removal treatments were not included (NI) in 2019.

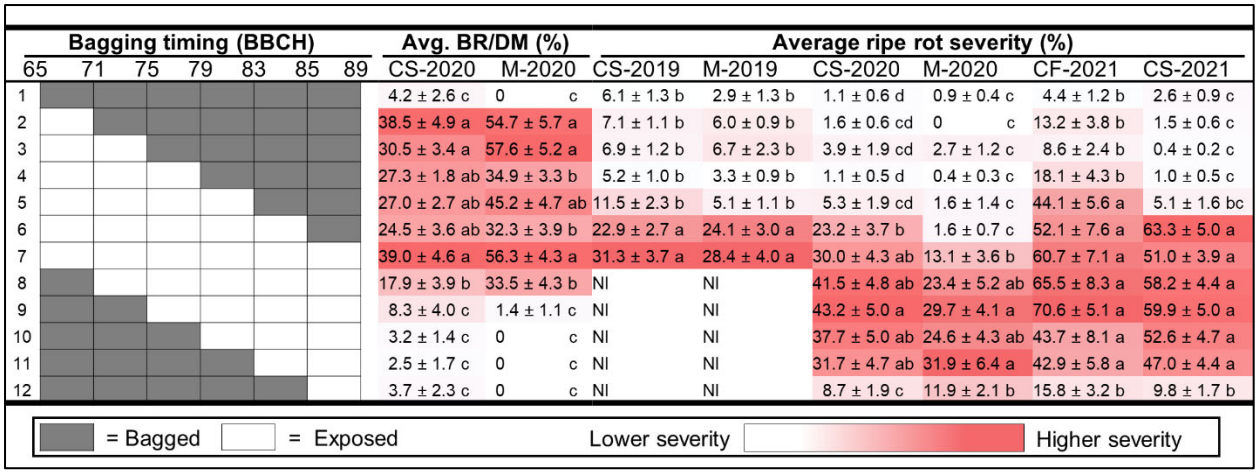

Fig. A9. Severity ± standard error of the mean of the fruit rot diseases black rot (BR), downy mildew (DM), and ripe rot from six trials conducted with the cultivars Cabernet Sauvignon (CS), Cabernet Franc, and Merlot (M) with grape clusters protected by bags at different phenological stages starting at bloom (BBCH 85) and ending at full ripeness (BBCH 89). The effect of bagging timing was evaluated on the square root transformed disease severity for each trial separately with ANOVA followed by a post hoc Tukey's HSD test. Disease severity values followed by a different letter are significantly different. Bag removal treatments were not included (NI) in 2019.

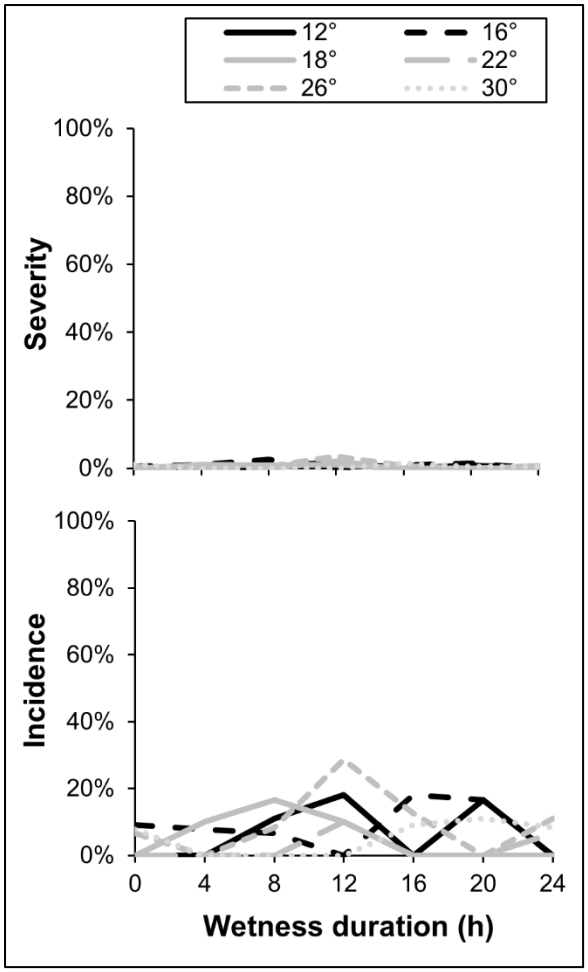

Fig. A10. The severity (top) and incidence (bottom) of ripe rot disease on mature grape clusters of potted grapevines that were inoculated with *C. fioriniae* at the bloom stage under multiple wetness duration and temperature conditions.

Bibliography

Abarca, M. L., Accensi, F., Cano, J., and Cabañes, F. J. 2004. Taxonomy and significance of black aspergilli. Anton. Leeuw. 86:33-49.

Adamo, N. R. 2016. Fungicide resistance of *Botrytis cinerea* from Virginia wine grapes, strawberry, and ornamental crops. Thesis. Virginia Tech.

Albakri, A. H., Al-Shuhaib, M. B. S., Alwan, S. L., AbdulAzeez, S., and Borgio, J. F. 2021. Deleterious missense variants in the aflatoxin biosynthesis genes explain the low toxicity of *Aspergillus flavus* from infected rice. Microbial Pathogenesis 152:104605.

Ali, M. E., Gunn, M., Stackhouse, T., Waliullah, S., Guo, B., Culbreath, A., and Brenneman, T. 2021. Sensitivity of *Aspergillus flavus* isolates from peanut seeds in Georgia to azoxystrobin, a quinone outside inhibitor (QoI) fungicide. J. Fungi 7:284.

Amiri, A., and Peres, N. A. 2014. Diversity in the erg27 gene of *Botrytis cinerea* field isolates from strawberry defines different levels of resistance to the hydroxyanilide fenhexamid. Plant Dis. 98:1131-1137.

Amiri, A., Heath, S. M., and Peres, N. A. 2014. Resistance to fluopyram, fluxapyroxad, and penthiopyrad in *Botrytis cinerea* from strawberry. Plant Dis. 98:532-539.

Amiri, A., Zuniga, A. I., and Peres, N. A. 2018. Potential impact of populations drift on *Botrytis* occurrence and resistance to multi- and single-site fungicides in Florida Southern highbush blueberry fields. Plant Dis. 102:2142-2148.

Amiri, A., Zuniga, A. I., Cordova, L. G., and Peres, N. A. 2019. The importance of selecting appropriate rotation and tank-mix partners for novel SDHIs to enhance botrytis fruit rot control in strawberry. Plant disease 103:729-736.

Austin, C. N., and Wilcox, W. F. 2011. Effects of fruit-zone leaf removal, training systems, and irrigation on the development of grapevine powdery mildew. Am. J. Enol. Vitic. 62:193.

Avenot, H. F., and Michailides, T. J. 2020. Occurrence and extent of boscalid resistance in populations of *Alternaria alternata* from California pistachio orchards. Plant Dis. 104:306-314.

Badali, H., Fakhim, H., Zarei, F., Nabili, M., Vaezi, A., Poorzad, N., Dolatabadi, S., and Mirhendi, H. 2016. In vitro activities of five antifungal drugs against opportunistic agents of *Aspergillus nigri* complex. Mycopathologia 181:235-240.

Baggio, J. S., Forcelini, B. B., Wang, N.-Y., Ruschel, R. G., Mertely, J. C., and Peres, N. A. 2021. Outbreak of leaf spot and fruit rot in Florida strawberry caused by *Neopestalotiopsis* spp. Plant Dis. 105:305-315.

Banno, S., Fukumori, F., Ichiishi, A., Okada, K., Uekusa, H., Kimura, M., and Fujimura, M. 2008. Genotyping of benzimidazole-resistant and dicarboximide-resistant mutations in *Botrytis cinerea* using real-time polymerase chain reaction assays. Phytopathology 98:397-404.

Barbetti, M. J. 1980. Bunch rot of Rhine Riesling grapes in the lower south-west of Western Australia. Aust, J. Exp. Ag. 20:247-251.

Barkai-Golan, R. 1980. Species of *Aspergillus* causing post-harvest fruit decay in Israel. Mycopathologia 71:13-16.

Bensch, K., Groenewald, J. Z., Braun, U., Dijksterhuis, J., de Jesús Yáñez-Morales, M., and Crous, P. W. 2015. Common but different: The expanding realm of *Cladosporium*. Stud. Mycol. 82:23-74.

Beruski, G. C., Gleason, M. L., Sentelhas, P. C., and Pereira, A. B. 2019. Leaf wetness duration estimation and its influence on a soybean rust warning system. Australasian Plant Pathol. 48:395-408.
Bolton, S. L. 2016. Assessment of mycotoxigenic fungi and mycotoxins in the *Vitis Vinifera* wine industry of the Southeastern United States. University of Georgia.
Bolton, S. L., Brannen, P. M., and Glenn, A. E. 2016. A novel population of *Fusarium fujikuroi* isolated from southeastern U.S. winegrapes reveals the need to re-evaluate the species' fumonisin production. Toxins 8:254.
Bradley, A. P. 1997. The use of the area under the ROC curve in the evaluation of machine learning algorithms. Pattern recognition 30:1145-1159.
Broome, J. C., English, J. T., Marois, J. J., Latorre, B. A., and Aviles, J. C. 1995. Development of an infection model for *Botrytis* bunch rot of grapes based on wetness duration and temperature. Phytopathology 85:97-102.
Bulger, M. A., Ellis, M. A., and Madden, L. V. 1987. Influence of temperature and wetness duration on infection of strawberry flowers by *Botrytis cinerea* and disease incidence of fruit originating from infected flowers. Phytopathology 77:1225-1230.
Burley, S. K., and Petsko, G. A. 1985. Aromatic-aromatic interaction: a mechanism of protein structure stabilization. Science 229:23-28.
Cabañes, F. J., Accensi, F., Bragulat, M. R., Abarca, M. L., Castellá, G., Minguez, S., and Pons, A. 2002. What is the source of ochratoxin A in wine? Int. J. Food Microbiol. 79:213-215.
Cao, Z. W., Han, L. Y., Zheng, C. J., Ji, Z. L., Chen, X., Lin, H. H., and Chen, Y. Z. 2005. Computer prediction of drug resistance mutations in proteins. Drug Discov. 10:521-529.
Carbone, I., and Kohn, L. M. 1999. A method for designing primer sets for speciation studies in filamentous ascomycetes. Mycologia 91:553-556.
Chen, S. N., Luo, C. X., Hu, M. J., and Schnabel, G. 2016. Fitness and competitive ability of *Botrytis cinerea* isolates with resistance to multiple chemical classes of fungicides. Phytopathology 106:997-1005.
Chi, M.-H., Park, S.-Y., and Lee, Y.-H. 2009. A quick and safe method for fungal DNA extraction. Plant Pathol. J. 25:108-111.
Cordova, L. G., Madden, L. V., Amiri, A., Schnabel, G., and Peres, N. A. 2017. Meta-analysis of a web-based disease forecast system for control of anthracnose and *Botrytis* fruit rots of strawberry in Southeastern United States. Plant Dis. 101:1910-1917.
Cosseboom, S., and Hu, M. 2021a. A SYBR Green qPCR method for detecting and quantifying spores of *Colletotrichum acutatum* and *C. gloeosporioides* species complexes causing ripe rot of grape. Plant Health Prog. 23:65-71.
Cosseboom, S. D., and Hu, M. 2021b. Identification and characterization of fungicide resistance in *Botrytis* populations from small fruit fields in the Mid-Atlantic United States. Plant Dis. doi:10.1094/PDIS-03-20-0487-RE.
Cosseboom, S. D., and Hu, M. 2021c. Diversity, pathogenicity, and fungicide sensitivity of fungal species associated with late-season rots of wine grape in the Mid-Atlantic United States. Plant Dis. 105:3101-3110.
Cosseboom, S. D., and Hu, M. 2022. Ontogenic susceptibility of grapevine clusters to ripe rot, caused by the C*olletotrichum acutatum* and C*. gloeosporioides* species complexes. Phytopathology:doi.org/10.1094/PHYTO-1001-1022-0004-R.
Cosseboom, S. D., Ivors, K. L., Schnabel, G., and Holmes, G. J. 2018. First report of Botrytis mali causing gray mold on strawberry in California. Plant Disease 102:679.

Cosseboom, S. D., Ivors, K. L., Schnabel, G., Bryson, P. K., and Holmes, G. J. 2019. Within-season shift in fungicide resistance profiles of *Botrytis cinerea* in California strawberry fields. Plant Dis. 103:59-64.

Da Rocha Rosa, C. A., Palacios, V., Combina, M., Fraga, M. E., Rekson, A. D. O., Magnoli, C. E., and Dalcero, A. M. 2002. Potential ochratoxin A producers from wine grapes in Argentina and Brazil. Food Addit. Contam. 19:408-414.

Dalla Lana, F., Madden, L. V., and Paul, P. A. 2021. Logistic models derived via LASSO methods for quantifying the risk of natural contamination of maize grain with deoxynivalenol. Phytopathology 111:2250-2267.

Damm, U., Cannon, P. F., Woudenberg, J. H. C., and Crous, P. W. 2012. The *Colletotrichum acutatum* species complex. Stud. Mycol. 73:37-113.

Daykin, M. E., and Milholland, R. D. 1984. Histopathology of ripe rot caused by *Colletotrichum gloeosporioides* on muscadine grape. Phytopathology 74:1339-1341.

Dean, R., Van Kan, J. A. L., Pretorius, Z. A., Hammond-Kosack, K. E., Di Pietro, A., Spanu, P. D., Rudd, J. J., Dickman, M., Kahmann, R., Ellis, J., and Foster, G. D. 2012. The Top 10 fungal pathogens in molecular plant pathology. Mol. Plant Pathol. 13:414-430.

Debode, J., Van Hemelrijck, W., Baeyen, S., Creemers, P., Heungens, K., and Maes, M. 2009. Quantitative detection and monitoring of *Colletotrichum acutatum* in strawberry leaves using real-time PCR. Plant Path. 58:504-514.

Deng, J. X., Sang, H. K., Hwang, Y. S., Lim, B. S., and Yu, S. H. 2013. Postharvest fruit rot caused by *Pestalotiopsis* sp. on grape in Korea. Australas. Plant Dis. Not. 8:111-114.

Deytieux-Belleau, C., Geny, L., Roudet, J., Mayet, V., Donche, B., Fermaud, M., Roudet, J., Mayet, V., and Fermaud, M. 2009. Grape berry skin features related to ontogenic resistance to *Botrytis cinerea*. Eur. J. Plant Pathol. 125:551-563.

Dowling, M., Peres, N., Villani, S., and Schnabel, G. 2020. Managing *Colletotrichum* on fruit crops: A "complex" challenge. Plant Dis. 104:2301-2316.

Dowling, M. E., Hu, M.-J., and Schnabel, G. 2017. Identification and characterization of *Botrytis fragariae* isolates on strawberry in the United States. Plant Dis. 101:1769-1773.

Doyle, V. P., Oudemans, P. V., Rehner, S. A., and Litt, A. 2013. Habitat and host indicate lineage identity in *Colletotrichum gloeosporioides* s.l. from wild and agricultural landscapes in North America. PLOS ONE 8:e62394.

Echeverrigaray, S., Delamare, A. P. L., Fontanella, G., Favaron, F., Stella, L., and Scariot, F. J. 2019. *Colletotrichum* species associated to ripe rot disease of grapes in the “Serra Gaucha” region of Southern Brazil. Proceedings of the 41st World Congress of Vine and Wine 12:01008.

Elmer, P. A. G., and Michailides, T. J. 2007. Epidemiology of *Botrytis cinerea* in orchard and vine crops. Pages 243-262 in: *Botrytis:* Biology, Pathology and Control. Y. Elad, B. Williamson, P. Tudzynski and N. Delen, eds. Springer, Dordrecht, The Netherlands.

Encardes, N. A. 2020. Causal factors of Macrophoma rot observed on Petit Manseng grapes. Virginia Tech.

Eskalen, A., and Gubler, W. D. 2001. Association of spores of *Phaeomoniella chlamydospora*, *Phaeoacremonium inflatipes*, and *Pm. aleophilum* with grapevine cordons in California. Phytopathol. Mediterr. 40:S429-S432.

Esposito, C., Landrum, G. A., Schneider, N., Stiefl, N., and Riniker, S. 2021. GHOST: Adjusting the decision threshold to handle imbalanced data in machine learning. J. Chem. Inf. Model. 61:2623-2640.

Esser, L., Quinn, B., Li, Y.-F., Zhang, M., Elberry, M., Yu, L., Yu, C.-A., and Xia, D. 2004. Crystallographic studies of quinol oxidation site inhibitors: a modified classification of inhibitors for the cytochrome bc1 complex. J. Mol. Biol. 341:281-302.

Fan, F., Hamada, M. S., Li, N., Li, G. Q., and Luo, C. X. 2017. Multiple fungicide resistance in *Botrytis cinerea* from greenhouse strawberries in Hubei Province, China. Plant Dis. 101:601-606.

Fernández-Ortuño, D., Chen, F., and Schnabel, G. 2012a. Resistance to pyraclostrobin and boscalid in *Botrytis cinerea* isolates from strawberry fields in the Carolinas. Plant Dis. 96:1198-1203.

Fernández-Ortuño, D., Tores, J. A., de Vicente, A., and Perez-Garcia, A. 2008. Mechanisms of resistance to QoI fungicides in phytopathogenic fungi. Int. Microbiol. 11:1-9.

Fernández-Ortuño, D., Li, X. P., Wang, F., and Schnabel, G. 2012b. First report of gray mold of strawberry caused by *Botrytis caroliniana* in North Carolina. Plant Dis. 96:914.

Fernández-Ortuño, D., Grabke, A., Li, X., and Schnabel, G. 2015. Independent emergence of resistance to seven chemical classes of fungicides in *Botrytis cinerea*. Phytopathology 105:424-432.

Fernández-Ortuño, D., Torés, J. A., Chamorro, M., Pérez-García, A., and de Vicente, A. 2016. Characterization of resistance to six chemical classes of site-specific fungicides registered for gray mold control on strawberry in Spain. Plant Dis. 100:2234-2239.

Fernández-Ortuño, D., Grabke, A., Bryson, P. K., Amiri, A., Peres, N. A., and Schnabel, G. 2014. Fungicide resistance profiles in *Botrytis cinerea* from strawberry fields of seven southern U.S. states. Plant Dis. 98:825-833.

Fernández-Ortuño, D., Pérez-García, A., Chamorro, M., de la Peña, E., de Vicente, A., and Torés, J. A. 2017. Resistance to the SDHI fungicides boscalid, fluopyram, fluxapyroxad, and penthiopyrad in *Botrytis cinerea* from commercial strawberry fields in Spain. Plant Dis. 101:1306-1313.

Fillinger, S., Leroux, P., Auclair, C., Barreau, C., Al Hajj, C., and Debieu, D. 2008. Genetic analysis of fenhexamid-resistant field isolates of the phytopathogenic fungus *Botrytis cinerea*. Antimicrob. Agents Chemother. 52:3933-3940.

Gadoury, D. M., Seem, R. C., Ficke, A., and Wilcox, W. F. 2003. Ontogenic resistance to powdery mildew in grape berries. Phytopathology 93:547-555.

Gadoury, D. M., Seem, R. C., Wilcox, W. F., Henick-Kling, T., Conterno, L., Day, A., and Ficke, A. 2007. Ecology and epidemiology effects of diffuse colonization of grape berries by *Uncinula necator* on bunch rots, berry microflora, and juice and wine quality. Phytopathology 97:1356-1365.

Gao, F., Chen, J., Xiao, J., Cheng, W., Zheng, X., Wang, B., and Shi, X. 2019. Microbial community composition on grape surface controlled by geographical factors of different wine regions in Xinjiang, China. Food Research International 122:348-360.

Garrido, C., Carbú, M., Fernández‐Acero, F. J., Boonham, N., Colyer, A., Cantoral, J. M., and Budge, G. 2009. Development of protocols for detection of *Colletotrichum acutatum* and monitoring of strawberry anthracnose using real‐time PCR. Plant Pathol. 58:43-51.

Gava, A., Emer, C. D., Ficagna, E., Fernandes de Andrade, S., and Fuentefria, A. M. 2021. Occurrence and impact of fungicides residues on fermentation during wine production- A review. Food Additives & Contaminants: Part A 38:943-961.

Glass, N. L., and Donaldson, G. C. 1995. Development of primer sets designed for use with the PCR to amplify conserved genes from filamentous ascomycetes. Appl. Environ. Microbiol. 61:1323-1330.
Grabke, A., and Stammler, G. 2015. A *Botrytis cinerea* population from a single strawberry field in Germany has a complex fungicide resistance pattern. Plant Dis. 99:1078-1086.
Greer, L. A., Harper, J. D. I., and Steel, C. C. 2014. Infection of *Vitis vinifera* (cv Chardonnay) inflorescences by *Colletotrichum acutatum* and *Greeneria uvicola*. J. Phytopathol. 162:407-410.
Greer, L. A., Harper, J. D. I., Savocchia, S., Samuelian, S. K., and Steel, C. C. 2011. Ripe rot of south-eastern Australian wine grapes is caused by two species of *Colletotrichum*: *C. acutatum* and *C. gloeosporioides* with differences in infection and fungicide sensitivity. Aust. J. Grape Wine R. 17:123-128.
Gubler, W. D., Bettiga, L. J., and Heil, D. 1991. Comparisons of hand and machine leaf removal for the control of *Botrytis* bunch rot. Am. J Enol. Vitic. 42:233-236.
Hahn, M. 2014. The rising threat of fungicide resistance in plant pathogenic fungi: *Botrytis* as a case study. J. of Chem. Biol. 7:133-141.
Hall, M. E., Loeb, G. M., and Wilcox, W. F. 2018. Control of sour rot using chemical and canopy management techniques. Am. J. Enol. Vitic. 69:342-350.
Hannah, L., Roehrdanz, P. R., Ikegami, M., Shepard, A. V., Shaw, M. R., Tabor, G., Zhi, L., Marquet, P. A., and Hijmans, R. J. 2013. Climate change, wine, and conservation. Proceedings of the National Academy of Sciences of the United States of America 110:6907-6912.
Hassan, O., Lim, Y.-S., and Chang, T. 2021. Phylogenetic and morphological characterization of *Cladosporium perangustum* associated with flyspeck on Shine Muscat grapes in South Korea. Mycobiology 49:183-187.
Hastie, T., Tibshirani, R., and Friedman, J. 2009. The elements of statistical learning. 2nd ed. Springer New York, New York, NY.
Herzog, K., Wind, R., and Töpfer, R. 2015. Impedance of the grape berry cuticle as a novel phenotypic trait to estimate resistance to *Botrytis cinerea*. Sensors 15:12498-12512.
Hilário, S., Gonçalves, M. F. M., and Alves, A. 2021. Using genealogical concordance and coalescent-based species delimitation to assess species boundaries in the *Diaporthe eres* complex. J. Fungi 7:507.
Hoffman, L. E., Wilcox, W. F., Gadoury, D. M., and Seem, R. C. 2002. Influence of grape berry age on susceptibility to *Guignardia bidwellii* and its incubation period length. Phytopathology 92:1068-1076.
Hoffmann, F., Bertram, T., Mikut, R., Reischl, M., and Nelles, O. 2019. Benchmarking in classification and regression. Wiley Interdisciplinary Reviews: Data Mining and Knowledge Discovery 9:e1318.
Hong, S.-B., Go, S.-J., Shin, H.-D., Frisvad, J. C., and Samson, R. A. 2005. Polyphasic taxonomy of *Aspergillus fumigatus* and related species. Mycologia 97:1316-1329.
Hu, M., and Cosseboom, S. D. 2019. Evaluation of fungicides at different timing for control of ripe rot of grapes, 2018. Plant Dis. Manag. Rep. 13:PF068.
Hu, M., Cosseboom, S. D., Schoeneberg, A., Johnson, C. S., Peres, N. A., and Lea-Cox, J. 2020. Validation of the strawberry advisory system in the Mid-Atlantic region. Plant Dis. 105:2670-2679.

Hu, M.-J., Fernández-Ortuño , D., and Schnabel, G. 2016. Monitoring resistance to SDHI fungicides in *Botrytis cinerea* from strawberry fields. Plant Dis. 100:959-965.

Hu, M.-J., Cosseboom, S., and Schnabel, G. 2019. *atrB*-associated fludioxonil resistance in *Botrytis fragariae* not linked to mutations in transcription factor *mrr1*. Phytopathology 109:839-846.

Iacomi-Vasilescu, B., Avenot, H., Bataillé-Simoneau, N., Laurent, E., Guénard, M., and Simoneau, P. 2004. In vitro fungicide sensitivity of *Alternaria* species pathogenic to crucifers and identification of *Alternaria brassicicola* field isolates highly resistant to both dicarboximides and phenylpyrroles. Crop Prot. 23:481-488.

Jain, A. K., Duin, R. P. W., and Jianchang, M. 2000. Statistical pattern recognition: a review. IEEE Transactions on Pattern Analysis and Machine Intelligence 22:4-37.

Jang, M. H., Moon, Y. S., Noh, J. H., Kim, S. H., Hong, S. K., and Yun, H. K. 2011. In vitro evaluation system for varietal resistance against ripe rot caused by *Colletotrichum acutatum* in grapevines. Hort. Environ. Biotech. 52:52-57.

Jarvis, W. R. 1962. The dispersal of spores of *Botrytis cinerea* in a raspberry plantation. Trans. Brit. Mycolog. Soc. 45:549-559.

Jayawardena, R. S., Hyde, K. D., Damm, U., Cai, L., Liu, M., Li, X. H., Zhang, W., Zhao, W. S., and Yan, Y. J. 2016. Notes on currently accepted species of *Colletotrichum*. Mycosphere 7:1192-1260.

Jayawardena, R. S., Zhang, W., Liu, M., Maharachchikumbura, S. S. N., Zhou, Y., Huang, J., Nilthong, S., Wang, Z., Li, X., Yan, J., and Hyde, K. D. 2015. Identification and characterization of *Pestalotiopsis*-like fungi related to grapevine diseases in China. Fungal Biol. 119:348-361.

Ji, T., Salotti, I., Dong, C., Li, M., and Rossi, V. 2021. Modeling the effects of the environment and the host plant on the ripe rot of grapes, caused by the *Colletotrichum* species. Plants 10:2288.

Kakalíková, Ľ., Jankura, E., and Šrobárová, A. 2009. First report of *Alternaria* bunch rot of grapevines in Slovakia. Australas. Plant Dis. Not. 4:68-69.

Karajeh, M. R. 2018. Pre-harvest bagging of grape clusters as a non-chemical physical control measure against certain pests and diseases of grapevines. Org. Agr. 8:259-264.

Kennelly, M. M., Gadoury, D. M., Wilcox, W. F., Magarey, P. A., and Seem, R. C. 2007. Seasonal development of ontogenic resistance to downy mildew in grape berries and rachises. Phytopathology 95:1445-1452.

Kepner, C., and Swett, C. L. 2018. Previously unrecognized diversity within fungal fruit rot pathosystems on *Vitis vinifera* and hybrid white wine grapes in Mid-Atlantic vineyards. Australas. Plant Path. 47:181-188.

Khodadadi, F. Gonzalez, J. B., Martin, P. L., Giroux, E., Bilodeau, G. J., Peter, K. A., Doyle, V. P., and Acimovic, S. 2020. Identification and characterization of *Colletotrichum* species causing apple bitter rot in New York and description of *C. noveboracense* sp. nov. Sci. Rep. 10:11043.

Kralik, P., and Ricchi, M. 2017. A basic guide to real time PCR in microbial diagnostics: definitions, parameters, and everything. Front. Microbiol. 8:108.

Kretschmer, M., Leroch, M., Mosbach, A., Walker, A. S., Fillinger, S., Mernke, D., Schoonbeek, H. J., Pradier, J. M., and Leroux, P. 2009. Fungicide-driven evolution and molecular basis of multidrug resistance in field populations of the grey mould fungus *Botrytis cinerea*. PLoS Pathog. 5:e1000696.

Kumar, S., Stecher, G., Li, M., Knyaz, C., and Tamura, K. 2018. MEGA X: molecular evolutionary genetics analysis across computing platforms. Mol. Biol. Evol. 35:1547-1549.

Latorre, B. A., Viertel, S. C., and Spadaro, I. 2002. Severe outbreaks of bunch rots caused by *Rhizopus stolonifer* and *Aspergillus niger* on table grapes in Chile. Plant Dis. 86:815-815.

Lederer, M. A., Nielsen, D. S., Toldam-Andersen, T. B., Herrmann, J. V., and Arneborg, N. 2013. Yeast species associated with different wine grape varieties in Denmark. Acta Agr. Scand. 63:89-96.

Lei, Y., Tang, X. B., Jayawardena, R. S., Yan, J. Y., Wang, X. D., Liu, M., Chen, T., Liu, X. M., Wang, J. C., and Chen, Q. X. 2016. Identification and characterization of *Colletotrichum* species causing grape ripe rot in southern China. Mycosphere 7:1177-1191.

Leroch, M., Plesken, C., Weber, R. W. S., Kauff, F., Scalliet, G., and Hahn, M. 2013. Gray mold populations in German strawberry fields are resistant to multiple fungicides and dominated by a novel clade closely related to *Botrytis cinerea*. Appl. Environ. Microb. 79:159-167.

Leroux, P., Gredt, M., Leroch, M., and Walker, A.-S. 2010. Exploring mechanisms of resistance to respiratory inhibitors in field strains of *Botrytis cinerea*, the causal agent of gray mold. Appl. Environ. Microbiol. 76:6615-6630.

Li, X., Fernández-Ortuño, D., Chen, S., Grabke, A., Luo, C.-X., Bridges, W. C., and Schnabel, G. 2014. Location-specific fungicide resistance profiles and evidence for stepwise accumulation of resistance in *Botrytis cinerea*. Plant Dis. 98:1066-1074.

Liu, Y. J., Whelen, S., and Hall, B. D. 1999. Phylogenetic relationships among ascomycetes: evidence from an RNA polymerse II subunit. Molec. Biol. Evol. 16:1799-1808.

Longo, A. V., Rodriguez, D., da Silva Leite, D., Toledo, L. F., Mendoza Almeralla, C., Burrowes, P. A., and Zamudio, K. R. 2013. ITS1 copy number varies among Batrachochytrium dendrobatidis strains: implications for qPCR estimates of infection intensity from field-collected amphibian skin swabs. PLoS One 8:e59499.

Lorenz, D. H., Eichhorn, K. W., Bleiholder, H., Klose, R., Meier, U., and Weber, E. 1995. Growth Stages of the grapevine: phenological growth stages of the grapevine (*Vitis vinifera* L. ssp. *vinifera*) - codes and descriptions according to the extended BBCH scale. Aust. J. Grape Wine R. 1:100-103.

Lorenzini, M., and Zapparoli, G. 2014. Characterization and pathogenicity of *Alternaria* spp. strains associated with grape bunch rot during post-harvest withering. Int. J. Food. Microb. 186:1-5.

Lorenzini, M., and Zapparoli, G. 2015. Occurrence and infection of *Cladosporium*, *Fusarium*, *Epicoccum* and *Aureobasidium* in withered rotten grapes during post-harvest dehydration. Anton. Leeuw. 108:1171-1180.

Lorenzini, M., Cappello, M. S., and Zapparoli, G. 2015. Isolation of *Neofusicoccum parvum* from withered grapes: strain characterization, pathogenicity and its detrimental effects on passito wine aroma. J. Appl. Microbiol. 119:1335-1344.

Ma, Z., Yan, L., Luo, Y., and Michailides, T. J. 2007. Sequence variation in the two-component histidine kinase gene of *Botrytis cinerea* associated with resistance to dicarboximide fungicides. Pestic. Biochem. Physiol. 88:300-306.

MacKenzie, S. J., and Peres, N. A. 2012. Use of leaf wetness and temperature to time fungicide applications to control anthracnose fruit rot of strawberry in Florida. Plant Dis. 96:522-528.

Madden, L. V. 1993. Aggregation of *Colletotrichum acutatum* in response to simulated rain episodes. J. Phytopathol. 138:145-156.
Mahaffee, W. F., and Stoll, R. 2016. The ebb and flow of airborne pathogens: monitoring and use in disease management decisions. Phytopathology 106:420-431.
Maharachchikumbura, S. S. N., Hyde, K. D., Groenewald, J. Z., Xu, J., and Crous, P. W. 2014. *Pestalotiopsis* revisited. Stud. Mycol. 79:121-186.
Manawasinghe, I. S., Dissanayake, A. J., Li, X., Liu, M., Wanasinghe, D. N., Xu, J., Zhao, W., Zhang, W., Zhou, Y., Hyde, K. D., Brooks, S., and Yan, J. 2019. High genetic diversity and species complexity of *Diaporthe* associated with grapevine dieback in China. Front. Microbiol. doi.org/10.3389/fmicb.2019.01936.
Martin, P. L., and Peter, K. 2021. Quantification of *Colletotrichum fioriniae* in orchards and deciduous forests indicates it is primarily a leaf endophyte. Phytopathology 111:333-344.
McClellan, W. D., and Hewitt, W. B. 1973. Early *Botrytis r*ot of grapes: time of infection and latency of *Botrytis cinerea* Pers. in *Vitis vinifera* L. Phytopathology 63:1151-1157.
Melksham, K. J., Weckert, M. A., and Steel, C. C. 2002. An unusual bunch rot of grapes in sub-tropical regions of Australia caused by *Colletotrichum acutatum*. Australas. Plant Pathol. 31:193-194.
Meng, X.-Y., Zhang, H.-X., Mezei, M., and Cui, M. 2011. Molecular docking: a powerful approach for structure-based drug discovery. Curr. Comput. Aided Drug Des. 7:146-157.
Mernke, D., Dahm, S., Walker, A. S., Lalve, A., Fillinger, S., Leroch, M., and Hahn, M. 2011. Two promoter rearrangements in a drug efflux transporter gene are responsible for the appearance and spread of multidrug resistance phenotype MDR2 in *Botrytis cinerea* isolates in French and German vineyards. Phytopathology 101:1176-1183.
Meunier, M., and Steel, C. C. 2009. Effect of *Colletotrichum acutatum* ripe rot on the composition and sensory attributes of Cabernet Sauvignon grapes and wine. Aust. J. Grape Wine R. 15:223-227.
Mikušová, P., Sulyok, M., and Šrobárová, A. 2014. *Alternaria* mycotoxins associated with grape berries in vitro and in situ. Biologia 69:173-177.
Mikušová, P., Ritieni, A., Santini, A., Juhasová, G., and Šrobárová, A. 2010. Contamination by moulds of grape berries in Slovakia. Food Addit. Contam. 27:738-747.
Miles, T. D., Gillett, J. M., Jarosz, A. M., and Schilder, A. M. C. 2013. The effect of environmental factors on infection of blueberry fruit by *Colletotrichum acutatum*. Plant Pathol. 62:1238-1247.
Molitor, D., and Berkelmann-Loehnertz, B. 2011. Simulating the susceptibility of clusters to grape black rot infections depending on their phenological development. Crop Prot. 30:1649-1654.
Mondy, N., Charrier, B., Fermaud, M., Pracros, P., and Corio-Costet, M.-F. 1998. Mutualism between a phytopathogenic fungus (*Botrytis cinerea*) and a vineyard pest (*Lobesia botrana*). Positive effects on insect development and oviposition behaviour. Comptes Rendus de l'Académie des Sciences-Series III-Sciences de la Vie 321:665-671.
Moral, J., Bouhmidi, K., and Trapero, A. 2008. Influence of fruit maturity, cultivar susceptibility, and inoculation method on infection of olive fruit by *Colletotrichum acutatum*. Plant Dis. 92:1421-1426.
Nair, N. G. 1985. Fungi associated with bunch rot of grapes in the Hunter Valley. Aust. J. Ag. R. 36:435-442.

Nair, N. G., and Allen, R. N. 1993. Infection of grape flowers and berries by *Botrytis cinerea* as a function of time and temperature. Mycol. Res. 97:1012-1014.
O'Donnell, K., and Cigelnik, E. 1997. Two divergent intragenomic rDNA ITS2 types within a monophyletic lineage of the fungus *Fusarium* are nonorthologous. Mol. Phylogenet. Evol. 7:103-116.
Oliveira, M. S., Amiri, A., Zuniga, A. I., and Peres, N. A. 2017. Sources of primary inoculum of *Botrytis cinerea* and their impact on fungicide resistance development in commercial strawberry fields. Plant Dis. 101:1761-1768.
Oliveira, M. S., Cordova, L. G., Marin, M. V., and Peres, N. A. 2018. Fungicide dip treatments for management of *Botrytis cinerea* infection on strawberry transplants. Plant Health Prog. 19:279-283.
Oliver, C. 2016. Investigation of wine grape cultivar and cluster developmental stage susceptibility to grape ripe rot caused by two fungal species complexes, *Colletotrichum gloeosporioides*, and *C. acutatum*, and the evaluation of potential controls. Thesis. Virginia Polytechnic Institute.
Oliver, C. 2018. Phylogeny, histological observation, and in vitro fungicide screening and field trials of multiple *Colletotrichum* species, the causal agents of grape ripe rot. Thesis. Virginia Polytechnic Institute.
O'Donnell, K., Kistler, H. C., Cigelnik, E., and Ploetz Randy, C. 1998. Multiple evolutionary origins of the fungus causing Panama disease of banana: Concordant evidence from nuclear and mitochondrial gene genealogies. Proceedings of the National Academy of Sciences 95:2044-2049.
Padgett, M., and Morrison, J. C. 1990. Changes in grape berry exudates during fruit development and their effect on mycelial growth of *Botrytis cinerea*. J. Am. Soc. Hort. Sci. 115:269-273.
Pan, F. Y., Huang, Y., Lin, L., Zhou, Y. M., Wei, R. F., Guo, W. F., Yin, L., and Lu, J. 2016. First report of *Colletotrichum capsici* causing grape ripe rot in Guangxi, China. Plant Dis. 100:2531-2531.
Panebianco, A., Castello, I., Cirvilleri, G., Perrone, G., Epifani, F., Ferrara, M., Polizzi, G., Walters, D. R., and Vitale, A. 2015. Detection of *Botrytis cinerea* field isolates with multiple fungicide resistance from table grape in Sicily. Crop Prot. 77:65-73.
Pavan, W., Fraisse, C. W., and Peres, N. A. 2011. Development of a web-based disease forecasting system for strawberries. Comp. Elec. Ag. 75:169-175.
Paňitrur-De La Fuente, C., Valdés-Gómez, H., Roudet, J., Acevedo-Opazo, C., Verdugo-Vásquez, N., Araya-Alman, M., Lolas, M., Moreno, Y., and Fermaud, M. 2018. Classification of winegrape cultivars in Chile and France according to their susceptibility to *Botrytis cinerea* related to fruit maturity. Australian J. Grape Wine Res. 24:145-157.
Peng, L.-J., Sun, T., Yang, Y.-L., Cai, L., Hyde, K. D., Bahkali, A. H., and Liu, Z.-Y. 2013. *Colletotrichum* species on grape in Guizhou and Yunnan provinces, China. Mycoscience 54:29-41.
Perrone, G., Varga, J., Susca, A., Frisvad, J. C., Stea, G., Kocsube, S., Toth, B., Kozakiewicz, Z., and Samson, R. A. 2008. *Aspergillus uvarum* sp. nov., an uniseriate black *Aspergillus* species isolated from grapes in Europe. J. System. Evol. Microbiol. 58:1032-1039.
Petit, A.-N., Vaillant-Gaveau, N., Walker, A.-S., Leroux, P., Baillieul, F., Panon, M.-L., Clément, C., and Fontaine, F. 2010. Determinants of fenhexamid effectiveness against

grey mould on grapevine: respective role of spray timing, fungicide resistance and plant defences. Crop Protection 29:1162-1167.
Pouzoulet, J., Mailhac, N., Couderc, C., Besson, X., Daydé, J., Lummerzheim, M., and Jacques, A. 2013. A method to detect and quantify *Phaeomoniella chlamydospora* and *Phaeoacremonium aleophilum* DNA in grapevine-wood samples. Applied Microbiol. Biotechnol. 97:10163-10175.
Primiano, I. V., Cia, M. C., Camargo, L. E. A., and Amorim, L. 2021. Early detection of *Neophysopella tropicalis* in grapevine leaves and on spore traps by qPCR. Plant Pathol. 70:358-366.
Quesada, T., Hughes, J., Smith, K., Shin, V. K., James, P., and Smith, J. 2018. A low-cost spore trap allows collection and real-time PCR quantification of airborne *Fusarium circinatum* spores. Forests 9:doi.org/10.3390/f9100586.
Rajput, N. A., Hussainullah, Huo, C., Cao, J., Atiq, M., Atif, R. M., Lodhi, A. M., Syed, R. N., Sarfraz, S., Hameed, A., and Zhao, Z. 2020. First report of *Curvularia verruculosa* causing leaf spot disease of grape (*Vitis vinifera*) in Afghanistan. J. Plant Pathol. 102:1337.
Rebollar-Alviter, A., Silva-Rojas, H. V., Fuentes-Aragón, D., Acosta-González, U., Martínez-Ruiz, M., and Parra-Robles, B. E. 2020. An emerging strawberry fungal disease associated with root rot, crown rot and leaf spot caused by *Neopestalotiopsis rosae* in Mexico. Plant Dis. 104:2054-2059.
Ren, W., Liu, N., Hou, Y., Li, B., Zhou, M., and Chen, C. 2020. Characterization of the resistance mechanism and risk of *Fusarium verticillioides* to the myosin inhibitor phenamacril. Phytopathology 110:790-794.
Rodríguez-Gálvez, E., Hilário, S., Lopes, A., and Alves, A. 2020. Diversity and pathogenicity of *Lasiodiplodia* and *Neopestalotiopsis* species associated with stem blight and dieback of blueberry plants in Peru. Eur. J. Plant Pathol. 157:89-102.
Rojas, E. I., Rehner, S. A., Samuels, G. J., Van Bael, S. A., Herre, E. A., Cannon, P., Chen, R., Pang, J., Wang, R., and Zhang, Y. 2010. *Colletotrichum gloeosporioides* sl associated with *Theobroma cacao* and other plants in Panama: multilocus phylogenies distinguish host-associated pathogens from asymptomatic endophytes. Mycologia 102:1318-1338.
Rousseaux, S., Diguta, C. F., Radoï-Matei, F., Alexandre, H., and Guilloux-Bénatier, M. 2014. Non-*Botrytis* grape-rotting fungi responsible for earthy and moldy off-flavors and mycotoxins. Food Microb. 38:104-121.
Roy, A., Kucukural, A., and Zhang, Y. 2010. I-TASSER: a unified platform for automated protein structure and function prediction. Nature Protocols 5:725-738.
Rupp, S., Plesken, C., Rumsey, S., Dowling, M., Schnabel, G., Weber, R. W. S., and Hahn, M. 2017. *Botrytis fragariae*, a new species causing gray mold on strawberries, shows high frequencies of specific and efflux-based fungicide resistance. Appl. Environ. Microb. 83:83:e00269-00217.
Saju, K. A., Mech, S., Deka, T. N., and Biswas, A. K. 2011. In vitro evaluation of biocontrol agents, botanicals and fungicides against *Pestalotiopsis* sp. infecting large cardamom (*Amomum subulatum* Roxb.). J. Spices Arom. Crop. 20:89-92.
Salah, H., Lackner, M., Houbraken, J., Theelen, B., Lass-Flörl, C., Boekhout, T., Almaslamani, M., and Taj-Aldeen, S. J. 2019. The emergence of rare clinical *Aspergillus* species in Qatar: molecular characterization and antifungal susceptibility profiles. Front. Microbiol. 10:1677.

Samson, R. A., Visagie, C. M., Houbraken, J., Hong, S. B., Hubka, V., Klaassen, C. H. W., Perrone, G., Seifert, K. A., Susca, A., and Tanney, J. B. 2014. Phylogeny, identification and nomenclature of the genus *Aspergillus*. Stud. Mycol. 78:141-173.

Samuelian, S. K., Greer, L. A., Savocchia, S., and Steel, C. C. 2011. Detection and monitoring of *Greeneria uvicola* and *Colletotrichum acutatum* development on grapevines by real-time PCR. Plant Dis. 95:298-303.

Samuelian, S. K., Greer, L. A., Savocchia, S., and Steel, C. C. 2012. Overwintering and presence of *Colletotrichum acutatum* (ripe rot) on mummified bunches, dormant wood, developing tissues and mature berries of *Vitis vinifera*. Vitis 51:33-37.

Samuelian, S. K., Greer, L. A., Savocchia, S., and Steel, C. C. 2014. Application of Cabrio (ai pyraclostrobin) at flowering and veraison reduces the severity of bitter rot (*Greeneria uvicola*) and ripe rot (*Colletotrichum acutatum*) of grapes. Aust. J. Grape Wine R. 20:292-298.

Santos, G. S., Mafia, R. G., Aguiar, A. M., Zarpelon, T. G., Damacena, M. B., Barros, A. F., and Ferreira, M. A. 2020. Stem rot of eucalyptus cuttings caused by *Neopestalotiopsis* spp. in Brazil. J. Phytopathol. 168:311-321.

Santos, L., Alves, A., and Alves, R. 2017. Evaluating multi-locus phylogenies for species boundaries determination in the genus *Diaporthe*. PeerJ 5:e3120.

Schweigkofler, W., Donnell, K., and Garbelotto, M. 2004. Detection and quantification of airborne conidia of *Fusarium circinatum* the causal agent of pine pitch canker, from two California sites by using a real-time PCR approach combined with a simple spore trapping method. Appl. Environ. Microbiol. 70:3512-3520.

Scott, P. M., Lawrence, G. A., and Lau, B. P. Y. 2006. Analysis of wines, grape juices and cranberry juices for *Alternaria* toxins. Mycotoxin Res. 22:142-147.

Serey, R. A., Torres, R., and Latorre, B. A. 2007. Pre-and post-infection activity of new fungicides against *Botrytis cinerea* and other fungi causing decay of table grapes. Cienc. Investig. Agrar. 34:215-224.

Sergeeva, V., Priest, M., and Nair, N. G. 2005. Species of *Pestalotiopsis* and related genera occurring on grapevines in Australia. Australas. Plant Path. 34:255-258.

Serra, R., Mendonça, C., and Venâncio, A. 2006. Fungi and ochratoxin A detected in healthy grapes for wine production. Lett. Appl. Microbiol. 42:42-47.

Shahoveisi, F., Riahi Manesh, M., and del Río Mendoza, L. E. 2022. Modeling risk of *Sclerotinia sclerotiorum*-induced disease development on canola and dry bean using machine learning algorithms. Sci. Rep. 12:864.

Shiraishi, M., Koide, M., Itamura, H., Yamada, M., Mitani, N., Ueno, T., Nakaune, R., and Nakano, M. 2007. Screening for resistance to ripe rot caused by *Colletotrichum acutatum* in grape germplasm. Vitis 46:196-200.

Sperschneider, J. 2020. Machine learning in plant–pathogen interactions: empowering biological predictions from field scale to genome scale. New Phyt. 228:35-41.

Staats, M., van Baarlen, P., and van Kan, J. A. L. 2005. Molecular phylogeny of the plant pathogenic genus *Botrytis* and the evolution of host specificity. Mol. Biol. Evol. 22:333-346.

Stammler, G., and Speakman, J. 2006. Microtiter method to test the sensitivity of *Botrytis cinerea* to boscalid. J. Phytopathol. 154:508-510.

Steel, C. C., Greer, L. A., and Savocchia, S. 2007. Studies on *Colletotrichum acutatum* and *Greeneria uvicola*: Two fungi associated with bunch rot of grapes in sub-tropical Australia. Aust. J. Grape Wine R. 13:23-29.
Steel, C. C., Greer, L. A., and Savocchia, S. 2012. Grapevine inflorescences are susceptible to the bunch rot pathogens, *Greeneria uvicola* (bitter rot) and *Colletotrichum acutatum* (ripe rot). Eur. J. Plant Pathol. 133:773-778.
Steel, C. C., Greer, L. A., Savocchia, S., and Samuelian, S. K. 2011. Effect of temperature on *Botrytis cinerea*, *Colletotrichum acutatum* and *Greeneria uvicola* mixed fungal infection of *Vitis vinifera* grape berries. Vitis 50:69-71.
Sturgess, O. W. 1957. A ripe fruit rot of the strawberry caused by a species of *Gloeosporium*. Queensland J. Ag. Sci. 14:241-251.
Sung, G.-H., Sung, J.-M., Hywel-Jones, N. L., and Spatafora, J. W. 2007. A multi-gene phylogeny of Clavicipitaceae (Ascomycota, Fungi): Identification of localized incongruence using a combinational bootstrap approach. Mol. Phylogen. Evol. 44:1204-1223.
Sutton, T. B., and Shane, W. W. 1983. Epidemiology of the perfect stage of *Glomerella cingulata* on apples. Phytopathology 73:1179-1183.
Swart, A. E., and Holz, G. 1994. Colonization of table grape bunches by *Alternaria alternata* and rot of cold-stored grapes. S. Afr. J. Enol. Vitic. 15:19-25.
Tardaguila, J., de Toda, F. M., Poni, S., and Diago, M. P. 2010. Impact of early leaf removal on yield and fruit and wine composition of *Vitis vinifera* L. Graciano and Carignan. Am. J. Enol. Vitic. 61:372-381.
Templeton, M. D., Rikkerink, E. H. A., Solon, S. L., and Crowhurst, R. N. 1992. Cloning and molecular characterization of the glyceraldehyde-3-phosphate dehydrogenase-encoding gene and cDNA from the plant pathogenic fungus *Glomerella cingulata*. Gene 122:225-230.
Thiessen, L. D., Neill, T. M., and Mahaffee, W. F. 2017. Timing fungicide application intervals based on airborne *Erysiphe necator* concentrations. Plant Dis. 101:1246-1252.
Thiessen, L. D., Keune, J. A., Neill, T. M., Turechek, W. W., Grove, G. G., and Mahaffee, W. F. 2016. Development of a grower-conducted inoculum detection assay for management of grape powdery mildew. Plant Pathol. 65:238-249.
Thomidis, T., Michailides, T., and Exadaktylou, E. 2009. Contribution of pathogens to peach fruit rot in Northern Greece and their sensitivity to iprodione, carbendazim, thiophanate-methyl and tebuconazole fungicides. J. Phytopathol. 157:194-200.
Tracey, J., Bomford, M., Hart, Q., Saunders, G., and Sinclair, R. 2007. Managing bird damage to fruit and other horticultural crops. Bureau of Rural Sciences, Canberra, Australia.
Tracey, J. P., and Saunders, G. 2003. Bird damage to the wine grape industry. Bureau of Rural Sciences, Canberry, Australia.
USDA-NASS. 2017. Quick stats. USDA National Agricultural Statistics Service.
Vail, M. E., and Marois, J. J. 1991. Grape cluster architecture and the susceptibility of berries to *Botrytis cinerea*. Phytopathology 81:188-191.
Valero-Jiménez, C. A., Veloso, J., Staats, M., and Van Kan, J. A. L. 2019. Comparative genomics of plant pathogenic *Botrytis* species with distinct host specificity. BMC Genom. 20:203.

Veloukas, T., Markoglou, A. N., and Karaoglanidis, G. S. 2013. Differential effect of sdhB gene mutations on the sensitivity to SDHI fungicides in *Botrytis cinerea*. Plant Dis. 97:118-122.

Verma, N., MacDonald, L., and Punja, Z. K. 2007. Environmental and host requirements for field infection of blueberry fruits by *Colletotrichum acutatum* in British Columbia. Plant Pathol. 56:107-113.

Verweij, P. E., Snelders, E., Kema, G. H. J., Mellado, E., and Melchers, W. J. G. 2009. Azole resistance in *Aspergillus fumigatus*: a side-effect of environmental fungicide use? Lancet Infect. Dis. 9:789-795.

Vesth, T. C., Nybo, J. L., Theobald, S., Frisvad, J. C., Larsen, T. O., Nielsen, K. F., Hoof, J. B., Brandl, J., Salamov, A., Riley, R., Gladden, J. M., Phatale, P., Nielsen, M. T., Lyhne, E. K., Kogle, M. E., Strasser, K., McDonnell, E., Barry, K., Clum, A., Chen, C., Labutti, K., Haridas, S., Nolan, M., Sandor, L., Kuo, A., Lipzen, A., Hainaut, M., Drula, E., Tsang, A., Magnuson, J. K., Henrissat, B., Wiebenga, A., Simmons, B. A., Mäkelä, M. R., De Vries, R. P., Grigoriev, I. V., Mortensen, U. H., Baker, S. E., and Andersen, M. R. 2018. Investigation of inter- and intraspecies variation through genome sequencing of *Aspergillus* section Nigri. Nat. Genet. 50:1688-1695.

Walker, A. S., Gautier, A., Confais, J., Martinho, D., Viaud, M., Le Pêcheur, P., Dupont, J., and Fournier, E. 2011. *Botrytis pseudocinerea*, a new cryptic species causing gray mold in French vineyards in sympatry with *Botrytis cinerea*. Phytopathology 101:1433-1445.

Weber, R. W. S. 2011. Resistance of *Botrytis cinerea* to multiple fungicides in northern German small-fruit production. Plant Dis. 95:1263-1269.

Weber, R. W. S., and Hahn, M. 2011. A rapid and simple method for determining fungicide resistance in *Botrytis*. J. Plant Dis. Prot. 118:17-25.

Weir, B. S., Johnston, P. R., and Damm, U. 2012. The *Colletotrichum gloeosporioides* species complex. Stud. Mycol. 73:115-180.

White, T. J., Bruns, T., Lee, S., and Taylor, J. 1990. Amplification and direct sequencing of fungal ribosomal RNA genes for phylogenetics. Pages 315-322 in: PCR protocols: a guide to methods and applications. M. A. Innis, D. H. Gelfand, J. J. Sninsky and T. J. White, eds. Academic Press, New York.

Wilcox, W. F., Gubler, W. D., and Uyemoto, J. K. 2015. Compendium of grape diseases, disorders, and pests. Second edition. ed. APS press, The American Phytopathological Society, St. Paul, Minnesota.

Wilson, L. L. 1990. Influence of temperature and wetness duration on infection of immature and mature strawberry fruit by *Colletotrichum acutatum*. Phytopathology 80:111-116.

Woudenberg, J. H. C., Groenewald, J. Z., Binder, M., and Crous, P. W. 2013. Alternaria redefined. Stud. Mycol. 75:171-212.

Woudenberg, J. H. C., Aveskamp, M. M., de Gruyter, J., Spiers, A. G., and Crous, P. W. 2009. Multiple *Didymella* teleomorphs are linked to the *Phoma clematidina* morphotype. Persoonia 22:56-62.

Xu, L., Kusakari, S.-i., Hosomi, A., Toyoda, H., and Ouchi, S. 1999. Postharvest disease of grape caused by *Pestalotiopsis* species. Jpn. J. Phytopathol. 65:305-311.

Yan, J.-Y., Jayawardena, M. M. R. S., Goonasekara, I. D., Wang, Y., Zhang, W., Liu, M., Huang, J.-B., Wang, Z.-Y., Shang, J.-J., Peng, Y.-L., Bahkali, A., Hyde, K. D., and Li, X.-H. 2015. Diverse species of *Colletotrichum* associated with grapevine anthracnose in China. Fungal Divers. 71:233-246.

Yokosawa, S., Eguchi, N., and Sato, T. 2020. Characterization of the *Colletotrichum gloeosporioides* species complex causing grape ripe rot in Nagano Prefecture, Japan. J. General Plant Pathol. 86:163-172.

Yong, Y. C., Chen, Y. J., Fang, B. Y., and Chung, W. H. 2014. Sensitivity of *Pestalotiopsis* spp. from guava to benzimidazoles in Taiwan. Plant Pathol. Bull. 23:271-275.

Yoshioka, I., Takahashi, H., Kusuya, Y., Yaguchi, T., Kirimura, K., and Cuomo Christina, A. 2020. Draft genome sequence of *Aspergillus tubingensis* WU-2223L, a citric acid-producing filamentous fungus belonging to *Aspergillus* section *Nigri*. Microbiol. Resour. Announc. 9:e00702-00720.

Zapparata, A., Da Lio, D., Sarrocco, S., Vannacci, G., and Baroncelli, R. 2017. First report of *Colletotrichum godetiae c*ausing grape (*Vitis vinifera*) berry rot in Italy. Plant Dis 101:1051.

Zhang, X., Batzer, J. C., Li, X., Peres, N. A., and Gleason, M. L. 2019. Validation of a Florida strawberry anthracnose fruit rot (AFR) warning system in Iowa. Plant Dis. 103:28-33.

Zoecklein, B. W., Wolf, T. K., Duncan, N. W., Judge, J. M., and Cook, M. K. 1992. Effects of fruit zone leaf removal on yield, fruit composition, and fruit rot incidence of Chardonnay and White Riesling (*Vitis vinifera* L.) Grapes. Am. J. Enol. Vitic. 43:139-148.

Zuniga, A. I., Oliveira, M. S., Rebello, C. S., and Peres, N. A. 2020. Baseline sensitivity of *Botrytis cinerea* isolates from strawberry to isofetamid compared to other SDHIs. Plant Dis. 104:1224-1230.